THE RESPONSE OF MUON DETECTORS TO THE PRIMARY COSMIC RAY FLUX

by

D.J. Cooke, B.Sc. (Melb.)

submitted in fulfilment of the

requirements for the degree of

Doctor of Philosophy

UNIVERSITY OF TASMANIA

HOBART

March 1971

Thesis
(Ph.D)

This thesis contains no material which has been accepted for the award of any degree or diploma in any university.

To the best of my knowledge and belief, the thesis contains no material previously published or written by another person except where due reference is made in the text.

D.J. Cooke

CONTENTS

CHAPTER 7: ASYMPTOTIC CONE OF ACCEPTANCE OF MUON DETECTORS

SUMMARY

This thesis presents the results of some investigations into problems associated with the determination of the relationship between the sea level directional muon flux, as observed by muon detectors, and the primary cosmic ray flux.

Previous estimates of muon coupling coefficients (which express the primary-secondary intensity relationship) have been in poor agreement, and insufficient to define the zenith angle dependence of the coefficients. A new determination was therefore undertaken. The following are summaries of the main phases of the determination:

Chapter 2: In order to acquire data suitable for deducing the coupling coefficients, an extensive latitude-azimuth survey was carried out, in which detailed directional muon intensity observations were made over the latitude range from Hobart to Mossman, along the Eastern Australian coast (vertical cut-off range, 2.0 - 13.2 GeV/c; inclined cut-offs to 31.1 GeV/c). The design and conduct of the survey are discussed in this chapter, and the data are presented in Section 2.3.4.

Chapter 3: Techniques are developed to allow the determination of telescope radiation sensitivities in the presence of any given geomagnetic cut-off distribution, and methods are devised to allow the accurate determination of the mean effective cut-offs pertaining to detectors in any particular situation.

Chapter 4: The distribution of cut-off momenta at the latitude survey sites is deduced. A peculiar fine structure is apparent in these results, which appears to account for reported anomalies in the observations of other investigators. The effect is interpreted, in Section 4.7, in terms of the "loop cone", a phenomenon produced by the looping of trajectories around field lines at longitudes local to the sites. The sensitivity of the structure to changes in the contributions to the geomagnetic field from internal and external sources is examined, in Section 4.12.

Chapter 5: The atmospheric asymmetry effect, responsible for portion of the azimuthal asymmetry in the sea level muon flux, is investigated. A series of calculations is made to establish the dependence of the intensity perturbations (produced as a result of the deflection of muons in the geomagnetic field) on direction, atmospheric structure, local magnetic field configuration, altitude, and geomagnetic cut-off. The latitude survey data are corrected to remove the effects of the atmospheric asymmetry, in Section 5.12.4. The atmospheric asymmetry, although responsible for very considerable effects at low latitudes, has been overlooked by most investigators. It appears to be responsible, in part, for the discrepancies between the various previous coupling coefficient estimates.

Chapter 6: A new technique, involving the use of data expressed in the form of inclined/ vertical intensity ratios, is used in analysing the latitude survey data. This method (described in Sections 2.3.4 and 6.2) allows the dependence of muon intensity to be

obtained without the necessity for making detailed corrections to remove the dependence of muon intensity on atmospheric structure.

Unidirectional coupling coefficients are deduced from the data, and extrapolated to high zenith angles (to $\approx 85^{o}$) and high momentum values. The coefficients, presented in Section 6.8, are expressed in terms of continuous functions of momentum and zenith angle. The dependence of the coupling coefficients on changes in primary and secondary conditions are examined, and a technique is devised to allow the azimuth dependence of the coefficients to be deduced.

Chapter 7: Finally, to illustrate the use of the unidirectional muon coupling coefficients, a computer technique (described in Sections 7.5 and 7.6) is developed to allow the rapid, automatic determination of the asymptotic cone of acceptance, and thus the anisotropic response, of any sea level muon telescope to be calculated. This technique, in addition to introducing an increased degree of accuracy into telescope response calculations, is found to facilitate the effective optimization of telescope configuration for use in particular investigations. By carrying out this optimization, it appears possible to obtain gains of the order of five in the efficiency of anisotropy detection over equivalent experiments designed in terms of detectors of commonly used geometries.

ACKNOWLEDGEMENTS

The successful execution of the research reported in this thesis depended to no small extent on the willing cooperation of a number of people and organizations.

The supervision and valuable support of Dr. A.G. Fenton and Dr. K.B. Fenton through all phases of this work is gratefully acknowledged. I thank Dr. A.G. Fenton for undertaking the administrative organization of the latitude survey.

It is a pleasure to acknowledge the important contributions made by Mr. J.E. Humble towards the work reported in Chapter 4, namely in making available the computer program used to make the trajectory tracing computations, and in carrying forward, in the absence of the author during the period of the latitude survey, the task of mapping the cut-off distributions pertaining to the latitude survey sites. I am very grateful to Mr. Humble for this generous assistance and for many stimulating discussions. The culmination of this collaboration was the publication, under joint authorship, of the paper "Directional Cosmic Ray Cut-offs and the Loop Cone Phenomenon at Mid Latitude Sites" (Cooke and Humble [1970]). This paper, with only minor changes, constitutes Sections 4.4, 4.5, 4.7 - 4.9 of the chapter. Mr. Humble also kindly supplied the computer procedure used to effect the time-dependence calculation in the "asymptotic cone" computer program described in Chapter 7.

I am indebted to Dr. R.M. Jacklyn for his interest and valuable

comments on aspects of the asymptotic cone work in Chapter 7, and for his constructive criticism of the draft copy of this thesis.

The useful discussions with Dr. K.G. McCracken, on the loop cone effect, are remembered with pleasure.

I thank Mr. R.F. Francey for supplying the polynomial fitting procedure used in Chapter 6, and the design of the oscillator circuit used in the latitude survey telescope EHT supplies (Chapter 2).

The latitude survey project was supported by a grant from the Australian Research Grants Committee. For assistance in the preparation and conduct of the survey I would like to thank:

: My wife, for her help as, among other things, cook, relief observer, and balloon launcher during the course of the observations.

: Dr. F. Van der Woude for his assistance in the mechanical design of the telescopes.

: Mr. G. Wagner, Mr. R. Wheatley, Mr. G. Kirwan and their respective staffs for the construction and preparation of the equipment.

: The Australian Meteorological Bureau, the Royal Australian Air Force, the Civil Aviation Department, the Darling Downs Aero Club, and the Douglas Shire council, for the use of their sites and facilities.

: Mrs. L. Jackson and Miss K. Haynes, for their assistance in processing the data.

Finally, I gratefully acknowledge the support of a Commonwealth post-graduate scholarship.

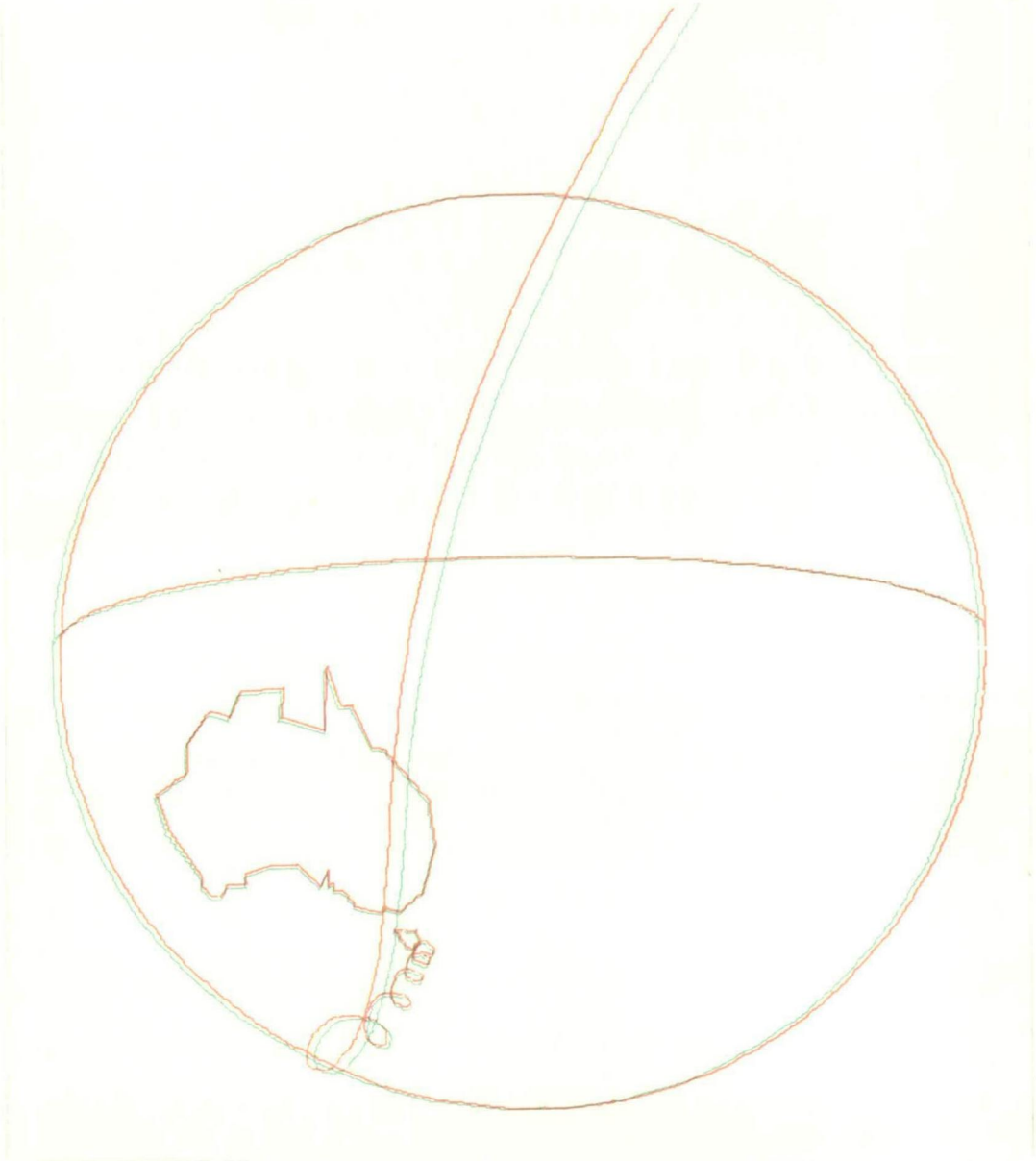

Frontispiece. Computer drawn stereoscopic representation of the trajectory followed by a 4 GeV/c proton which arrives at Hobart at a zenith angle of 60^{o} and a geographic azimuth of 180^{o}. View with the colour filter "spectacles" (see Appendix 2), under incandescent or day-light.

CHAPTER 1

RELATIONSHIP BETWEEN PRIMARY AND SECONDARY COSMIC RAYS

1.1 Introduction

Directional intensity measurements of cosmic rays of energies in excess of a few GeV, in yielding information on anisotropies occurring at distances of the order of 1 AU and greater from the earth, provide a means for pursuing the study of the solar system and the nearer regions of our galaxy. The only practical detectors so far employed at these energies are used at the surface of the earth or underground.

Interpretation of the data from such instruments has a two-fold complexity. As nearly the entire cosmic ray flux which can be studied in this way consists of charged particles, deflected as they are by the terrestrial magnetic field in their motion towards the detector, the directional intensity distribution that existed at the outer boundary of the geomagnetic field is seriously modified. Consequently the directions of viewing of detectors on the surface of the earth are not simply related, except for very high energy particles, to the directions of motion outside the field.

In addition, since detectors deep in the atmosphere are observing not the original cosmic rays, but rather the secondary descendants of these particles, produced on interaction of the primary rays with the oxygen and nitrogen nuclei higher in the

atmosphere, the detailed intensity relationship between the primary and secondary components has to be known accurately if precise interpretation of the data is to be undertaken.

The first of these difficulties may be readily overcome since accurate calculations of the trajectories of primary particles in the geomagnetic field can be performed with the aid of computers, and thus the "asymptotic cone of viewing" (the cone containing all the directions of viewing) of the detector may be deduced.

The second difficulty, that of knowing the intensity relationship between the primary and secondary particle fluxes, has not yet been brought to a satisfactory conclusion for the muon component of the secondary radiation. The muon flux at sea level and below ground is of particular interest in cosmic ray astronomy because of the relatively high average momentum of the parent primaries, and the consequently large region of space about which information may be obtained.

In this thesis coefficients are derived which relate the intensity of muons, at any zenith angle, to the primary particle intensity. Techniques are developed to use these coefficients in the complete specification of the differential response of cosmic ray detectors to anisotropy in the primary particle flux.

As an essential step towards this result it has been necessary to investigate several other aspects of the geophysical effects on the cosmic radiation. This research is reported in detail in this thesis, which is complete in as much as the investigations and the

summaries of the associated literature are covered. The more general aspects of primary-secondary phenomena are well understood and thoroughly reported elsewhere, in review articles and text-books (for example, Vallarta [1961], Fowler and Wolfendale [1961], and Sandstrom [1965]).

1.2 Relating Muon Intensity to Primary Particle Flux

The primary cosmic ray flux consists mainly of protons (≈85%), α-particles (≈10%), and the remainder nuclei with $Z \geq 3$. When these primary particles interact with nuclei in the atmosphere, they give rise to three main secondary components: mesons, nucleons, and the so-called soft component (electron - γ showers). Great numbers of muons (μ-mesons) penetrate to sea level where they are readily observed by normal charged particle detection methods (Geiger counters, plastic scintillators, etc.).

The process of muon production are diverse and complex. The main mechanism is via charged pion (π-meson) production by the primaries. Most pions are produced in the initial interaction and then, because of their short mean life time (2.65×10^{-8} sec.) most decay, giving muons of the same charge. A small proportion are removed by collision, but these further interactions may produce more pions, which then decay to muons, so that the pion-muon decay is the predominant overall result. The other processes that give rise to muons together produce considerably fewer muons than are produced as a result of pion decay.

Measurements show that, although muons may be produced at any level in the atmosphere, most originate at high altitudes. Because of their low interaction cross-section and their relatively long life at relativistic velocities (mean life at rest 2.21×10^{-6} sec.), muons penetrate in large numbers to sea level, and significant numbers to great depths underground. They retain the general direction of motion of the parent primary, but there may be appreciable departures from parallel motion of primary and secondary particles. These deviations are produced partly in the initial pion production (because of multiple pion production the particles leave the struck nucleus in a cone relative to the laboratory co-ordinate system), partly during the subsequent decay of pions into muons, and partly when muons experience coulomb scattering in the atmosphere. Sandstrom [1965] reviews these factors in detail. In addition, the geomagnetic field causes deflections of the muons within the atmosphere.

The momentum possessed by a muon at production is not uniquely related to the momentum of the parent primary, and so the possession of detailed spectral information in relation to the muon flux at any level is of no assistance in determining the role of primaries of particular momentum in giving rise to the muons. It is necessary to determine by some other means the extent to which primaries of any momentum contribute to the muon flux at any level.

This information may be obtained in two different ways. In principle, theoretical calculations may be carried out, if

sufficiently detailed data are available describing the probabilities and cross-sections of the various interactions within the atmosphere. This approach, however, is very difficult due to the inherent complexity of the problem, and the scarcity of detailed information about the interaction processes. As a result theoreticians, as for example Pal and Peters [1964], Brooke et al. [1964], Krimsky et al. [1965], have found it necessary to use many approximations, such as the assumption that muon production is a one-dimensional process. The most sophisticated treatment appears to be that of Astrom [1968], who used information on muon production processes derived from accelerator studies. He derived a set of multiplicities for muon production by primaries of any momentum, for a range of angles relative to the velocity vector of the primary. Nevertheless his work of necessity involves certain approximations, and is limited to momentum values $\leq$ 50 GeV/c. Sea level spectra calculated using this technique agree well with experiment, and it appears that further developments of this theoretical approach may ultimately provide complete specification of the primary-secondary relationship. Because of the scope of the theory the calculations involved in the application to particular problems are themselves complex and time consuming.

The most straightforward means of determining the relationship is the alternate semiempirical method which utilizes a direct experimental approach. This technique is a powerful one because it avoids the need to introduce detailed assumptions about the muon

production and interaction processes, but rather determines the actual, existing relationship. If, in the future, the results of this approach are outstripped by the greater possibilities of the theoretical determinations, the experimental method is nevertheless invaluable, as it yield information which is readily utilized in cosmic ray astronomy, and provides a check on the detailed results of the theoretical calculations.

The semiempirical technique uses the geomagnetic field as a spectrum analyser, the latter preventing as it does primaries of less than a particular momentum from reaching the top of the atmosphere in a given direction. In any direction at any point on the earth, truncation of the primary spectrum therefore occurs at a certain calculable "cut-off" momentum (see Chapter 4). Correlation of the total muon intensity at any given level, in any direction, enables the contribution of primaries within any portion of the primary spectrum to be derived.

If, following Fonger [1953], we use the specific yield function $S(P,x)$ to express the relationship between the vertical intensity of muons at an atmospheric depth x, and the vertical intensity of primaries of momentum P, then the total vertical intensity of muons at that level is

$$N(P_c,x) = \int_{P_c}^{\infty} J(P)\ S(P,x)\ dP \qquad (1.1)$$

where P_c is the vertical cut-off momentum, and $J(P)$ is the primary spectrum. $N(P,x)$ is called the integral response function.

If we assume for the moment that the structure of the atmosphere is latitude invariant, then $S(P,x)$ is also latitude invariant.

More generally we may relate the intensity of muons at any zenith angle θ to the primary directional intensity by introducing a zenith dependent specific yield function $S(\theta,P,x)$.

Thus

$$N(\theta,P_c(\theta,\emptyset),x) = \int_{P_c(\theta,\emptyset)}^{\infty} J(P)\ S(\theta,P,x)\ dP \qquad (1.2)$$

where $P_c(\theta,\emptyset)$ is the cut-off momentum in the direction specified by the zenith and azimuth angles θ and $\emptyset$.

The yield function describes the effective multiplicity in the production of muons by primaries, for muons detectable at sea level. It is independent of azimuth in the absence of a magnetic field in the atmosphere, as then a cylindrically symmetric situation exists about the vertical.

A factor which seems to have been overlooked in previous calculations of specific yield functions is that this symmetry does not exist in real situations. In reality, of course, a magnetic field is present in the atmosphere, and systematic deflections of the muons occur. Owing to the predominance of positively charged muons in the secondary flux, an azimuthal variation arises, superimposed on the azimuthal intensity pattern due to the asymmetrical distribution of cut-off momenta at any site. Intensities tend to be enhanced at western azimuths and reduced in the east. This atmospheric asymmetry effect is largely responsible for the

azimuthal asymmetry observed at high geomagnetic latitudes ($\gtrsim 30^{o}$), but is also of importance at lower latitudes. This phenomenon is discussed in detail, and quantitatively investigated in Chapter 5. For the present it is sufficient to appreciate the existence of the effect.

The magnitude of the atmospheric asymmetry effect is dependent on the atmospheric depth x of the detection level, on the zenith and azimuth angles of viewing θ and ϕ, on the geomagnetic cut-off $P_c(\theta,\phi)$ and on the local magnetic field $\underline{B}$.

Experimental observations yield values of intensity $I(\theta,\phi,P_c,x,\underline{B})$, where the intensity is modified by the magnetic field in the atmosphere. In order to obtain the intensity $N(\theta,P_c,x)$ that would exist in the given set of conditions in the absence of the field, we assume that a function $A(\theta,\phi,P_c,x,\underline{B})$ exists which relates these intensity values, such that

$$N(\theta,P_c,x) = I(\theta,\phi,P_c,x,\underline{B})\ A(\theta,\phi,P_c,x,\underline{B}) \qquad (1.3)$$

If the function A is known, then, in principle, N may be determined, as discussed in Chapter 5. The specific yield function may then be obtained in an azimuth independent form by means of equation (1.2).

Dorman [1957] introduced the concept of coupling coefficients - a particularly convenient form in which the primary-secondary relationship may be expressed. If atmospheric conditions are constant so that $S(\theta,P,x)$ is invariant (data normalized to standard

atmospheric conditions), and if the primary spectrum J(P) is invariant, then partial differentiation of equation (1.2) yields

$$\frac{\delta N}{\delta P_c} = -J(P)\ S(\theta,P,x)$$

Dividing both sides by the intensity $N'(\theta,P_c=0,x)$,

$$\frac{1}{N'}\frac{\delta N}{\delta P_c} = -\frac{J(P)\ S(\theta,P,x)}{N'} = -W(\theta,P,x) \qquad (1.4)$$

$W(\theta,P,x)$ is the so-called coupling coefficient function, expressing the differential contribution to the directional muon intensity at zenith angle θ, and at atmospheric depth x, from the primaries of momentum P. Since at low momenta $S(\theta,P,x)$, and at high momenta J(P), tend to zero, the coupling coefficient function possesses a maximum at some intermediate momentum.

The coupling coefficients may be expressed in the units % per GeV/c, so that at any site, in any direction

$$\int_{P_c}^{\infty} W(\theta,P,x) = 100\ \% \qquad (1.5)$$

If the dependence of N on P_c for any particular θ is determined from experimental observations, then $\frac{\delta N}{N\,\delta P_c}$ is known, and $W(\theta,P,x)$ may be deduced. An upper limit exists in the range of P_c available in the geomagnetic field at any zenith angle. In the

vertical direction this range extends to ≈ 18 GeV/c, and at high zenith angles to ≈ 60 GeV/c. It is necessary to extrapolate the experimental coefficients in order to obtain the complete specification of the coupling coefficients. Dorman [1957] showed that the extrapolation to high momenta could be carried out by application of the known restraints on the function, viz.

a) Total area under the coupling coefficient curves must be 100 % (equation 1.5),

b) Continuity of slope and equality of absolute value required at the point where the extrapolation function joins the experimentally determined function.

A further difficulty arises in practice because of the significant latitude dependence of the muon intensity in any particular direction at a particular atmospheric level, due to variation in the temperature - height structure of the atmosphere. The intensity of muons at any site is dependent on both the pressure and temperature conditions existing at any instant. Increase in pressure alone will lead to a decrease in muon intensity, due to the increased mass of air above the site. Variation in temperature, however, has a more devious effect on the observed intensity. With increase in temperature the atmosphere expands, resulting in an increase in height of the mean production level, and an increase in the distance the muons have to travel to the observing level. The muons consequently have an increased probability of decay. At the same time, due to the decreased density of the atmosphere, there

will be a decrease in the probability of pion loss by collision, causing increase in numbers of muons produced. The relative importance of these processes will depend on the actual configuration of the atmosphere at any particular place and time.

If observations of muon intensity at different sites are to be used in conjunction to derive the coupling coefficients, then it is necessary to have some means of normalizing the data to some standard set of conditions.

We may summarize the requirements necessary for the successful determination of muon coupling coefficients by the method adopted in this thesis as follows. It is desirable to have:

a) Accurate observational data,

b) Knowledge of the values of the function $A(\theta,\phi,P_c,x,\underline{B})$ pertaining to the directions of viewing of the muon detectors,

c) Accurate knowledge of the geomagnetic cut-offs in the directions of viewing,

d) The means of taking into account the finite acceptance cone of the detectors,

e) The means for correcting or normalizing the experimental data to remove the effects of latitude variation of atmospheric configuration.

f) Experimental evidence of the form of the coupling coefficient function in the region of the maximum.

To date, although numerous experimental determinations of muon coupling coefficients have been carried out, particularly for the

vertical muon component, there is great diversity in the results, evidently due to failure to take into account some or all of these factors. We now review the various determinations of the muon coupling coefficients.

1.3 Review of Previous Coupling Coefficient Determinations

The results of the various experimental determinations of the muon coupling coefficients are briefly summarized, and consideration is then given to the effects of the factors listed in Section 1.2 to see if these can account for the disparity between the estimates.

Dorman [1957] deduced the form of the coefficients for the vertical muon component, using the results of a latitude survey of vertical muon intensity. Corrections for atmospheric effects were applied to normalize the data, and then the intensity observations were correlated with vertical cut-off momentum. The coefficients were extrapolated to high momenta using an empirical formula of the form

$$W_{P>P_o} = K\left[\frac{P}{P_o}\right]^{(-\alpha + bP_o/P)} \qquad (1.6)$$

where P = momentum, and P_o, K, α, and b are constants. The resulting estimate differed considerably from that of Webber and Quenby [1959], who used an essentially different technique to obtain the vertical coefficients. Rather than measure the latitude variation of intensity with a single detector during a period of cosmic ray calm, they noted the response of telescopes at sites distributed over a wide latitude range to a large cosmic ray

flare. The spectrum of the isotropic phase of the flare was deduced using the observed response of neutron monitors to the flare in conjunction with the previously established neutron specific yield function. The muon specific yield function was then deduced using the observed amplitudes of response of the muon telescopes. By combining the specific yield function with the quiet period primary spectrum, the muon coupling coefficients were deduced. This technique, unlike the standard latitude survey, avoids the need for detailed correction of data for removal of atmospheric effects, since the information used is essentially the percentage increase in observed muon intensity, rather than absolute intensity, over a very short period of time.

Webber [1962] recalculated the vertical muon coupling coefficients from the data of Webber and Quenby, using improved cut-off values and neutron yield function. He extended the calculations to deduce the coupling coefficients pertaining to 45^{o} zenith angle. These coefficients show the expected shift of the momentum of greatest response to higher momenta with increase in zenith angle. Extrapolation of the functions to high momenta was effected using the Dorman method.

Kane [1962] used the data from all the currently available published surveys of azimuthal variation of muon intensity, to obtain information on the intensity variation as a function of directional main cone cut-off at a number of zenith angles. He found very considerable differences between the estimates made

from individual data sets, also observing inconsistencies among the coefficients obtained from a single set. Typically the empirical coupling coefficient functions he derived show no sign of a maximum, rather being irregular functions, decreasing in value with increasing momentum.

Mathews [1963] used a different technique again to derive the coupling coefficients relating to the vertical sea level muon flux. By means of a method similar to that used by Dorman [1959] to relate coupling coefficients underground to those at sea level (discussed in Chapter 6), Mathews effected the conversion to sea level of Webber and Quenby's [1959] muon differential response curve pertaining to 312 gm cm^{-2} atmospheric depth. The resulting coefficients are more akin to those of Webber [1962] than to those of Dorman [1957]. Although based on a purely empirical method, Mathews' determination is a valuable one, because the estimate of the position of the maximum in the sea level coefficients derives from direct experimental evidence, as against the extrapolation procedure used in other determinations.

Mazaryuk [1966] used data from a latitude survey conducted between Russia and Australia to deduce coupling coefficients for the vertical muon flux, also for the muon component inclined at 30^{o} zenith angle in the north-west and south-east. Separate estimates for the two azimuths were necessary because of the marked differences in the integral response functions (observed intensity vs cut-off momentum relationship) for the two azimuths.

The coefficients for the inclined directions show, contrary to reasonable expectations, maxima at lower momentum values than the maximum in the vertical coupling coefficient function.

Dorman, Kovalenko and Milovidova [1967] carried out a latitude survey using vertical and inclined muon telescopes. The data so obtained were corrected for atmospheric temperature and pressure, then correlated with directional cut-off momenta. Like Mazaryuk, Dorman et al. found it necessary to deduce three separate sets of coefficients, for east, west and north-south combined. The experimental coefficients, for these azimuthal headings and for zenith angles of 0^{o}, 33^{o} and 53^{o} exhibit increases with increasing momentum. The predicted position of the maxima are not indicated, as the extrapolation to high momenta was not carried out.

An interesting attempt to extend the range of momentum for which the vertical coupling coefficients have been experimentally determined was made by Mathews and Sivjee [1967]. The dependence of muon intensity on cut-off momentum in inclined directions at elevated sites was measured, with the aim of using the atmospheric depth so obtained (sensibly equivalent to the atmospheric depth in the vertical direction at sea level) in conjunction with the large cut-off values existing in the inclined directions at the equator to extend the vertical sea level integral response curve. It was found, however, that considerable disparity in slope existed between the sea level curve and the experimentally obtained extension, and Mathews and Sivjee were unable to make use

of the additional information.

Dorman, Kovalenko and Cherkov [1969] carried out latitude survey observations between Russia and South America, and deduced the muon coupling coefficients pertaining to zenith angles of 0^{o}, 45^{o} and 55^{o}. These results show evidence of a maximum in the experimentally determined portions of the functions. It is not stated by Dorman et al. whether the inclined coupling coefficients apply to any particular azimuth.

The most recent determination of coupling coefficients appears to be that of Bel'skiy, Dmitriyev and Romanov [1969]. At a site having geomagnetic latitude 57^{o} the azimuthal variation of intensity at zenith angles as great as 84^{o} was investigated. Coupling coefficients were deduced from the resulting integral response curves. These coefficients are functions diminishing in value with increasing cut-off momentum, with no evidence of a maximum in the range of cut-offs investigated.

1.4 Discussion

Examining these various coupling coefficient estimates critically in respect of the requirements as stated in Section 1.2, it is evident that certain of them show deficiencies. The most obvious failing is lack of consideration of the effects of the atmospheric asymmetry in data from inclined directions. It is necessary, in fact, to reject outright the coefficients of Bel'skiy et al., because it is quite clear that a sea level site with a geomagnetic

latitude of 57^{o} is well beyond the latitude "knee" (see Chapter 5) for all zenith angles, and consequently the observations were simply measurements of the atmospheric azimuthal asymmetry alone.

The atmospheric asymmetry effect seems to have been responsible, too, for the disparity between the integral response curves for different azimuths found by Mazaryuk [1966], and Dorman et al. [1967], producing as it does depression of eastern intensities and enhancement of those in the west.

Although for many purposes it is obviously necessary to know the coupling coefficients pertaining to particular azimuths, it is invalid to deduce these from integral response functions constructed directly from data applying to the particular azimuths, since it is then implicitly assumed that the magnitude of the atmospheric asymmetry is independent of cut-off value and magnetic field configuration. This, as is shown in Chapter 5, is contrary to expectation.

For this reason, then, the determinations of specific azimuth coupling coefficients effected in this way must be regarded as invalid. At the same time, however, it is invalid simply to take the mean of the estimates for a number of azimuths as being the generalized coupling coefficient function for that zenith angle. The reason for this cannot simply be explained in this chapter, arising as it does out of the observed peculiarities of the azimuthal asymmetry effect, as investigated in Chapter 5.

It must, therefore, be assumed that the inclined coefficients of Mazaryuk [1966], and Dorman et al. [1967] contain significant

errors. It will be shown later in this thesis that failure to remove the effects of the atmospheric asymmetry from observational data can introduce distortion in the integral response curves, flattening the curves and even introducing curvature concave upwards. This distortion characteristically causes displacement of the maxima in the inclined direction coupling coefficients towards low momentum values.

This phenomenon appears to account for the failure of Mathews and Sivjee to achieve their object, as, without correction of the data from inclined directions to remove the atmospheric asymmetry, continuity of the two portions of the integral response curve could not be achieved. The basic technique is a very valuable one, and advantage is taken of the data of Mathews and Sivjee in later work.

The observations of Dorman et al. [1969], pertaining to inclined directions, are combined in some manner, without explanation, to obtain a mean coefficient estimate for zenith angles of 33^{o} and 53^{o}. Without knowledge of how this was carried out, the results cannot be critically examined for evidence of distortion by the atmospheric asymmetry effect. In the absence of specific discussion by Dorman et al. it must be assumed that the results probably are affected.

The estimates that are free of first order contamination from this source, then, are the vertical coefficients of Dorman [1957], Webber [1962], Mathews [1963], Mazaryuk [1966], and Dorman et al.

[1969], also the coefficients of Webber [1962], corresponding to a zenith angle of 45^{o}.

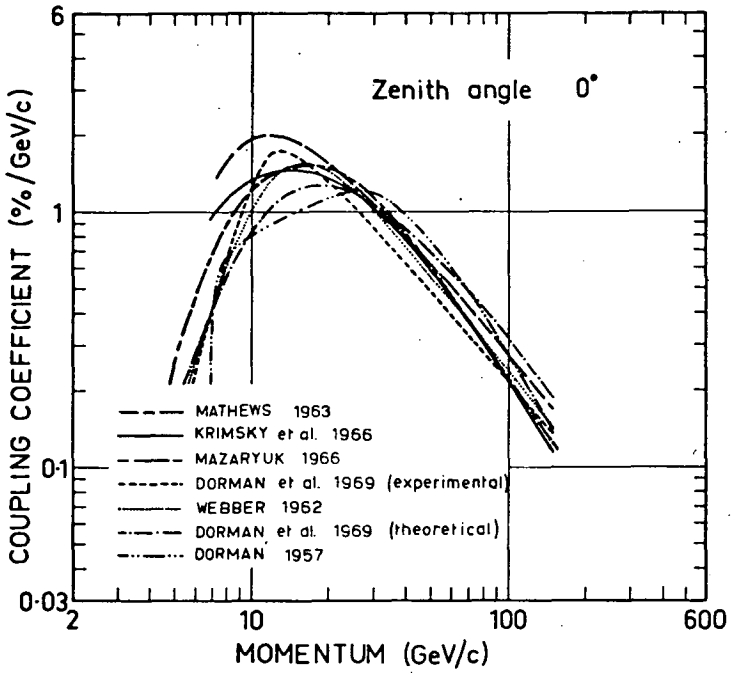

Figure 1.1. Coupling coefficients applying to vertically incident muon flux at sea level, according to the various investigators. In this diagram, and in Figure 1.2, the functions are normalized so that $\int_0^\infty W(\theta,P,x) = 100\ \%$.

It appears that no detailed account has been made in any of these estimates for the finite cone of acceptance of the muon detectors, or for variation of primary cut-off momentum over the opening angle. In addition, these estimates, apart from those of Webber, involve the use of corrections of large magnitude to compensate for variation with latitude of atmospheric temperature and pressure. Any deficiencies, in particular the presence of

systematic errors, will tend to introduce large changes in the form of the coupling coefficients, related as they are to the first derivative of the integral response curves.

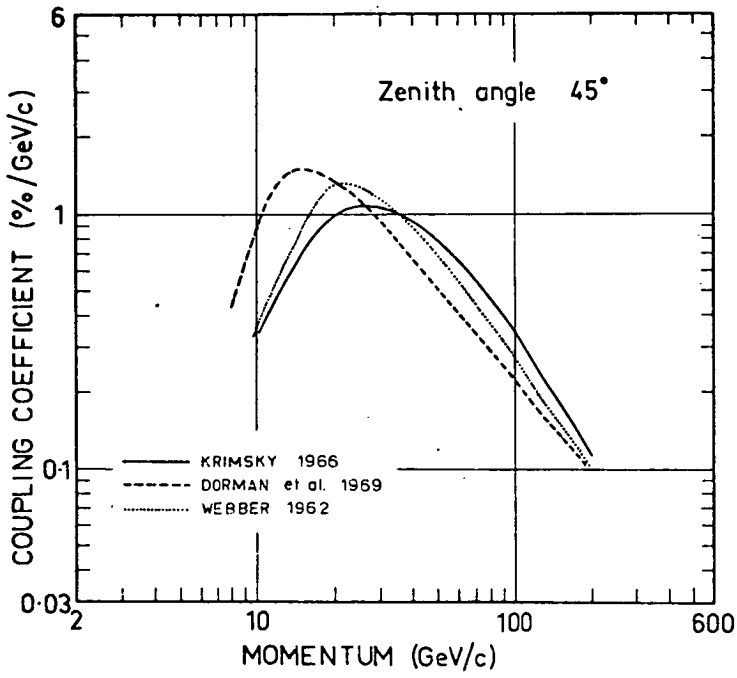

Figure 1.2. Coupling coefficients pertaining to 45^{o} zenith angle.

None of the estimates has made use of detailed, real field models of the geomagnetic field, and so the possibility must be accepted of significant errors in the detailed cut-off momentum values used. Uncertainty in this respect would probably be considerably less than the errors introduced by the use of axial direction cut-offs in conjunction with wide angle detector data. This aspect of the use of cut-off data is examined in detail in Chapter 4, and shown to be of importance in the interpretation of data.

It is not surprising, therefore, that large disparities exist between the estimates of the vertical coupling coefficients, as may be seen in Figure 1.1. The inclined coupling coefficient function of Webber is presented in Figure 1.2. For comparison with this estimate, the theoretical coupling coefficients of Krimsky et al. [1965], and those quoted by Dorman et al. [1969], are also presented.

The need is obvious for an accurate experimental determination of the muon coupling coefficients, in order to clarify the situation in the vertical direction, to determine in detail the zenith angle dependence of the coupling coefficient function, and to locate accurately the position of the maxima in the coefficients, so that accurate extrapolation of the functions to high momenta can be effected. In principle such an undertaking is possible only if the various factors affecting the interpretation of experimental intensity observations (listed in Section 1.2) are effectively taken into account.

These problems are investigated in the following chapters.

CHAPTER 2

LATITUDE SURVEY

2.1 Introduction

In order to take advantage of techniques developed to remove spurious effects from muon intensity data, it is of prime importance to acquire observational data of a high order of accuracy. So that the zenith angle dependence of the muon coupling coefficient function may be investigated, complete sets of observations over a wide range of zenith angles are required. In the absence of suitable existing data it is obvious that a new experiment must be carried out, specifically designed to allow the resolution of the problem.

The Webber and Quenby method (described in Section 1.3) of determining coupling coefficients from data acquired during solar flares could not be employed at this time. Successful utilization of this technique necessitates the use of multiple beamed telescope arrays at a number of sites, and requires the occurrence of a suitable flare event. The resources were not available to build and maintain such a network of detectors, and in any case, at the 1966-67 epoch, a large flare was most unlikely to occur.

The present determination therefore, of necessity, was to be carried out using a latitude-azimuth survey. Because of failure to take into account the factors discussed in Section 1.2, invest-

igators in the past generally have had difficulty reconciling intensity vs cut-off data obtained from azimuth and latitude surveys. As is found in the following chapters, there are distinct advantages to be gained in combining data from both types of measurements, in order to make use of the desirable features of each.

2.2 Design of the Experiment

In essence the experiment consists of the transportation of a number of muon detectors of accurately known characteristics to sites over a wide latitude range, in order to establish by observation the distribution of muon intensity over the observing hemisphere at each site.

Whilst ideally it would be desirable to utilize fully the complete range of cut-offs available in the geomagnetic field, for practical and economic reasons the present survey was restricted to observations at sites within Australia covering the cut-off range 2-13 GeV/c in the vertical direction.

An experiment was therefore planned in which a set of muon detectors was to be transported to a number of sites widely spaced over the latitude range available. It was fortunate that a large airconditioned semi-trailer unit became available at this time, and was purchased for the purposes of the survey. This vehicle was eminently suitable, having internal partitions conveniently arranged for division into laboratory and living space (see Figures 2.1 and 2.2).

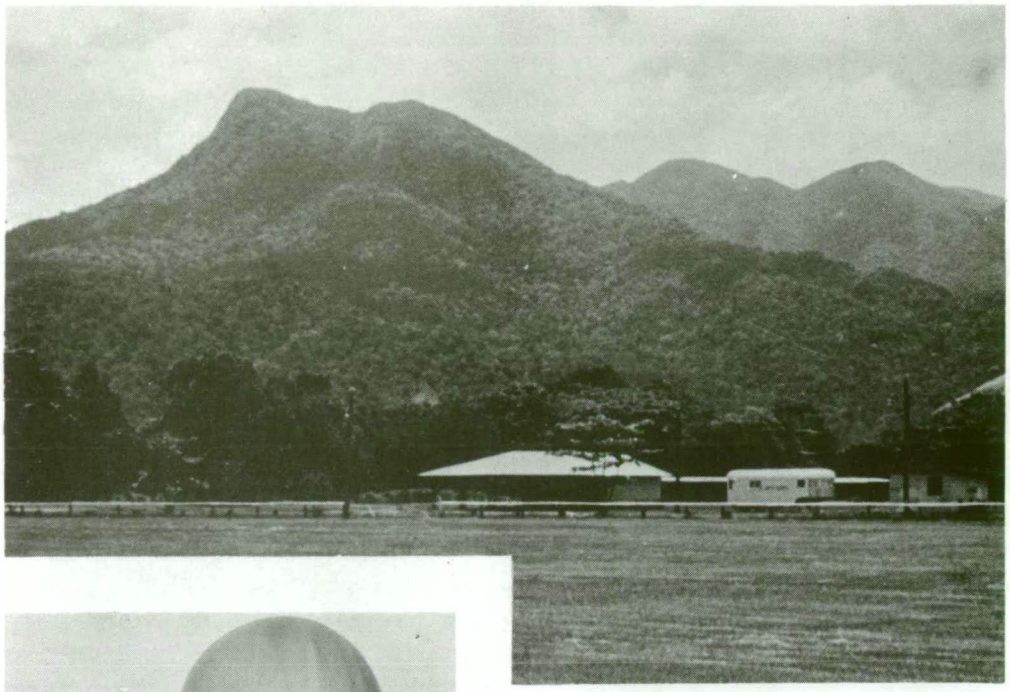

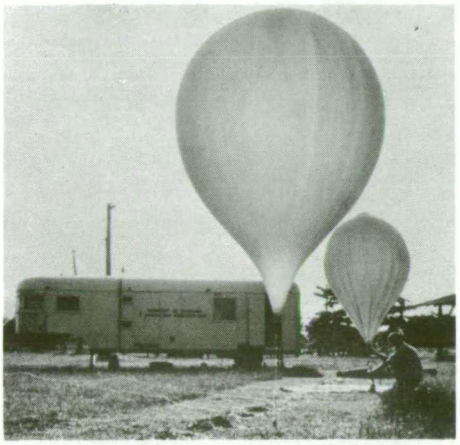

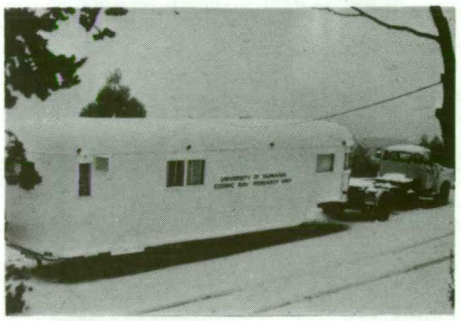

Necessarily the size and shape of the equipment to be carried was dictated to a great extent by the space available in the unit.

Figure 2.1 (opposite). Some "on location" scenes:
Figure 2.1a (top) Trailer set up at the northern-most site of the survey, Mossman, in tropical northern Australia.
Figure 2.1b (centre left) Balloon inflation prior to launch at Mossman.
Figure 2.1c (centre right) The other climatic extreme - the trailer set up at the Springs, near Hobart.
Figure 2.1d (lower left) Rock quarry at Townsville, where cosmic ray shower measurements were carried out.
Figure 2.1e (lower right) Tribulations en route. Moving the heavily laden semi-trailer from site to site was far from "plain sailing". In addition to a number of mechanical breakdowns, and eight tyre blowouts, difficulties were experienced due to the poor road conditions in northern Australia. During an unsuccessful attempt to reach Cooktown, the unit was on two occasions marooned in dry creekbeds for 24 hour periods, being of too low power to negotiate the steep exit tracks. Figure 2.1e shows the semi-trailer being towed from the bed of the Desailly River.

Because of the extensive experience of the Hobart cosmic ray research group in the design and use of Geiger counters, triple

coincidence Geiger counter telescopes were chosen as the muon detectors. In addition to the muon detectors, it was planned to carry further detectors in the mobile unit, to facilitate other cosmic ray measurements. An IGY type neutron monitor was especially designed and built for the survey, to enable continuous measurements of neutron intensity to be carried out. The trailer was also fitted as a receiving station to receive and record data transmissions from high altitude balloon-borne neutron detectors. Sufficient equipment was carried to enable pre-flight checks to be made on the balloon rigs, and for the inflation and launch of the balloons (see Figure 2.1b). The neutron data are not presented in this thesis.

Figure 2.2 (opposite). Details of mobile research unit:
Figure 2.2a (left) Plan view of the trailer unit, showing the location of the cosmic ray detectors and associated recording equipment.
Figure 2.2b (top right) Unit set up for observations at Williamtown. The antenna visible in this photograph was used for receiving telemetered data from balloon-borne equipment flown as part of the latitude survey program.
Figure 2.2c (centre right) A view in the forward compartment of the unit. A telescope unit is visible on the left, the neutron monitor in the foreground, and printing registers above.
Figure 2.2d (lower right) Section of the living quarters in the

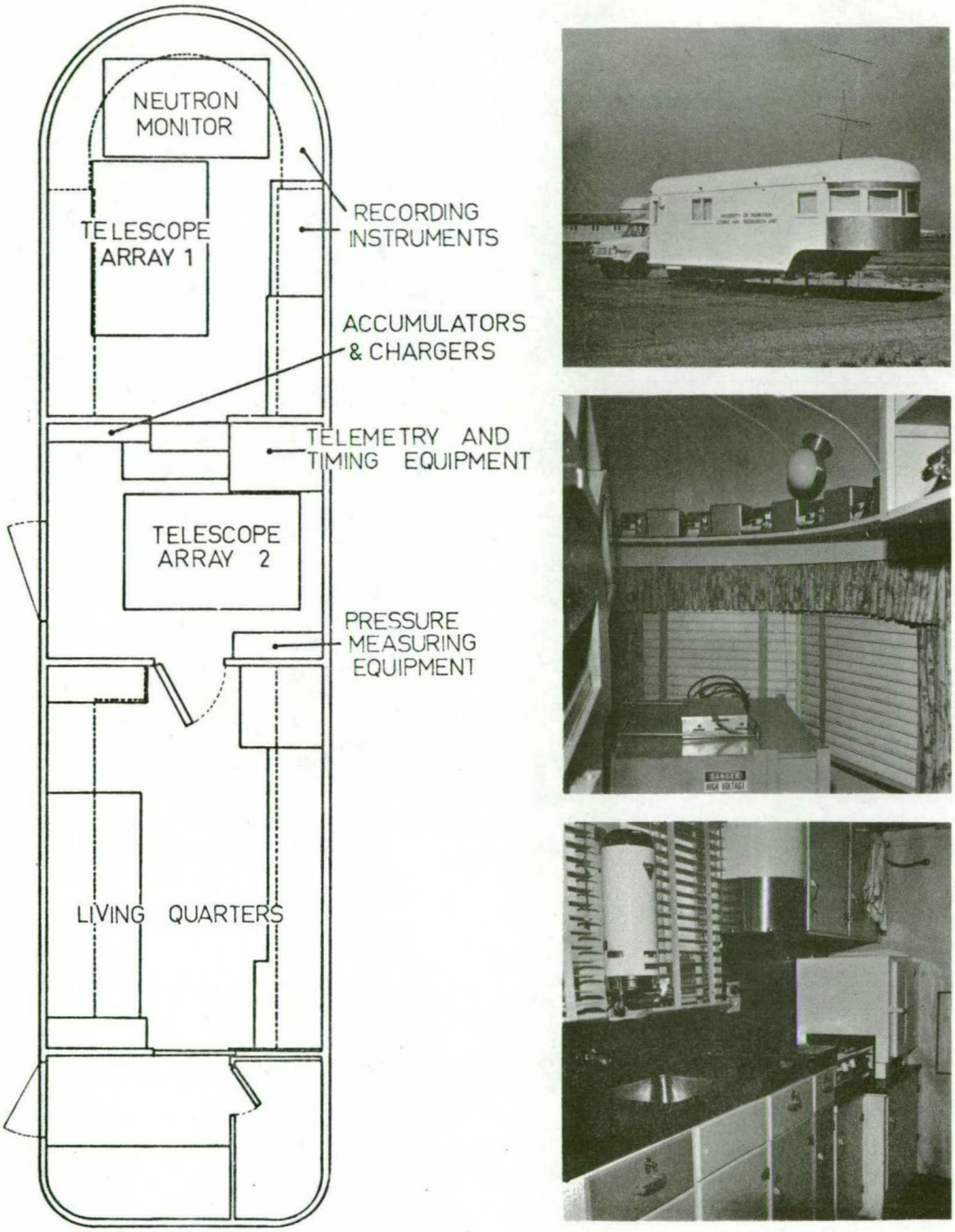

trailer unit, showing the well equipped kitchen area. For a year (August 1966 - August 1967) the trailer was "home" to the author, his wife, and daughter.

2.2.1 Design of the Muon Telescopes

The configuration of the muon telescopes was carefully chosen to be an optimum one for the present purpose, giving a relatively narrow angle of response in conjunction with usefully high coincidence rates at each of four equally spaced zenith angles - nominally 0^{o}, 22.5^{o}, 45^{o} and 67.5^{o}. The following basic requirements were considered when designing the telescopes:

a) To minimize the total time for the survey, it was desirable to carry the maximum number of telescopes that could conveniently be transported, so that observations in a number of directions could be carried out simultaneously.

b) Whilst, in order to shield the telescopes from the soft component of the cosmic ray flux it was necessary to use 10 cm. of lead absorber normal to the axis of each telescope, the total mass of lead had to minimized.

c) Intercalibration of all the telescopes had to be easily effected.

These specialized requirements were satisfied by a "cart-wheel" type of telescope array, in which the telescopes were arranged about a central axle (see Figure 2.3). All the telescopes were of the same dimensions and had the required 10 cm. of lead absorber normal to their axes. The centre tray was common to all seven telescopes in the array. Glass wall Geiger counters of 60 cm. length and 4 cm. diameter were used as the detecting elements. The sensitive area in the extreme trays in each telescope, which

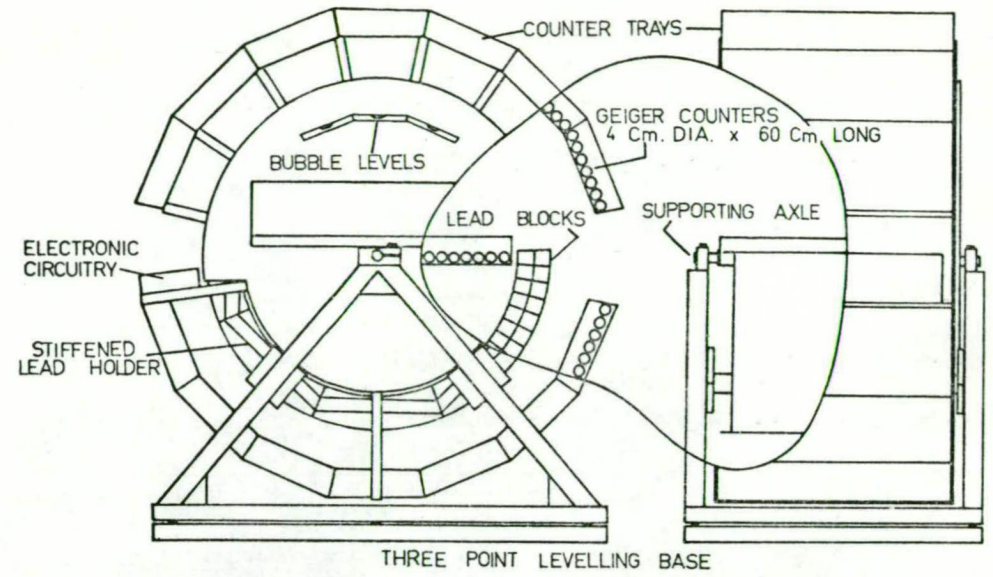

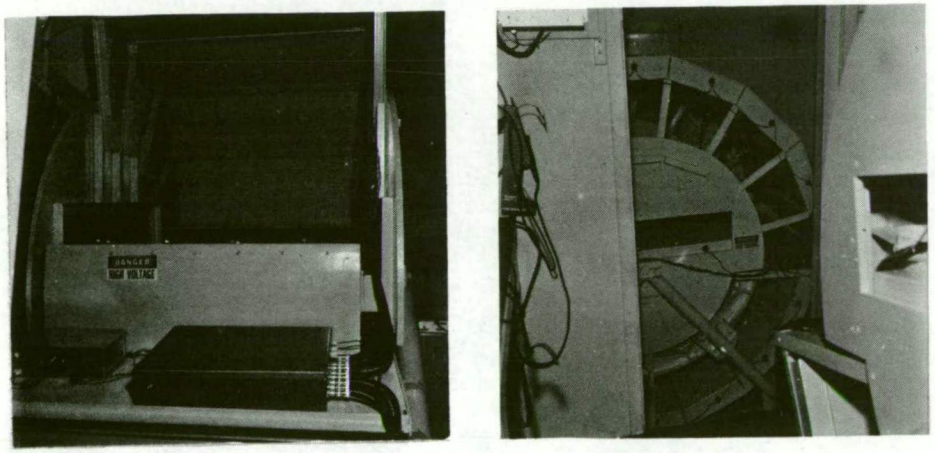

Figure 2.3. Muon telescope design:

Figure 2.3a (top) Details of the construction of the "cart-wheel" telescope arrays.

Figure 2.3b (lower left) A view of the telescope array 1 (see Figure 2.1a), showing EHT and scaling electronics.

Figure 2.3c (lower right) Telescope array 2, viewed through a doorway in the trailer.

was formed by seven such counters, had the dimensions 60 x 29.5 cm. (the larger dimension parallel to the axle supporting the array), and the effective axial length of the telescopes was 159 cm.. The measured axial zenith angles of the detectors as constructed were 0^{o}, 22.6^{o}, 45.2^{o} and 67.8^{o}. The telescope arrays were axle mounted to facilitate the intercalibration of the telescopes. By rotating an array through one position and comparing the telescope counting rates before and after, counting efficiencies could be obtained relative to each other and to those in a second array.

Two such units were constructed, one full array of seven telescopes, and one partial array which, due to the lack of space in the mobile unit, contained sufficient trays to form only one telescope at each of the four zenith angles. The two units were mounted in the trailer with their supporting axles at right angles in the horizontal plane. Intercalibration of the telescopes at the same zenith angle in the two arrays was effected by inter-comparing rates after turning the mobile unit through 90^{o} in azimuth. By turning in this way and to intermediate 45^{o} azimuth points, and continuing observations until a statistically significant number of counts was recorded by each telescope, a set of related intensity measurements over the observing hemisphere at each site was obtained.

In addition to the narrow angle telescopes, a vertical wide angle telescope was used, formed by the top three trays, the centre tray, and the bottom three trays of the complete array. The wide

angle telescope had an effective tray size of 60 x 91 cm., and axial length 159 cm..

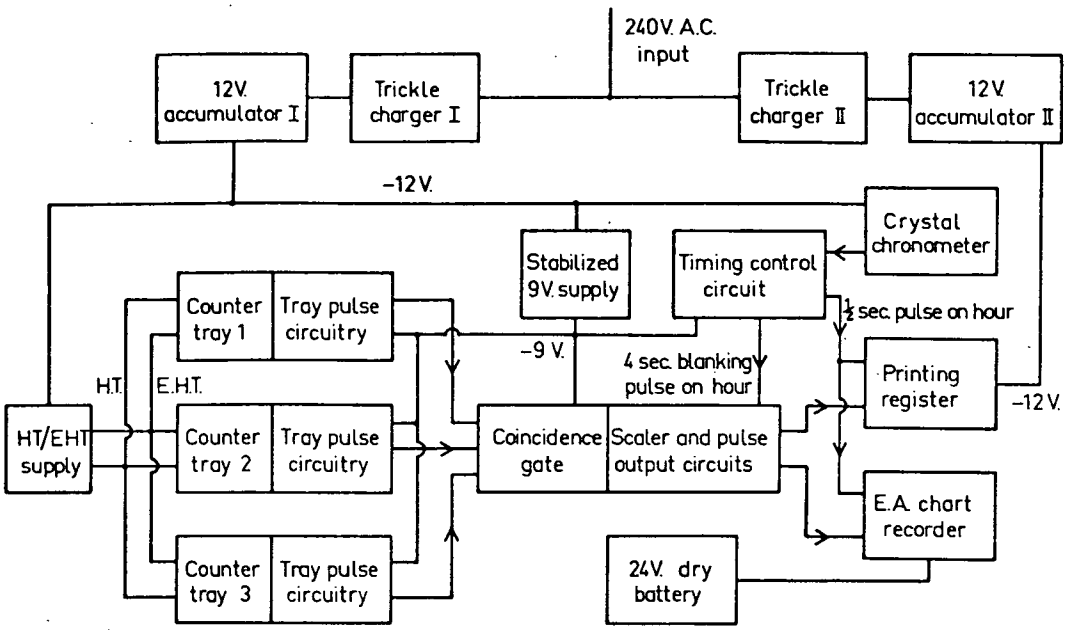

Figure 2.4. Block diagram of the circuitry associated with the muon telescopes.

2.2.2 Telescope Circuitry, Recording Equipment

As the existing observatory-type equipment operated by the Hobart cosmic ray group in 1966 was vacuum tube operated, it was necessary to design a completely new, transistorized, electronics system for the latitude survey equipment, in order to comply with the requirements of low power consumption, small component size, minimum weight, and maximum reliability in mobile operation. The circuits were required to be stable over wide variations in operating voltage and temperature. To this end great care was

taken in developing and testing the circuitry to ensure that these requirements were satisfactorily fulfilled. The circuits were designed to be of relatively low impedance, to ensure stability of operation in the presence of electrical "noise", and tests were carried out on the operating system to check that the events recorded could not be produced by other than counter discharges. A block diagram of the system is shown in Figure 2.4. The main components and functions of the circuitry will be described briefly here.

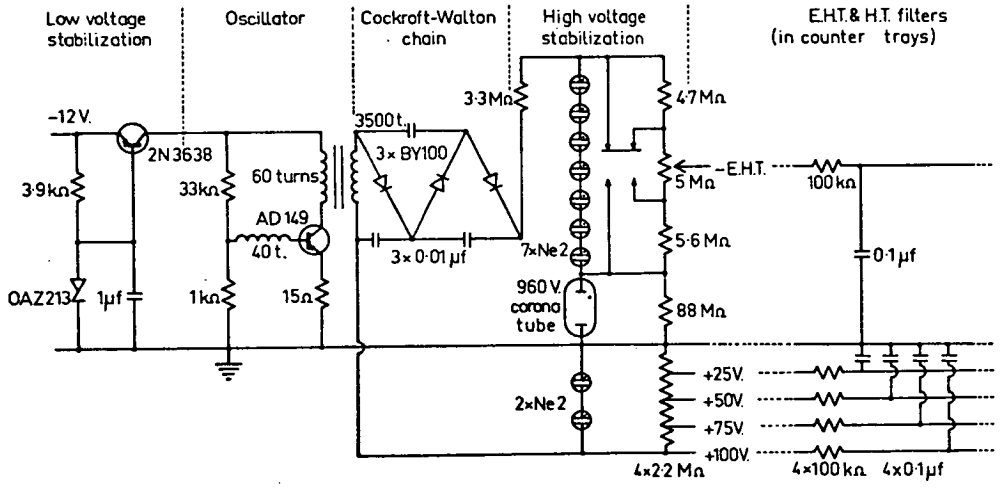

Figure 2.5. Circuit of muon telescope EHT supply.

The basic muon detecting elements, the Geiger counters, required a high voltage, of the order of 1100 volts, for their operation. Simple neon stabilized EHT supplies (see Figure 2.5) provided this voltage, all counters in the one telescope array being supplied by a single power pack. The voltage to the

In order to obtain a short, sharp pulse suitable for use in coincidence circuitry, the pulses from all counters in each tray were first added through emitter follower stages into a common line, and then fed through a forward biassed diode acting as a noise discriminator, into a Schmitt trigger circuit (see Figure 2.6). This circuit, used to square the waveform, was triggered by the first few percent of the Geiger pulses. The output of the Schmitt circuit was used to fire a single shot multivibrator, producing a 2.5 microsec. positive pulse with sharp leading and trailing edges. Figure 2.7 shows the waveforms present in the different portions of the circuitry.

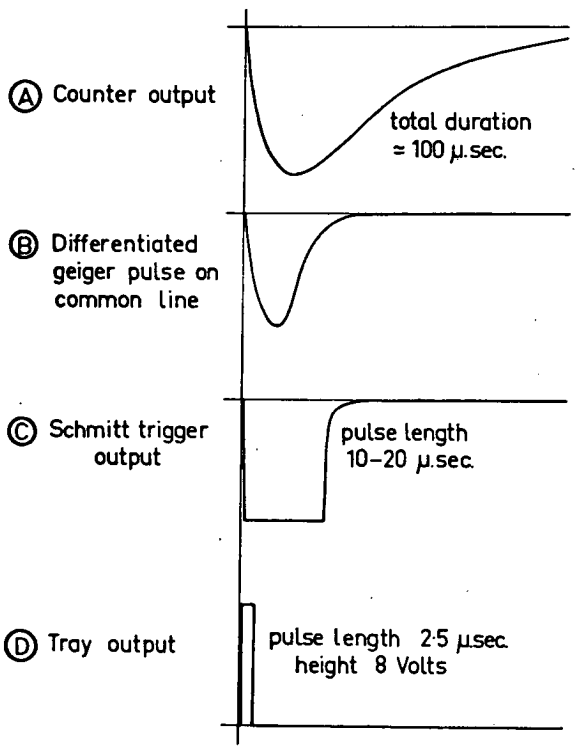

Figure 2.7. Circuit waveforms. The points A, B, C and D at which these waveforms occur are identified in Figure 2.6.

counters was adjusted by means of a single control on the power supplies, and if it was necessary to adjust the voltage to individual counters, then this could be accomplished by connecting the anode resistors to one of five buss bars carrying 0, +25, +50, +75 and +100 volts. The Geiger counters, as operated in the telescopes with a 3.3 megohm load, produced a 10 volt negative pulse, with rise time of ≈6 microsec., and of about 100 microsec. duration.

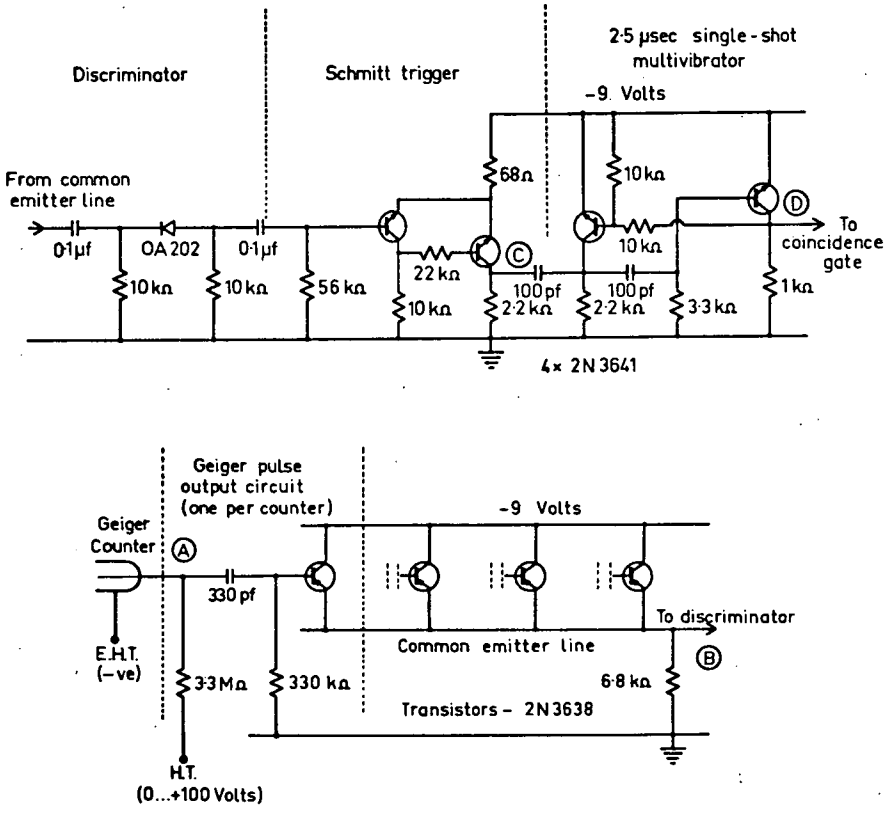

Figure 2.6. Telescope counter tray circuits:

Figure 2.6a (upper diagram) Circuitry associated with each counter, and emitter follower Geiger pulse adding circuit.

Figure 2.6b (lower diagram) Output pulse shaping circuit.

By means of these circuits, charged particles passing through each counter tray initiated short, square pulses, which were then fed through shielded cables into diode coincidence circuits. Events common to the three trays constituting each telescope were detected as short pulses present at the output of these circuits. These pulses were then pre-scaled by a given constant factor, and then counted by electro-mechanical printing registers. These registers were originally 240 V. operated, but were transistorized and adapted to low voltage operation for the survey. An Esterline-Angus event recorder was used as a backup recording system. The circuitry employed to detect the events and drive the recording devices is shown in Figure 2.8.

Power for the electronic circuitry was supplied by two 12 V. car type accumulators, one used for powering the high current consumption printing printing registers, and the other supplying current to the remainder of the circuits. The batteries were normally trickle-charged by mains operated power supplies, but in the absence of a mains supply at a site, a portable, 1 kW generator unit was run to provide the 240 V. input to the battery chargers. The batteries, without charging, were capable of operating the equipment for a period of approximately 24 hours.

Recording was carried out on an hourly basis. A crystal chronometer, designed by Dr. A.G. Fenton of the Hobart research group, supplied the hour pulse used to initiate the printout sequence. As the printers took between two and three seconds

to print the accumulated count totals, the actual time varying from one printer to the next, a common dead time of 4 seconds was introduced on all channels, at the end of each hour, to cover the print-out time.

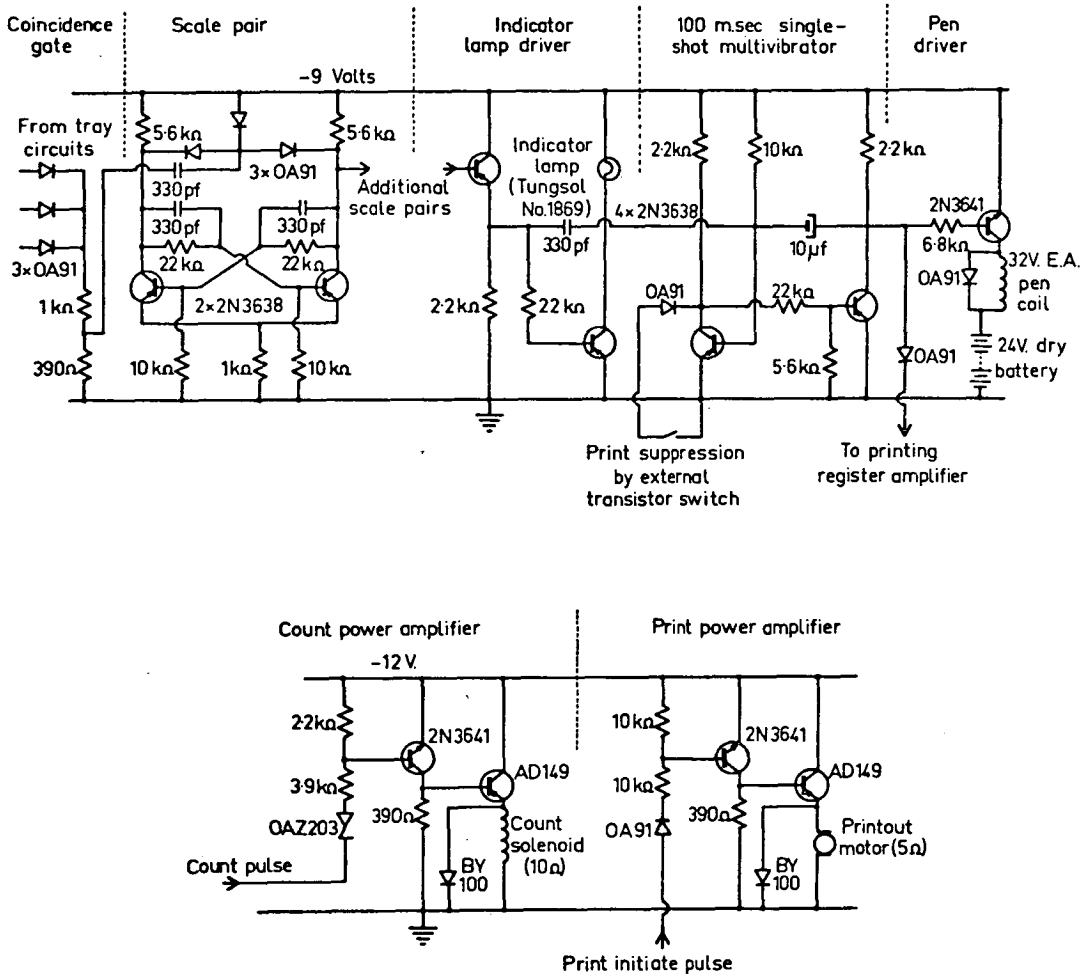

Figure 2.8. Event registration circuits.

Figure 2.8a (upper diagram) Coincidence, scaling and output circuits.

Figure 2.8b (lower diagram) Power amplifiers, controlling the count and print operations of the printing registers.

It was necessary to have continuous recording of barometric pressure for use in conjunction with the cosmic ray observations. To this end an aneroid barograph and a Fortin mercury barometer were carried, and during the course of the survey pressure information was obtained using standard meteorological bureau procedures - regular three hourly Fortin barometer observations for use in conjunction with readings from the barograph trace, to obtain the mean hourly pressure.

The stable operation of the equipment was dependent on the maintainance of reasonably constant temperature and humidity conditions in the trailer throughout the survey. The air-conditioning unit was found to be effective in controlling humidity and in maintaining the temperature of the equipment within quite acceptable bounds over the extremes of climatic conditions encountered. The mean temperature in the trailer was held in the range 75 ± 5° F, and maximum excursions to 75 ± 10°F, this range falling well inside the stable operating range of the equipment.

The overall design and operation of the equipment was found most satisfactory, and a number of features of the muon telescope mechanical and electronic design were incorporated into the design of later transistorized observatory telescopes at Hobart (for example, the use of buss bar supplied HT voltages for facilitating the adjustment of individual counter EHT voltages, and the use of the particular method of clamping counters in the trays).

2.3 Execution of the Latitude Survey

2.3.1 Choice of Sites, Observing Procedures

Seven major sea level sites were selected at which observations of directional muon intensity were to be made. The sites, approximately equally spaced in latitude, were chosen to fulfil where possible the requirements of level terrain, accurately known position coordinates, and regular upper atmospheric soundings. The sites were Hobart, Laverton, Williamtown, Brisbane, Rockhampton, Townsville and Mossman (see Figure 2.9 and Table 2.1 for site positions and details). In addition, measurements were made at two elevated sites, namely Toowoomba (near Brisbane, 610 m. above S.L.), and Mt. Wellington (near Hobart, 1250 m. above S.L.). Short, subsidiary series of observations were carried out in a deep rock quarry in Townsville, at Coolangatta (near Brisbane, S.L.), and at the Springs, Hobart, site of the Mt. Wellington neutron monitor.

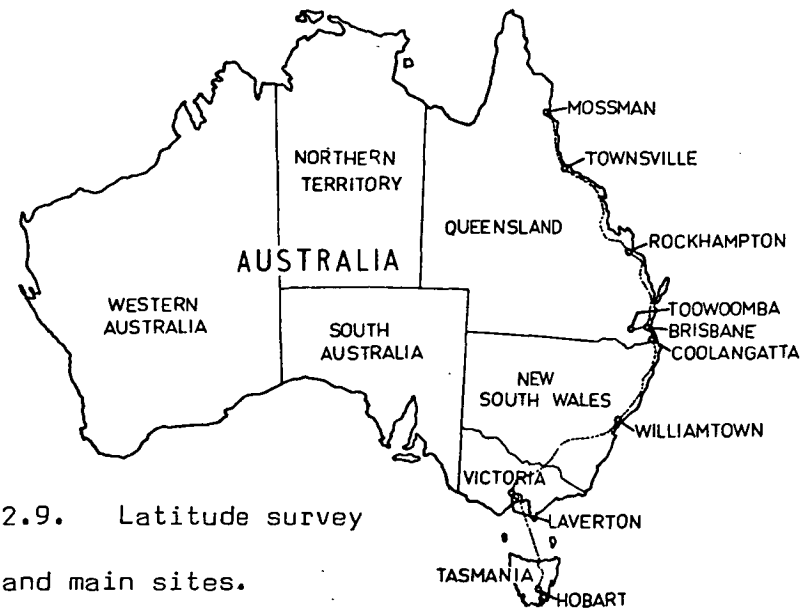

Figure 2.9. Latitude survey route, and main sites.

Table 2.1 Details of latitude survey main sites.

Site	Geog. Coords.		Alt. (km)	Obs. period	Mean press. (mb)	Vert. Int.* (press. corr.)	
	Lat(S)	Lon(E)				(site)	(Hob.)
Moss.	16°28'	145°18'	SL	30/12/66-13/1/67	1008.0	86.86	99.96
Towns.	19°15'	146°46'	SL	17/1/67-19/3/67	1009.1	89.53	100.42
Rock.	23°22'	150°29'	SL	24/3/67-18/4/67	1016.0	93.21	100.83
Brisb.	27°25'	153°05'	SL	22/4/67-17/5/67	1021.6	97.03	100.71
Toow.	27°34'	151°55'	0.48	21/5/67-3/6/67	946.3	-	100.76
Will.	32°48'	151°50'	SL	22/6/67-7/7/67	1018.2	98.93	100.40
Lav.	37°52'	144°45'	SL	12/7/67-28/7/67	1018.8	99.65	100.74
Hob.	42°50'	147°30'	SL	4/8/67-31/8/67	1015.5	100.00	100.00
Mt. W.	42°50'	147°25'	1.25	9/11/67-26/11/67	864.7	-	97.32

* In % relative to intensity during period of latitude survey observations at Hobart.

At each site the trailer was aligned to the required azimuth with the aid of a prismatic compass and then raised on a set of rigid jacks (visible in Figure 2.2b). Care was taken to position the trailer away from buildings and trees, and to ensure that the

directions of viewing of the telescopes were completely clear of obstructions. The telescopes were accurately levelled using a three-point screw adjustment on their bases. Sensitive bubble levels were used as references to enable the required zenith angles of the telescopes to be accurately re-established after azimuth and site changes.

Observations were normally continued for about a week in each direction to accumulate usefully large count totals. At each site a full intercalibration of all telescopes was carried out, to enable the intensity relationship between observations in all directions at each site to be deduced.

The survey was conducted in the period from August 1966 to October 1967. Observations were made at each of the seven major sites on both the north-bound and south-bound legs of the survey, although in fact only the results of measurements carried out on the return half of the survey were finally used in the analysis which produced the coupling coefficients. The data acquired on the north bound section of the survey were rejected due to major deficiencies in the observational data, which arose as follows:

a) Serious interruptions were experienced during observations, due to the failure of many Geiger counters as a result of the cracking of glass-metal seals, brought about by vibration and temperature cycling during travel. This problem was overcome by applying a coating of epoxy resin over the seals of all counters.

b) Failure to carry out the intercalibration process at each site. This technique was introduced as a regular part of the operations at each site during the return half of the survey. Whilst this repeated calibration process added an extra two months to the survey work, it enabled results of greatly improved accuracy to be obtained, and in fact, it was due only to the implementation of this procedure that the ratio method of analysis could be developed (described in Section 2.3.4), allowing effective data analysis.

The data used in the coupling coefficient determination, described in later chapters, were acquired over the period December 1966 to August 1967. The period of time spent at each site is listed in Table 2.1. Information about the relative muon intensities at the sites and at Hobart during these periods is also contained in Table 2.1.

2.3.2 Investigation of Air Shower Effect

Geiger counter telescopes obtain their directional sensitivity by detecting simultaneous occurrence of pulses that accompany the passage of a charged particle through the trays of the telescope. The charged particles in the sea level flux are mostly muons and electrons; however, a layer of 10 cm. of lead, inserted between two of the trays of the telescope, is able to prevent all but the highest energy electrons from being detected after entering within the opening angle of the telescope, whilst allowing the passage of

most of the muons.

Many electrons originate in cosmic ray "shower" events, in which a high energy primary or secondary particle suffers a collision in the atmosphere, producing a cascade of electrons travelling downwards through the atmosphere (Janossy [1948] presented a detailed discussion of the morphology of cosmic ray showers). If such a shower impinges upon a telescope, bypassing the lead (incident from a direction outside the opening angle of the detector), a spurious event may be detected by the telescope, because the electrons can then produce simultaneous discharges in each of the counter trays constituting the telescope. Such events must be rejected if true directional muon intensities are to be measured.

The actual effect that showers of this type have on any detector is found to be dependent on the configuration of the particular detector (the position of the absorber, the size, number and position of the trays, the inclination of the telescope, etc.), and the spurious event rate must normally be experimentally determined by means of extra circuitry incorporated into the detector electronics.

The present series of observations were made using no direct suppression of the recording of shower produced events, although, because of the narrow angle of the telescopes, such events would be expected to contribute significantly to the total coincidence rate. It was found necessary to make regular direct observations

of the shower rates involved in order to subtract these from the observed rates. As will be shown presently, the removal of the effects of showers from the data is very important as the shower events are responsible for a marked zenith dependent increase in the atmospheric pressure coefficients of the total telescope rates. It is particularly important to remove this effect in order that the ratio technique of data analysis be successfully applied. The measurements of the coincidence rates produced by showers was made using the standard shower detection technique of recording four-fold coincidences, in this case between the three trays of the telescope involved and the summed outputs of other trays nearby, but outside, the acceptance angle of the telescope.

The shower events as they affected the telescopes were found to have a very large pressure coefficient, varying from approximately 0.72 % per mb. for telescopes inclined at 67.8^{o} to the zenith (from now on referred to as the 67.8^{o} telescopes), to 0.4 % per mb. for the 0^{o} telescopes. The shower rate - pressure relationship for showers affecting the various telescopes was observed to differ significantly from a simple exponential dependence.

As a means of investigating the nature of the shower effect, an experiment was conducted in a deep rock quarry at Townsville (see Figure 2.1d). Telescopes inclined at 45.2^{o} and 67.8^{o} to the zenith were directed into a rock face, with a minimum thickness of approximately 24 m. of granite obscuring their cones of

acceptance. It was found that the three-fold coincidence rates dropped to approximately 15% of the normal rates. The four-fold rates, on the other hand, were not so greatly affected - the 67.8^{o} telescope four-fold rate dropped by 8 ± 11 % (S.D.error), and that of the 45.2^{o} telescope by 34 ± 4 %. These observations tend to support the view that the showers affecting the telescope rates come predominantly from directions away from the acceptance cones.

In order to investigate quantitatively the nature of the shower events, a further experiment was carried out, at Toowoomba, in which the four-fold events characterising the occurrence of showers were recorded individually on an event recorder for a three hour period, to find the number of detectors affected in each event. Analysis of these results showed that the ratio of the number of events in which one telescope was affected, to the number in which two or more were simultaneously excited, varied markedly with the zenith angle of viewing, from 0.49 for a vertical telescope, to 0.29 for one at 67.8^{o}.

This result, together with the observed variation from exponential dependence of shower rate on pressure, can be explained in terms of two components in the shower flux. One component corresponds to the multiple particle electron shower, initiating spurious coincidences by impinging on the telescopes from the sides, outside the cones of acceptance. The other component evidently is a hard shower component, consisting of a limited number of particles approaching the telescopes within the acceptance cones,

one of the particles at least (probably a muon), penetrating the absorber.

Analysis of the shower rate vs pressure data for the telescopes at each zenith angle, using the measured ratios of the two components, produced independent estimates of the pressure coefficients of the two components which agree well with one another (even though the ratios were derived as the result of the rather arbitrary division of the showers into those affecting one, or more than one telescope simultaneously). The pressure coefficient estimates were made by determining the two exponential components which together are required to make up the observed pressure dependence. It may be shown that, if the total shower rates I_1, I_2 and I_3 are known at three pressures $P - \delta P$, P, and $P + \delta P$, and the ratio of hard to soft shower rates I_h/I_s is known at pressure P (where $I_2 = I_h + I_s$), then the pressure coefficients are given by

$$k_1 = -\frac{\ln X}{\delta P} \quad \text{and} \quad k_2 = -\frac{\ln Y}{\delta P}$$

$$\text{where} \quad X = \frac{I_h^2 - I_s^2 + I_1 I_3}{2 I_h I_1} \pm \left[\left(\frac{I_s^2 - I_h^2 - I_1 I_3}{2 I_h I_1} \right) - \frac{I_3}{I_1} \right]^{\frac{1}{2}}$$

$$\text{and} \quad Y = \frac{I_3 - I_h X}{I_s}$$

It is found that the alternate pairs of solutions predict essentially the same pressure coefficients. The calculated coefficient values were: -0.29 ± 0.05 % per mb. for the "hard"

component, and -0.81 ± 0.06 % per mb. for the "soft" shower component.

The two-component picture of the showers explains well the observed Townsville quarry results. On the basis of the two-component assumption, the expected decrease in shower rate for a 67.8^{o} telescope is 22 ± 10 %, and 32 ± 10 % for one at 45.2^{o}, as the result of blocking of the telescope cones of viewing (cf. 8 ± 11 % and 34 ± 4 % respective experimental values). These calculated values do not take into account the slight reduction expected in the shower event rate due to the diminuition of the solid angle from which soft showers could arrive.

Ideally, all the soft component shower events and that portion of the hard component produced by particles entering at some angle outside the telescope acceptance cone should be taken into account when corrections to the three fold coincidence rates are made. As, during the survey, only total shower event rates were measured, correction has been carried out to remove all detected shower events. It is apparent that a small overcorrection is being made in that a significant number of muons enter the viewing cones of the telescopes, as discussed, accompanied by a second particle and are rejected as undesirable, although in fact forming part of the directional muon flux. This overcorrection, however, appears only as a small systematic change in the apparent zenith angle dependence of the muon intensity. Calculations of the magnitude of the effect, included in the error estimates in

the following section, show that no serious errors are introduced into the corrected data.

The freedom of the final results from other spurious shower effects depends very much on the efficiency of the shower detection. If the detection efficiency is low, then, because of the high pressure coefficient of the residual uncorrected shower component, the resultant apparent muon pressure coefficient will be greater than the true value. The magnitude of the increase will vary with zenith angle, since the proportion of showers in the total rate varies greatly with zenith angle, and since the admixture of hard and soft components in the showers, each with a different pressure coefficient, is also a function of zenith angle. A low detection efficiency would be expected to be manifested as an artificial rise in the value of the pressure coefficient with increasing zenith angle.

In order to obtain an estimate of the efficiency of shower detection, an experiment was carried out in which the rate of the wide angle telescope (denoted A in Figure 2.10) was compared, over a wide pressure range, with the summed rates of the three narrow angle telescopes B, C and D, whose trays together constituted the wide angle telescope. The three narrow angle telescopes together covered the same total field of view as the wide angle telescope, and in so far as their summed rates were equivalent to the wide angle rate, the observed pressure coefficient should have been the same, in the absence of showers.

Consider the effect of showers on the telescope rates. Whilst the genuine single event rate, dependent as it is on both the area of the trays and the solid angle of acceptance, varies approximately as $(\text{area})^2$ for a telescope of given axial length, the soft shower rate, as it is sensibly independent of the acceptance angle of the telescope, would be expected to vary approximately as $(\text{area})^1$ in a telescope of given axial length.

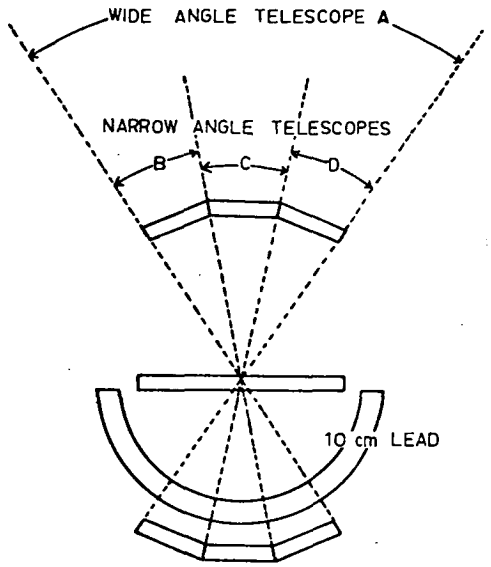

Figure 2.10. The physical relationship between the three narrow angle telescopes and the wide angle telescope.

In the experiment, the wide angle telescope had the same axial length as the narrow angle telescopes, but had a tray area three times as large. Thus, from the preceding discussion, the genuine muon event rate would be expected to be nine times larger, and this is in fact observed. The shower rate would be expected to be approximately three times as large, compared with the factor of four observed.

Because of the disproportionate increase of the genuine event rate compared with the shower rate, the pressure coefficient of the uncorrected wide angle rate would be expected to be lower than that of the summed narrow

angle rates. The ratio of the uncorrected telescope rates $\frac{B + C + D}{A}$ is seen, in Figure 2.11, to vary markedly with pressure. For comparison, the shower corrected ratio is also shown. Little residual pressure variation is observed. As the "guard tray" systems for the wide and narrow angle telescopes were similar, it is reasonable to assume that the efficiency of shower detection is essentially the same for all the telescopes. On this assumption, the shower detection efficiency, estimated from a comparison of the corrected and uncorrected ratio pressure dependence, as shown in Figure 2.11, is of the order of 70 %.

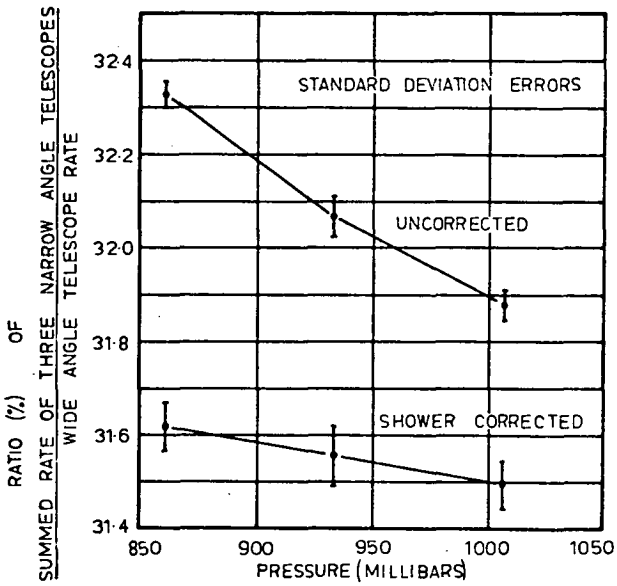

Figure 2.11. Observed dependence of the ratio of the summed narrow angle telescope rate to the wide angle telescope rate, as deduced from both the shower corrected and uncorrected data.

2.3.3 Analysis of Errors

The errors affecting the experimental results may be divided into three classes:

2.3.3.1 Errors in individual telescope observations

These errors arise from four main sources:

a) The limited statistical accuracy of the observations.

Each measurement consisted of the detection of a finite number of events. Since, for the population of events detected by coincidence telescopes, Poisson statistics are found to apply, the standard errors were deduced in a straight forward manner. Further statistical error was introduced in the process of inter-calibration of the various telescopes inclined at any particular zenith angle. The statistical errors of observation and of calibration have been combined to produce a single standard deviation error on each estimate. It may be shown that the precision of an estimate derived as the ratio or product of two quantities, each with known statistical errors, is given by

$$\sigma = (\sigma_1^2 + \sigma_2^2)^{\frac{1}{2}}$$

where σ, σ_1, and σ_2 are the percentage S.D. errors of the estimate and the individual quantities respectively.

b) Errors due to the uncertainty of telescope orientation in azimuth and zenith.

The possible azimuth angle error was estimated to be $\pm 1.5^{o}$, made up of the summed uncertainties in the effective telescope heading relative to the trailer, and in the trailer heading relative to an established azimuth bearing. The magnitude of the error so produced in the results is dependent upon the value of $\frac{dI}{d\theta}$ at the particular azimuth and zenith, where I represents the muon intensity, and θ the azimuth. The greatest value observed was at Mossman, where, for the 67.8^{o} telescope, $\frac{dI}{d\theta} \approx 0.15$ % per ^{o}. The possible errors from this source have been computed from the observational data and applied accordingly. In general, errors due to azimuth uncertainties are small compared with the statistical errors.

The zenith angles of the telescopes were reproducible (with the aid of bubbles levels) to ± 15 seconds of arc. Assuming a cosine squared form of zenith dependence of intensity (to which all the results approximate), this uncertainty could result in errors of ± 0.01 % in 22.6^{o} telescope results, ± 0.02 % at 45.2^{o}, and ± 0.05 % at 67.8^{o}. Calibration of the telescopes at any zenith angle against one "standard" telescope at each inclination was unaffected by slight differences in zenith angle of the individual telescopes, as these differences appeared merely as differences in relative efficiency.

c) Errors due to uncertainties in the shower correction process.

Overlooking for the moment the effects of inefficient

shower detection (discussed in Section 2.3.3.3 b), the effects are considered of inaccuracy arising in the estimates of the shower total corresponding to any particular recording period. The shower rates were regularly measured, and these data were compiled in the form of graphical plots of shower rate as a function of pressure for each telescope. The shower correction for any particular set of muon intensity data was found by interpolating the value of the shower correction appropriate for that period. The possible error in any value so derived is estimated to be ± 3 %. The resulting errors in the intensity data are ± 0.06 % at 0^{o}, ± 0.09 % at 22.6^{o}, ± 0.12 % at 45.2^{o}, and ± 0.3 % at 67.8^{o}.

d) Errors resulting from the assumption that the inclined/vertical intensity ratios are independent of changes in atmospheric conditions.

The analysis technique adopted for deriving the coupling coefficients depends critically upon this assumption for its validity (this technique is discussed in Section 2.3.4, and justified in Chapter 6). The behaviour of the ratios was studied experimentally for large changes in atmospheric conditions, in particular, observations were made at the summit of Mt. Wellington, and the observed ratio values compared with those at sea level. The mean changes in the shower-corrected ratios were found to be, for a decrease in pressure of 150 mb., + 0.10 ± 0.15 % at 22.6^{o}, - 0.3 ± 0.2 % at 45.2^{o}, and - 2.7 ± 0.4 % at 67.8^{o}. No significant

differential change in the ratio values was observed in the ratio values with variation in azimuth. The effects of correction for the "hard" shower over-compensation would tend to reduce these observed ratio changes to the point where little residual variation would remain; however, because of the incomplete knowledge of the precise proportion of such showers, no attempt was made to introduce this factor.

The mean pressure values at the sea level sites were found to lie within a 13 mb. range. The calculated changes in the inclined / vertical intensity ratio for pressure variation in this range, relative to the ratios existing at the average pressure over the period of the entire survey, may be considered an estimate of the errors associated with the use of the ratio values. These errors are small: ± 0.005 % at 22.6^{o}, ± 0,015 % at 45.2^{o}, and ± 0.12 % at 67.8^{o}.

2.3.3.2 Intercalibration systematic errors

These errors limit the accuracy to which comparison of data, for any particular zenith angle at any two sites, may be made. They arise in the process of intercalibration of the "standard" telescopes at the different zenith angles. Calculation of the magnitude of these errors has been carried out, taking into account the statistical accuracy of the count totals used to derive the relative efficiencies. Because intercalibration was carried out at each site, these errors are constant for any one

set of observations, but vary from site to site. The effects of long term changes in operating levels of the detectors were overcome by this repeated intercalibration. The values of the intercalibration systematic errors at each site are tabulated in Tables 2.2, 2.3, and 2.4, in conjunction with the tabulated ratio values.

2.3.3.3 Fixed systematic errors

These errors produce a systematic shift in the apparent zenith angle of the different "standard" telescopes, introducing errors into the data for each zenith angle data set which are constant throughout the entire series of measurements, affecting all observations for each particular zenith angle to the same extent. They arise in two ways:

a) A significant uncertainty exists in the measured value of the zenith angles of the standard telescopes, estimated to ± 20 minutes of arc. The resulting possible errors are ± 0.8 % in the 22.6^{o} results, ± 1.6 % in the 45.2^{o} results, and ± 4 % at 67.8^{o}.

b) Appreciable systematic errors could arise out of uncertainties associated with the shower correction process. Taking into account the estimated shower detection efficiency and the effects of over-correction for the "hard" shower component, the systematic errors are estimated to be: $^{+\ 0.2}_{-\ 1.0}$ % at 0^{o}, $^{+\ 0.4}_{-\ 1.3}$ % at 22.6^{o}, $^{+\ 0.8}_{-\ 1.6}$ % at 45.2^{o}, and ± 2 % at 67.8^{o}.

The total fixed systematic errors in the inclined/vertical intensity ratios are as follows: $^{+\ 1.0}_{-\ 1.1}$ % at 22.6°, ± 2 % at 45.2°, and $^{+\ 4.8}_{-\ 5.0}$ % at 67.8°.

2.3.4 Presentation of Experimental Data

The experimental results are presented in tabular and graphical form, in Tables 2.2, 2.3, and 2.4, and in Figures 2.12, 2.13, and 2.14. Table 2.5 specifies the azimuth angles referred to by number in Tables 2.2 - 2.4.

The data are in the form of ratios of inclined/vertical muon intensities; or, more specifically, the ratio of the corrected counting rate of a narrow angle telescope (as described in Section 2.2) directed in the specified viewing direction, to the rate of the same telescope directed vertically at the same site. The magnitude of the different types of errors discussed in Section 2.3.3 are indicated in both the tables and the diagrams.

The inclined/vertical mode of presentation is a very important one, as it is the means by which the necessity for detailed correction for atmospheric effects in the data is avoided. The technique, justified in Chapter 6, relies on the fact that the muon pressure and temperature coefficients are sensibly independent of zenith and azimuth angle in the atmosphere. As a result, it is possible to assume that, in the absence of the geomagnetic field (i.e. zero value cut-offs, and no atmospheric asymmetry effect), the ratio [to page 62]

Table 2.2. Value of inclined/vertical intensity ratio for range of values of azimuth at the latitude survey sites - zenith angle of inclined detector: 22.6°. Note - bracketed errors are in %.

Site	Inclined/vertical ratio at specified azimuths (1)								Error (2)
	1	2	3	4	5	6	7	8	
Moss.	0.8548 (0.26)	0.8171 (0.23)	0.8547 (0.36)	0.8780 (0.23)					0.29
Towns.	0.8475 (0.10)	0.8268 (0.11)	0.8146 (0.13)	0.8308 (0.19)	0.8450 (0.15)	0.8606 (0.18)	0.8692 (0.12)	0.8633 (0.12)	0.17
Rock.	0.8431 (0.13)	0.8235 (0.18)	0.8299 (0.14)	0.8412 (0.27)	0.8521 (0.27)	0.8618 (0.26)	0.8528 (0.29)		0.37
Brisb.	0.8401 (0.17)	0.8354 (0.14)	0.8360 (0.29)	0.8403 (0.28)	0.8480 (0.28)	0.8471 (0.29)	0.8440 (0.14)		0.18
Toow.	0.8347 (0.18)	0.8329 (0.16)	0.8389 (0.33)	0.8452 (0.33)	0.8528 (0.33)	0.8530 (0.32)	0.8447 (0.16)		0.29
Will.	0.8450 (0.14)	0.8406 (0.31)	0.8413 (0.30)	0.8429 (0.15)					0.26
Lav.	0.8415 (0.16)	0.8359 (0.30)	0.8356 (0.30)	0.8400 (0.15)					0.26
Hob.	0.8391 (0.08)	0.8373 (0.08)	0.8387 (0.10)	0.8410 (0.09)					0.12
Mt. W.	0.8421 (0.26)	0.8346 (0.26)	0.8412 (0.13)	0.8428 (0.14)					0.27

a) [1] See Table 2.5.

b) [2] Intercalibration systematic error (%), see Section 2.3.3.2.

c) Bracketed figures denote S.D. statistical error (%) applicable. A ± 0.13 % error also applies to each value (see Section 2.3.3.1).

d) Fixed systematic error (see Section 2.3.3.3): $^{+\ 1.0}_{-\ 1.1}$ %.

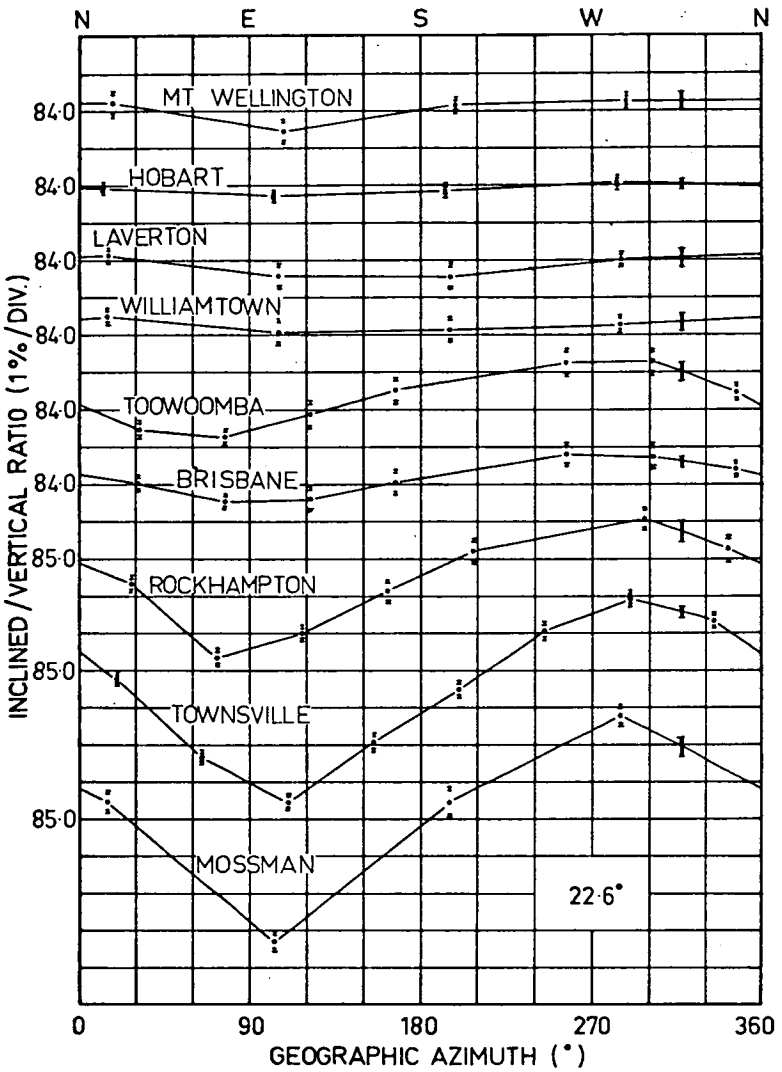

Figure 2.12. Graphical representation of observed inclined/vertical intensity ratio - zenith angle of inclined detector: 22.6^{o}. Inner and outer segments of error bars represent statistical and additional errors on points, double error bars at 315^{o} azimuth indicate the magnitude of the intercalibration systematic error; the fixed systematic error applicable is $^{+\ 1.0}_{-\ 1.1}$ % (see Sections 2.3.3.1, 2 and 3).

Table 2.3. Value of inclined/vertical intensity ratio for range of values of azimuth at the latitude survey sites - zenith angle of inclined detector: 45.2°. Note - bracketed errors are in %.

Site	Inclined/vertical ratio at specified azimuths (1)								Error (2)
	1	2	3	4	5	6	7	8	
Moss.	0.4994 (0.35)	0.4611 (0.24)	0.4999 (0.50)	0.5155 (0.24)					0.41
Towns.	0.4872 (0.15)	0.4716 (0.17)	0.4562 (0.16)	0.4766 (0.27)	0.4931 (0.21)	0.5005 (0.25)	0.5030 (0.17)	0.5019 (0.16)	0.24
Rock.	0.4851 (0.17)	0.4693 (0.24)	0.4677 (0.19)	0.4838 (0.40)	0.4930 (0.38)	0.4936 (0.36)	0.4937 (0.45)		0.54
Brisb.	0.4743 (0.21)	0.4734 (0.15)	0.4731 (0.36)	0.4736 (0.35)	0.4849 (0.35)	0.4840 (0.36)	0.4829 (0.17)		0.26
Toow.	0.4735 (0.23)	0.4677 (0.21)	0.4665 (0.43)	0.4687 (0.43)	0.4800 (0.38)	0.4771 (0.38)	0.4766 (0.21)		0.41
Will.	0.4759 (0.18)	0.4683 (0.38)	0.4733 (0.39)	0.4790 (0.20)					0.38
Lav.	0.4712 (0.20)	0.4684 (0.39)	0.4640 (0.39)	0.4715 (0.19)					0.38
Hob.	0.4720 (0.10)	0.4668 (0.12)	0.4719 (0.15)	0.4749 (0.12)					0.17
Mt. W.	0.4710 (0.34)	0.4644 (0.34)	0.4695 (0.16)	0.4739 (0.17)					0.39

a) [1] See Table 2.5.

b) [2] Intercalibration systematic error (%), see Section 2.3.3.2.

c) Bracketed figures denote S.D. statistical error (%) applicable. A ± 0.17 % error also applies to each value (see Section 2.3.3.1).

d) Fixed systematic error (see Section 2.3.3.3): ± 2.2 %.

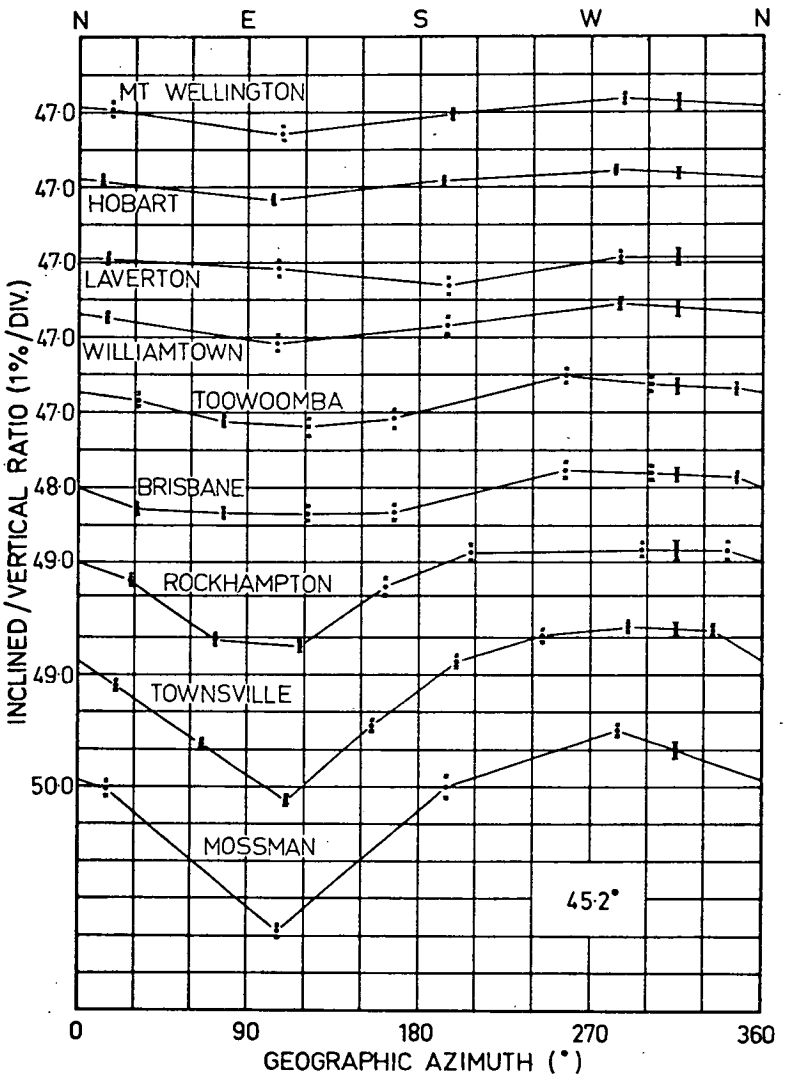

Figure 2.13. Graphical representation of observed inclined/vertical intensity ratio - zenith angle of inclined detector: 45.2^{o}. Inner and outer segments of error bars represent statistical and additional errors on points, double error bars at 315^{o} azimuth indicate the magnitude of the intercalibration systematic error; the fixed systematic error applicable is $\pm$ 2.2 % (see Sections 2.3.3.1, 2 and 3).

Table 2.4. Value of inclined/vertical intensity ratio for range of values of azimuth at the latitude survey sites - zenith angle of inclined detector: 67.8°. Note - bracketed errors are in %.

Site	Inclined/vertical ratio at specified azimuths ([1])								Error
	1	2	3	4	5	6	7	8	([2])
Moss.	0.1467 (0.65)	0.1364 (0.53)	0.1467 (0.92)	0.1538 (0.53)					0.57
Towns.	0.1428 (0.31)	0.1390 (0.32)	0.1353 (0.30)	0.1408 (0.48)	0.1432 (0.38)	0.1465 (0.44)	0.1472 (0.31)	0.1465 (0.32)	0.34
Rock.	0.1410 (0.31)	0.1390 (0.45)	0.1386 (0.35)	0.1400 (0.72)	0.1441 (0.72)	0.1463 (0.65)	0.1437 (0.72)		0.74
Brisb.	0.1374 (0.41)	0.1363 (0.33)	0.1366 (0.68)	0.1367 (0.67)	0.1426 (0.62)	0.1423 (0.68)	0.1398 (0.37)		0.36
Toow.	0.1346 (0.43)	0.1325 (0.39)	0.1339 (0.79)	0.1338 (0.79)	0.1378 (0.80)	0.1402 (0.78)	0.1365 (0.39)		0.57
Will.	0.1383 (0.35)	0.1334 (0.71)	0.1346 (0.73)	0.1394 (0.38)					0.53
Lav.	0.1350 (0.38)	0.1313 (0.73)	0.1341 (0.73)	0.1369 (0.37)					0.52
Hob.	0.1351 (0.21)	0.1340 (0.22)	0.1342 (0.23)	0.1370 (0.23)					0.23
Mt. W.	0.1306 (0.64)	0.1306 (0.63)	0.1322 (0.31)	0.1329 (0.33)					0.54

a) [1] See Table 2.5.

b) [2] Intercalibration systematic error (%), see Section 2.3.3.2.

c) Bracketed figures denote S.D. statistical error (%) applicable. A ± 0.49 % error also applies to each value (see Section 2.3.3.1).

d) Fixed systematic error (see Section 2.3.3.3): $^{+\ 4.8}_{-\ 5.0}$ %.

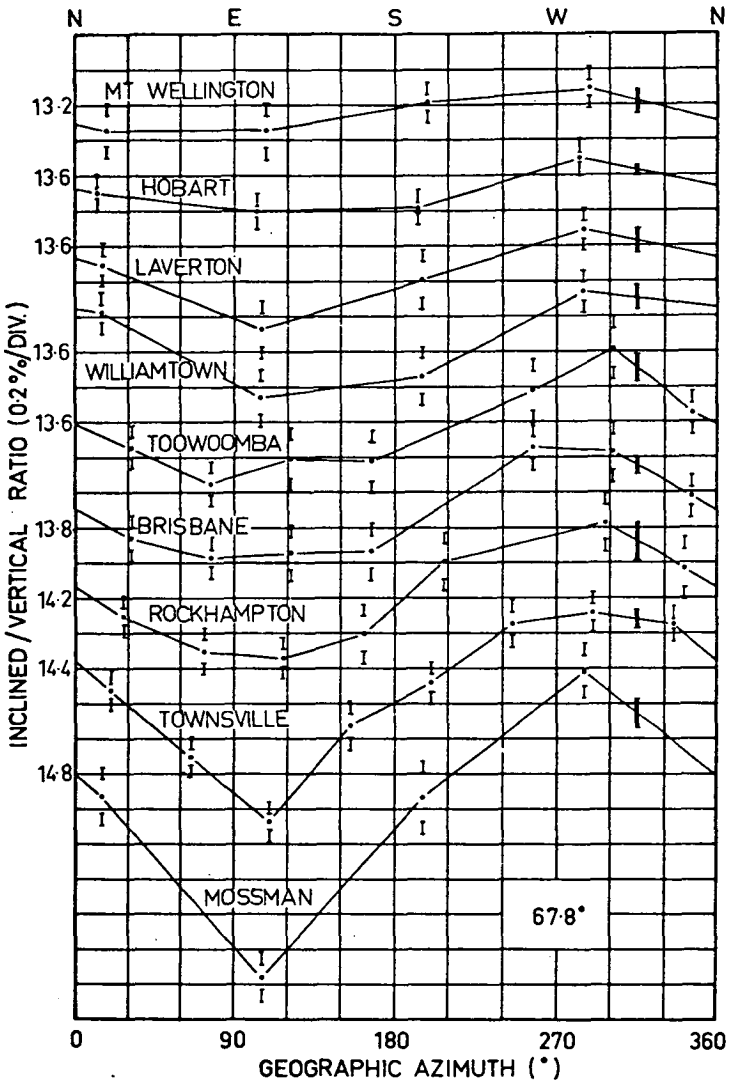

Figure 2.13. Graphical representation of observed inclined/vertical intensity ratio - zenith angle of inclined detector: 67.8^{o}. Inner and outer segments of error bars represent statistical and additional errors on points, double error bars at 315^{o} azimuth indicate the magnitude of the intercalibration systematic error; the fixed systematic error applicable is $^{+\ 4.8}_{-\ 5.0}$ % (see Sections 2.3.3.1, 2 and 3).

Table 2.5. Identification of numbers used to represent azimuth angles in Tables 2.2 - 2.4.

Site	Azimuth (^{o}E of geographic N) equivalent of numbers							
	1	2	3	4	5	6	7	8
Moss.	15.5	105.5	195.5	285.5				
Towns.	20.5	65.5	110.5	155.5	200.5	245.5	290.5	335.5
Rock.	28.0	73.0	118.0	163.0	208.0	298.0	343.0	
Brisb.	32.0	77.0	122.0	167.0	257.0	302.0	347.0	
Toow.	32.0	77.0	122.0	167.0	257.0	302.0	347.0	
Will.	15.0	105.0	195.0	285.0				
Lav.	15.5	105.5	195.5	285.5				
Hob.	13.0	103.0	193.0	283.0				
Mt. W.	13.0	103.0	193.0	283.0				

[from page 55] of inclined to vertical intensity, for a particular pair of detectors, is effectively dependent only on zenith angle, and is independent of the latitude of the observing site. Departure from the basic zenith angle dependence would occur in the presence of significant primary momentum cut-offs.

Consider the situation at two sites, which, while being free of the manifestations of the atmospheric asymmetry effect, possess significant cut-off values over the observing hemisphere. At each of these sites, we may, in principle, deduce the azimuthal asymmetry pattern at any particular zenith angle by making a series of

observations with an inclined detector, and calculating the ratio of the rate of this detector to that of a vertically directed detector operating simultaneously. Comparison of the ratio values at the two sites would reveal that, for observations in inclined directions having the same cut-off value, the ratios have the same value if the vertical cut-offs were also of equal value. On the other hand, if the vertical cut-offs were not of equal value, the resulting difference in the ratio values would be a measure of the change in vertical muon intensity from one site to the other, due to the difference in vertical cut-off value, independent of the structure of the atmosphere.

The presence of the geomagnetic field in the atmosphere complicates analysis by this technique, as directional asymmetries are produced due to the deflection of the muons. This problem is investigated in Chapter 5, and it is shown that these effects may be removed from the data.

Analysis of the corrected ratio data, in order to extract the uni-directional coupling coefficients as a function of zenith angle, necessitates detailed understanding of the response characteristics of the detectors used in the latitude survey. In the following chapter the telescope characteristics are considered, and in particular, techniques are developed for determining the detector response in the presence of geomagnetic cut-offs.

CHAPTER 3

DETECTOR CHARACTERISTICS

3.1 Introduction

In many aspects of cosmic ray research, information is required, in principle, about unidirectional particle intensities. In practice, because of the low fluxes involved, it is usually necessary to resort to the use of detectors of relatively wide angle of response, in order to measure particle intensities to sufficient statistical accuracy.

Such a situation exists in the determination of muon coupling coefficients by latitude survey. Because of the limitations on detector size imposed by the requirements of easy transportability, together with the limited time of observation, investigators have, in general, made use of wide angle detectors, of cubic or semi-cubic geometry. In spite of the obvious desirability of rigorously taking into account the finite width of the detector acceptance cone, the lack of information about several factors in the problem (distribution of cut-off momentum value over the acceptance cone, zenith dependence of response characteristics, etc.) has led to the use of a simplified approach in data analyses. The cut-off momentum effective in any direction of viewing of a detector has therefore been assumed to be equal to that pertaining to the axial direction, and the coupling coeff-

icient estimates have been interpreted as applying to the zenith angle of the detector axis. Thus coefficients obtained by the use of vertically directed telescopes are usually assumed to be those applying to a zenith angle of 0^{o}, even though, in fact, the mean zenith angle of response of such detectors is necessarily non-zero.

In order to derive the unidirectional dependence of coupling coefficients on zenith angle from the results of the latitude survey, the finite cone of acceptance of the telescopes must be taken into account. Calculations must allow for the contributions from all portions of the acceptance cone, with account taken of variation of geometric sensitivity, muon intensity dependence on zenith angle, and the effects of a directional cut-off structure over the acceptance cone of the detector. It is in the consideration of this last factor that the problem becomes complex.

At high latitudes the situation is relatively straightforward, as the geomagnetic cut-offs are masked by atmospheric absorption, and a simple zenith-dependent, azimuth-independent, expression may be used to represent the muon intensity distribution, in determinations of detector characteristics. A number of previous investigations have been made of detector response under these conditions. The more significant of these are reviewed here.

3.2 Review of Investigations of Telescope Response in Absence of Cut-offs

In discussing detector characteristics, it is convenient to use the terms "geometric" and "radiation" sensitivity. The detector sensitivity calculated on the assumption that the particle flux is isotropic is called the geometric sensitivity (or geometric factor), whilst the radiation sensitivity is that calculated taking into account the directional dependence of the particle intensity reaching the detector.

Calculations of telescope sensitivity are usually carried out to allow either:

a) the determination of the relationship between directional intensities and observed detector rates, or

b) the establishment of the sensitivity pattern of a particular telescope in a particular situation, as a necessary step in, for example, the interpretation of observed time variations in the cosmic ray flux, where it is important to know precisely the range of directions viewed by the detector.

Investigations typical of the first type include those by Tidman and Ogilvie [1957], and Stern [1960], who derived integrable expressions representing the radiation sensitivity of a small element of a telescope, and from these deduced detector sensitivities. Tidman and Ogilvie carried out the integration process numerically, and, by varying the parameters representing the dimensions and inclination of a generalized detector, and the form

of the muon intensitivity zenith dependence $f(\theta)$, obtained sets of values of a constant, C, which, when inserted into the expression

$$I = I(0)\ f(\theta)\ (\text{area})\ (\text{solid angle})\ C$$

allowed the counting rate of a detector of any configuration to be predicted. Due to certain approximations introduced into the calculations, the technique is limited to telescopes with $(\text{tray side}) / (\text{length}) \leq 0.75$.

In his approach, Stern derived, by analytical integration, an expression giving the rate of a telescope of any dimensions in a radiation flux with variable zenith dependence. This expression, however, is applicable only to vertically directed telescopes.

Parsons [1957,1959], Brunberg [1958], and Lindgren [1965], on the other hand, have investigated the sensitivity patterns of detectors - the manner in which the sensitivity of a telescope varies over the acceptance cone. Parsons' approach is typical of these. He developed general relationships expressing the variation of radiation sensitivity of a telescope, of any geometry, with zenith angle, and carried out calculations of the sensitivity pattern of a number of telescopes of commonly used geometry and inclinations. Brunberg and Lindgren similarly have developed techniques for calculating sensitivity patterns of detectors, and have deduced the response characteristics of particular detectors, in high latitude situations.

It can be seen that the techniques for calculating telescope sensitivities at high latitudes are well established, and in

principle may be applied in any related situation. At low latitudes these techniques cannot be applied, because of the presence of geomagnetic cut-offs, and it appears that in the past no investigations have been made into the problem of taking the cut-offs into account.

In order to interpret the present latitude survey observations it has been necessary to investigate this problem. A method of determining telescope response in any situation, in the presence or absence of geomagnetic cut-offs, has been developed, in a form particularly suited to computer solution.

3.3 Generalized Technique for Calculating Telescope Response

3.3.1 Geometric Sensitivity of Element

Consider the telescope, of dimensions a x b x l, represented in Figure 3.1. It is readily shown that a solid angle element whose position is defined by the angles $\alpha - \delta\alpha/2$, $\alpha + \delta\alpha/2$, $\beta - \delta\beta/2$, $\beta + \delta\beta/2$, as indicated in this diagram, has solid angle

$$\delta\Omega = \frac{\delta\alpha\ \delta\beta\ \cos^3\gamma}{\cos^2\alpha\ \cos^2\beta}$$

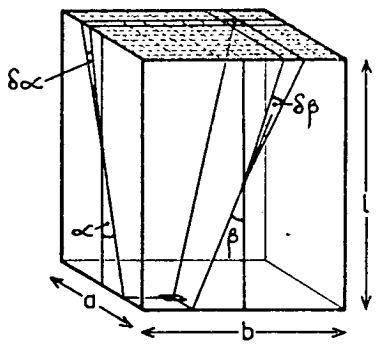

Figure 3.1. Mode of division of acceptance cone of telescope into solid angle elements.

where $\gamma = \arctan[\sqrt{(\tan^2\alpha + \tan^2\beta)}]$

This method of defining the element was chosen as it conveniently allows the

division of the acceptance cone of any telescope into rectangular elements for the purpose of summing the contributions from all elements. The cross-sectional area of the telescope presented to particles entering within the solid angle element may be shown to be

$$A = \cos\gamma \, (a - 1 \, |\tan\alpha|) \, (b - 1 \, |\tan\beta|)$$

The geometric sensitivity G of the element is simply $G = A \, \delta\Omega$.

3.3.2 Determination of Position of Element

Calculation of the radiation sensitivity requires that the zenith and azimuth angles defining the position of the element be known, so that the directional distribution of muon intensity may be taken into account.

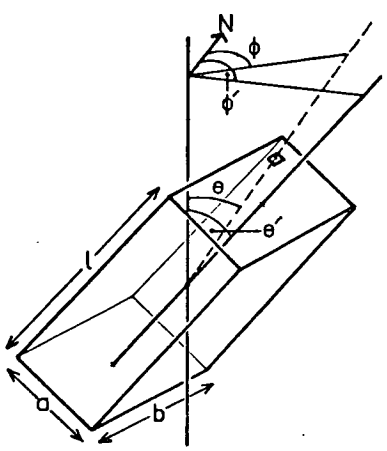

Figure 3.2. Position of telescope after being tilted through angle θ', and directed at azimuth Ø.

If the telescope is tilted about an axis parallel to the side b, so that the telescope is inclined at an angle of θ' to the zenith, and directed at azimuth heading of Ø', as shown in Figure 3.2, then the zenith and azimuth angles θ, Ø of the element are given by the expressions:

$$\theta = \arccos[\cos(\theta + \alpha)\ \cos(\arctan(\cos\alpha\ \tan\beta))]$$
$$\phi = \phi' + \arctan\left[\frac{\cos\alpha\ \tan\beta}{\sin(\theta' + \alpha)}\right] \qquad (3.1)$$

For certain applications it is desirable to rotate the telescope through an angle σ about the axis of the acceptance cone, as shown in Figure 3.3. (This step is taken in Chapter 4, where

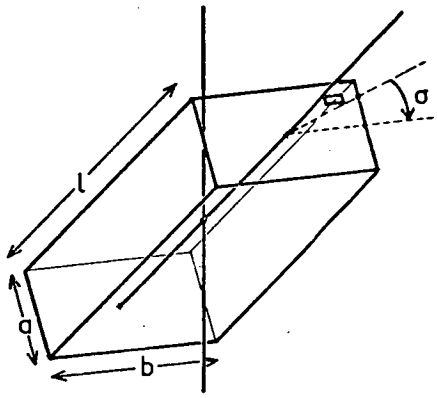

Figure 3.3. Inclined telescope, after rotation through an angle σ about the axis of the telescope acceptance cone.

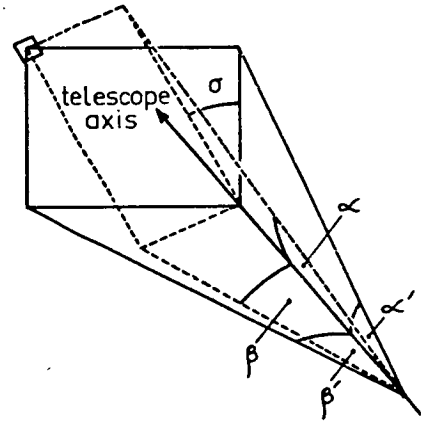

Figure 3.4. Relationship between α', β' and α, β after telescope rotation.

the response of a narrow angle telescope, viewing in the direction of main cone folding, is determined. A further use of a rotation of this kind lies in cosmic ray astronomy, where it could be used as a means of optimizing the overall response of a multiple beam array of telescopes to a primary anisotropy).

After rotation, the zenith and azimuth angles defining the position of a telescope element may be found by firstly transforming

the angles α and β defining the element position in the telescope frame of reference, to angles α' and β' fixed in the frame of reference coinciding with that existing in the telescope before the rotation was carried out (see Figure 3.4). The relationship between α', β' and α, β is given by the equations:

$$\alpha' = \arctan(\tan\alpha \cos\sigma - \tan\beta \sin\sigma)$$

$$\beta' = \arctan(\tan\beta \cos\sigma + \tan\alpha \sin\sigma)$$

The position of the element is found by using α' and β' in place of α and β in equations (3.1).

3.3.3 Radiation Sensitivity of Element in Absence of Cut-offs

The radiation sensitivity R of a telescope element is given quite generally by

$$R = G\, f(\theta,\emptyset) \qquad (3.2)$$

where $f(\theta,\emptyset)$ is a function describing the directional distribution of muon intensity. In the absence of geomagnetic cut-offs (at high latitudes and low altitudes), the total muon intensity is almost independent of azimuth, and the radiation sensitivity may be expressed as

$$R = G\, f(\theta) \qquad (3.3)$$

where $f(\theta)$ is an expression describing the relative intensity of muons at zenith angle θ. If a function $I(\theta)$ represents the absolute intensity of muons as a function of zenith

angle, then it is convenient to define $f(\theta)$ as the ratio of the muon intensity at zenith angle θ to that in the vertical direction, i.e.

$$f(\theta) = I(\theta) / I(0)$$

The zenith dependence of muon intensity is found to be closely represented by an empirical function of the form

$$I(\theta) = I(0) \cos^{n}\theta$$

over a wide range of conditions. Investigators have studied the value of the exponent n in various situations - Moroney and Parry [1954], for example, and Beiser [1954], have examined the dependence of n on muon momentum, whilst Gill and Mitra [1958] investigated the dependence of n on azimuth at low latitudes.

For the muon component capable of penetrating 10 cm. of lead absorber at sea level, n is found to have value close to 2.2, for zenith angles as great as 70^{o} approximately, in the absence of appreciable cut-offs (the various determinations of n have been reviewed by Fenton [1952] and Parsons [1959]). At higher zenith angles the intensity predicted by this function falls significantly below that observed, and at 90^{o} a finite muon flux is observed, compared with the zero value predicted. Wilson [1959] suggested that an expression of the form

$$I(\theta) = I(0) \cos^{n}\theta + K$$

could be used to represent the high zenith angle

variation of muon intensity (where K is of the order of I(0)/300). The data of Jakeman [1956], and Judge and Nash [1965], indicate that the value of the second term is I(0)/330, at 90^{o} zenith angle.

A simple function that takes into account the presence of the high zenith angle muon flux, whilst remaining essentially the basic empirical function at lower zenith angles, is

$$I(\theta) = I(0) \left[\cos^{n}\theta + \frac{\theta}{90} \times 1/330\right] \qquad (3.4)$$

where θ is in degrees.

This expression, with n = 2.2, evidently represents to an acceptable accuracy the zenith dependence of the total muon intensity on zenith angle at sea level, at high latitudes, and has been utilized in later work; for example, in the high zenith angle extrapolation of the muon coupling coefficients.

For more immediate purposes it was desirable to find an expression capable of representing the basic zenith dependence of muon intensity in the latitude survey data, for use in the data analysis. Because of the appreciable magnitude fixed systematic errors (see Section 2.3.3.3), the unidirectional zenith dependence of the muon intensity as deduced from the high latitude data (those from Hobart) differed significantly from the dependence predicted by equation (3.4). Although the differences lay within the limits of the fixed systematic errors, because these errors introduced a constant shift in the data from each zenith angle, it was desirable to obtain a function capable of representing

accurately the observed high latitude zenith angle dependence of muon intensity, which expression could then be modified to take into account the effects of cut-offs at the low latitude sites.

An expression similar in form to equation (3.4) was found suitable for this purpose, viz.

$$I(\theta) = I(0)\ [\cos^{2.2}\theta + 2.5 \times 10^{-6} \times \theta^2] \qquad (3.5)$$

(for $0 < \theta < \approx 70^{o}$). In the presence of the fixed systematic errors, it is unlikely that the second term has the same high zenith angle significance as that in equation (3.4).

In Section 5.9 a comparison is made of the predictions of the functions (3.4) and (3.5) with the theoretically calculated zenith dependence of muon intensity.

3.3.4 Radiation Sensitivity of Element in Presence of Cut-offs

In order to calculate the radiation sensitivity of a telescope element in the presence of a directional distribution of muon intensity having azimuth, in addition to zenith, dependence, it is necessary to invoke equation (3.2), viz.

$$R = G\ f(\theta,\phi)$$

At low latitude sites, an azimuth dependence of intensity arises out of the asymmetric distribution of geomagnetic cut-offs (in this discussion we do not consider the effects of the atmospheric asymmetry effect, which also produces azimuthal asymmetries; this

factor, which does not invalidate the present discussion, is discussed in Chapter 5). It is therefore possible to rewrite equation (3.2) as

$$R = G\ f(\theta, P_c)$$

where P_c is the geomagnetic cut-off in the direction θ, $\emptyset$.

The cut-offs have the effect of diminishing the directional muon intensity relative to the intensity that would exist in the absence of cut-offs. In particular, the relative intensity of muons existing in the presence of a cut-off momentum of value P_c, at any particular zenith angle θ, is given by the so-called integral response function $N_\theta(P_c)$ (see Section 1.2).

Because they affect the directional intensities in this manner, the cut-offs may be considered to have the effect of perturbing the basic high latitude zenith dependence function $f(\theta)$. The function $f(\theta, P_c)$ may therefore be considered to be made up of separable functions of zenith and cut-off, as follows

$$f(\theta, P_c) = f(\theta)\ N_\theta(P_c)$$

The radiation sensitivity is thus simply

$$R = G\ f(\theta)\ N_\theta(P_c)$$

Normally, of course, a penumbral structure exists in most directions over the observing hemisphere, rather than a simple unique cut-off value. Consider the situation at a site having a certain structure of main cone cut-off and penumbra, where the main

cone cut-off, and the upper and lower boundaries of the n allowed penumbral bands are known functions $P_m(\theta,\phi)$ and $P_{11}(\theta,\phi)$, $P_{12}(\theta,\phi)$; $P_{21}(\theta,\phi)$, $P_{22}(\theta,\phi)$; ..... $P_{n1}(\theta,\phi)$, $P_{n2}(\theta,\phi)$; respectively, of zenith and azimuth (in the penumbral terms, the second subscript denotes the upper edge (1), or lower edge (2), of the particular penumbral band).

The radiation sensitivity of an element in the direction θ, ϕ is, in terms of these functions

$$R = f(\theta)\, G \{N_\theta[P_m(\theta,\phi)] + N_\theta[P_{12}(\theta,\phi)] - N_\theta[P_{11}(\theta,\phi)] + N_\theta[P_{22}(\theta,\phi)] - N_\theta[P_{21}(\theta,\phi)] + \ldots\ldots \ldots + N_\theta[P_{n2}(\theta,\phi)] - N_\theta[P_{n1}(\theta,\phi)]\}$$

In practice the functions $P_m(\theta,\phi)$ etc. are not known explicitly. On the other hand, information is available about the discrete values P_m, P_{11}, P_{12}, P_{21}, P_{22}, ... P_{n1}, P_{n2}, of the main cone cut-off, and upper and lower edges of the penumbral bands pertaining to any one of a large number of representative directions at any site, in principle, as the result of cut-off calculations of the type described in Chapter 4.

In order to avoid the complexities of considering in detail the often finely detailed structure of the penumbra, it has proved convenient to introduce the concept of the "equivalent" penumbra. This consists of a single penumbral band equivalent in width to the summed widths of allowed penumbral bands, in any particular direction. Thus, in any direction, the cut-off

structure may be represented by three numbers: P_m, P_u and P_l, where P_m denotes the main cone cut-off, and P_u and P_l the upper and lower edges of the equivalent penumbra respectively. In terms of these values, the radiation sensitivity is, simply,

$$R = G\ f(\theta)\ [N_\theta(P_m) + N_\theta(P_l) - N_\theta(P_u)]$$

for an element directed at the zenith angle θ, in the particular direction.

As P_m, P_u and P_l are not explicit functions, analytical integration of contributions to the radiation sensitivity from all portions of the acceptance cone of a telescope is out of the question, and a simple summation process is used to determine the total radiation sensitivity.

As part of the summation process it is necessary to calculate the values of P_m, P_u and P_l applying to any direction. To facilitate this calculation, the values of these quantities pertaining to closely spaced directions over the observing hemisphere at the sites of interest are grouped in the form of a matrix of values, from which the values corresponding to any intermediate direction may be obtained by interpolation.

3.3.5 Calculation of Telescope Response

A computer program was written to carry out calculations of telescope response using the techniques described. Because of the rapidity of operation of the program in carrying out the

calculations, there is no disadvantage in having resorted to numerical methods. In practice any desired degree of accuracy may be attained by reduction of the size of the elements.

As input data this "telescope response" program requires the matrix of values describing the cut-off configuration at the site of interest (in the case of a low latitude site), and details of the detector for which the particular calculations are to be carried out - zenith and azimuth of viewing, the dimensions of the telescope, the angle of rotation about the axis of the cone of acceptance, and the nominated element size. During calculations involving the optimization of the coupling coefficient functions, parameters in the functions describing the momentum and zenith angle dependence of the integral response function were also inserted as data.

In calculating the radiation sensitivity of a given detector, the program first determines the number i and j of elements $\delta\alpha$ and $\delta\beta$ spanning the acceptance cone in each direction (taking into account, if necessary, the fractional portions of elements at the edges of the acceptance cones), and then systematically sums the radiation sensitivities of all the elements, i.e.

$$R_{tot} = \sum_i \sum_j G(\alpha,\beta)\ f(\theta)\ [N_\theta(P_m) + N_\theta(P_l) - N_\theta(P_u)]$$

to obtain an estimate of the response of the particular telescope in the given situation.

The element size required to produce the desired degree of accuracy was determined by carrying out test calculations for

progressively reduced element dimensions. The dependence of the calculated value of integrated telescope radiation sensitivity on element size is demonstrated in Table 3.1.

Table 3.1 Dependence of calculated radiation sensitivity, and inclined/vertical ratio, of latitude survey telescopes on element size (the radiation sensitivity has units cm^2 ster.).

Element size (^{o})	Radiation sensitivity for given inclination telescope				Inclined/vertical ratio for given inclination telescope			
	0^o	22.6^o	45.2^o	67.8^o	0^o	22.6^o	45.2^o	67.8^o
10 x 10	113.35	95.40	53.61	15.461	1.0000	0.8416	0.4730	0.1364
5 x 5	113.70	95.65	53.66	15.333	1.0000	0.8413	0.4719	0.1349
3 x 3	116.67	98.14	55.03	15.687	1.0000	0.8412	0.4717	0.1345
2 x 2	113.79	95.72	53.67	15.298	1.0000	0.8412	0.4717	0.1344
1 x 1	114.13	96.00	53.83	15.335	1.0000	0.8412	0.4716	0.1344
$\frac{1}{2}$ x $\frac{1}{2}$	113.81	95.74	53.67	15.292	1.0000	0.8412	0.4716	0.1344

It is evident from these figures that, whilst a certain variability exists in the estimates of radiation sensitivity, the inclined/vertical ratio values stabilize at element sizes of 2^o and less. Because the latitude survey data analysis is carried out in ratio form, an element size of 2×2^o was adopted, and used throughout the series of calculations of telescope response at the latitude survey sites.

3.4 Utilization of the "Detector Response" Program

The zenith angle dependence of radiation sensitivity of the latitude survey telescopes, in the absence of cut-offs, have been calculated in order to illustrate the general response characteristics of these narrow angle detectors (see Figure 3.5).

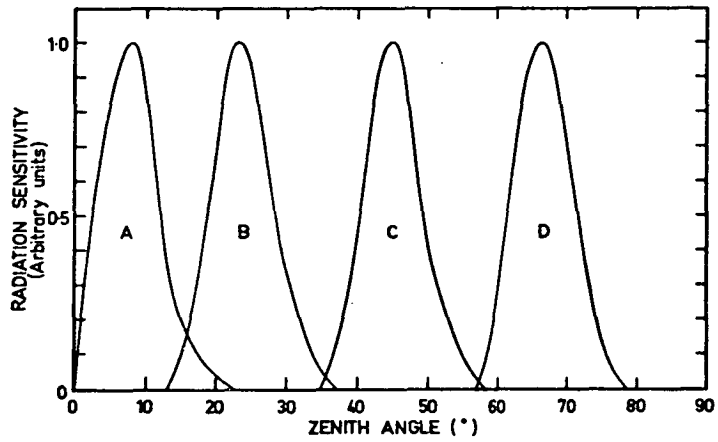

Figure 3.5. Zenith angle dependence of radiation sensitivity of the latitude survey telescopes, curve corresponds to telescope inclination 0^{o}, B to 22.6^{o}, C to 45.2^{o}, and D to 67.8^{o}. In each case the maximum differential response is normalized to unity.

At low latitudes these response patterns would be modified to an extent dependent on the form of the cut-off distribution over the acceptance cones of the telescopes in any particular situation. In the numerous calculations of telescope response at the latitude survey sites, the details of the detector response were not explicitly determined, as only the integrated radiation sensitivities were required.

A facility was included in the "detector response" program to expedite calculation of detector radiation sensitivity in the presence of any given, constant, value of cut-off. It was by means of such calculations that it was possible to deduce accurate mean effective cut-off values in the direction of viewing of detectors in any situation - information of great importance in the data analysis associated with the coupling coefficient determination.

The detailed role of the "constant cut-off" technique is discussed in the following chapters.

3.5 Conclusion

Having, by virtue of the techniques described in this chapter, the means for accurately taking into account the details of directional cut-off and penumbral structure at all points within the cone of acceptance of muon detectors, it is necessary to acquire detailed information about the structure of cut-offs at the latitude survey sites. This problem is investigated in the following chapter.

CHAPTER 4

PRIMARY RADIATION CUT-OFFS IN THE GEOMAGNETIC FIELD

4.1 Introduction

The geomagnetic field, by deflecting charged primaries, effectively limits the access of low energy cosmic rays to points within the field. Arrival at any given location, in any particular direction, is restricted to primary particles with energy (or momentum*) exceeding a certain minimum (cut-off) value. It may be shown, by means of Liouville's theorem (see, for example, Vallarta [1961]), that the intensity of primaries in any allowed direction in the field is the same, in the absence of energy changes, as that at large distances from the earth, assuming primary isotropy. This fact is a most important one in cosmic ray physics, as it

* In the first three sections of this chapter, particle motion is referred to in terms of **energy**, because of the fundamental importance of this quantity in the analytical theories of particle motion in a magnetic field. In the later sections, **momentum** is the variable utilized, once again because of the significance of this unit in the techniques discussed. Later again, in Chapter 7, primary particle motion (in particular, in connection with asymptotic directions of approach) is discussed in terms of particle **rigidity** (momentum / unit charge).

simplifies the interpretation of cosmic ray astronomy studies made using detectors situated within the geomagnetic field.

The problem of determining cut-offs at sites on the earth's surface is one that has been intensively studied because of the relevance of this information in many aspects of geophysics and cosmic ray physics. As the degree of specialization in experimental observations developed, so the demands on the accuracy of theoretical cut-off estimates increased.

It is not entirely true to say that the methods used to derive this information have become more sophisticated. The field is one in which, at each stage in development, a very great degree of sophistication has existed - the techniques employed in determining geomagnetic cut-offs have developed largely as the result of the availability of vastly improved computational methods (the introduction of mechnical, and later electronic computers). The emphasis has changed, as a result, from analytical methods, involving the use of approximations to the actual physical situation, to comprehensive numerical techniques, capable of taking into account the many complicating factors in the problem. Historically, three main phases are evident in this development. These are briefly reviewed here, with particular reference to certain aspects of the predicted behaviour of trajectories which are of interest later in this chapter.

4.2 Stormer Theory

A first approach to the problem was provided by the theory of Stormer (reviewed in detail by Montgomery [1949], Vallarta [1961], and others). Stormer showed that in an axially symmetric field (for example the geomagnetic field, to a first approximation) an integral of the charged particle equation of motion exists, as a consequence of the axial symmetry. In this integral equation - the "Stormer equation", a variable may be introduced to represent the angle between the particle velocity vector and the local meridian plane. As the value of the trigonometric function containing the angle must lie within a known range, a means was thus available for delimiting the regions of the magnetic field to which particle entry is forbidden.

To allow the shape of the regions to be quite generally investigated and graphically represented, Stormer introduced a technique of using a unit of length related to the particle energy (the unit corresponds to the radius at which a particle of the particular energy traces a circular orbit in the equatorial plane). It is thus possible to use the diagrams representing the shape of the forbidden regions to obtain information about particles of any energy, simply by scaling the diagrams appropriately. A variable, γ, incorporated in the Stormer equation (equivalent to the impact parameter of the particle at large displacements from the earth), is found to have values lying within certain well defined ranges for different characteristic forms of the forbidden regions (Figure

4.1 illustrates typical forms of these regions).

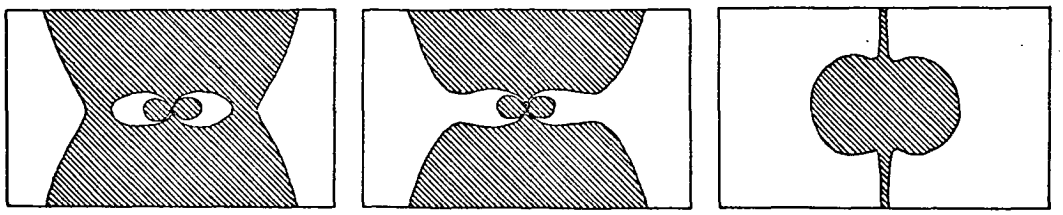

$\gamma = +1.016$ $\gamma = +0.97$ $\gamma = -0.03$

Figure 4.1. Form of the regions of a dipole field inaccessible to charged particles, for different values of γ, as predicted by Stormer theory.

At any point in the field it may be shown that the velocity vectors of positive particles of given energy or lower are expressly forbidden from lying within a particular range of directions, the range having the form of a circular cone with axis normal to the meridian plane and directed towards the east. The size of the **Stormer cone** is dependent on primary particle energy, the half angle of the cone increasing with decreasing energy.

At any location in the field, in any direction, a Stormer cut-off may be calculated which gives the energy below which the particle entry is debarred. The Stormer cut-off R (GeV) in the dipole representation of the geomagnetic field is given by

$$R = 59.6 \cos^4\lambda \left[1 + \sqrt{(1 - \sin\theta \cos\phi \cos^3\lambda)}\right]^{-2}$$

where λ is the latitude, and θ, ϕ are the zenith and azimuth angles defining the given direction.

Stormer theory, whilst providing a means for examining the character of the forbidden regions, does not, on the other hand, yield information about particle accessibility to those regions not specifically forbidden. It was the development of a mechanical analogue computer (the differential analyser of Bush [1931]) that enabled Lemaitre and Vallarta [1936a, 1936b] to investigate this problem.

4.3 Lemaitre and Vallarta Theory of the Allowed Cone of Radiation

At any point in the geomagnetic field, the allowed, or **main cone** for particles of any particular energy is the region into which access is unrestricted to particles of the given energy or greater. Lemaitre and Vallarta showed that the edge of the main cone is a boundary between domains of trajectories travelling direct from infinity (non-reentrant) and those having re-entrant sections (where the term **re-entrant**, which may be taken as referring to reversals in the sense of motion relative to the centre of the earth, is defined more precisely in Appendix 1), and that the generators of the main cone, the transition trajectories between re-entrant and non-reentrant orbits, have the property of being asymptotic to bound periodic orbits. These bound orbits, investigated originally by Stormer, lie in the allowed pass between the "jaws" of the forbidden region (see Figure 4.1, $\gamma = +0.97$, for

example) for values of γ in the range $0.78856 < \gamma < 1$.

Lemaitre and Vallarta determined the characteristics of the bound periodic orbits in the dipole field for various values of γ, and traced the path (as a projection on the moving meridian plane) of representative members of the families of trajectories asymptotic to these periodic orbits. Figure 4.2 reproduces Figure 2 of Lemaitre and Vallarta [1936b], which illustrates the family of trajectories for $\gamma = 0.93$. In this diagram (and in Figure 4.3) latitude is plotted on the vertical axis, whilst the parameter X plotted on the horizontal axis is related to the Stormer unit of length. The earth's surface is represented by a straight vertical line, whose position with respect to the trajectories is determined by the particle energy in question.

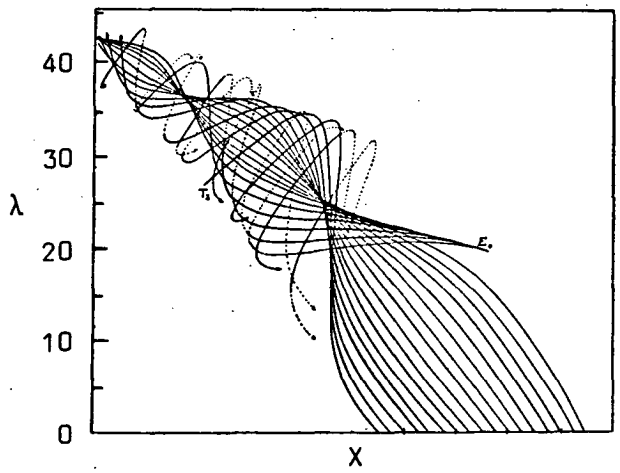

Figure 4.2. A family of asymptotic trajectories. $\gamma = 0.93$. (Lemaitre and Vallarta [1936b]).

As part of their investigation Lemaitre and Vallarta located

the envelopes defining the limits of the various sections of the trajectories constituting the families, for a range of values of γ. The change in position of the envelopes for change in γ is shown in Figure 4.3, a reproduction of Figure 1 of Lemaitre and Vallarta [1936a].

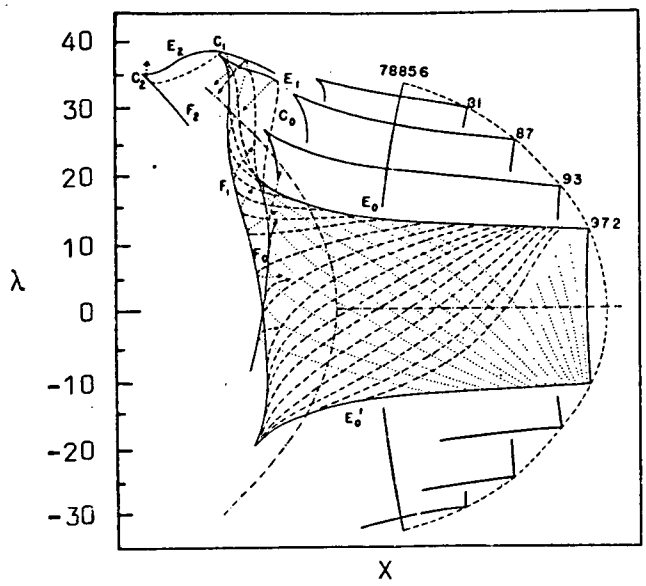

Figure 4.3. The family of envelopes and periodic orbits, and a typical family of asymptotic trajectories. (Lemaitre and Vallarta [1936a]).

The delineation of the main cone structure for primaries of any energy, using plots like these, is a complicated procedure, involving the location of points on the diagrams pertaining to the latitude of interest and position on the earth's surface for given values of trajectory inclination to the meridian plane, and the determination of the slope of the trajectories intersecting these

points. Lemaitre and Vallarta calculated the form of the main cone structure for a range of values of particle energy, at latitudes of 0^{o}, 20^{o} and 30^{o} North in the dipole field.

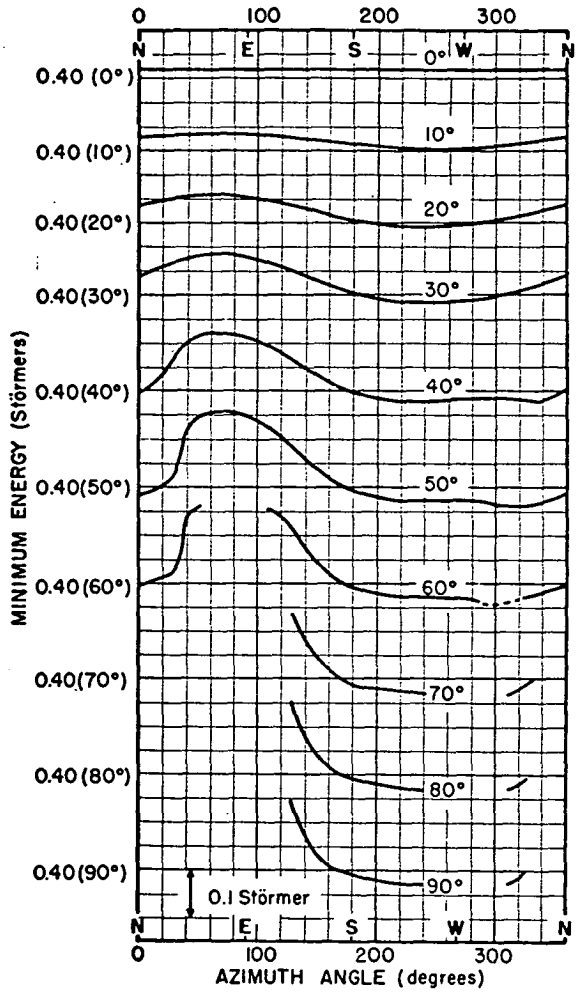

Figure 4.4. Main cone cut-off energy vs azimuth for various zenith angles at 30^{o} N. geomagnetic latitude. (Alpher[1950])

Presentation of the information contained in these plots in a rather more convenient form is due to Alpher [1950]. Alpher's graphs show the dependence of main cone cut-off energy (in Stormer units) on azimuth at a number of zenith angles (see Figure 4.4, which reproduces Figure 3c of Alpher, the distribution of main cone cut-off value at 30^{o} North geomagnetic latitude). The main cone cut-off energy, in any direction, corresponds to the energy value above which particle entry in that direction is unrestricted.

Lemaitre and Vallarta found that the main cone edge in certain ranges of directions is formed by trajectories that are

tangential to the earth in re-entrant sections. In cut-off plots the shadow cone edge so produced is manifested as a hump in the cut-off curves at eastern azimuths (this effect, although not visible in Figure 4.4, is readily distinguished in the cut-off diagrams presented in Section 4.5, for example Figure 4.9). The region between the edges of the main and Stormer cones consists of alternate allowed and forbidden directions, and is known as the **penumbra.** The presence of the solid earth intersecting trajectories in re-entrant sections is a major factor contributing to the complexity of the penumbral structure.

Hutner [1939a, 1939b] investigated the detail in the penumbra for a single energy at latitude 20^{o} North, using the techniques of Lemaitre and Vallarta. Because of the complexity of the structure, Hutner concluded that a study restricted in this way could not form the basis for making general predictions about the behaviour of the penumbral structure in different situations, other than indicating that penumbra associated with low energy particles tend to have greater transparency (greater numbers of allowed bands) than penumbra at higher energies.

The basic techniques of Stormer, and of Lemaitre and Vallarta, are restricted to consideration of particle motion in axially symmetric fields. The theoretical predictions are, as a result, of limited use when real field situations are being considered in detail. Improvement in the accuracy of estimated cut-off values has resulted from the efforts of investigators to adapt these

theories to take account of non-symmetric field components (for example, the work of Rothwell [1958], Rothwell and Quenby [1958], Quenby and Webber [1959], and Quenby and Wenk [1962]). These techniques, and that of Sauer [1963], which utilizes the "guiding centre" approximation to particle motion in the determination of high latitude cut-offs, have been largely superseded by a later, more powerful technique, which relies on the use of extensive trajectory tracing calculations to examine particle accessibility to points in the real field.

4.4 Trajectory Derived Cut-offs

The development of this method has been possible because of the advent of fast electronic computers. Apparently first used by Kellogg and Schwartz [1959], the technique has been adopted by many other investigators, amongst them Kellogg [1960], Freon and McCracken [1962], Kondo and Kodama [1965], Shea, Smart and McCracken [1965], Daniel and Stephens [1966], Shea and Smart [1967, 1970], Shea, Smart and McCall [1968], and Smart, Shea and Gall [1969]. Shea et al. [1965] have presented a comprehensive review of the operation of the method, in which they discussed the optimum value of the various parameters in the calculations, and the dependence of the results on the model used to represent the geomagnetic field. In practice, the technique, capable as it is of producing results of a high order of accuracy, has proved flexible, if time consuming, and has been

used almost exclusively in determinations of geomagnetic cut-offs in the past decade.

The process of trajectory tracing involves the numerical integration, in a starting point calculation, of the differential equations representing the motion of a charged particle in the magnetic field, establishing in a cyclic sequence of operations successive points on the trajectory.

The Lorentz equation has the form (in MKS units)

$$m \ddot{\underline{R}} = q \dot{\underline{R}} \times \underline{B}$$

where m, q, $\underline{R}$ are the mass, charge, and position vector of the particle, and $\underline{B}$ is a vector representing the magnetic field.

In order that the trajectory pertaining to a particular direction and point of arrival in the field may be deduced for a particle of particular momentum, a trace is made of the trajectory of a negatively charged "proton", projected with specified zenith and angles away from a given site. It is readily seen that the path followed will be the same as, but traversed in the opposite direction to, that followed by an incoming positive proton having the same momentum, arriving at the site with the particular zenith and azimuth angles.

McCracken et al. [1962] published a Fortran computer program designed to carry out this trajectory tracing operation in a high order simulation of the earth's magnetic field (McCracken et al., and subsequently many other investigators have utilized this program to

carry out extensive investigations of cosmic ray trajectories, and determinations of cut-off values in the geomagnetic field).

The use of such trajectory traces in the determination of directional cut-offs involves essentially the examination of the freedom of access in a given direction, at a given site, of protons from infinity as a function of momentum. To facilitate further discussion, terms used to describe the features of the structure in the distribution of allowed and forbidden directions of approach are summarized here.

Studies of charged particle motion in the geomagnetic field show that the allowed directions of arrival of a proton of given momentum at a given location are distributed in a well-determined manner. The following regions may be distinguished:

Main Cone - The solid angle containing directions of arrival which are accessible to an incident proton with momentum between the given value and infinity.
This definition is an equivalent re-statement of the "full light" definition of Lemaitre and Vallarta [1936a], that the main cone is the solid angle of directions along non-reentrant trajectories (see notes in Appendix 1).

Stormer Cone - The solid angle of directions outside of which all directions are forbidden to particles of the given momentum or lower.

Shadow Cone - The solid angle outside of which all directions are forbidden to particles of the given momentum, due to the presence of the solid earth. In some directions the shadow cone edge constitutes the main cone edge.

In any particular direction there exist momentum values at which an edge of each of these cones is encountered. These momentum values are known as the **main cone cut-off, Stormer cone cut-off,** or **shadow cone cut-off,** depending on which cone edge is under consideration.

The term Penumbra is used to describe a region consisting of alternate allowed and forbidden trajectories. The term is used in two situations:

a) In a given direction it refers to the momentum interval between the edges of the main and Stormer cones.

b) At a given momentum, the solid angle region between the main and Stormer cone edges constitutes the penumbra.

In practice, to determine the cut-off values pertaining to a particular direction, trajectory traces are carried out in a sequence of descending values of momentum, commencing with a high value, and continued until a value is found for which the trajectory is unable to leave the field. This momentum value is, by definition, the main cone cut-off in that direction. Examination

of the form of the trajectory reveals whether the cut-off is also the shadow cone cut-off. Trajectory traces carried out for lower values of momentum again permit penumbral details to be established, and also in principle allow the Stormer cut-off to be located, although this is not always distinct.

4.5 Determination of Cut-off Distributions at Survey Sites

The trajectory technique for deriving cut-offs has been used to obtain detailed information about the directional distribution of the primary radiation cut-offs over the observing hemisphere at the six northern-most major latitude sites (see Section 2.3.1). The trajectory traces have been carried out on an Elliott 503 digital computer, using an Algol version (written by Mr. J.E. Humble, of the Hobart research group) of the McCracken et al. [1962] program. The Finch and Leaton [1957] sixth order coefficients were used to represent the geomagnetic field during the major part of the calculations, although in certain additional calculations, described in Section 4.12, the Jensen and Cain [1962] and Leaton et al. [1965] coefficients were utilized.

The details of the trajectory tracing program (choice of step length, integration technique, method of generation of the field potential terms etc.) are essentially the same as published by McCracken et al. [1962].

In the process of locating the directional main cone cut-off, and establishing the form of the penumbra in a number of repres-

entative directions at each site, momentum steps of from 0.1 to 0.01 GeV/c were used, depending on the particular requirements in hand. An automatic search procedure was developed to facilitate the location of main cone cut-off; the approximate cut-off value was first found in a coarse momentum step search, and then finally the accurate value in a fine, 0.01 GeV/c interval search.

Integration of each trajectory was commenced at a point 20 km above sea level at each site and continued until one or other of the following applied:

a) a radial distance of 10 earth radii from the centre of the earth was reached (this point was sufficiently distant from the earth to be clearly outside the jaws of the Stormer forbidden regions for particles with momenta close to the cut-off values at the latitudes considered, even in the presence of the non-dipole field components). At this point the trajectory was deemed accessible to a positive proton coming from infinity, and so was termed an allowed trajectory.

b) the trajectory re-approached within 20 km of the earth's surface, in which case the trajectory was deemed forbidden to a proton from infinity.

c) 5000 integration steps had been performed, representing about 7 minutes' computer time. It is known that such trajectories can proceed to a very large number of integration steps before reaching a definite result, and it was considered that the expenditure of the required computer time was not warranted.

Calculations were therefore terminated and referred to as an integration failure. Uncertainty in cut-off value due to integration failures were negligably small at sites other than Laverton, where, due to numerous such failures, a possible error of up to 0.25 GeV/c applies to some of the main cone cut-offs.

The cut-offs were calculated for sufficiently closely spaced directions to enable tracing of the finest detail in the directional main cone cut-off distributions. Penumbral detail was investigated for a number of representative directions at each site and summarized in the form of the "equivalent" penumbra. We define the equivalent penumbra in any direction as the penumbral band equal in width to the sum total of allowed trajectories in the penumbra multiplied by the momentum interval interval between trajectories, centred on the arithmetic mean of the allowed trajectory momenta. This presentation was adopted in favour of subtracting the total penumbral width from the main cone cut-off as done by some investigators (for instance, Shea et al. [1965]) to obtain an "effective" cut-off, so that the penumbral information could be retained, to allow, in principle, increased accuracy in the utilization of the cut-off data.

The distribution of cut-off momenta over the observing hemisphere at Mossman, Rockhampton, Brisbane, Williamtown and Laverton (site locations given in Figure 4.5 and Table 4.1) are presented in Figures 4.6 to 4.11 inclusive, in the form of graphs showing the dependence of cut-off momentum on azimuth for a [to page 100]

Table 4.1 Position coordinates of the sites for which detailed cut-off calculations have been carried out. The invariant latitude values were obtained from the charts of Kilfoyle and Jacka [1968].

Site	Geographic		Geomagnetic		Invariant
	Latitude (°South)	Longitude (°East)	Latitude (°South)	Longitude (°East)	Latitude
Mossman	16°28'	145°18'	25°50'	216°54'	24°
Townsville	19°15'	146°46'	28°36'	218°53'	27°
Rockhampton	23°22'	150°29'	31°59'	223°30'	31.5°
Brisbane	27°25'	153°05'	35°39'	227°03'	36°
Williamtown	32°48'	151°50'	41°07'	226°51'	42°
Laverton	37°52'	144°45'	47°05'	220°06'	48.5°

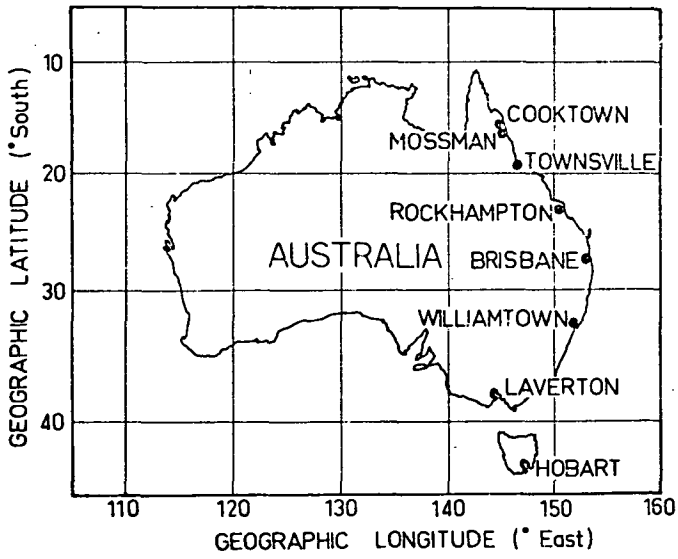

Figure 4.5. Location of the sites for which detailed cut-off distributions have been determined.

[from page 97] range of zenith angles (this presentation is the same as that used by Alpher, see for example Figure 4.4). These cut-offs, momentum cut-offs for protons, are numerically equal to the value of the rigidity cut-offs for other primary particles.

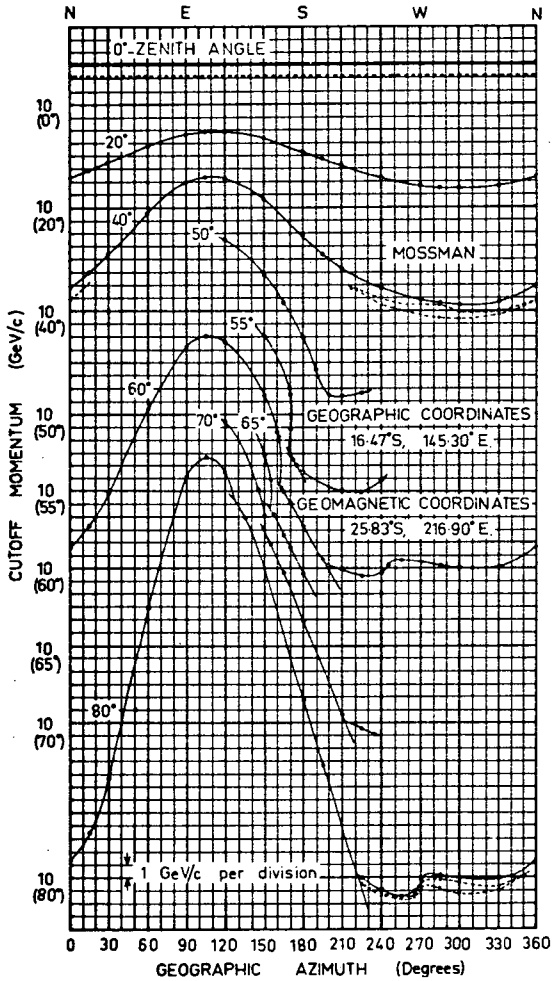

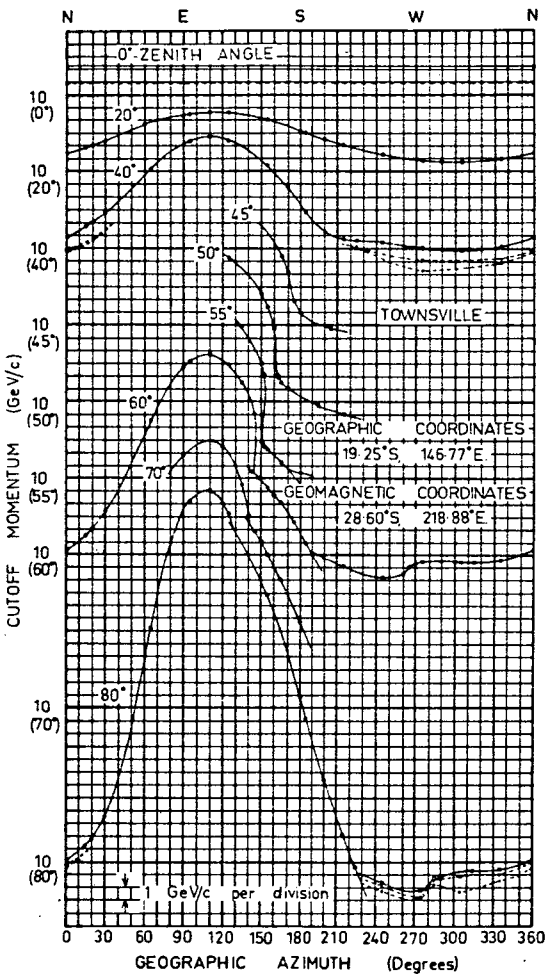

Figure 4.6 (left) and 4.7 (right). Variation of main cone cut-off with geographic azimuth for various zenith angles at Mossman and Townsville respectively. Calculated cut-off values are shown as dots. The equivalent penumbra for 0^{o}, 40^{o} and 80^{o} are represented by dashed lines.

4.6 Calculation of Mean Effective Cut-off Values in the Directions of Viewing at the Latitude Survey Sites

Interpretation of directional muon intensity observations at the sites necessitates a knowledge of the average (or "mean

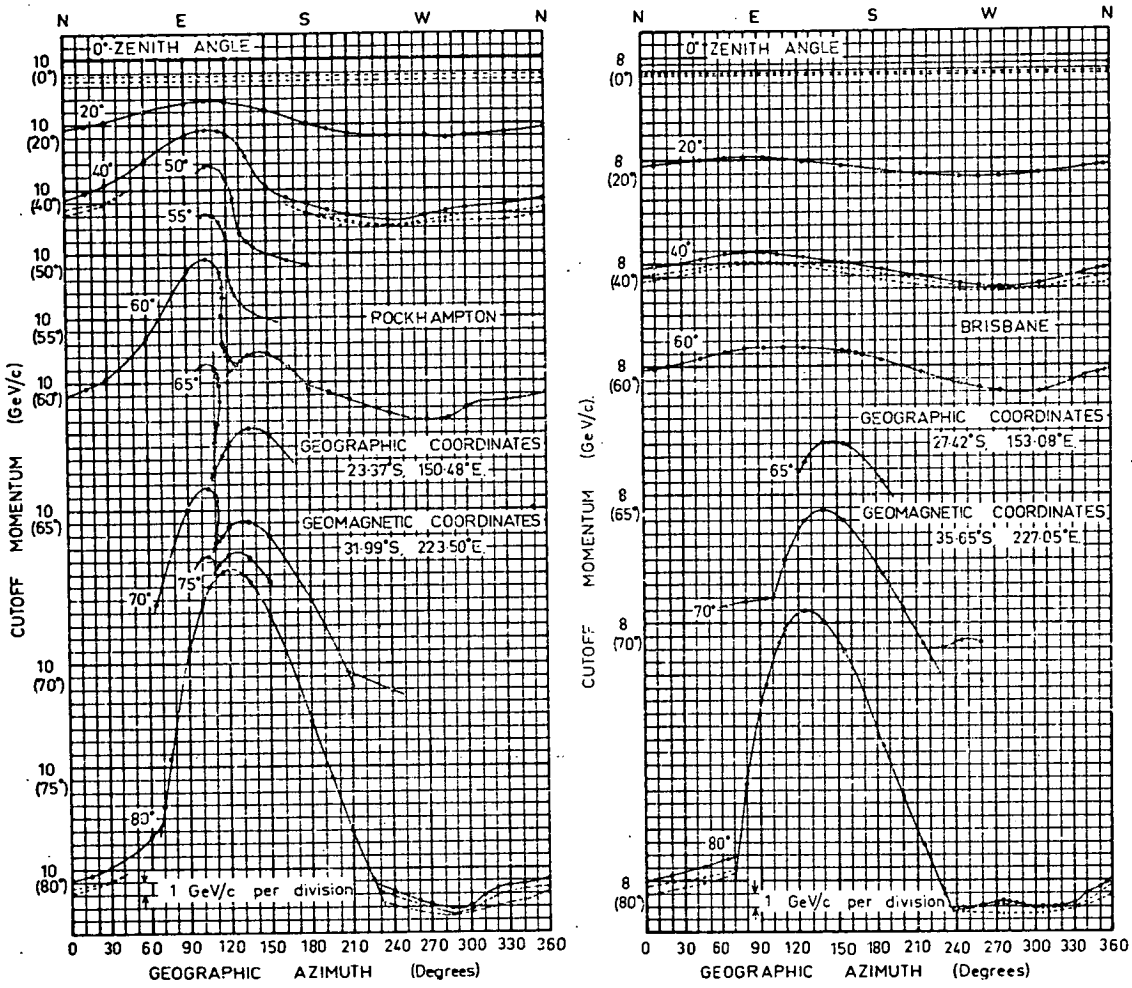

Figure 4.8 (left) and 4.9 (right). Variation of main cone cut-off with geographic azimuth for various zenith angles at Rockhampton and Brisbane respectively. Calculated cut-off values are shown as dots. The equivalent penumbra for 0^{o}, 40^{o} and 80^{o} are represented by dashed lines.

effective") cut-off pertaining to each direction of viewing of the muon telescopes. Previous investigators, with the apparent exception of Carmichael et al. [1968, 1969] and Shea and Smart [1970b], have made use of the cut-off value in the axial direction of detectors as an approximation to the true mean effective cut-off value.

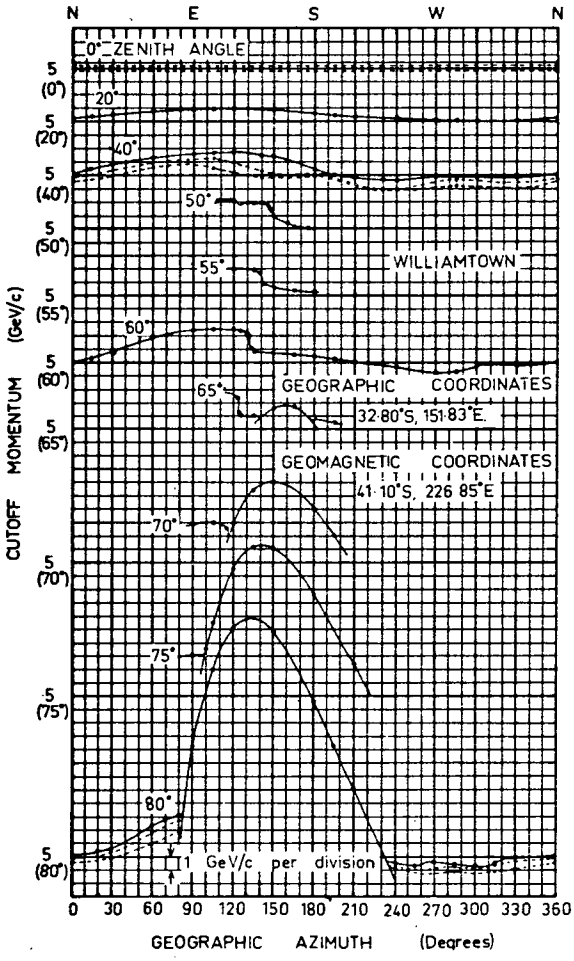

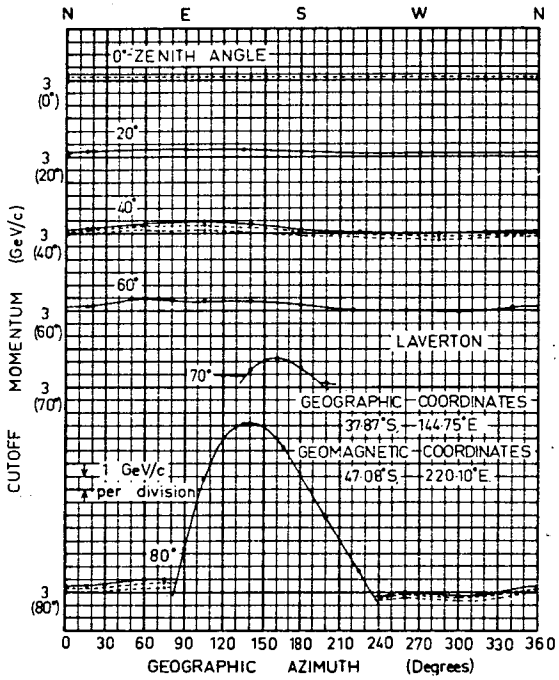

Figure 4.10 (left) and 4.11 (above). Variation of main cone cut-off with geographic azimuth for various zenith angles at Williamtown and Laverton respectively. Calculated cut-off values are shown as dots. The equivalent penumbra for 0^{o}, 40^{o} and 80^{o} are represented by dashed lines.

The axial effective cut-off values in the directions of viewing at each latitude survey site have been deduced, and are presented in Table 4.2. For comparison, the mean effective (m.e.) cut-off values applicable to each viewing direction are also tabulated. These values were calculated using the "constant cut-off" technique mentioned in Section 3.4 (and described more fully in Section 4.10), in conjunction with the integral response functions developed in Chapter 6. Where the atmospheric cut-offs exceed the geomagnetic cut-offs, the m.e. cut-offs are not determinable by this method.

Table 4.2. Axial and mean effective cut-off momentum values in directions of viewing at the latitude survey sites (m.e. values bracketed).

Direction Ze.	Az.*	Mossman	Towns.	Rock.	Brisbane	Will.
0^{o}	-	13.0(13.2)	11.2(11.7)	9.8(10.0)	7.3(7.3)	5.1(5.1)
22.6^{o}	1	12.9(13.0)	11.6(11.9)	9.9(10.1)	7.6(7.7)	5.0(5.0)
	2	16.3(16.4)	13.9(14.0)	11.6(11.5)	8.2(8.1)	5.5(5.6)
	3	13.8(13.9)	14.9(14.9)	12.0(11.9)	7.8(7.8)	5.0(5.2)
	4	10.7(11.0)	14.0(14.1)	10.2(10.4)	7.2(7.1)	4.5 -
	5	-	12.0(12.2)	8.9(9.0)	6.4(6.5)	-
	6	-	10.5(10.4)	8.4(8.5)	6.6(6.5)	-
	7	-	9.7(10.0)	8.9(9.0)	7.1(7.2)	-
	8	-	10.0(10.4)	-	-	-

Table 4.2 (continued).

Direction Ze.	Az.*	Mossman	Towns.	Rock.	Brisbane	Will.
45.2°	1	13.3(13.6)	11.8(12.1)	10.0(10.2)	7.8(7.9)	5.1(5.2)
	2	22.1(21.7)	17.3(17.1)	13.8(13.7)	8.8(8.7)	6.4(6.5)
	3	14.2(14.1)	20.2(19.9)	15.2(14.4)	8.4(8.5)	4.9 -
	4	9.6(9.9)	17.0(16.4)	9.5(9.6)	7.6(7.6)	4.3 -
	5	-	9.8(10.6)	8.0(8.0)	6.1(6.1)	-
	6	-	9.6(9.6)	7.7(7.9)	6.0(6.2)	-
	7	-	9.0(9.2)	8.1(8.4)	6.9(7.0)	-
	8	-	9.6(9.7)	-	-	-
67.8°	1	13.5(13.8)	12.1(12.3)	10.1(10.1)	8.1 -	-
	2	33.0(31.1)	23.1(22.3)	16.8(16.5)	9.4 -	-
	3	13.3(12.5)	29.6(28.1)	17.9(17.9)	13.1(11.7)	-
	4	9.4(9.5)	20.2(19.1)	16.3(14.5)	12.9(11.3)	-
	5	-	11.8(11.0)	9.1 -	6.1 -	-
	6	-	7.8 -	7.2 -	5.7 -	-
	7	-	8.5 -	8.0 -	6.9 -	-
	8	-	9.0 -	-	-	-

* Table 2.5 identifies the azimuth angles denoted here by numbers.

It is to be observed, on examination of Table 4.2, that very appreciable differences exist between the axial effective and mean

effective cut-off values in some directions, differences of up to 1.9 GeV/c, and 12 % in relative magnitude.

It is not unreasonable that differences do occur, as, in inclined directions, the zenith angle of maximum detector response may differ significantly from the inclination of the telescope axis (see figure 3.5), and it would be expected that, for any particular detector geometry, systematic differences between the axial effective and mean effective cut-off values would exist. It is, however, at first sight surprising that the largest differences do not always occur in conjunction with the greatest cut-off values (see, in Table 4.2 for example, the 67.8^{o} zenith angle cut-off values at azimuth 4 (163^{o}) at Rockhampton).

An indication of the reason for this behaviour may be found in an examination of the distribution of cut-off values at the sites. A structure is to be observed in the main cone cut-off distribution, associated with which are very large changes in cut-off value within small azimuth ranges, in particular, in the south-east at Townsville and Rockhampton. This structure is very clearly depicted in the stereo pair diagrams representing the cut-off distribution at these sites (Figures 4.12a and 4.12b). That the presence of such a structure could be responsible for large differences between the axial and mean effective cut-offs can be seen by considering the changes in cut-off value for a telescope scanning past the cut-off "discontinuity". It is evident that the axial effective cut-off changes drastically within a few degrees [to page 106]

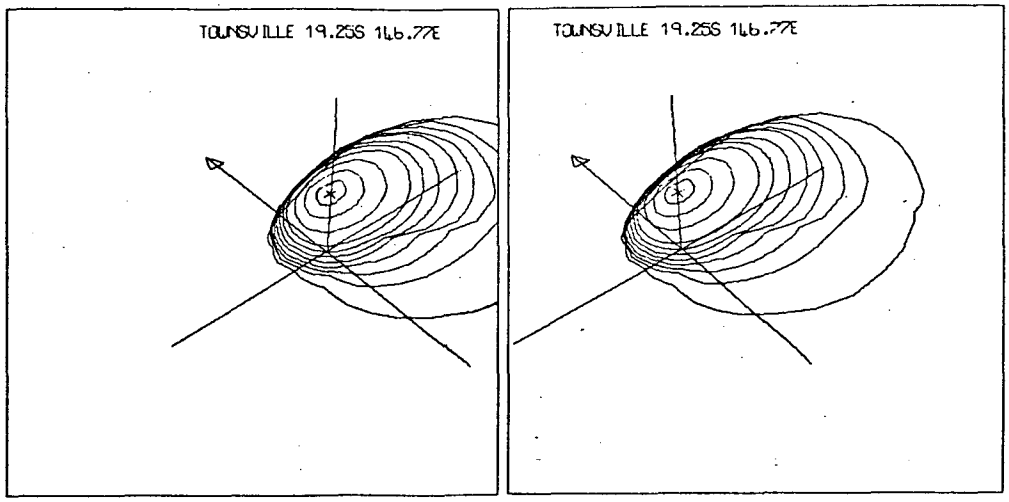

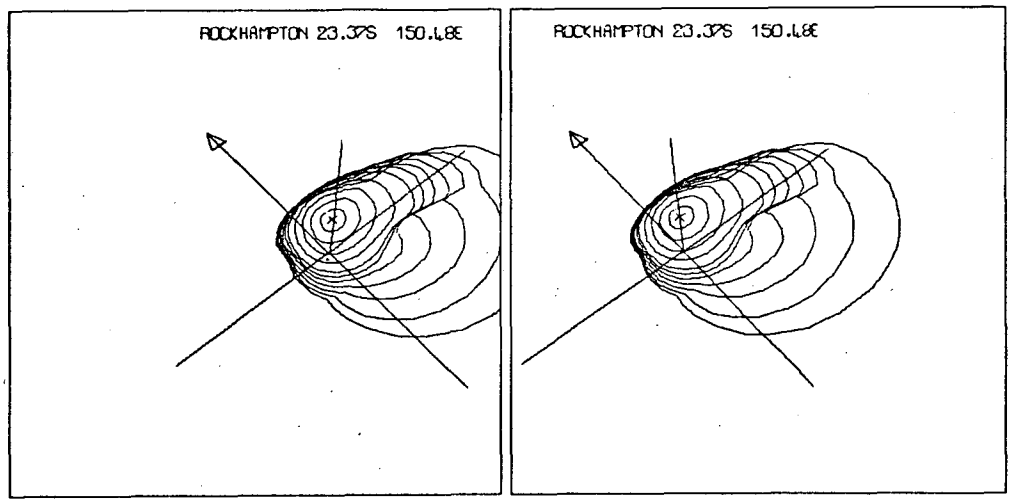

Figures 4.12a (above) and 4.12b (below). Computer drawn stereo pair pictures of the directional cut-off distributions at Townsville and Rockhampton respectively. Viewpoints: 220^{o} azimuth in each case, and 45^{o}, 30^{o} zenith respectively. The "contour lines" show the variation of m.c. cut-off momentum with azimuth at various zeniths (cut-off value is proportional to the displacement of each point from the origin of the cartesian reference frames; the arrows point geogr. north). View with prism (see Appendix 2).

[from page 104] (for example, a drop of ≈ 6 GeV/c within 2^{o}azimuth, at 60^{o} to the zenith and 116^{o} azimuth at Rockhampton, as shown in Figure 4.8). The mean effective cut-off, on the other hand, because of the finite acceptance angle of the telescope, will change from high to low cut-off value over a considerably wider azimuth range. Over this range, then, large differences between the axial and mean effective cut-off values can arise.

Because of the possible effects of the structure on directional cosmic ray intensity, and therefore on the ordering of corresponding observational data by the use of directional cut-off values, and in view of the fact that difficulty has commonly been experienced in the interpretation of data in terms of axial cut-offs (as, for example, by Carmichael et al. [1968]), it is of considerable interest to investigate this effect further.

4.7 Main Cone Fold Effect - the Loop Cone

At very low geomagnetic latitudes the dependence of main cone cut-off on azimuth , for a constant zenith angle, is observed to be a smoothly varying function with a maximum in the east and a minimum in the west, and sensibly symmetric about an approximately east-west directed azimuthal plane (see, for example, the results of Daniel and Stephens [1966], and the 0^{o} latitude results of Lemaitre and Vallarta [1936b] as presented by Alpher [1950]).

The calculated main cone cut-off distributions at low and mid-latitude sites (Figures 4.6 to 4.11) show significant departures

from this north-south symmetry, due to the presence of certain distinct features in the main cone cut-off values at southern azimuths. Such an effect can also be observed in Alpher's presentation of the 30^{o} North latitude results of Lemaitre and Vallarta, as reproduced in Figure 4.4. In this case the structure occurs at north-western azimuths.

Hutner [1939a, 1939b] investigated the structure evident in Lemaitre and Vallarta's 20^{o} North latitude data, using the Lemaitre-Vallarta technique with fine spatial resolution. She found a complex penumbral structure over a small azimuth range in the north-western quadrant (Northern hemisphere) which she predicted should be observable as humps in experimental muon intensity vs azimuth results. Perhaps partly because of limited observational accuracy, experimental results (reviewed by Kane [1962] have failed to show positive evidence of the structure at the expected azimuth.

We have investigated the phenomenon and find it to be produced by the looping of trajectories. Trajectories with such looping, as will be shown presently, are able to approach a site more freely than those without the loops, enabling depressed values of main cone cut-off to exist in certain well defined ranges of directions. The penumbra, if present in any such direction, may also be affected; however, the predominant effect is the structure of the main cone edge, which may be present in the absence of a penumbra. It is an effect produced basically by the dipole field, and the introduction of higher order field terms merely modifies the

predicted size and position of the structure.

A typical example of the phenomenon is to be seen in Figure 4.13. We refer to the fine structure visible at 145° and 260° as **folds**, and call the intermediate azimuth range labelled A, in which depressed values of cut-off exist, the "folded" region of the main cone cut-off curve. The reason for the formation of the folds is to be found in an examination of the trajectories associated with the main cone edge.

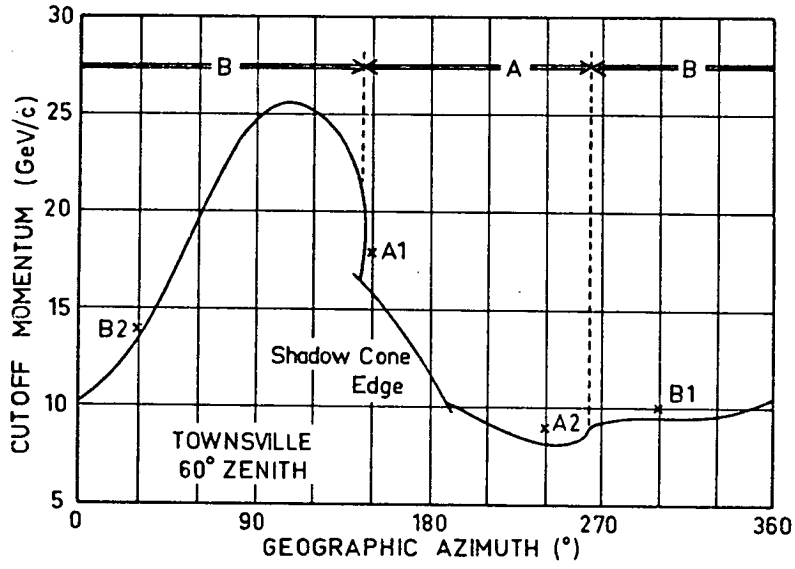

Figure 4.13. Variation of main cone cut-off with geographic latitude at 60° to the zenith at Townsville, showing folding over a well defined azimuth region. Trajectories corresponding to the directions of arrival, and momenta, indicated by the crosses, and denoted A1, A2, B1 and B2, have been plotted in part in Figure 4.14 to illustrate the looping that is responsible for the folding. These momentum values lie just above the main cone cut-off.

As first stated by Lemaitre and Vallarta, the edge of the main cone is associated with two types of trajectories: those asymptotic to the Stormer periodic orbits (constituting in Figure 4.13 the entire main cone edge except that labelled "shadow cone edge"), and those which intersect the earth tangentially in a looped section, forming the shadow cone edge.

Asymptotic trajectories (we are now considering the form of trajectories of negative "protons" that are travelling away from the earth) originating at mid latitude sites are observed to approach the equatorial regions within a narrow range of longitudes and then take on the characteristic form of closed periodic orbits, moving from west to east and swinging back and forth in quasi-periodic motion across the equator. It is due to the peculiarities of the initial aperiodic sections of the asymptotic trajectories that the folding of the main cone cut-off distribution is produced. The significance of the form of these trajectory sections will be illustrated for a typical mid-latitude site, Townsville.

It is observed (see Figure 4.14) that the initial sections of trajectories originating inside the folds at Townsville (i.e. within region A in Figure 4.13) have at some point reversals in the direction of crossing of the local magnetic meridians. In these reversals the general west to east motion with concave downwards curvature develops into east to west crossing of meridians, with the consequent reversal of the sense of the curvature relative to the surface of the earth. A loop thus forms in these traject-

ectories. On the other hand, trajectories originating outside the folds are seen in Figure 4.14 to be free of these reversals from west-east to east-west crossings of the magnetic meridians, and so do not possess loops. These unlooped trajectories do not have the

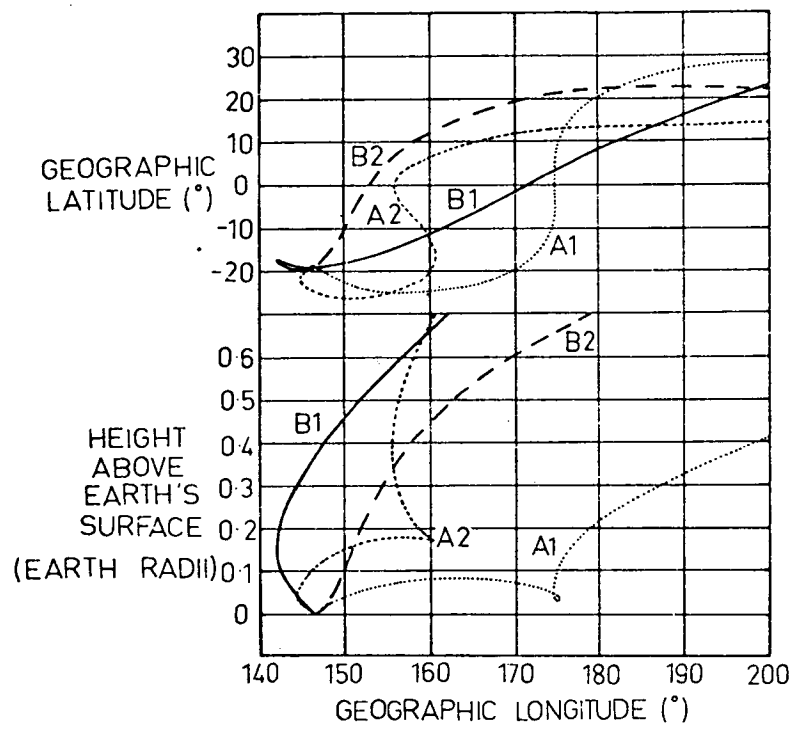

Figure 4.14. Sections of the trajectories of protons, whose directions of arrival and momenta are indicated in Figure 4.13, are plotted in detail on a latitude versus longitude plot (upper part of diagram) and on a height versus longitude plot(lower part). Trajectories A1 and A2 (situated within the folded region of the main cone edge) are seen to loop in their south to north motion, whilst B1 and B2 (situated outside the folded region) are seen to be free of loops.

advantage of being re-projected away from the earth as do those with a loop, and so the cut-offs in the directions at the site from which the unlooped trajectories originate are observed to be relatively higher than those which, although perhaps pertaining to adjacent directions, are associated with looped orbits. If the loop intersects the surface of the earth the shadow cone edge is formed. Such an intersection occurs in the main cone edge trajectories at Townsville, producing the shadow cone edge evident in Figure 4.13.

The solid angle of all the directions from which looped trajectories originate is found to have the form of portion of a nearly circular cone directed away from the equator. We propose to call this cone the **loop cone**, formally defining it after further discussion. At Townsville the loop cone has a half angle of 84^{o}, and the axis of the cone is oriented 35^{o} below the horizontal towards the South. Inside this cone the main cone edge is formed by looped trajectories, and outside by unlooped trajectories. Figure 4.15a shows, in the form of a stereo pair picture, an unlooped trajectory characteristic of those outside the loop cone at Townsville, and Figure 4.15b illustrates a singly looped trajectory typical of those associated with the loop cone.

The loop cone is bounded by an annular region of approximately 10^{o} width, across which, instead of an abrupt discontinuity in main cone cut-off value occuring, a fold, or transition from high to low cut-off value is produced by the gradual [to page 113]

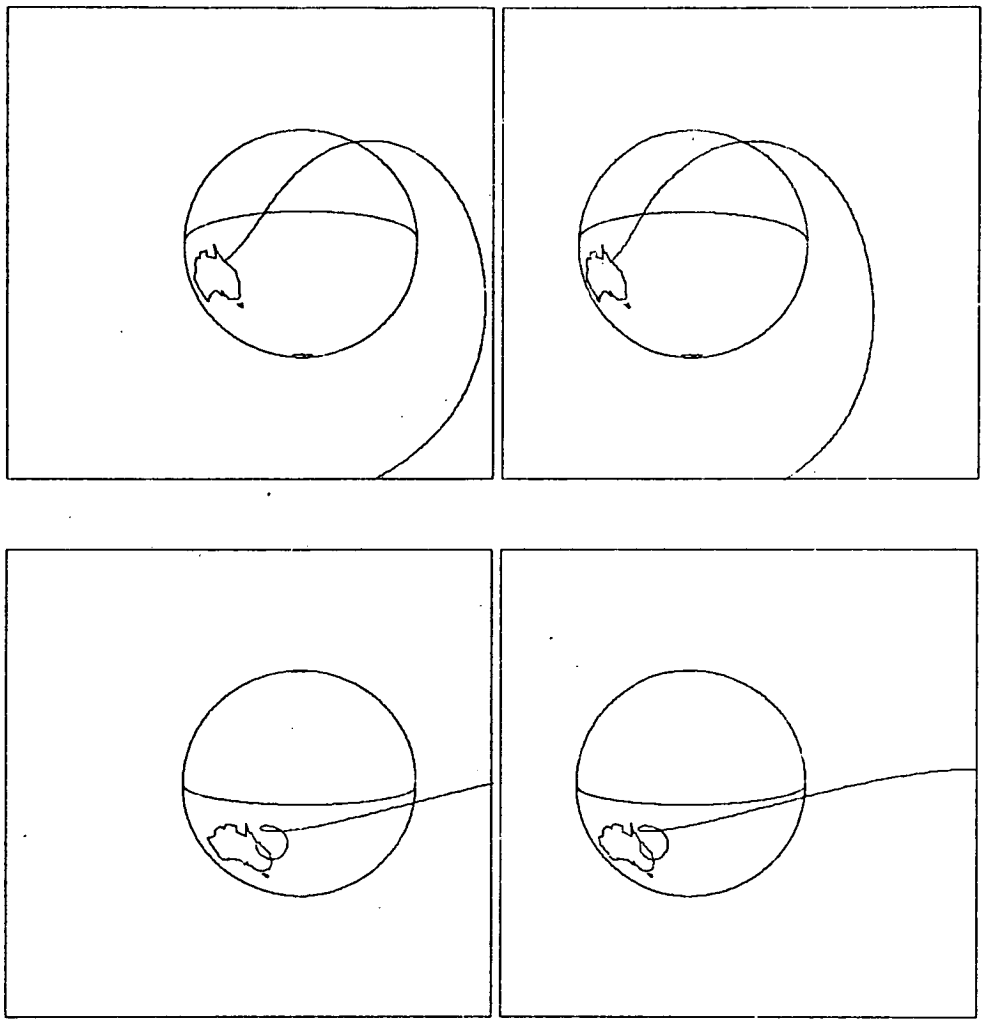

Figures 4.15a (top) and 4.15b (bottom). Stereo pair pictures of unlooped and singly looped trajectories characteristic of those arriving outside and inside the first order loop cone at Townsville respectively. View with prism (see Appendix 2).

Figure 4.15a shows path of a 25 GeV/c proton, arriving at zenith angle 60^{o}, azimuth 90^{o}. Viewed from latitude -15^{o}, longitude 190^{o}.

Figure 4.15b shows path of a 10.4 GeV/c proton, arriving at zenith angle 60^{o}, azimuth 190^{o}. Viewed from latitude 10^{o}, longitude 170^{o}.

[from page 111] establishment of the looping condition in the trajectories. Because of the presentation, in Figures 4.6 to 4.11, of the cut-off data in the form of graphs of cut-off vs azimuth for constant zenith angle, the transition region is greatly exaggerated in apparent width at low zenith angles.

An interesting feature of the fold visible in the south-east at Townsville (and at Rockhampton) is that the main cone curve turns back under itself. Thus, in any direction within a finite range of directions, asymptotic trajectories may originate which correspond to the passage of protons with any one of a number of momentum values. The lower values, by strict definition, should be regarded as penumbral structure. Nevertheless, taken together, these values are part of a smooth bounding main cone cut-off curve, and must therefore be regarded as genuine main cone structure. The Rockhampton 65^{o} zenith angle cut-off data show this effect particularly

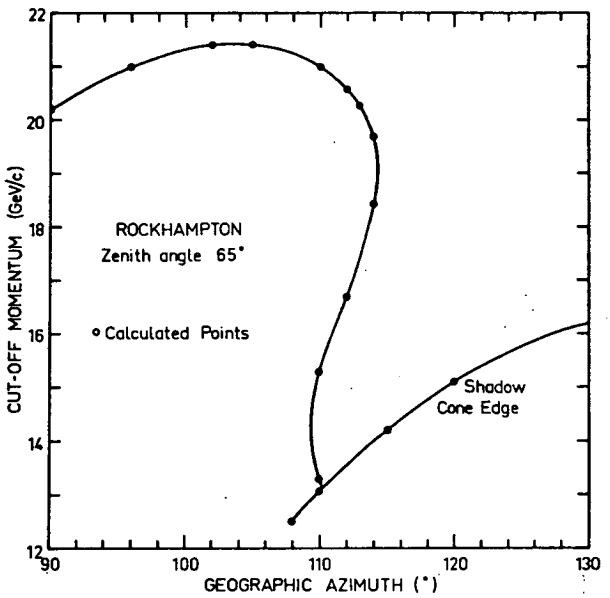

Figure 4.16. Variation of main cone cut-off with azimuth, for 65^{o} zenith angle at Rockhampton. An "overhang" of approximately 5^{o} is visible between 110^{o} and 115^{o} azimuth.

clearly. In Figure 4.16 the calculated cut-off values defining the main cone edge are seen to lie on a smooth curve, in spite of an "overhang" of 5^{o}. Extensive calculations have revealed no trace of penumbral structure in this azimuth range.

Investigation has shown that the mechanism by which the overhang is produced is associated with the exit angle of trajectories from loops. Within a narrow range of azimuths the situation arises where, for decreasing momentum, trajectories, initially unlooped, acquire a loop, the exit angle from which is unsuitable to allow escape from the field. At a lower momentum again the exit direction has rotated to the point where trajectory escape is permitted. On further momentum reduction, the exit angle again becomes unsuited to escape, or in some situations, the lower section of the loop intersects the surface of the earth, giving rise to the shadow cone edge. On either side of the band of azimuths where the conditional trajectory escape occurs, the loop orientation evidently is such as either to allow completely, or to forbid, the escape of these trajectories.

4.8 Latitude Dependence of the Loop Cone

Having discussed in the preceding section the loop cone as observed at Townsville, we now consider the latitude dependence of the loop cone structure. The size of the loop cone is latitude dependent, a small opening angle being found at low latitudes (indeed, it is evident from the results of Lemaitre and Vallarta

[1936], and Daniel and Stephens [1966] that it is non-existent at very low latitudes), with the main cone edge in most directions being formed by unlooped trajectories. With increasing latitude, although the zenith and azimuth angles of the loop cone axis remain sensibly constant (see Table 4.3), the half angle of the cone increases, as illustrated in Figure 4.17, until by mid-latitudes the cone has almost entirely opened out and the main cone edge is formed predominantly by looped trajectories.

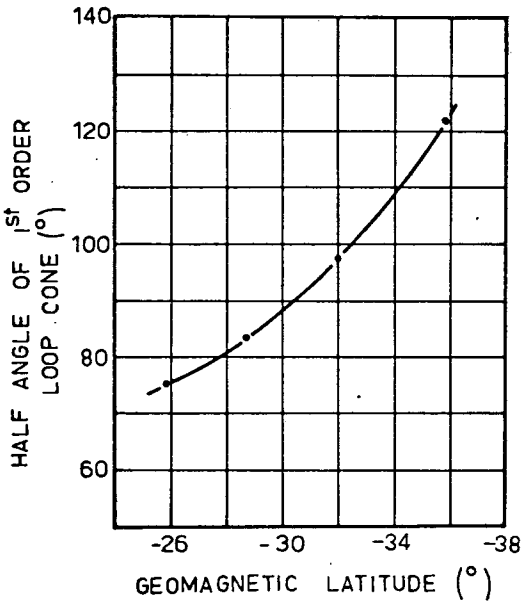

Figure 4.17. Geomagnetic latitude dependence of the first order loop cone half angle, at the longitudes investigated.

At about these latitudes in the Southern hemisphere a further cone is observed to open in the south, distinguishable by the presence of folds in the main cone directional cut-off distribution (as exhibited by the 60^{o} zenith curve in Figure 4.10). This new loop cone contains directions from which doubly looped trajectories originate, whereas outside this cone the main cone edge consists of singly looped trajectories. Figures 4.18 and 4.19 illustrate typical single and double looped trajectories originating at Williamtown. With further increasing

latitude this cone opens and other cones form, containing trajectories with greater numbers of loops again, and evident by the presence of further folds in the main cone cut-off distributions.

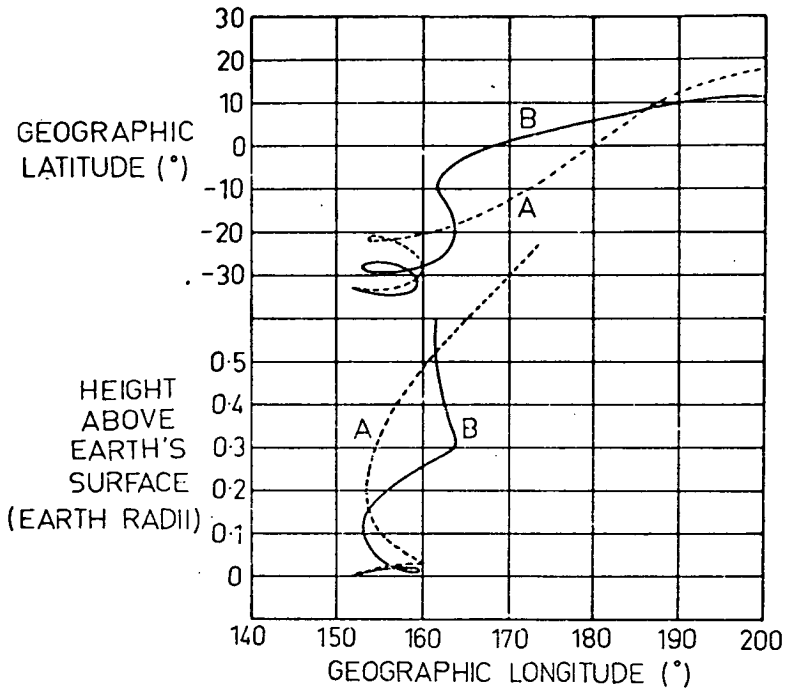

Figure 4.18. Trajectories (plotted as two different projections in upper and lower portions of the diagram) typical of those arriving outside (trajectory A) and inside (trajectory B) the second order loop cone at Williamtown. Trajectory A: 6 GeV/c proton arriving at zenith angle 60°, azimuth 150°; trajectory B: 7.8 GeV/c proton arriving at zenith angle 60°, azimuth 120°.

The systematic trajectory looping responsible for the formation of main cone folding is clearly indicated in the trajectory plots of Lemaitre and Vallarta [1936a, 1936b] [to page 118]

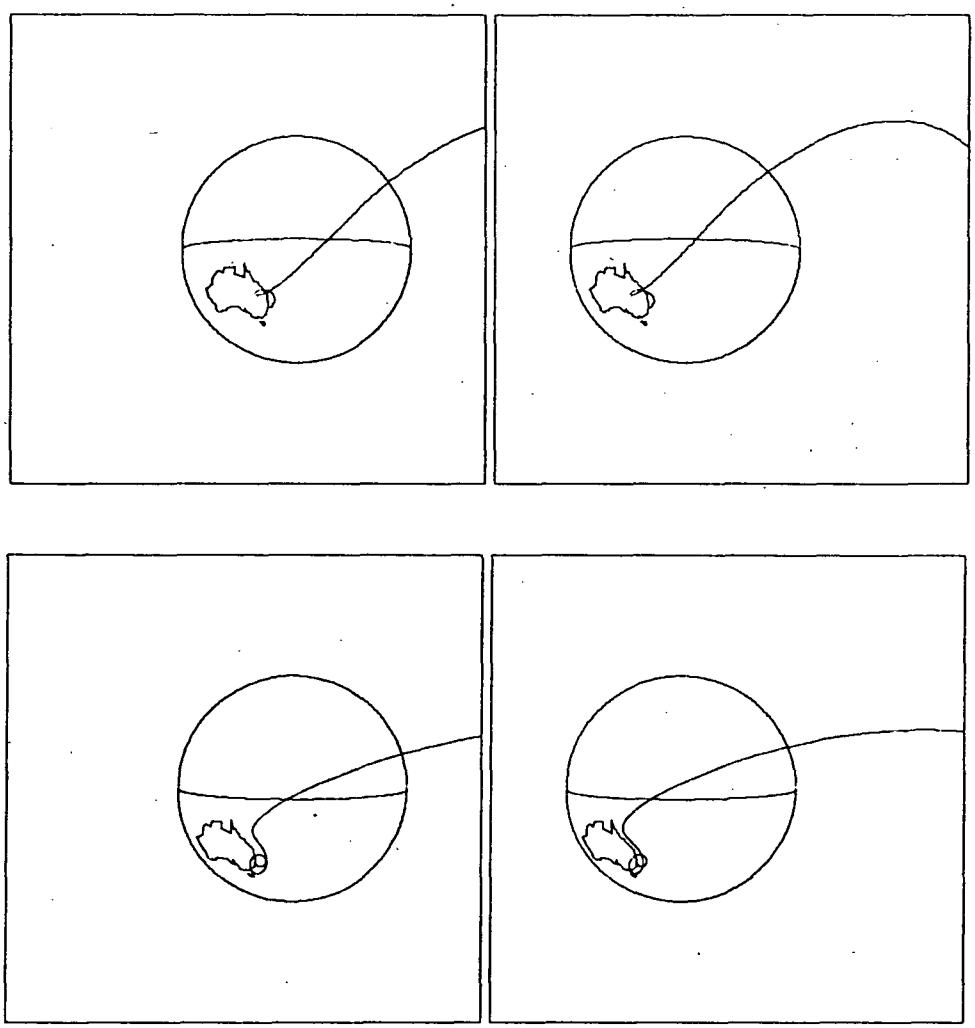

Figures 4.19a (top) and 4.19b (bottom). Stereo pair pictures of singly and doubly looped trajectories characteristic of those arriving outside and inside the second order loop cone at Williamtown respectively. View with prism (see Appendix 2).

Figure 4.19a shows path of a 7.5 GeV/c proton, arriving at zenith angle 60^{o}, azimuth 90^{o}. Viewed from latitude -5^{o}, longitude 170^{o}.

Figure 4.19b shows path of a 6.0 GeV/c proton, arriving at zenith angle 60^{o}, azimuth 150^{o}. Viewed from latitude 5^{o}, longitude 175^{o}.

[from page 116] (see for example, Figure 4.2) by the reversals in the sense of the curvature of the trajectories. Although not indicated in such drawings (which represent the projection of the trajectories onto the moving meridian plane), the trajectories in these sections remain within a relatively narrow band of longitudes, looping around field lines. Particles approaching higher latitude sites, with momenta close to cut-off values, are very closely tied to the field lines, and perform many loops. A typical example of this multiple looping is seen in the Frontispiece to this thesis, a computer drawn stereoscopic representation* of the trajectory of a proton of 4.0 GeV/c momentum approaching Hobart, destined to arrive at a zenith angle of 60^{o} and a geographic azimuth of 180^{o}. In this particular trajectory six loops are clearly visible.

It is precisely because of the close adhesion of low energy particle trajectories to field lines that the "guiding centre" approximation to particle motion in the geomagnetic field may be applied, as, for example, by Sauer [1963] in the determination of high latitude cut-offs.

* As an aid to trajectory visualization in the presently reported investigation, a computer program was developed to allow the preparation of stereoscopic drawings of cosmic ray trajectories by computer. The basic techniques involved are described in Appendix 2. The Frontispiece and Figures 4.12, 4.15, and 4.19 were drawn by means of this program.

At low and mid-latitudes the tying of particle trajectories to field lines is not so complete, because of the considerably higher momentum values involved and the consequent large scale size of the loops. The formation of the folding around the perimeter of the loop cones at such sites is due to the progressive establishment of loops in main cone edge trajectories with increasing latitude of arrival.

That the main cone folding is in fact a genuine main cone structure, rather than a penumbral effect, such as could be produced by the progressive baring of underlying major penumbral bands with increasing latitude, may be shown by reference to the Lemaitre and Vallarta diagrams, Figures 4.2 and 4.3. If the phenomenon were merely penumbral then it would be reasonable to suppose that there exists above the cut-off value within the loop cone a "virtual" main cone edge corresponding to periodic orbit entry via unlooped trajectories. The Lemaitre and Vallarta diagrams clearly show that such an undetected edge cannot exist. In Figure 4.2 it is apparent that trajectories passing through a point above the cusp point at latitude 25^{o} must possess at least one loop (or above 37^{o} two loops). Figure 4.3 shows the locus of the cusp point for changing γ. It is clear that asymptotic entry to the periodic orbits from a point at a latitude greater than approximately 35^{o} in a dipole field cannot occur via other than looped trajectories, and thus the cut-off value associated with the looped trajectories is uniquely the main cone cut-off.

Having illustrated the significance of trajectory looping in the formation of the structure of the main cone edge, we now define the loop cone.

The Loop Cone is the solid angle of directions in which a systematic depression of the main cone cut-off occurs due to the looping of trajectories. The loop cone may be of first or higher order according to the number of loops in the trajectories at the main cone edge within the loop cone.

Table 4.3 lists the angular size and position of the loop cones more readily distinguishable in the cut-off results for the six sites. Although cones of order as high as four are visible, only the first and second order cones are sufficiently well defined to

Table 4.3 Configuration of the local magnetic field at the survey sites, and details of loop cones clearly evident in cut-off data.

Site	Magnetic Dip Angle	Geog. Azimuth of		Loop Cone Details			
		Mag. N. (^{o}E)	Geom. N. (^{o}E)	Order	Half angle η	Inclination of axis ρ	Geom. Azim. of axis λ
Moss.	-43^{o}53'	6^{o}	7^{o}	1	76.5^{o}	-36^{o}	196^{o}
Towns.	-47^{o}57'	7^{o}	7.5^{o}	1	84^{o}	-35^{o}	196.5^{o}
Rock.	-52^{o}56'	9^{o}	8.5^{o}	1	98^{o}	-34^{o}	197.5^{o}
Brisb.	-57^{o}12'	10^{o}	9.5^{o}	1	≈122^{o}	≈-30^{o}	≈200^{o}
Will.	-62^{o}54'	12^{o}	10.5^{o}	2	78^{o}	-23^{o}	204.5^{o}
Lav.	-68^{o}37'	10.5^{o}	9.5^{o}	-	-	-	-

allow estimation of size and position.

Figure 4.20 illustrates diagramatically the intersection of the first order loop cone and the observing hemisphere at each site. The lines representing these intersections indicate the position of the first order folds, in direction, relative to the sites.

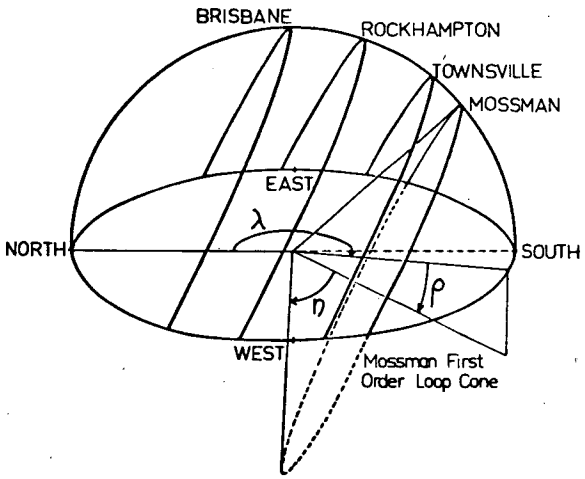

Figure 4.20. Intersection of the first order loop cone and the observing hemisphere at the different sites. The angles η, ρ and λ are used in Table 4.3 to indicate the size and position of the cones.

When the first order loop cone has small opening angle (at low latitude sites, such as Townsville), the differences in cut-off value associated with the folds are large. With increasing opening angle (i.e. with increasing site latitude), the size of the first order folds decrease, until at the latitude of Brisbane and greater, the folds are barely visible in the cut-off distributions.

The higher order folds are of small magnitude, even when the opening angle of the cones is small. Like the first order folds, they evidently tend to decrease in size with increasing opening angle. Save for the second order cone at Williamtown, there is

insufficient information available from the current series of calculations to deduce the accurate size and position of the higher order loop cones. We may, however, infer their behaviour with change in latitude by examining the change in azimuth position of the associated folds at given zenith angles. Figures 4.21a and 4.21b show the observed azimuth bearings of the folds at each site for zenith angles of 60^{o} and 80^{o} respectively. In these diagrams lines have been drawn to indicate more clearly the sequence of opening of the first and higher order cones with increasing latitude. As indicated in Figure 4.21b, small folds are present in the Williamtown and Laverton cut-off data (as displayed in Figures 4.10 and 4.11), associated with cones of order as high as four. In Figure 4.21, too, is to be seen the effect of the shadow cone edge intruding through the main cone edge and obscuring the folds within a certain range of azimuths, as indicated by the shading. The rapid change in position of the eastern edge of this region between Townsville and Rockhampton is due to the effect of the first order cone opening and exposing the underlying shadow cone edge.

From these diagrams it is to be seen that at any particular zenith angle, as the order of the fold increases, there is a slight increase in the rate at which the folds sweep around in azimuth. This tendency is to be expected, since the momentum of the particles moving in trajectories associated with the main cone edge in these directions decreases, and so the dimensions of the loop (its wavelength) will decrease, with a consequent decrease in the rate of

opening of the loop cone.

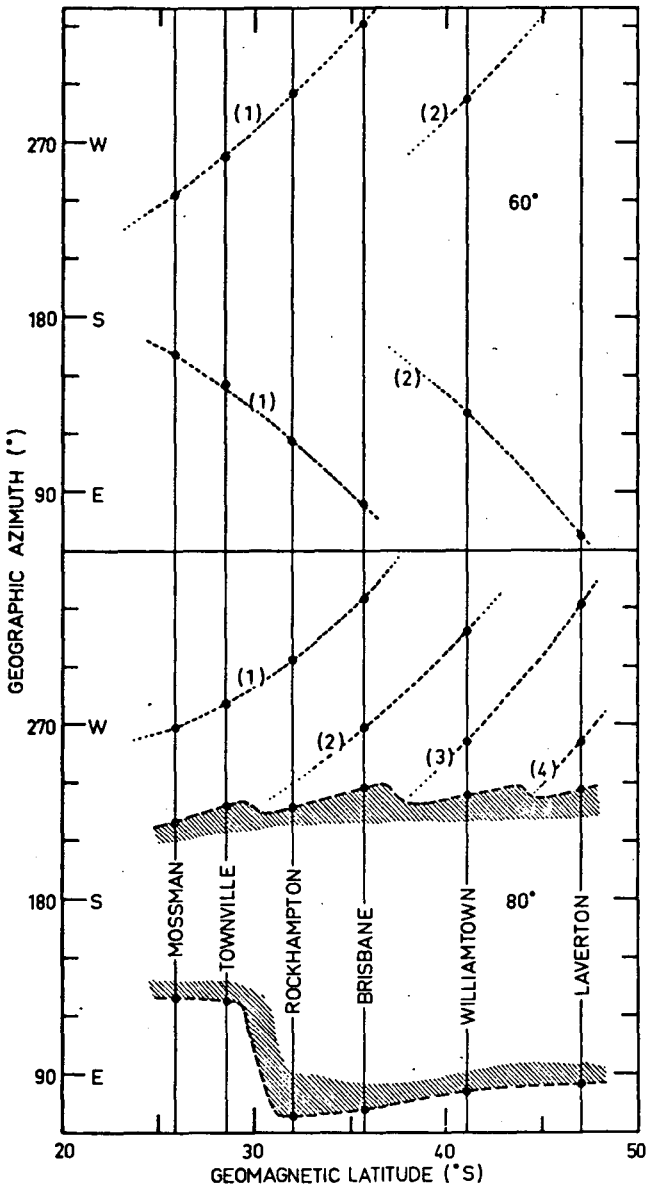

Figures 4.21a (upper part of diagram) and 4.21b (lower part). Observed variation in azimuth position of the main cone folds at 60^{o} and 80^{o} zenith angle respectively. Dashed lines indicate the locus of the folds, of order indicated, with change in latitude.

The magnitude of the cut-off reduction across a fold varies along the perimeter of the loop cone, in addition to the decrease in the average cut-off reduction across the folds with increasing latitude. At low latitudes the folds are of very appreciable magnitude, and reductions of up to 35 % are observed as the first order folds are crossed in the south east at Townsville and Rockhampton (see Figures 4.7 and 4.8).

It was shown, by means of the calculations carried out in Section 4.6 to determine the mean effective cut-offs for the latitude survey detectors, that the loop cone structure could significantly modify the estimates of mean effective cut-offs. On the other hand, to this point in the discussion we have not yet demonstrated the actual observable reality of the loop cone effect. Later in the following section we consider the evidence supporting the assumption of reality.

4.9 Effect of the Loop Cone on Directional Cosmic Ray Intensities

We have the situation where, as opening of the first order cone proceeds with increasing southern latitude, the first order fold, with its appreciable associated cut-off reduction sweeps upwards from the south over observing hemisphere. (Correspondingly, the cones open in the north in the Northern hemisphere.) This phenomenon would be expected to influence significantly the manner in which the directional cosmic ray intensity varies with latitude.

In inclined directions, in particular at high zenith angles,

there is a rapid change in the azimuth position of the folds with latitude ($\approx 7^{o}$ in azimuth per 1^{o} in latitude at a zenith angle of 60^{o}, as shown in Figure 4.21a). This sensitivity suggests that the real field model used in the cut-off computations could be checked in part by the experimental observation of the actual position of the folds at a suitable latitude and zenith angle.

In the vertical direction the movement of the first order fold significantly influences the dependence of the vertical cut-off on latitude. As the first order cone expands, the section of the fold associated with the upper edge of the loop cone passes overhead, producing a distinct reduction in the vertical cut-off. In Figure 4.22, a graph of main cone cut-off vs zenith angle in the

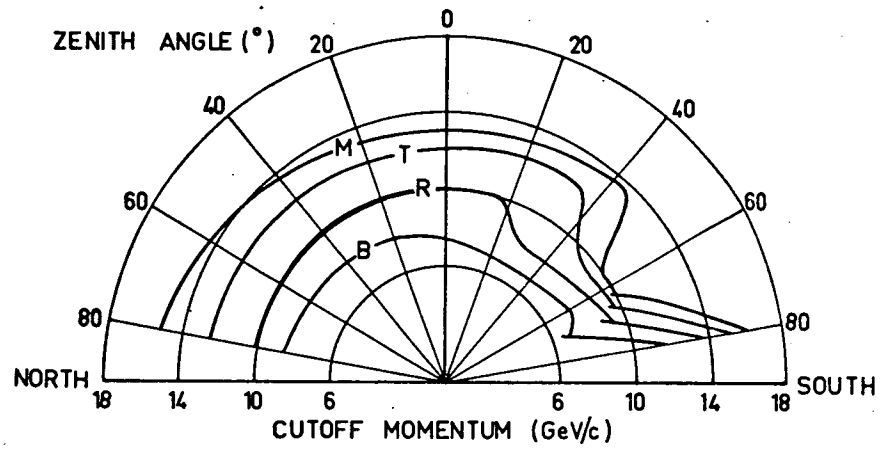

Figure 4.22. Variation of main cone cut-off with zenith angle in the azimuthal plane containing the axis of the first order loop cone. M, Mossman; T, Townsville; R, Rockhampton; B, Brisbane. At 65^{o} zenith angle in the South, the Brisbane curve shows second-order folding.

plane containing the loop cone axis for the four northernmost sites, the movement of the fold with latitude is evident. It is seen to pass the zenith between Rockhampton and Brisbane, and the resultant drop in vertical main cone cut-off is seen in Figure 4.23. The effect is to be observed on a world scale in the graphs of Kondo and Kodama [1965], manifested as the bunching of the lines of equal main cone cut-off at low to mid latitudes (see Figure 4.24, a reproduction of Figure 1 of Kondo and Kodama).

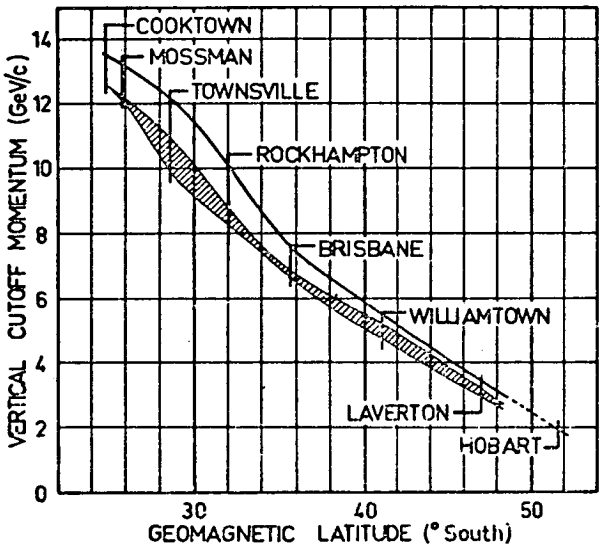

Figure 4.23. Variation of vertical main cone cut-off (uppermost curve) and equivalent penumbra (shaded band) with geomagnetic latitude, in the longitude range of Eastern Australia.

The loop cone would thus be expected to modify the observed variation of counting rate with latitude for a vertically directed detector, but not necessarily to a degree predictable from the vertical cut-off values. At low latitudes a smooth variation of cut-off exists over the observing hemisphere, and it would be expected that both the main cone and effective cut-off values would vary in a reasonably linear manner with mean effective cut-off for a given vertical detector, although not necess-

arily at any point being equal to it. However, in the latitude region where the first order loop cone edge nears the vertical this is not the case, since we have in the fold what may be regarded as an abrupt cut-off discontinuity propagating across the viewing cone. In addition to the main cone structure, the penumbra is similarly dependent on the trajectory looping and would be expected to have an appreciable effect on the latitude dependence of the mean effective cut-off. It is clear that the determination of mean effective cut-offs must incorporate details of main cone cut-off and penumbra at all points inside the detector viewing cone, if observed responses are to be accurately interpreted.

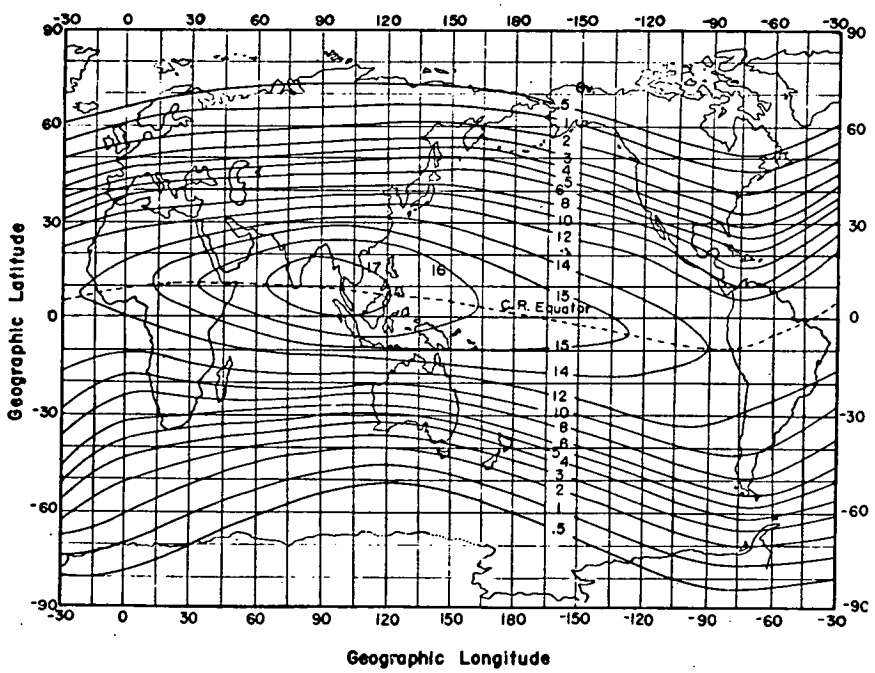

Figure 4.24. Variation of vertical main cone cut-off with geographic latitude and longitude (Kondo and Kodama [1965]).

The data of Carmichael et al. [1968] provide unmistakeable evidence of the loop cone phenomenon. In the analysis of their neutron monitor latitude survey data they find that the calculated vertical effective cut-off values poorly represent the variation of the actual mean effective cut-off with latitude in the region of Mexico City. It is apparent from the manner in which the vertical main cone cut-off varies with latitude that the first order loop cone is well developed at this location, and could be expected to influence significantly the detector counting rate. Carmichael et al. [1968, 1969] have obtained satisfactory ordering of data by the introduction of "geographically smoothed" geomagnetic cut-offs. These smoothed cut-offs, deduced empirically from the experimental data, implicitly take into account the effect on the detector of cut-offs in inclined directions, and so in principle are equivalent to mean effective cut-offs.

Shea and Smart [1970b] investigated the problem of ordering data using estimated cut-off values, and showed that the procedure used to obtain the effective cut-offs (that of subtracting the total width of the allowed bands from the main cone values, neglecting the momentum dependence of the response constants) could not account for the difference between the geographically smoothed and vertical effective cut-off values. Shea and Smart showed that calculated mean effective cut-offs for a neutron monitor in the region of Mexico City (which they refer to as " angular compensated" cut-offs) agreed closely with the geographically smoothed cut-off values of

Carmichael et alia.

A program of investigation was undertaken to make use of the Australian cut-off data in the further study of the problem, particularly as applied to muon detectors, but also to test generally the findings of Carmichael et al., and of Shea and Smart.

4.10 Dependence of Mean Effective Cut-off on Telescope Geometry

Calculations have been made of the mean effective cut-off values pertaining to vertical muon telescopes of various geometries at the six sites for which detailed cut-off distributions have been calculated. The constant cut-off technique, as described in Section 3.4, was employed in these calculations (in conjunction with the integral response functions deduced in later sections of this thesis). In detail, the constant cut-off technique involves establishing the precise form of the integral response function of a detector by determining the detector response in the presence of known cut-off values. It is then possible to interpolate from this function the cut-off value required to give the same response as that calculated to be produced in the presence of any particular cut-off distribution, this cut-off value constituting the mean effective cut-off in the particular situation.

A number of telescope geometries were considered, varying from a very narrow angle detector of dimensions (1 x 1) x 8 units in length, to a wide angle "semi-cube" telescope of dimensions (1 x 1) x 0.5 units in length. The mean effective cut-off values calc-

ulated theoretically to apply to these detectors at the latitude survey sites are plotted as a function of geomagnetic latitude in Figure 4.25.

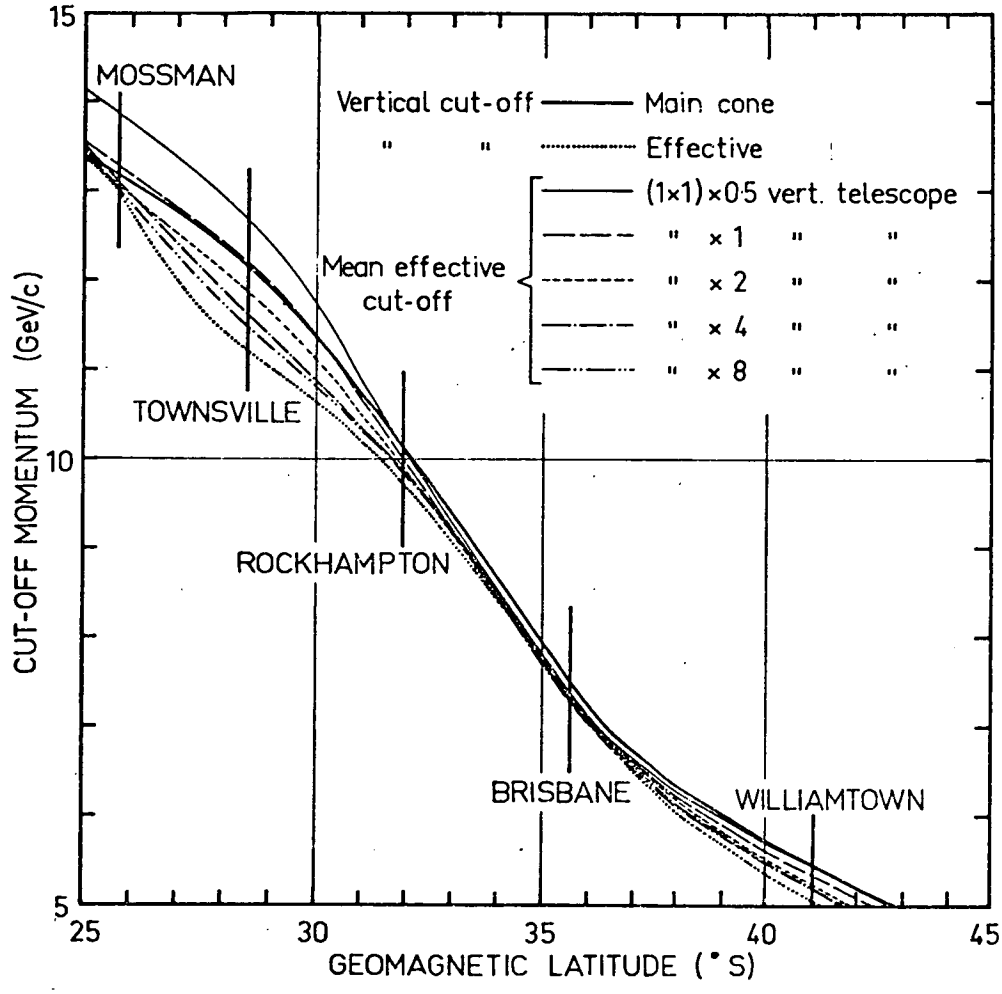

Figure 4.25. Theoretically calculated mean effective cut-offs applying to muon telescopes of various geometries, as function of geomagnetic latitude. The main cone and effective cut-off values in the vertical direction are also plotted.

In this diagram the large range of values of mean effective

cut-off at the sites for detectors of different geometries is immediately obvious, particularly at Townsville and Rockhampton. The mean effective cut-off is evidently a very sensitive function of opening angle at these sites. As expected, the mean effective cut-offs for a very narrow angle detector are very close in value to the vertical effective cut-off values. On the other hand, the mean effective cut-offs for the semi-cube telescope are of considerably greater value than the vertical effective cut-off, with a difference of 1.5 GeV/c, for example, occurring at Townsville. Calculations to test the change in mean effective cut-off for rotation of the squared trayed telescopes about the vertical axis show that a quite negligible variation, of the order of 10^{-4} GeV/c, is produced in the estimate of the mean effective cut-off. (For detectors with rectangular trays an appreciable variation in mean effective cut-off may accompany rotation about the vertical axis. The magnitude of the effect for the vertical latitude survey detectors is still small, nevertheless, at 0.07 GeV/c.)

The situation in the longitude range of Eastern Australia is evidently very similar to that in the region of Mexico City, because of the close similarity between the latitude dependence of the vertical main cone and effective cut-off values in the two regions (compare the cut-offs in Figure 4.26, a reproduction of Figure 2 of Carmichael et al. [1968], with the main cone and effective cut-offs in Figure 4.25).

Carmichael et al. noted that the main cone cut-off values

tended to exhibit the same form of latitude dependence as the geographically smoothed cut-offs pertaining to a neutron monitor, but with a small, nearly constant difference (see Figure 4.26). It is interesting to note in Figure 4.25 that the mean effective cut-off for a telescope of geometry (1 x 1) x 2 units similarly has mean effective cut-off values bearing the same relationship to the vertical main cone cut-off. Evidently there is some sort of equivalence between a telescope of this geometry and a neutron monitor, as far as mean effective cut-off values are concerned.

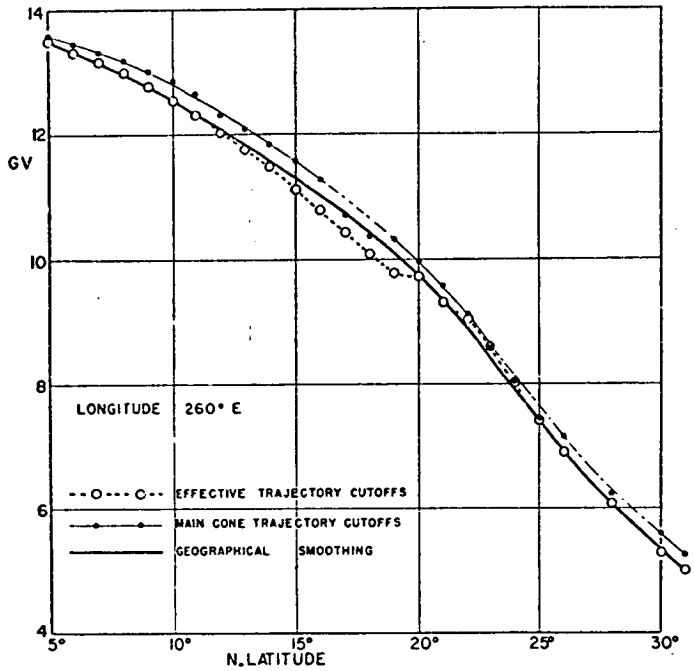

Figure 4.26. Main cone and effective cut-offs in the vertical direction, in addition to the "geographically smoothed" cut-off values, as function of geographic latitude, for longitude 260° (Carmichael et al. [1968]).

A further observation may be made from Figure 4.25. Although a large range in mean effective cut-off values for the different telescopes occurs at most latitudes, at Brisbane the spread is quite small, the total range there being 0.2 GeV/c. This result is not unexpected, since Brisbane lies at a latitude which is just outside the range for which the first order loop cone has an appreciable effect on the directional cut-off distribution, but at a point at which the second order cone is not yet well developed, so that a relatively smooth variation of cut-off exists over the observing hemisphere.

It is of interest to examine the geographically smoothed cut-offs of Carmichael et al. in the light of this observation. It is evident from Figure 4.26 that, as predicted, the effective cut-off and geographically smoothed cut-off have the same value at a point just below the "step" associated with the fold passage overhead.

Obviously there are limitations to the validity of the generalizations to be drawn from observations for any particular longitude range (and indeed hemisphere). Whilst the situation for Eastern Australia and Mexico are evidently very similar, at other longitudes it is possible that significant differences in cut-off dependence on latitude might exist. Carmichael et al. [1969] have published graphs of the geographically smoothed cut-offs in the Northern hemisphere, for longitudes in the range 195 - 285^{o} East. At points west of Mexico, these curves show that the fold passage overhead tends to be associated with higher momentum cut-

off values, and to cause a slightly more abrupt step. It is possible, in this case, that at these longitudes the first order fold may have some effect on the mean effective cut-offs after passing the zenith. This conjecture would of necessity have to be tested by calculation.

The close agreement between the form of the geographically smoothed cut-offs and the angular-compensated cut-offs, on the one hand, and the general nature of the calculated mean effective cut-offs in a similar situation, on the other, strongly supports the validity of the various approaches, and independently the reality of the loop cone phenomenon. It is interesting to conjecture upon the possibility of using observations of the intensity gradients associated with the folds and related penumbral structure to obtain information on the configuration of the geomagnetic field.

4.11 On the Possible Direct Observation of Main Cone Folding

It is obvious, both from the presently reported calculations, and those of Carmichael et al., and Shea and Smart, that whilst a characteristic structure is introduced into the vertical effective cut-off dependence on latitude as a consequence of the movement of the upper edge of the first order loop cone in the region of the zenith, the mean effective cut-off (geographically smoothed cut-off, angular-compensated cut-off) for a wide angle vertical detector has a relatively smooth dependence on latitude.

It is possible that narrow angle detectors could be used to

detect the fine structure in the zenith direction, at longitudes where the effect is most pronounced (for example, at 285° East longitude, for which the vertical effective cut-offs are given by Carmichael et al. [1969], and reproduced in Figure 4.27a). If a sufficiently sensitive experiment could be carried out, then it is conceivable that useful information could be obtained about the geomagnetic field. As noted by Shea and Smart [1970a] and predicted in Section 4.10, the precise form of the mid-latitude cut-off dependence on latitude is evidently appreciably field sensitive.

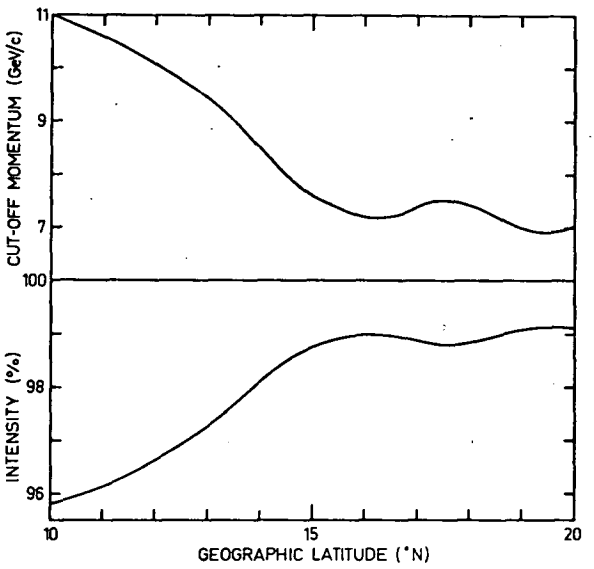

Figure 4.27a (upper part of plot) and Figure 4.27b (lower part). Figure 4.27a shows the variation of vertical effective cut-off, at 285° longitude (Carmichael et al. [1969]). Figure 4.27b shows the calculated relative counting rate of a vertical narrow angle telescope over the same latitude range.

Calculations have been carried out to ascertain the response of a narrow angle telescope to the fine structure exhibited in the vertical effective cut-off latitude distribution at 285° longitude. The expected intensity dependence on latitude is shown

in Figure 4.27b. It can be seen that the slope of the dependence curve changes from 0.8 % per degree to zero within an interval of 1^{o} at 15.5^{o} North latitude. It is possible that by the use of narrow angle detectors this "knee" could be located; however, in practice difficulties would probably be experienced in the removal of atmospheric effects from the observational data.

The sensitivity of this method of locating the fine structure associated with the loop cones is obviously restricted, both by the fact that the change in vertical effective cut-off over this latitude range, although large, is relatively smooth; and by the limitations on the experimental method.

At directions away from the zenith the intensity gradients associated with the first order folding are very much greater than those in the zenith direction, and it is possible that observations at inclined directions might enable the accurate location of main cone folds. An additional advantage of a determination in inclined directions is that the observations necessary for the execution of the experiment may be carried out at a single location, thus avoiding the uncertainties associated with the detailed corrections necessary for the removal of spurious atmospheric effects, for the reasons given in Section 1.3.

Calculations have been carried out to estimate the sensitivity of a determination made using directional muon detectors. Obviously, if the effects of main cone folding are to be seen clearly in the sea level muon intensity distribution then it is desirable that the

cut-off values associated with the main cone folding be as great as possible relative to the atmospheric cut-off (see Section 5.10). A suitable situation exists at Townsville, where cut-off changes of up to 5 GeV/c occur within azimuth ranges of one or two degrees, associated with the first cone edge in the south-east (see for example the cut-off structure at 55^{o} to the zenith, at 152^{o} azimuth in Figure 4.7). It was unfortunate that, at the time when the latitude survey observations were being carried out at Townsville, the cut-off calculations were not sufficiently advanced to allow interpretation of the peculiarities in the cut-off distribution, and no attempt was made to observe the folding experimentally. The observations made as part of the normal program pertain to directions away from the folds, and whilst tending to exhibit general north-south asymmetry, show no direct evidence of folding.

In the absence of suitable experimental observations, calculations have been carried out to explore the practicability of detecting the folding. Calculations have been made of the response of a narrow angle telescope when viewing in directions close to the folds. The detector configuration simulated during the calculations corresponds to a geometry that could be readily obtained in practice, but particularly suited to such observations. This telescope consists of four trays of Geiger counters, each tray being 1 metre square. By connecting various groups of counters in coincidence (assuming 4 cm diameter counters) it would be possible to obtain 36 telescope elements of dimensions (0.330 x 0.084) x 1

metres in length, having a cone of acceptance of $18.5^{o} \times 4.7^{o}$ and total counting rate of 1000/hour approximately (this telescope is illustrated in Figure 4.28). The telescope orientation best suited to the detection of the folds would be obtained by tilting the telescope from the position in which the elements are viewing vertically, to a zenith angle of 55^{o} (so that the long side of the element "fan" beams remain in a vertical plane), and then rotating the telescope about the long axis of the elements by 50^{o} (clockwise rotation when telescope viewed from behind). In this position the long side of the element "fan" beams are able to lie parallel to the expected inclination of the first order folds at zenith angle 55^{o}.

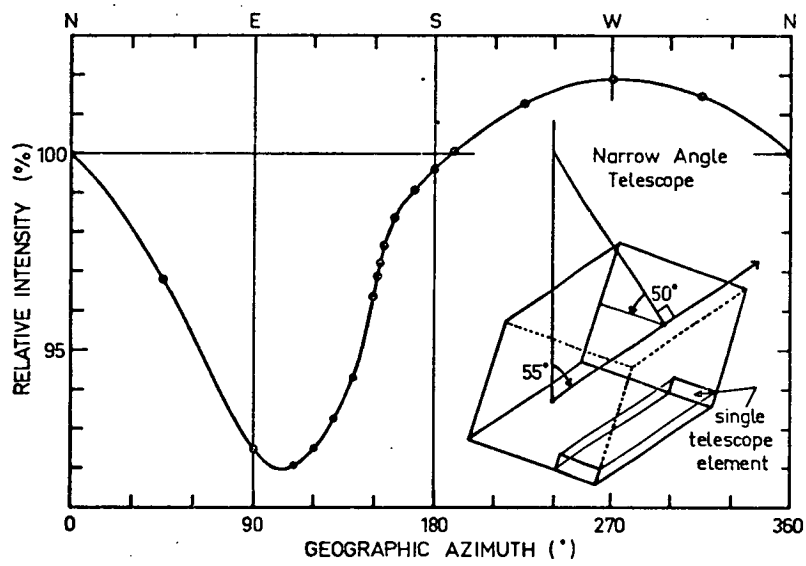

Figure 4.28. Calculated variation of inclined telescope counting rate as function of azimuth at Townsville, for the particular narrow angle detector illustrated. The direction of viewing of the telescope is indicated by an arrow in this diagram.

By varying the azimuth heading of the telescope array within the south-eastern quadrant at Townsville, the structure in the directional muon intensity distribution due to the first order fold could be examined.

In practice, a very useful technique to apply in the analysis of data from this instrument would be that of expressing the narrow angle telescope counting rate as a fraction of the rate of a high counting rate vertical wide angle telescope operating at the same site. It would be possible by this means (for the reasons outlined in Section 2.3) to avoid the uncertainties associated with the detailed correction for atmospheric effects. The dependence of the counting rate of the narrow angle detector on azimuth would be indicated by the form of the inclined/vertical telescope rate ratio.

The expected dependence of muon intensity on azimuth has been calculated, with allowance made for the atmospheric asymmetry effect (discussed in the following chapter), and the results presented in Figure 4.28. This calculation does not take into account the effects of muon scattering, which would, however, not be expected to introduce a systematic shift in the apparent fold position, but would tend to diminish the value of the intensity gradient in the fold direction. The maximum intensity gradient that could be expected in the region of the fold would be $\frac{1}{2}$ % per degree in azimuth, and it estimated that in this case the fold could be located with an accuracy of $\pm 2^{o}$ in azimuth. Taking into account

the rate of change in position of the fold with change in latitude, this accuracy corresponds to an error of $\pm 1/3^{o}$ in latitude.

It appears that this method of locating the main cone folds is capable of greater accuracy than the method described earlier, involving the use of narrow angle vertical telescopes in a latitude survey.

4.12 Sensitivity of Azimuth Position of Fold to Field Changes

A particular advantage in making observations of fold position in inclined directions at a fixed location is that, in principle, it would be possible to detect movement in the position of the fold, if such a shift were to occur in conjunction with perturbations in the geomagnetic field. Such an observation could be effected by directing the fan beam of a narrow angle telescope, similar to that described in the preceding section, to the azimuth at which the intensity gradient is a maximum (in Figure 4.28, 152^{o} azimuth). In this direction the fold shift would be most sensitively indicated by a change in telescope rate. For the dependence of intensity shown in Figure 4.28, a shift of 1^{o} would be accompanied by a $\frac{1}{2}$ % change in intensity. In using this technique, it would of course be necessary to discriminate between changes in detector rate produced by shift in fold position and those resulting from changes in mean primary intensity (the inclined/vertical ratio method of analysis strictly only pertains to conditions of invariant spectrum). In principle, if the multiple telescope segments were to be hodoscoped, then

directions of viewing could be obtained on either side of the fold, allowing the muon intensities to be monitored in these directions.

Having established the general sensitivity of the experimental technique in locating fold position, it is of interest to obtain information about the dependence of the fold position on the configuration of the geomagnetic field, and hence to ascertain whether useful information could be obtained about the field by such experimental observations.

As mentioned previously, the calculations of cut-offs at the latitude survey sites were carried out using the Finch and Leaton [1957] sixth order field coefficients. These particular coefficients were utilized because at the time the computations were made, the Finch and Leaton coefficients were widely used as the "standard" magnetic field model. Whilst for most applications, such as in the calculation of cut-offs in equatorial regions, their use has been shown to produce effective cut-off values essentially equivalent to those derived from other available field models, Shea and Smart [1970a] have shown that in the mid-latitude region the cut-offs are to a degree dependent on the choice of model. This result is not unexpected, since, as was discussed in Section 4.9, the rapid rate of opening of the first order loop cone indicates a great sensitivity to field configuration. Shea and Smart found that, at any particular epoch, the calculated cut-offs were not greatly dependent upon the differences between models (and incidently that sixth and eighth order coefficients yielded

comparable results), but that a time dependence exists in the mid-latitude cut-off values. At Mexico City, Shea and Smart showed that the vertical cut-off has apparently diminished by approximately 1 GeV/c over the past thirty years.

In the presently reported investigation, a limited number of calculations has been carried out using the Jensen and Cain [1962], and Leaton et al. [1965] coefficients, to see if the differences between these models and the Finch and Leaton model could be detected experimentally as changes in fold position. The azimuth position of the eastern section of the first order fold at 60^{o} to the zenith at Townsville and Rockhampton have been calculated, using the different field models. The results are tabulated in Table 4.4.

Table 4.4 Geographic azimuth position of eastern section of first order folds at 60^{o} to the zenith, for various geomagnetic field models.

Site	Model: Epoch:	Finch & Leaton 1955	Jensen & Cain 1960	Leaton et al. 1965
Townsville		147.5 ± 0.25^{o}	147.5 ± 0.25^{o}	148.5 ± 0.25^{o}
Rockhampton		117.2 ± 0.1^{o}	115.75 ± 0.25^{o}	118.0 ± 0.25^{o}

At Townsville the change in fold position is very small, a total of less than 1^{o}. At Rockhampton a greater field sensitivity

is exhibited, the spread in fold positions in this case being about 2^{o}. That a greater sensitivity should exist at Rockhampton than at Townsville is seen to be reasonable when the discussion of Section 4.8 is recalled, in which the increase in rate of opening of the cones with latitude was attributed to the decreasing "wavelength" of the loops. Change in field configuration will obviously produce a larger percentage change in the number of loops traversed in reaching a higher latitude site than a lower. With increasing latitude, however, while the fold sensitivity to field configuration is increasing, the cut-off values and the relative size of the folds are diminishing, and it is unlikely that at higher latitude sites there will be improvement in the ability to detect changes in the geomagnetic field using observations of fold position.

It is to be noted in Table 4.4 that at Rockhampton the fold positions are not continuously displaced in one direction with increasing time. This fact, in conjunction with Shea and Smart's finding of relatively uniform change of cut-off with time at Mexico City, indicates that possibly the cut-offs in the region of Australia were not changing at a uniform rate over the period 1955 - 1965. Alternatively, the result may indicate that, in fact, there are appreciable differences between the predictions of the various models, contrary to Shea and Smart's finding.

In any case, it is apparent that the small shift in fold position, in conjunction with an experimental error likely to be of the

same order of magnitude, render Australia unsuitable as a site for making observations designed to discriminate between the models. At other longitudes, on the other hand, for example in the region of Mexico City, it appears that a greater fold sensitivity to field configuration would exist. A systematic investigation of directional cut-off distributions at such locations would have to be undertaken to test this possibility.

In addition to examining the loop cone dependence on mean field configuration it is of interest to examine the effect that perturbations of the mean field will have on the loop cone structure.

It has been shown that the trajectories associated with the main cone edge at particular sites become progressively more and more tied to field lines as the latitude of the site increases. The loop cone axes at high latitude sites are evidently related to the local field line direction at the site, and it would thus appear that the variation of the field could be manifested as an observable change in loop cone position as indicated by fold measurements, if the direction of the field line at the site changed during a magnetic disturbance. We may readily calculate the order of magnitude of this effect.

During a magnetic storm, typical disturbances to the local field at mid-latitude sites are $\frac{1}{2}$ % in the horizontal component H and 1 % in the vertical component Z (Parkinson, private communication).

Since $\tan I = Z/H$ where I is the dip angle of

the local field,

$$dI = \frac{h\,dZ - Z\,dH}{H^2 \sec^2 I}$$

It is readily shown, for the local field conditions at Townsville and Rockhampton, that such a disturbance will result in a change of 9' arc at Townsville and 1^{o} at Rockhampton. A considerably larger shift would be required to produce detectable changes in fold position, since, at the zenith angle where the folding is most pronounced, at between 50^{o} and 60^{o} to the zenith, because the loop cone axis lies along a line at the same inclination, the folds are disposed normal to the axis about which the tilting occurs, so that the azimuth change in fold position is small. At other zenith angles, although a larger shift in fold position would be expected (up to the full value of the dip angle shift at low zenith angles), because of the small intensity gradients associated with the folds in these directions, experimental observation of changes in fold position would present great difficulties.

It is likely, of course, that additional factors would be involved in the distortion of cosmic ray trajectories during magnetic field disturbances, thus affecting the loop cone structure. For example, a change in the half angle of the loop cone could possibly result as a consequence of fractional change in the number of loops in trajectories associated with mid-latitude sites, because of change in the length of the local field line bundle.

Calculations have been made to determine the order of magnitude

of the change in azimuth position of the first order folds in the presence of two types of magnetic field disturbance:

a) the presence of a storm field, and

b) the magnetospheric cavity distortion due to solar wind pressure on the geomagnetic field.

In order to simplify the calculations, the basic geomagnetic field was assumed to have the form of a simple centred dipole having the components:

$$B_r = -0.62 \cos\theta / r^3$$
$$B_\theta = -0.31 \sin\theta / r^3$$
$$B_\phi = 0 \qquad \text{gauss}$$

The storm field was simulated by the superposition of a linear 100 γ field antiparallel to the dipole field. In this case the total magnetic field has the components

$$B_r = -0.62 \cos\theta / r^3 + 0.001 \cos\theta$$
$$B_\theta = -0.31 \sin\theta / r^3 + 0.001 \sin\theta$$
$$B_\phi = 0$$

The magnetospheric current field was obtained by invoking the expressions developed by Mead [1964]. According to Mead this field may, to a first approximation, be represented by an axial uniform field in conjunction with a component having a constant field gradient along the earth-sun line, represented by the coefficients g_1 and g_2 respectively, where

$$g_1 = -0.2515 / r_b^3 \quad \text{and} \quad g_2 = 0.1215 / r_b^4 .$$

and r_b is a constant representing the distance to the magnetospheric boundary along the earth-sun line, in earth radii (taken in this work to be 10). In this case the total field has the components

$$B_r = -0.62 \cos\theta / r^3 - g_1 \cos\theta - 2\sqrt{3}\, g_2\, r \sin\theta \cos\theta \cos\phi$$
$$B_\theta = -0.31 \sin\theta / r^3 + g_1 \sin\theta - \sqrt{3}\, g_2\, r \cos\phi\, (2\cos^2\theta - 1)$$
$$B_\phi = \sqrt{3}\, g_2\, r \cos\theta \sin\phi$$

For these field simulations the azimuth position of the eastern section of the first order fold at 60° zenith angle has been calculated, for latitudes of 28° and 32° South (corresponding approximately to the positions of Townsville and Rockhampton respectively in the geomagnetic field). The results of these calculations are summarized in Table 4.5.

Table 4.5 Azimuth position of first order fold at 60° zenith angle in the south-east at sites at latitudes 28° and 32° South, in: A, Dipole field; B, Dipole + storm field; C, Dipole + magnetospheric field, with indication of the effect of rotation of the earth relative to the earth-sun line (D).

Field	28°	32°
A	149.9°	123.2°
B	149.8°	122.7°
C	149.8°	122.7°
D	$< \pm 0.02^\circ$	$\approx \pm 0.05^\circ$

It is apparent from these results that the external magnetic field sources exert only a very small influence on the first order folds at these latitudes (implying stability of the first order loop cone in the presence of the external sources). Rotation of the earth inside the magnetospheric cavity evidently produces a minute variation in the azimuth position of the first order folds (the azimuth positions of the folds were not, in fact, located to this accuracy, the small changes were deduced from variation in value of the cut-offs in the region of the folds).

The field perturbations are unlikely to be detectable from observations of fold position in the sea level muon intensity distribution because of the small magnitude of the effect produced. It is conceivable that observations at higher levels in the atmosphere could lead to the detection of changes in the loop cone structure (first or higher order order cones) during magnetic field disturbances.

4.13 Conclusions - Ordering of Latitude Survey Data

The variation of main cone cut-off value and of equivalent penumbral width over the observing hemisphere at six mid-latitude sites has been calculated in detail, and the results presented graphically. Fine structure visible in the results has been studied and found to be due to the loop cone phenomenon, an effect produced by either single of multiple looping of charged particle trajectories in the local longitude region about each site. With increasing latitude

a series of nearly circular cones opens up in the south at Southern hemisphere sites (and in the north at Northern hemisphere locations), the main cone edge within each being associated with trajectories having successively greater numbers of loops. Each loop cone may be distinguished by the presence of main cone folding.

The large magnitude of the cut-off change associated with the first order loop cone edge could be expected to produce appreciable intensity gradients in the sea level directional muon intensity distribution. The loop cone phenomenon may be used to account for the anomalous behaviour of the mid-latitude neutron monitor latitude survey data reported by Carmichael et al. [1968].

The possibility of using directional muon detectors to locate the main cone fold positions, and so to obtain information about the geomagnetic field, has been explored. It is evident that, whilst the fold positions are appreciably dependent on the main field configuration, the external field sources exert a smaller influence on the loop cone structure (the difference in dependence arises because the looping responsible for the structure occurs at relatively low altitudes ($\approx\frac{1}{2}$ e.r.), in regions of the geomagnetic field where external field contributions are small). In the longitude range of Eastern Australia the predicted change in fold position for change in main field configuration is of the same order of magnitude as the likely errors of observation, although it appears that a larger, detectable effect may occur at other longitudes.

It may, in fact, be possible to make use of the stability

of the folds at low and mid latitude sites. In principle, an effective way exists of studying the changes occuring during cosmic ray events (Forbush decreases, energetic flares), in particular differential momentum ranges of the primary cosmic ray flux. These observations could be made by means of pairs of narrow angle detectors viewing in directions either side of large first order folds, making use of the differences in cut-off momentum (up to 7 GeV/c approximately) existing in adjacent directions at low latitude sites.

It is clear, from the results of the present investigation, and from the work of Carmichael et al., and of Shea and Smart, that very appreciable errors may arise out of the use of axial effective cut-offs instead of mean effective cut-offs in ordering cosmic ray intensity data. The calculated mean effective cut-offs for the directions of viewing of the latitude survey telescopes have therefore been used for the purposes of ordering the observational data obtained during the latitude survey.

The ratio data for the telescopes inclined at 22.6^{o}, 45.2^{o} and 67.8^{o} to the zenith are plotted as a function of mean effective cut-off in Figure 4.29. In directions of viewing where the atmospheric cut-off value exceeds the mean effective cut-off, the mean effective cut-off is indeterminate by the methods employed in the current investigation, and so the axial direction cut-offs are used.

Whilst the various sets of data show general agreement in overall slope, the individual sections show peculiarities quite contrary to expectation, in particular, the data for 67.8^{o} zenith angle.

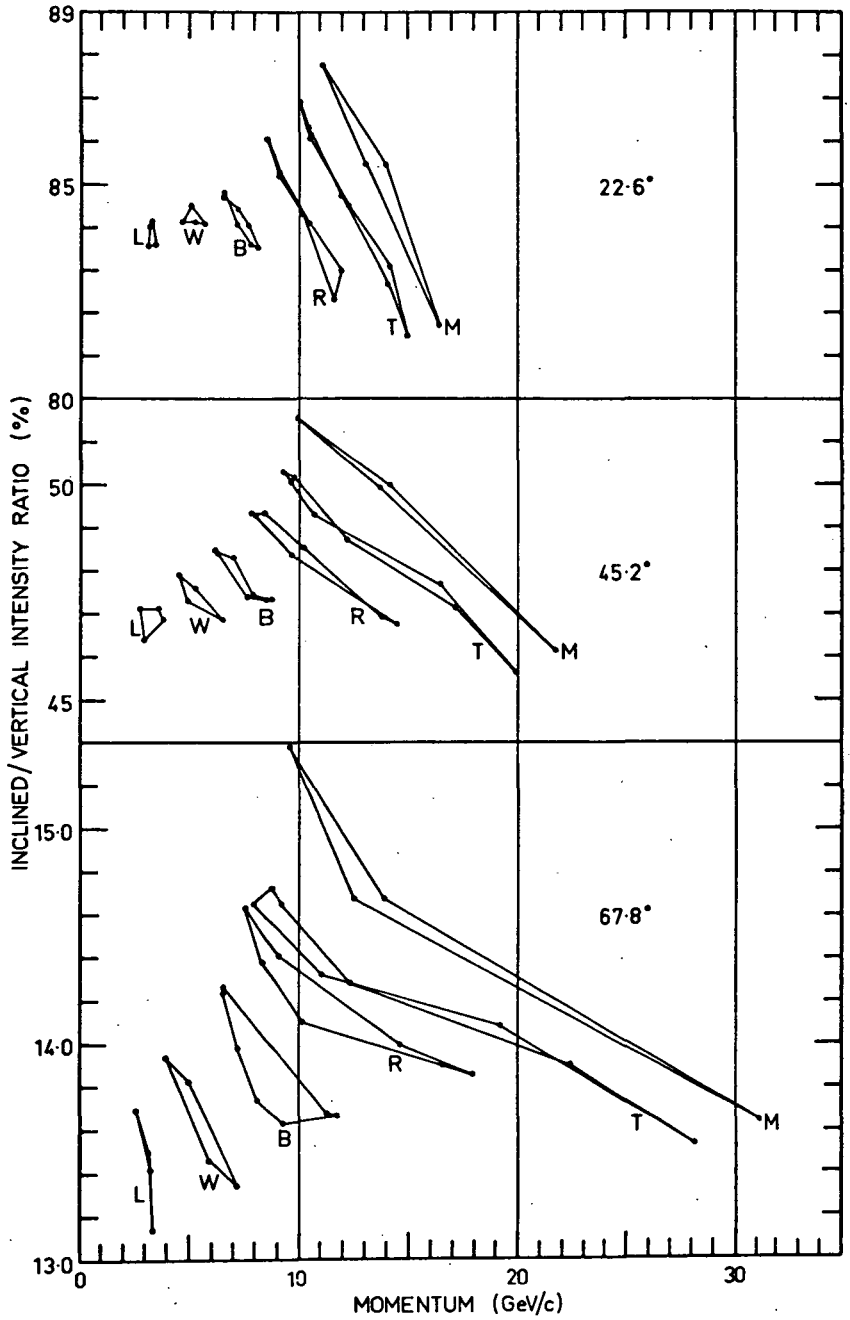

Figure 4.29. Latitude survey data, plotted in the form of rates relative to that of a vertical detector at each site, of detectors inclined to 22.6^{o}, 45.2^{o} and 67.8^{o}, as function of mean effective cut-off momentum in the inclined viewing direction.

The Townsville results, for example, indicate clearly a point of minimum slope at approximately 14 GeV/c, with maximum slope evidently associated with the lowest momentum values, indicating maximum differential response at these low values. The fact that the atmospheric cut-off is approximately equal to the primary cut-off at this point, indicating that the true differential response to the primary flux must be zero, is at first sight disconcerting.

The peculiar form of these graphs is produced as the result of the distortion of the directional intensity distributions at the sites by the atmospheric asymmetry effect - a phenomenon which arises as a consequence of the systematic deflection of muon trajectories by the geomagnetic field. It is apparent that very appreciable corrections must be applied if the distortion exhibited by the momentum-ordered data plots is to be removed.

In order that accurate correction factors may be deduced for this purpose, and in addition that a more detailed general understanding of the effect in various situations be gained, a detailed investigation of the atmospheric asymmetry effect has been carried out. This research is reported in the following chapter.

CHAPTER 5

THE ATMOSPHERIC ASYMMETRY EFFECT

5.1 Introduction

Measurements made with the aid of directional muon detectors reveal the presence of marked azimuthal asymmetries in the sea level directional muon flux, whose magnitude* is zenith angle and latitude dependent. Large asymmetries are observed near the geomagnetic equator, with muon intensities in the west of the order of ten percent greater than those in the east, due to the presence of high value primary radiation cut-offs in the geomagnetic field. As the cut-offs diminish with increasing latitude, the azimuthal asymmetries are observed to decrease. At latitudes beyond the latitude "knee" (at approximately 25^{o} geomagnetic latitude) the cut-offs are reduced to the point where the primary particles within the sections of the primary spectrum removed due to the presence of the cut-offs are incapable of giving rise to muons energetic enough to penetrate the atmosphere and be detected at sea level. Thus, beyond this latitude (actually a small latitude range, due to the difference in knee position at each zenith and azimuth angle)

* The quantitative asymmetry α between the radiation intensities I_1 and I_2, in two directions, is defined as

$$\alpha = \frac{2\,(I_1 - I_2)}{I_1 + I_2} \times 100 \quad \%$$

the geomagnetic cut-offs have no further effect on the sea level muon flux, and it would be expected that, since the primary radiation at these higher latitudes is observed to be sensibly isotropic, azimuthal asymmetry would vanish. Nevertheless, experimental observations show that small but significant azimuthal asymmetries do exist at these higher latitudes.

First observed by Johnson and Street [1933], the presence of a "high latitude" azimuthal asymmetry of the order of one percent was confirmed by the observations of Johnson and Stevenson [1933], Froman and Stearns [1934], and Seidl [1941]. The asymmetry, although of smaller magnitude than those at low latitudes, was shown to be superficially similar, in that the greater intensity was associated with the west, and that the asymmetry increased with increasing zenith angle.

5.2 Theory of the East-West Asymmetry at High Latitudes

Bowen [1934] suggested that directional east-west asymmetry of the muon flux in the atmosphere could arise as a result of the deflection of the muons in the magnetic field, if the numbers of positive and negative muons at production were unequal. The mechanism responsible may be quantitatively considered to operate as follows:

The sense of deflection of positive muons moving in the east-west azimuthal plane is such that a greater depth of atmosphere will be traversed in order to arrive at a particular zenith angle in the east than in the west. The reverse is true for negative muons.

Because there is a preponderance of positive muons, a greater total intensity will be observed in the west than in the east.

Bowen, after demonstrating that muon trajectories opproximate to equi-angular spirals, showed that the zenith angle intensity dependence in the east-west plane could be considered to be rotated through a small angle, and that the resulting intensity differences could account for the observed east-west asymmetry at medium and high latitudes.

Johnson [1941] formulated a considerably more detailed treatment of the asymmetry. He considered that at any point in the atmosphere the intensity of muons of one sign at a particular zenith angle θ in the magnetic east-west plane would be the same as that at the zenith angle $\theta - \delta\theta$ in the absence of energy losses in the air, where $\delta\theta$ is the additional deflection suffered by the muons due to energy loss. Because the normal zenith angle dependence of the total muon intensity in the absence of appreciable cut-offs was known, calculation of the dependence of $\delta\theta$ on muon momentum, followed by integration over the secondary spectrum allowed the mean value of the additional deflection and hence the asymmetry to be deduced. Several simplifying assumptions were made:

a) That the change in muon path length due to the small additional deflection is negligible.

b) That the height-pressure relationship within the atmosphere may be adequately represented by a simple exponential

function.

c) That the secondary spectrum is independent of zenith angle.

d) That the muons lose energy at a constant rate per gm cm^{-2} of air.

e) That the muons move in the magnetic east west azimuthal plane and are deflected in a horizontal magnetic field.

f) That if the muons did not lose energy, no asymmetry would exist.

g) That the ratio of the numbers of positive and negative muons has a constant value, independent of momentum.

Johnson showed that the asymmetry could be represented by an expression of the form

$$\alpha = 2\ \bar{\delta}\ n\ \left(\frac{r - 1}{r + 1}\right)\ \tan\theta$$

where n is the exponent in the empirical function expressing the zenith angle dependence of total muon intensity (see Section 3.3), $\bar{\delta}$ is the mean additional deflection of the muons produced by the energy losses in the atmosphere, and r is the ratio of the number of positive to negative muons.

The asymmetry values thus calculated were shown to give an adequate representation of the available experimental data.

Burbury and Fenton [1952], having access to observational data of greater accuracy (from their work, and that of Fenton and Burbury [1948], and Burbury and McClaren [1952]), introduced certain refinements into the Johnson theory in order to improve the theoretical

asymmetry calculations. They used numerical techniques to facilitate the use of empirically determined data for the representation of the atmosphere, and for the rate of energy loss by muons. Rather than calculating merely the additional deflections due to the energy loss in the atmosphere, they computed the total deflections as they considered that the asymmetry arose as a consequence of these. As a result, their calculated values are significantly greater than corresponding values derived using the additional deflections alone, the disparity arising mainly from the large difference between the total and additional deflections at high muon momenta. Burbury and Fenton showed that their theoretical results gave good agreement with the experimental observations at Hobart and Macquarie Island at zenith angles up to about 60^{o}, but overestimated the asymmetry values at higher zenith angles. They showed that, as predicted by theory, the values of the east-west asymmetry at a given zenith angle are evidently proportional to the horizontal component of the magnetic field, within the experimental errors.

Fenton [1952] examined Johnson's theory with the view of ascertaining the effect of muon decay on the quantitative theoretical results. The original theory of Johnson assumes that the additional deflection of muons due to energy loss merely has the effect of rotating the observed zenith angle dependence of muon intensity through a small, energy dependent angle in the east-west plane, and that it is unnecessary to introduce specific

considerations of the lifetime of the muons. Fenton demonstrated by calculation that, on the assumption that muon production occurs at a single atmospheric level, in the absence of energy loss by muons in the atmosphere an east-west asymmetry will arise of magnitude about half that of the Johnson value at 45^{o} to the zenith, due to the decay of muons. Thus Johnson's assumption that the additional deflection alone produces the asymmetry is not justified. Fenton pointed out that, ideally, integration should be carried out along the actual muon trajectory in order to determine the energy loss and survival probabilities of the muons. Because the means of carrying out the complex associated numerical calculations were not available, it was necessary to follow Johnson, and Burbury and Fenton in resorting to the use of integration along a straight line path to determine the required deflections. Fenton introduced the refinement of the Bethe-Bloch relationship for obtaining the rate of energy loss by the muons, and utilized a zenith angle-dependent secondary spectrum, derived from the vertical sea level muon spectrum of Rossi [1948] on the assumption of muon production at the 100 mb level.

The more detailed theoretical calculations of east-west asymmetry to date, those of Johnson, Burbury and Fenton, and Fenton, are essentially similar, disparities arising out of the use of the additional deflection by Johnson and the total deflection by the other authors, and the degree of refinement in the introduction of the variables into the muon deflection calculations. Several approx-

imations are common to these approaches. Firstly, that the magnetic field is considered to be horizontally directed and of magnitude equal to the horizontal component of the field at any site. Secondly, that the calculation of muon deflection has been carried out by integration along a straight line path of the equation representing the instantaneous curvature of the trajectory. A consequence of the straight line path integration is that the deflection of a positive muon is calculated to be equal in magnitude and opposite in sense to that of a negative muon arriving at the same zenith angle. Thus the resultant asymmetry is predicted to be manifested as an enhancement of the western intensity by an amount equal to the diminuition of the eastern intensity. It is readily apparent, in fact, that the deflections suffered by positive and negative muons in arriving at a particular zenith angle will in general not be the same, because of the difference in path length along the actual trajectories. An accurate theoretical approach, using trajectory tracing techniques as suggested by Fenton, would as a matter of course resolve this difficulty.

In the past most study on azimuthal asymmetry has been devoted to that in the east-west azimuthal plane. This concentration has arisen for two reasons. Firstly, theoretical considerations become relatively simple if the field is assumed to be normal to the plane containing the particle trajectory, as may be done to a first approximation in the magnetic east-west plane. Secondly, azimuthal asymmetries are found to have their greatest magnitude

in directions close to the magnetic east-west azimuthal plane and thus are the most easily observed experimentally. However, the asymmetry in this plane is only one portion of an overall asymmetry affecting all azimuths, produced by systematic muon deflections in the magnetic field. It is desirable to have an understanding of the asymmetry effect at other azimuths.

Fasoli et al. [1957] carried out theoretical calculations of low momentum ($\leq$ 2 GeV/c) muon intensity dependence on azimuth in the presence of a horizontal magnetic field. Their approach was essentially similar to that used in the earlier east-west asymmetry calculations of Johnson, Fenton, and others. For example, total muon deflections were calculated by analytical integration of expressions representing the instantaneous curvature of the trajectories, along straight line paths. Like the earlier work, too, a constant charge ratio value was utilized, and muon decay was not considered. Their final theory is more genral, however, as it applies to all azimuths. Because of the assumption of a horizontal magnetic field, the theory predicts an intensity distribution symmetrical about the magnetic east-west azimuthal plane, and as a consequence of the straight line path integration, the eastern intensity diminuition is equal in magnitude to the enhancement of the western intensity. Fasoli et al. found that their experimental observations exhibited agreement with the theoretical predictions, and claimed that the assumption of a horizontal magnetic field was acceptable.

Contrary to the findings of Fasoli et al., it may readily be shown that a north-south asymmetry can arise at sites where a vertical magnetic field component exists.

5.3 The North-South Asymmetry at High Latitudes

That a north-south asymmetry should exist may be seen by considering the situation at, say, a southern hemisphere site for which the local magnetic field line is inclined in the magnetic north at a zenith angle θ. Secondaries approaching from the north at this zenith angle will be travelling along field lines and so will be undeflected. Those approaching from the south, on the other hand, will be crossing field lines and consequently will be deflected. The slight additional energy loss and increased time of flight will reduce the southern intensity relative to that from the north. In contrast to the east-west asymmetry effect, the north-south asymmetry is produced independently of the magnitude of the charge ratio. In the northern hemisphere the asymmetry would, by its nature, be expected to have opposite sign (i.e. a southern excess) to that in the southern hemisphere, as the field lines are there inclined in the south.

The existence of a significant north-south asymmetry at high latitudes was demonstrated by Burbury and McClaren [1952]. In an experiment carried out at Hobart they found an asymmetry of approximately half the magnitude of the east-west asymmetry at 45^{o} zenith angle. Burbury [1952] presented a theoretical treatment of the

effect in which he showed that the north-south asymmetry could be represented as

$$\alpha_{ns}(\theta) = \frac{2\,(\cos^{2.2}\bar{\delta}_n - \cos^{2.2}\bar{\delta}_s)}{\cos^{2.2}\bar{\delta}_n + \cos^{2.2}\bar{\delta}_s}$$

where $\bar{\delta}_n$, $\bar{\delta}_s$ are the mean deflections of particles arriving from the north and south at the particular zenith angle θ. Muon deflections calculated in the same way as by Burbury and Fenton [1952] in their study of the east-west asymmetry were used in the asymmetry calculations, which were shown to predict satisfactorily the observed asymmetry at Hobart.

Certain measurements of the north-south asymmetry at higher latitudes reveal that the observed asymmetries are markedly different from the theoretical values. Hovi and Aurela [1961] experimentally measured the north-south asymmetry at a geomagnetic latitude of 58° north and compared the result with values calculated from Burbury's theory. The experimental value was shown to be significantly greater than predicted (i.e. a higher intensity from the south than expected), and they concluded that the discrepancy was produced by anisotropy in the primary radiation.

It is interesting to bear this result in mind when considering the results of an experiment conducted by the author at Mawson. This investigation, reported in detail by Cooke [1965], is briefly described here.

5.4 Investigation of the Azimuthal Asymmetry Pattern at Mawson

During the period July 1963 to January 1964 inclusive, observations were carried out to investigate the dependence of muon intensity on azimuth at Mawson (Geographic coordinates $67^{o}36'$ S, $62^{o}53'$ E, Geomagnetic coordinates 73^{o} S, 103^{o} E). Measurements were made at equally spaced azimuths using high counting rate telescopes inclined at 45^{o} to the zenith. The telescopes, described in detail by Parsons [1957], were a "wide angle" telescope of dimensions (1 x 1) x 1.5 m. long, and a "narrow angle" telescope, (0.4 x 0.4) x 1.5 m. long.

The azimuthal asymmetry pattern was deduced, by calculating the asymmetry between the muon intensity at each azimuth to that in the geomagnetic west. The resultant asymmetry pattern is presented in Figure 5.1. Analysis of the data for each individual month revealed that no appreciable secular change occurred in this distribution over the six months observing period, although marked short term variation was observed. In particular, on September 23rd 1963, the east-west asymmetry changed sign during a Forbush decrease to become negative (i.e. an eastern excess).

The expected east-west and north-south asymmetries were calculated using the theoretical results of Burbury and Fenton [1952], and Burbury [1952]. The east-west asymmetry values for several zenith angles were obtained by multiplying the asymmetry values, calculated for Macquarie Island by Burbury and Fenton, by the ratio

of the horizontal field components at the two sites. Similarly the north-south asymmetry values for several zenith angles were obtained using the formula of Burbury. The asymmetry values for these zenith angles were then used in conjunction with the telescope radiation sensitivity differential values for the same angles as derived by Parsons [1959], to obtain weighted mean estimates of the expected asymmetry values at Mawson. The experimental and theoretical east-west and north-south asymmetries, together with the estimated errors in the interpolated experimental values, are given in Table 5.1.

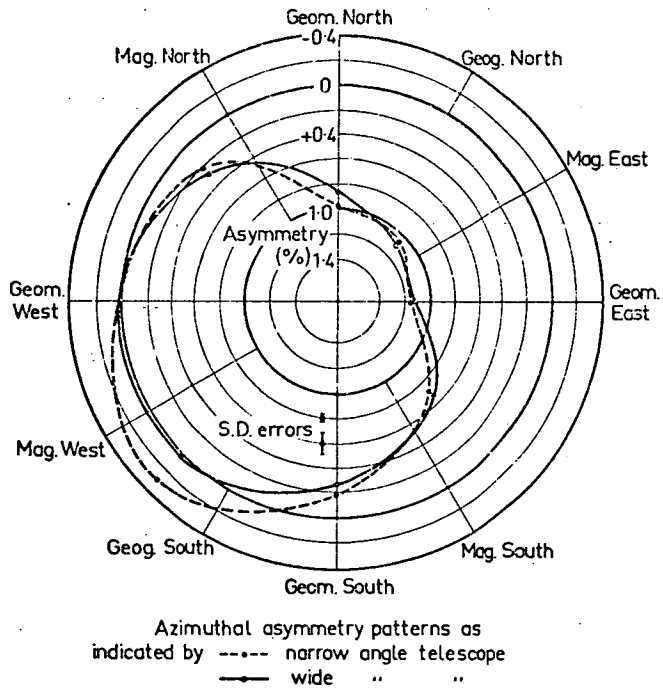

Figure 5.1. Experimentally determined azimuthal asymmetry pattern at 45^{o} zenith angle at Mawson. The intensity in the geomagnetic west used as reference in calculating asymmetry values.

Table 5.1 Comparative experimental and theoretical values of magnetic east-west and north-south asymmetries at Mawson, as observed by the inclined "wide angle" telescope.

Azimuthal Plane	Asymmetry Value (%) Experimental	Theoretical
East-west	1.16 ± 0.03	0.90
North-south	0.00 ± 0.05	0.68

Whilst the theoretical east-west asymmetry value is in reasonable agreement with experiment, there is marked disagreement for the north-south asymmetry. The low experimental value of north-south asymmetry corresponds to a higher value of southern intensity than expected relative to that in the north. To check that geomagnetic cut-offs were not responsible for this result the cut-off calculations of Kasper [1959] were consulted to find if the cut-offs in any direction at a site with the geomagnetic latitude of Mawson could exceed the atmospheric cut-offs. It was apparent, however, that in all directions the geomagnetic cut-offs are ineffective, and this source of perturbation of the azimuthal asymmetry pattern had to be discounted.

Parsons carried out an experiment at Mawson, in 1956, in which the wide angle telescope, described earlier, was used to investigate the daily variation in the muon component at four azimuths - geomagnetic east, south, west and north. The intensity

data, as published by Parsons [1960], although relating to directions too widely spaced in azimuth to allow estimation of the precise value of the magnetic east-west and north-south asymmetries in 1956, nevertheless support the general intensity distribution as observed in 1963, and tend to indicate a low value of the north-south asymmetry. Thus the apparent southern excess of radiation at the top of the atmosphere appears consistent.

5.5 Evidence for Primary Anisotropic Contributions to Azimuthal Asymmetry

As noted in Section 5.3, Hovi and Aurela [1961], in their experiments at a high northern latitude, also found an apparent southern excess of primary radiation. The similar findings from both north and south hemispheres could be explained by the presence of a steady primary anisotropic component, with southern intensities higher than those from the north, such as could be produced by a density gradient of cosmic ray intensity normal to the ecliptic plane. Accurate investigation of the problem would require precise knowledge of muon coupling coefficients and asymptotic directions of approach of trajectories pertaining to the two sites, in order that the asymptotic cones of viewing of the detectors could be derived.

The presence of primary anisotropy is also indicated by the variability in the magnitude of the east-west asymmetry with time at high latitudes. Temporary, short period fluctuations are obs-

served during, for example, Forbush decrease events, and appreciable secular changes are observed over longer periods.

Jacklyn and Fenton [1957] observed changes in the east-west asymmetry at Hobart over the period 1947-1956, in which the magnitude of the asymmetry varied by a factor of three, apparently correlated with relative sunspot number. They considered the factors contributing to the atmospheric asymmetry to find if these could be responsible for significant asymmetry changes in the presence of primary isotropy. Since the horizontal magnetic field change associated with field disturbances is normally less than one percent they reasoned that the asymmetry could not change by more than approximately one percent, whilst primary spectrum changes would have to be drastic to produce significant effects. They concluded that variable primary anisotropic components were responsible for the observed asymmetry variability.

Jacklyn [1959a] reported significant recurrence tendencies in the east-west asymmetry data from Mawson, with evidence for a 27-day type of intensity variation. He suggested that unipolar magnetic disturbances on the sun were responsible for the effect. Stensland [1965] also found marked recurrence tendencies in muon intensity data recorded at Malmberget, Sweden, which were evidently related to the passage of active areas across the disc of the sun.

Forbush decreases are normally accompanied by small asymmetry changes (Jacklyn [1959b]), although occasionally very large changes are observed, in which the east-west asymmetry is depressed for a

period of one or more days. Sometimes an eastern excess of intensity is observed. Both Jacklyn and Stensland reported a large effect during the cosmic ray storm of July 1959, whilst, as reported in the preceding section, one occurred in September, 1963. Jacklyn investigated the phenomenon and concluded that factors contributing directly to the atmospheric asymmetry production could not be responsible for the changes. He suggested that a mechanism operated which tends to reduce the intensity of protons reaching the earth from directions at right angles to the ecliptic plane, relative to the intensity closer to the plane. The asymptotic cones of west pointing telescopes at high southern latitudes lie close to the south polar axis, whilst the asymptotic cones of east pointing telescopes lie close to the equatorial plane. Jacklyn proposed that ecliptic latitude dependent hardening of the primary spectrum could occur during a Forbush type event, which would be manifested as a decrease in east-west asymmetry, as the result of the anisotropy produced in the distribution of primaries at the top of the atmosphere. (The magnitude of the anisotropy responsible for any particular asymmetry change is not necessarily large, as the asymmetry is very sensitive to departures from primary isotropy. A change of 100 % in a directional asymmetry of one percent may be brought about by an increase of only one percent in the intensity in one direction.)

It is to be expected that the maximum sensitivity of asymmetry measurements to primary anisotropy would occur at high latitudes,

since it is there that the most distinct separation of the cones of viewing of detectors "looking" towards opposite azimuths occurs. At lower latitudes the geomagnetic field the geomagnetic field tends to exert a greater influence on the primary particle trajectories, resulting in the tendency for the predicted asymptotic cones of viewing to merge. Thus the anisotropy of the primaries would, if present, affect asymmetry measurements less and less with decreasing latitude, and for this reason, together with the fact that the magnitude of the atmospheric asymmetry increases appreciably with decreasing latitude, the observed azimuthal asymmetry would be expected, in the absence of appreciable geomagnetic cut-offs, to correspond more and more to those calculated from a knowledge of the atmospheric asymmetry effect, on the assumption of primary isotropy. Removal of the lower energy particles by the action of the cut-offs would, in any case, tend to decrease the sensitivity of the total sea level muon intensity to primary anisotropies. For this reason, too, it could be expected that the magnitude of the atmospheric asymmetry at low latitudes would be adequately predicted by calculations carried out on the assumption of primary isotropy.

5.6 Aims of the Present Atmospheric Asymmetry Investigation

Ample evidence exists to verify the operation of the atmospheric asymmetry mechanism as proposed by Johnson, despite the possible confusion at high latitudes with asymmetry components

produced by primary anisotropies. It should be borne in mind that the object of the current study is not merely to examine the atmospheric asymmetry effect as an isolated phenomenon. If accurate investigations are to be carried out on the effects of the geomagnetic field on the primary cosmic radiation (one of the objects of this thesis), and the primary solar and siderial anisotropies, then it is necessary to establish by theoretical study the nature of the atmospheric asymmetry effect, in order that data from directional muon intensity studies at any latitude may be corrected to remove the effects of the overlaid atmospheric asymmetry.

Evidence of the co-existence of the atmospheric asymmetry and the asymmetry produced by geomagnetic cut-offs at mid to low latitudes is distinct in the latitude survey data. From a graph of the observed east-west asymmetry at three zenith angles as a function of geographic latitude (Figure 5.2), it may be seen that the curves each exhibit a very distinct, abrupt change of slope. This discontinuity occurs at the point where, with decreasing latitude, the eastern geomagnetic cut-offs have reached a value where they are able to influence significantly the directional muon intensity at sea level, adding to the asymmetry already present as a result of the atmospheric asymmetry effect. The position of the changes of slope correspond to the latitude "knee" at eastern azimuths for these particular zenith angles.

The effect is equally as clear in the published results of Dorman et al. [1967], who, apparently not aware of the atmospheric

asymmetry mechanism, interpreted their data in terms of geomagnetic cut-off action alone.

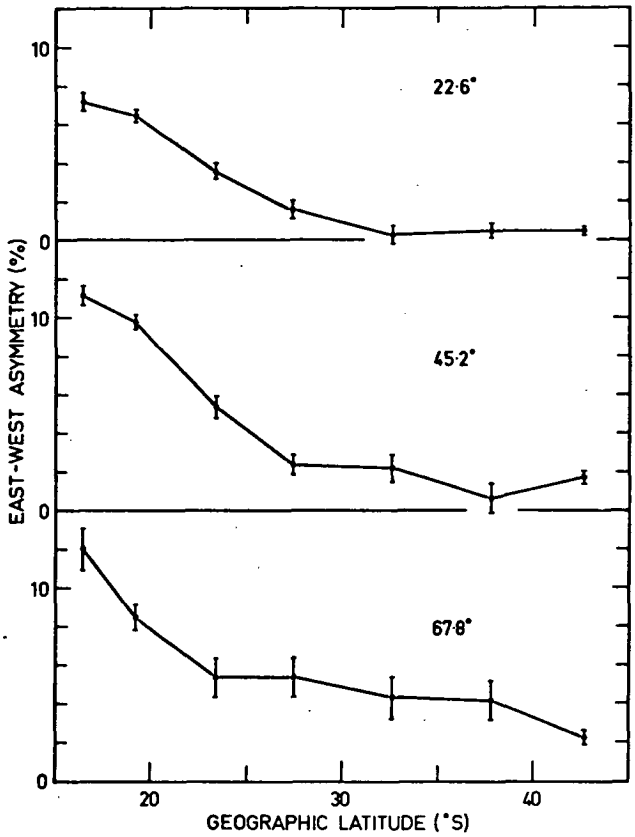

Figure 5.2. Dependence of east-west asymmetry on geographic latitude, as measured by telescopes inclined at three zenith angles during the latitude survey.

At very low latitudes, although the change in secondary spectrum due to the presence of primary cut-offs would be presumed to modify the atmospheric asymmetry, there is no reason to suppose that the asymmetry is of negligible magnitude. In spite of this, most investigators, in interpreting the results of observations

with inclined telescopes at low latitudes, have assumed that azimuthal asymmetries arise solely because of the action of the geomagnetic cut-offs. The unfortunate choice of the name "high latitude" asymmetry may have been partly responsible for this oversight, as it tends to imply that the phenomenon affects only observations at high latitudes.

Kane [1962] pointed out that interpretation of low latitude azimuthal intensity patterns in terms of cut-offs alone was not satisfactory, following attempts to derive directional muon coupling coefficients from a number of sets of directional intensity data published by other authors. It is evident that both the presence of the atmospheric asymmetry effect, and poor statistics, were responsible for the lack of success.

The only workers to be fully aware of the atmospheric asymmetry effect at low latitudes appear to have been Harris and Escobar [1955, 1956], who showed, by the use of theoretical calculations based on the production spectrum of Olbert [1954], that the observed east-west asymmetry in the low momentum muon component at the equator consists of both primary and secondary effects.

In the current general investigation of the atmospheric asymmetry effect, it will obviously be necessary to introduce geomagnetic cut-off as a variable. Precise knowledge of the behaviour of the total intensity with cut-off implicitly assumes the availability of muon coupling coefficients (through the integral response functions), even though, in fact, the atmospheric asymmetry effect is being

investigated primarily in order that accurate coupling coefficients may be derived. This situation can be unambiguously resolved, as will be shown in Chapter 6, and for the purposes of this investigation we anticipate the result and use the final estimated muon response functions.

We now undertake a detailed examination of the atmospheric asymmetry effect, to determine the dependence of the azimuthal asymmetry pattern on zenith, azimuth, cut-off, magnetic field strength and orientation, altitude and atmospheric structure. The complexity of the asymmetry calculations, when considerations such as the determination of muon trajectories are introduced, has necessitated the development of the problem in a form suitable for computer solution.

5.7 Theoretical Investigation of the Atmospheric Asymmetry Effect

5.7.1 Introduction of the Asymmetry Function

We treat as separable effects the atmospheric asymmetry effect and the basic directional muon intensity distribution due to the presence of the atmosphere and geomagnetic cut-offs.

If, in the presence of a magnetic field in the atmosphere, a certain directional intensity distribution $I(\theta,\phi,P_c,x,\underline{B})$ is observed at an atmospheric depth x, then the directional distribution that would be observed in the absence of the magnetic field may be represented as

$$N(\theta,P_c,x) = I(\theta,\phi,P_c,x,\underline{B})\ A(\theta,\phi,P_c,x,\underline{B})$$

where θ, ϕ are zenith and azimuth angles respectively, P_c is the primary cut-off momentum, and $\underline{B}$ the magnetic field.

The dimensionless function A is a quantity we call the **asymmetry function.** In principle, experimental muon intensity data may be corrected to remove the effects of the atmospheric asymmetry if theoretical knowledge of the values of the asymmetry function **(asymmetry factors)** pertaining to the given conditions is available.

In the present investigation it is desirable that the dependence of the asymmetry function on the various parameters be investigated in detail sufficient to allow the deduction of values of the asymmetry factor applying to any given set of conditions, in particular so that the latitude survey data may be corrected.

5.7.2 Determination of Secondary Spectra

A basic requirement for investigating the atmospheric asymmetry is the knowledge of the spectrum of the muons on arrival at the observing point. Essentially, the investigation involves calculating the perturbations of the muon spectrum due to variation of the parameters of interest in the problem. Having determined the modified spectrum, the directional muon intensity may then be obtained by integrating over the spectrum.

In order to determine the secondary spectrum we have utilized the production spectrum of Olbert [1954], modified in several respects to render it more suitable for use in the present calculations. Olbert, using a technique originated by Sands [1950], derived an

empirical muon production spectrum expressing the production rate of muons by primary cosmic rays at any level in the atmosphere. This spectrum may be used in conjunction with expressions representing muon survival probability and proton intensity to obtain the contribution to the vertical muon intensity at any observing level from any higher levels in the atmosphere. Integration over all contributing levels allows the differential intensity to be obtained, and a further integration over any particular momentum interval yields the total vertical muon intensity within that interval.

The Olbert theory assumes that, because of the extremely short lifetime of the pions, the muons are produced in the initial proton interaction. The process of muon production, and the subsequent passage through the atmosphere is assumed to be one-dimensional. Olbert justified the one-dimensional treatment of the muon production by showing firstly that experimental evidence indicated good collimation of the muon beam relative to the direction of motion of the parent proton for muon momenta in the range of interest, and secondly that the mean square angle of scattering of muons in the atmosphere is negligible.

Harris and Escobar [1955, 1956] found it necessary to introduce a small empirical correction into the Olbert theory to account for discrepancies they found in the sea-level muon flux for muon momenta at production of approximately 3.4 GeV/c. Our work involves mainly calculations corresponding to appreciably higher

momenta than this, and accordingly we feel justified in following Olbert and using the one-dimensional model. That the results of the calculations satisfactorily represent reality is demonstrated in Section 5.9.

According to Olbert, at a latitude λ the vertical differential intensity of muons with residual range R at a level s in the atmosphere may be expressed as

$$I(R,s,\lambda) = \int_0^s G(R',\lambda)\ e^{(-x/L)}\ w(x,s,R)\ dx$$

where w is the survival probability of a muon of range R' produced at the atmospheric level x arriving at the level s. L is the mean free path for absorption of protons in air (taken by Olbert to be 120 gm cm^{-2}), and $G(R',\lambda)$ is the production spectrum, where

$$G(R',\lambda) = \frac{7.3 \times 10^4}{[H(\lambda) + R']^{3.58}} \quad gm^{-2}\ cm^2\ sec^{-1}\ sterad^{-1} \qquad (5.1)$$

where H is a latitude dependent constant.

We assume (following Kraushaar [1949]) that at a zenith angle θ the differential intensity may be expressed as

$$I(R,s,\lambda,\theta) = \int_0^s G(R',\lambda)\ \frac{e^{(-x/L\cos\theta)}}{\cos\theta}\ w(x,s,R,\theta)\ dx \qquad (5.2)$$

In the absence of a magnetic field in the atmosphere the muons are not deflected, and the evaluation of this integral is carried

out over a straight line path at a constant zenith angle. The total muon intensity may then be found by integration over all ranges in the given direction, i.e.

$$I(s,\lambda,\theta) = \int_0^\infty I(R,s,\lambda,\theta)\, dR$$

In our calculations it was found most convenient to use muon momentum P as the variable rather than range R, so the empirical range-momentum relationship quoted by Olbert [1953] as being accurate for momenta up to approximately 14 GeV/c was employed to effect the conversion. This relationship is

$$R = \frac{53.5\ P}{2.07\times10^{-3}\ P + 0.10573} - 56 \quad \text{gm cm}^{-2} \tag{5.3}$$

assuming the muon mass to be 207 x electron mass, and where P is in GeV/c.

In terms of momentum, then, the total intensity of muons in any direction is represented by the following expression

$$I(s,\lambda,\theta) = \int_0^\infty \int_0^s G(P',\lambda)\, \frac{e^{(-x/L\cos\theta)}}{\cos\theta}\, w(x,s,P,\theta)$$

$$\frac{5.6566}{(2.07\times10^{-3}\ P + 0.10573)^2}\, dx\, dP \tag{5.4}$$

where P' is the muon momentum at the level x in the atmosphere. The intensity has the units particles per cm^2 per

steradian per second.

5.7.3 Production Spectrum Dependence on Geomagnetic Cut-off

5.7.3.1 Dependence as Predicted by Olbert

In the production spectrum (equation 5.1) Olbert used the constant H to introduce the latitude (cut-off) dependence. He estimated the form of the dependence by using the best information available at the time, and this relationship was subsequently confirmed and extended by Harris and Escobar [1955]. From Olbert's graph of the variation of H with latitude, it is evident that a sensibly linear relationship exists between vertical cut-off momentum and H, which may empirically be described by the equation

$$H = K P_c + 506 \quad \text{gm cm}^{-2} \qquad (5.5)$$

where K is a constant of value 9.9, if P_c is in GeV/c.

Test calculations carried out using this expression show that it leads to a poor representation of the observed integral muon intensity dependence on cut-off (neither Olbert's nor Harris and Escobar's applications of the production spectrum were critically dependent on the predicted form of the integral response). This arises out of the failure of the function to take into account an important factor in the problem.

In equation (5.1) it is evident that variation of H changes the differential muon intensity at all points on the secondary spectrum. This does not correspond strictly to reality, since

the muons produced by primaries of momentum above the geomagnetic cut-off P_c are unaffected by the presence of a cut-off. It is evidently necessary to modify the production spectrum to allow this factor to be taken into account.

5.7.3.2 Calculation of the Muon Cut-off

If we define $f(P_c)$ as the maximum momentum of a muon which a primary proton of momentum P_c can produce, the portion of the muon spectrum of momentum above $f(P_c)$ at production is unaffected by the presence of the geomagnetic cut-off P_c. Only that portion of the production spectrum below $f(P_c)$ will be affected by the presence of a cut-off. At the observing level, we define the **muon cut-off** as the point on the muon spectrum above which the geomagnetic cut-offs exert no influence.

The muon cut-off $P_{\mu c}$ for any particular primary cut-off value and zenith angle through the atmosphere may be found by determining $f(P_c)$, and then subtracting the momentum loss δP sustained by the muon in passing through the atmosphere at the particular zenith angle. Thus

$$P_{\mu c} = f(P_c) - \delta P \qquad (5.6)$$

The determination of $f(P_c)$ necessitates the examination of the muon production process. Most muons in the atmosphere are generated by protons via pion production. For each of the two stages in the muon production, the maximum energy that can be passed on to the descendant particle may be deduced. In Appendix 3 we

present equations representing the maximum energy transferred in the interactions, and from these derive a set of equations relating the maximum momentum of a muon to the momentum of the parent proton.

We may calculate the other parameter, δP, as follows. Muons lose energy in passing through the atmosphere, and the final momentum on reaching the observing level will depend on the atmospheric depth involved, the inclination of the muon path to the vertical (and the curvature of the path), and the mean energy of the muon. The rate of energy loss by a fast charged particle per gm cm^{-2} of any gas is given by the Bethe-Bloch relationship

$$-\frac{dE}{dx} = \frac{4\pi e^4 N(Z/A)}{m_o c^2 \beta^2} \left[\ln\left(\frac{2m_o c^2}{I} \frac{\beta^2}{(1-\beta^2)}\right) - \beta^2\right] \qquad (5.7)$$

where N is Avogadro's number, e the electronic charge, Z the atomic number of the absorber, A the atomic weight of the absorber, m_o the rest mass of electron, c the velocity of light, βc the velocity of the particle, I the mean energy of excitation of the absorber electrons (taken as 80.5 eV), and E the kinetic energy of the particle.

For muons in air this expression reduces to

$$-\frac{dE}{dx} = \frac{1.5375\times10^5}{\beta^2} \left[\ln\left(\frac{1.274\times10^4 \beta^2}{1-\beta^2}\right) - \beta^2\right]$$

Integration of this expression along the path traversed by a muon yields the energy loss and hence the momentum loss δP suffered

by the muon.

Thus for any particular set of conditions δP and $f(P_c)$ may be calculated and, with the aid of equation (5.6), the muon cut-off determined.

If we let P_{min} be the momentum threshold of muon detection at the observing level (essentially P_{min} corresponds to the muon momentum necessary for penetration of the telescope shielding; for 10 cm of lead, P_{min} = 0.25 GeV/c), then it may be seen that for $P_{\mu c} \leq P_{min}$ the primary cut-offs can have no effect on the secondary spectrum at the observing level. The latitude for which $P_{\mu c} = P_{min}$ at any particular zenith and azimuth angle is called the "latitude knee" in that direction. For the muon component at sea level the knee in most directions lies in the range 25^o to 35^o geomagnetic latitude. There is further discussion on the latitude knee effect in Section 5.12.4, with reference to the observed latitude dependence of the latitude survey data.

When $P_{\mu c} = P_{min}$, then the value of the primary cut-off momentum P_c is equal to the **atmospheric cut-off** P_{at}, the lowest momentum that a primary entering the atmosphere at any particular zenith angle may possess to give rise to a muon that can be detected at the level of observation. In Section 5.10 we present the calculated dependence of atmospheric cut-off on zenith angle for muon arrival at sea level in the standard N.A.C.A. atmosphere (see Section 5.7.7).

5.7.3.3 Introduction of Modified Cut-off Variable

From the preceding discussion it will be obvious that the simple form of cut-off dependence of H in the Olbert production spectrum cannot possibly allow satisfactory reproduction in all respects of the chacteristic observed dependence of the total muon intensity on latitude, as there is no facility for taking into account the proton-muon momentum relationship or the screening effect of the atmosphere.

It has proved possible to effectively introduce these factors into the calculations by making equation (5.5) momentum dependent, in particular, introducing the dependence of P_c on the momentum of the muons at the observing level. Initially a very simple form of dependence was used. In determining the value of H it was assumed that the parameter P_c had value equal to the primary cut-off for muon momenta below the muon cut-off, but zero value otherwise. As such a dependence introduced a discontinuity into the secondary spectrum at the muon cut-off, it was evidently preferable to employ some method of "tapering" the value of P_c in equation (5.5), from the actual primary cut-off value, at a momentum value below the muon cut-off, to zero at the muon cut-off.

To effect the tapering it was found satisfactory to use a third order polynomial to express the variation of the parameter P_c from full value to zero (see Figure 5.3). The constant D was introduced to represent the momentum interval over which the tapering takes place. Assuming arbitrarily a curve antisymmetric about the

point $X = X' - D/2$, $P_c = P_c'/2$, having zero slope at $X = X'$ and $X = X' - D$ (the limits of the momentum range within which the function is used), the polynomial may be shown to be

$$P_c = \frac{P_c'}{D^3}\left[2X^3 - 3(2X' - D)X^2 + 6X'(X' - D)X + X'^2(3D - 2X')\right] \quad (5.8)$$

where the parameters are defined by Figure 5.3.

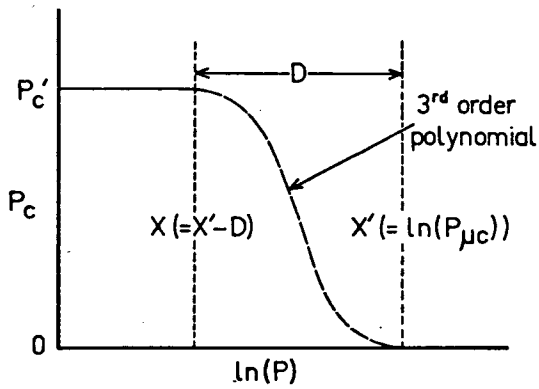

Figure 5.3. Assumed dependence of the parameter P_c in equation (5.5) on muon momentum P, as introduced into the modified Olbert production spectrum.

It was found that the precise form of the integral muon intensity dependence on primary cut-off momentum, as calculated using this model, could be adjusted to some extent by suitable matched choice of the values of the constant D and the constant K in equation (5.5). In particular, an optimum pair of values (D = 23.5, K = 200.0) was found to exist for which the observed form of experimental muon integral response curves could be accurately reproduced. (A comparison of the calculated and experimental integral response functions is made in Section 6.8.) Close agreement was obtained, too, between the calculated integral response functions and the extrapolated portions of the experimental functions, for momenta up to several hundred GeV/c.

It will be shown later that, in spite of the possible departure of certain of the individual equations from reality (equations (5.1) and (5.3) strictly only apply for momenta less than approximately 14 GeV/c), the production spectrum model nevertheless is capable, without further modification, of predicting accurately the form of the sea level muon spectra and integral response functions at momenta up to hundreds of GeV/c.

5.7.4 Trajectory Tracing, Calculation of Survival Probabilities

The paths of the muons in the atmosphere will in general be curved as the result of deflections in the geomagnetic field. In order to obtain the greatest degree of accuracy in the present investigation, it is desirable that the inner integral in equation (5.4) be evaluated along the actual path described by the muons. To allow calculations to be carried out corresponding to specific zenith and azimuth angles of arrival at the observing level of interest, we have followed the general practice used in the tracing of cosmic ray trajectories in that the trace is carried out in the reverse direction to the sense of motion of the actual particles. This is done by reversing the sign of the charge and the sense of the velocity vector of the particle. In our calculations it was assumed that the magnetic field is uniform in the atmosphere.

The motion of a particle of charge q, mass m, and position vector $\underline{R}$, moving with velocity $\underline{V}$ through the atmosphere in the presence of a magnetic field $\underline{B}$, is expressed by the differential

equation of motion

$$m \ddot{\underline{R}} = q (\dot{\underline{R}} \times \underline{B}) - m \frac{dV}{dt}$$

$\frac{dV}{dt}$, the acceleration of the particle due to energy loss in the air, may be determined from knowledge of the rate of energy loss by the particle. (At any instant we can determine the rate of energy loss $\frac{dE}{dx}$ by a particle of given momentum by invoking the Bethe-Bloch relationship (equation 5.7).) If the parameter s is introduced to represent the displacement along the trajectory, then, for air of density ρ,

$$\frac{dE}{dx} = \frac{1}{\rho} \frac{dE}{ds}$$

and we may relate the rate of energy loss to the acceleration as follows

$$\frac{dV}{dt} = \frac{dE}{ds} \frac{ds}{dt} / \frac{dE}{dV}$$

where, since the kinetic energy $E = m_o c^2 (\gamma - 1)$ (where m_o is the rest mass of the particle, and $\gamma = 1/\sqrt{(1 - \beta^2)}$, where $\beta = V/c$)

$$\frac{dE}{dV} = m_o c^2 V \gamma^3$$

Therefore

$$\frac{dV}{dt} = \frac{\rho}{m_o \gamma^3} \frac{dE}{dx} \quad (= Y) \tag{5.9}$$

It is convenient to express the particle motion in terms of components in the cartesian coordinate system having its origin at the "observing" point (see Figure 5.4) in the atmosphere. The partial differential equations of motion are, then,

$$
\begin{aligned}
v_x &= V \sin\theta \sin\phi \\
v_y &= V \sin\theta \cos\phi \\
v_z &= V \cos\theta \\
a_x &= Y \sin\theta \sin\phi + q/m\ (v_y B_z - v_z B_y) \\
a_y &= Y \sin\theta \cos\phi + q/m\ (v_z B_x - v_x B_z) \\
a_z &= Y \cos\theta + q/m\ (v_x B_y - v_y B_x)
\end{aligned}
\qquad (5.10)
$$

where Y is defined in the preceding equation.

Having thus a set of instantaneous simultaneous differential equations representing the motion we may trace the trajectory by numerical integration in a starting point calculation. Part of this operation involves determining the velocity of the particle at each point on the trajectory in order that the Lorentz force, and hence the deflection term in the differential equation may be calculated. At low muon momenta the instantaneous velocity is directly determined in the course of the integration. At large momentum values, on the other hand, the

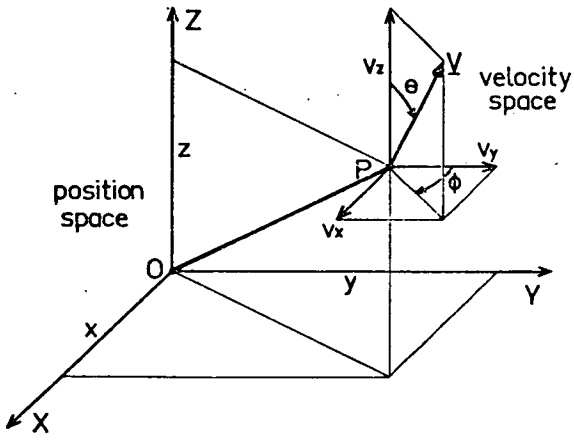

Figure 5.4. Diagram defining the relationship between the orientation of the axes of the cartesian coordinate system and the angles θ and Ø. The Y axis points geographic north, and the Z axis, vertical.

velocities are highly relativistic, with β very close to unity, and it was found that for calculations corresponding to muon momenta greater than 25 GeV/c, the number of digits used by the computer in its operation (9 significant figures) was too low to allow the required manipulation of the β values. At these momenta, then, it became necessary to determine the velocity from considerations of the muon energy and the known rates of energy loss in the atmosphere. It proved possible to estimate accurately the mean atmospheric density and mean rate of energy loss over the short trajectory segments used in the numerical integration, and from this information to calculate the instantaneous energy, and thus velocity.

Further differential equations may be set up to allow the determination of the time of flight of the muons, so that the survival probabilities corresponding to any particular situation (required in equation (5.4)) may be calculated. At the values of muon energy under consideration it is necessary to take into account the time dilatation in the c.m. system (the frame of reference in which the muon is at rest) due to the highly relativistic velocity in the laboratory system of coordinates.

If a period of time t elapses in the c.m. system of a particle which is travelling at velocity $\underline{V}$ towards the observer, the period of time which will elapse for the observer is t', where $\frac{dt'}{dt} = \frac{1}{\gamma}$.

Now,

$$\frac{d^2t'}{dt^2} = \frac{d(\frac{1}{\gamma})}{dt} = \frac{d(\frac{1}{\gamma})}{dV}\frac{dV}{dt}$$

Therefore, since

$$\frac{dV}{dt} = \frac{\rho}{m_o \gamma^3} \frac{dE}{dx}, \qquad \frac{d^2t'}{dt^2} = - \frac{\rho V}{m_o c^2 \gamma^2} \frac{dE}{dx}$$

Repeated numerical integration of the set of equations (5.10) and of the expressions for $\frac{dt'}{dt}$ and $\frac{d^2t'}{dt^2}$ in a starting point calculation allows the position of the muon to be calculated at successive points on the trajectory, and also the time of flight from each point to the origin, so that the survival probability may be evaluated for use, in conjunction with the production spectrum, in the determination of muon intensities.

The Gill [1951] modification of the Runge-Kutta integration process, as used by McCracken, Rao and Shea [1962], was employed in the present series of calculations. A step length of 3×10^{-6} was found to be suitable for most purposes, although the step length was reduced when the point on the trajectory was passed for which 2 gm cm^{-2} of atmosphere remained along the extrapolation of the trajectory path, in order to prevent overshoot of the height at which the atmosphere was assumed to terminate (see Section 5.7.7).

5.7.5 Calculation of Muon Intensity

As the numerical integration of the various differential equations proceeded, the numerical evaluation of the inner integral in equation (5.4) was also carried out, so that at the completion of any particular trajectory trace the differential intensity of

muons of one sign and of a particular momentum at the observing level, in a given direction, was known. Pairs of trajectory calculations (for both positive and negative muons) were carried out for muon momenta at the observing level of 1000, 200, 40, 16, 7, 3.5, 1.7, 0.8, 0.4 and 0.25 GeV/c.

Within each of these individual trajectory calculations it was necessary to have knowledge of the muon cut-off (see Section 5.7.3.2) in order that the tapering function described in Section 5.7.3.3 could be applied, even though the precise value of the muon cut-off in each case was determinable only as the result of the particular calculation. This difficulty was overcome by retaining, on the completion of each trajectory trace within a set (calculations relating to a given direction at the observing point), the momentum loss incurred in travelling from the 125 gm cm^{-2} level to the observing point. These stored values were then used in the calculation of the muon cut-off for muons of the same sign in the next lower momentum calculation of the set. The accuracy of estimates made in this way was found quite satisfactory.

In calculating the muon cut-off values, allowance was made for the momentum loss suffered by the primary protons in travelling down to the 125 gm cm^{-2} level (the approximate mean production level of the muons) at any zenith angle. Calculations showed that the momentum loss did not vary greatly with zenith angle and momentum, lying within the range 0.28 ± 0.08 GeV/c. In order to simplify the calculations a constant value of 0.25 GeV/c was assumed.

Thus, for the purposes of the calculations, equation (5.6) was used in the form

$$P_{\mu c} = f(P_c - 0.25) - \delta P$$

where δP is the momentum loss incurred by the muon in passing through the atmosphere from the 125 gm cm^{-2} level at the particular zenith angle to the observing level, determined from the preceding related trajectory calculation.

At the completion of each given set of trajectory tracing calculations, a series of differential muon intensities existed, defining the spectra of the positive and negative muons incident in the direction of interest. Calculation of the total intensity of muons of each sign was effected by numerical integration of these spectra. This integration was carried out by fitting 3rd order polynomial functions to each successive set of four calculated points on a log-log representation of the calculated spectra, then determining the area under the curves in natural units with the aid of a standard numerical integration procedure, and finally summing all these contributions to obtain the estimate of the total directional intensity of muons of each sign.

5.7.6 Muon Charge Ratio

It is necessary, in calculating the contributions to the total muon intensity in any situation from positive and negative muons, to know the relative numbers of these particles at production.

Baber, Nash and Rastin [1968] reviewed the results of the most

accurate muon charge ratio determinations in the vertical direction. These data are of interest because, with allowance made for momentum loss within the atmosphere, they indicate the momentum deendence of the ratio at production. In spite of the considerable disparity between results due to different investigators, it is evident that the charge ratio is only a slowly varying function of momentum, with an indication of a slight increase in magnitude for momenta in excess of approximately 100 GeV/c.

Although a specific non-constant charge ratio spectrum could have been readily incorporated into our calculations, in view of the still considerable uncertainty as to the precise form of the charge spectrum a constant value of charge ratio was employed. The value of 1.266 (= +/-) of Moroney and Parry [1954] was adopted, both because this value constitutes a reasonable approximation to the experimental charge spectrum, and because the computed spectra presented in this thesis may be checked readily against the observed muon spectra published by Moroney and Parry. This comparison is made in Section 5.9.2.

5.7.7 Representation of the Atmosphere

Because of the use of numerical integration techniques, actual atmospheric profiles could be readily incorporated into the calculations, and in practice were introduced as a set of values representing pressure and temperature at 25 altitudes in the atmosphere. Density values at any point in the atmosphere were obtained by first

interpolating values of temperature and pressure from the set, corresponding to the altitude of interest, then determining density using the relationship

$$\rho(p) = \frac{pMg}{RT(p)}$$

where p is the air pressure in cm water, M is the effective molecular weight of the air, g is the acceleration due to gravity, R is the universal gas constant, and T is the temperature in ^{o}K; $\frac{Mg}{R} = 3.484 \times 10^{-4}$ ^{o}K cm^{-1} (Olbert [1953]). The second order latitude dependence of this constant has been overlooked in the presently reported series of calculations.

For the general investigation of the atmospheric asymmetry effect, the N.A.C.A. standard atmosphere was employed to represent the typical mid-latitude atmosphere (details were obtained from Montgomery [1949]), and to represent low and high latitude atmospheres, profiles presented in the Handbook of Geophysics [1961] were adopted, and referred to as the "standard equatorial" and "standard polar" atmospheres respectively. In calculations corresponding to conditions at particular sites (for the purposes of data correction etc.), actual mean atmospheric profiles were used, derived from radiosonde data acquired during the observing periods at the sites. The three "standard" atmospheric profiles are presented in Figure 5.5, and certain of the profiles typical of the latitude sites, in Figure 6.7 (in the following chapter).

Whereas in fact the atmosphere extends to hundreds of kilometres, for the purposes of the calculations zero air density was

assumed to occur at 34 km. The correct atmospheric structure was used to a height of 28 km, and the termination effected above this

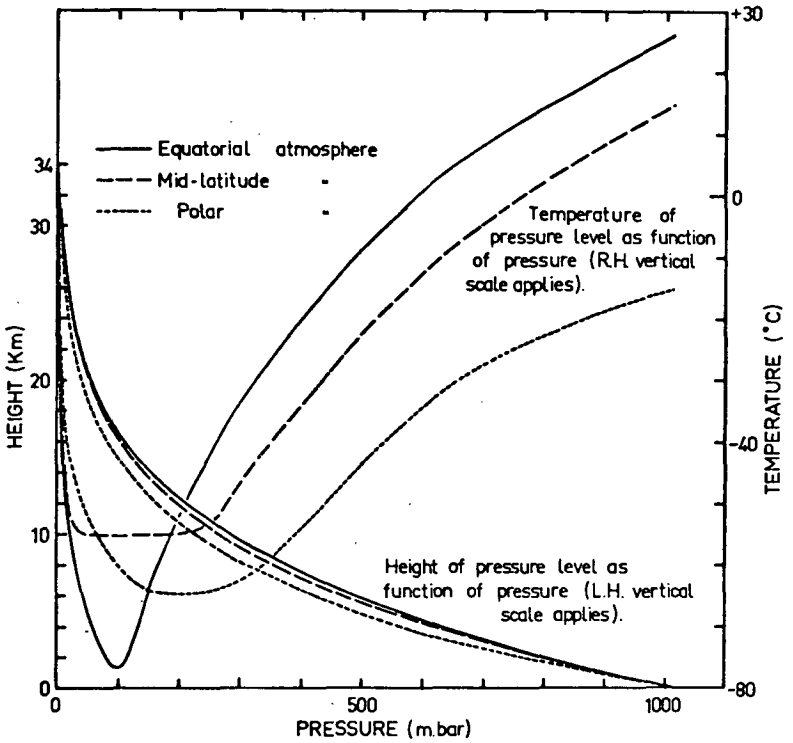

Figure 5.5. Graphical representation of the structure of the "standard" equatorial, mid-latitude, and polar atmospheres.

altitude. The main purpose of this truncation was to minimize the calculation time required to trace trajectories through the atmosphere. Tests showed that a barely discernible effect arose in the overall results, due to the low intensity of muons originating from this region.

5.7.8 Curved Earth Representation

Because of the inadequacies of a flat earth representation at high zenith angles, a curved earth simulation was employed in the calculations. It is readily shown that the height h of a point P in the curved atmosphere (see Figure 5.6) is given by

$$h = \sqrt{[(r_e + l\cos\sigma)^2 + l^2 \sin^2\sigma]} - r_e$$

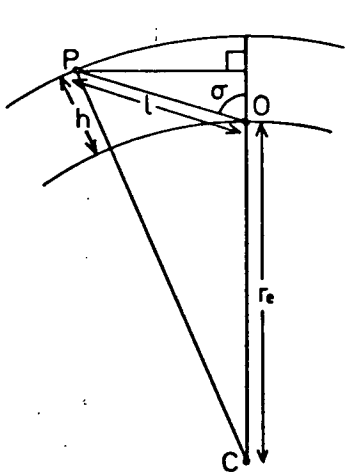

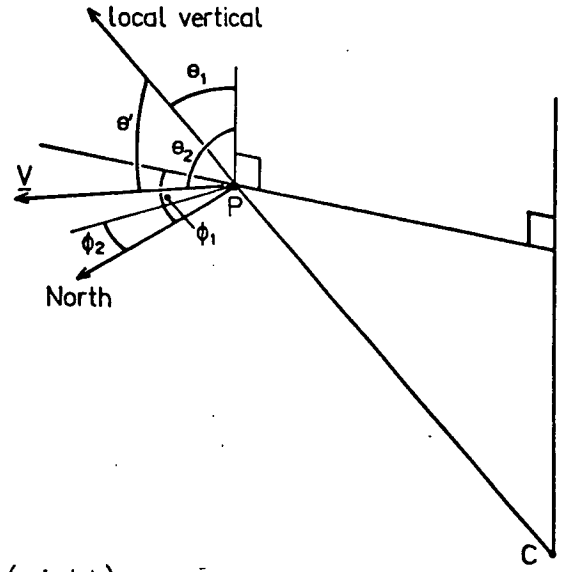

Figures 5.6 (left) and 5.7 (right).

Figure 5.6. Relationship between the variables used to define the position of a point P relative to the "observing" point O in the curved earth representation. C represents the centre of the earth.

Figure 5.7. Diagram defining the angle θ' between the velocity vector of the particle P and the local vertical through the atmosphere, and its relationship to the other angles that define the position of the particle and its velocity vector.

Similarly, at any point on a curvilinear trajectory in the curved atmosphere, the local zenith angle θ' (the zenith angle between the local vertical and the muon velocity vector (see Figure 5.7)) may be shown to be

$$\theta' = \arccos[\sin\theta_1 \cos\theta_2 \cos(\phi_1 - \phi_2) + \cos\theta_1 \sin\theta_2]$$

where ϕ_1 is the azimuth bearing of the point relative to the origin of the cartesian reference system (the site position), θ_1 the angle between the local vertical and the vertical axis of the cartesian system, and θ_2, ϕ_2 the known zenith and azimuth orientation of the velocity vector in velocity space (see Figure 5.4).

5.8 Accuracy and Speed of Computer Program

The computer program written to carry out the muon intensity calculations using the techniques described in the preceding sections, required as input data details of the atmospheric and magnetic field configurations at the site, altitude, the zenith and azimuth angles defining the directions of interest, together with associated cut-off values. Estimates were thereupon made of the total muon intensity, charge ratio, and, if required, the asymmetry factor pertaining to the given directions. The asymmetry factor estimates, of course, were produced as the result of a pair of calculations, one pertaining to the actual site conditions, and the other to "field-free" conditions. Printout was obtained after each

calculation of the details of the directional muon spectra.

A great deal of development and testing of the various sections of the program was carried out in order to allow results of sufficient accuracy to be obtained for use in the atmospheric asymmetry investigation, and later, in the coupling coefficient investigation. The requirements of the latter of these were more stringent in that the slope of the calculated integral response curves, as determined by taking differences between adjacent intensity values on the curves, was required to be continuous. The price to be paid in return for a high degree of accuracy in the intensity estimates, however, was the slow speed of operation of the program.

It was thus necessary, in the initial testing of the program, to establish the optimum between the degree of detail in the calculations (for example, the number of points calculated on the secondary spectra), and a practicable speed of operation. The program, in final form, was capable of producing muon intensity estimates internally consistent to within approximately 0.05% (i.e. a scatter of points lying within 0.05% of a continuous integral response curve). The operation time for calculation of a single directional intensity (involving 20 trajectory traces) varied between approximately 2 and 8 minutes, for low and high zenith angles respectively.

5.9 Test of Theoretical Predictions

5.9.1 Zenith Angle Dependence of Total Intensity

In Section 3.3.3 we discussed the dependence of total muon

intensity on zenith angle, and its representation in terms of empirical functions such as equation (3.4). We now compare the zenith angle dependence of this function with that predicted by the "muons in the atmosphere" computer program. The comparative results are shown in Figure 5.8.

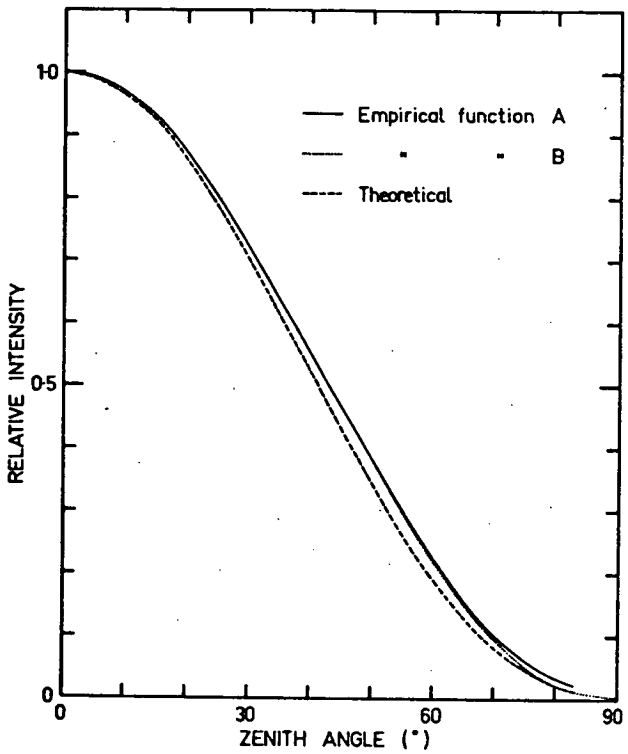

Figure 5.8. Zenith angle dependence of total muon intensity. Function A is the dependence indicated by the latitude survey data (equation 3.5); Function B (equation 3.4) a realistic empirical representation (see the discussion in Section 3.3); The "theoretical" curve represents the predictions of the program.

The maximum discrepancy between the calculated zenith depend-

ence curve and that representing the true dependence (as represented by equation (3.4)) is 15 %, at 65^{o} to the zenith. It is likely that the disparity arises out of the failure of the calculations to take into account the scattering of muons in the atmosphere. Such scattering would allow muons to arrive at any particular zenith angle from zenith angles up to several degrees lower than expected on the basis of deflections in the magnetic field alone, and produce a higher intensity because of the shorter path length in the atmosphere.

The effects of scattering were not considered to be of sufficient importance to warrant consideration in Olbert's development of his production spectrum (because the calculations applied to the vertical direction only relatively short path lengths were involved, and in addition, a symmetry existed about the zenith). Harris and Escobar [1955, 1956], on the other hand, did take muon scattering into account in their adaption of the Olbert production spectrum. In the present case, the percentage errors introduced into the calculated asymmetry factors, due to exclusion of such considerations, may be shown to be unimportant.

In Figure 5.8 it may be seen that the error in the calculated intensity values corresponds to the displacement of the predicted intensity distribution pattern through approximately 2^{o} relative to the true distribution. The error in the asymmetry factor estimate in this case would be expected to correspond approximately to the difference in asymmetry factor value for a change of 2^{o} in zenith

angle. The possible error, on this basis, is of the order of 3 % at 45^{o} zenith angle.

5.9.2 Sea Level Spectra

To obtain a detailed check on the validity of the calculations based on the modified Olbert production spectrum, the predicted sea level differential muon spectra have been compared with those experimentally observed. Firstly, the low momentum (< 50 GeV/c) portions of the spectra have been compared with the results of Moroney and Parry [1954], for both the vertical and inclined directions. These investigators measured the muon spectra at zenith angles of 0^{o}, 30^{o} and 60^{o} in the east-west plane at Melbourne, Australia. They themselves demonstrated the acceptable agreement between their results and estimates based on the production spectrum of Sands [1950]. Our test calculations of comparative spectra (based on the Olbert spectrum) were carried out using an atmospheric profile, and magnetic field configuration, representative of the site. The calculated and experimental spectra are shown in Figure 5.9. In conjunction with these spectra the calculated and observed charge ratio values are presented. It is to be seen, both from the form of the corresponding spectra, and the charge ratio values, that there is good agreement between theory and experiment.

A check on the predictions of the Olbert production spectrum at higher momenta may be made by comparing the calculated and experimental spectra in the momentum range 50 - 1000 GeV/c [to page 201]

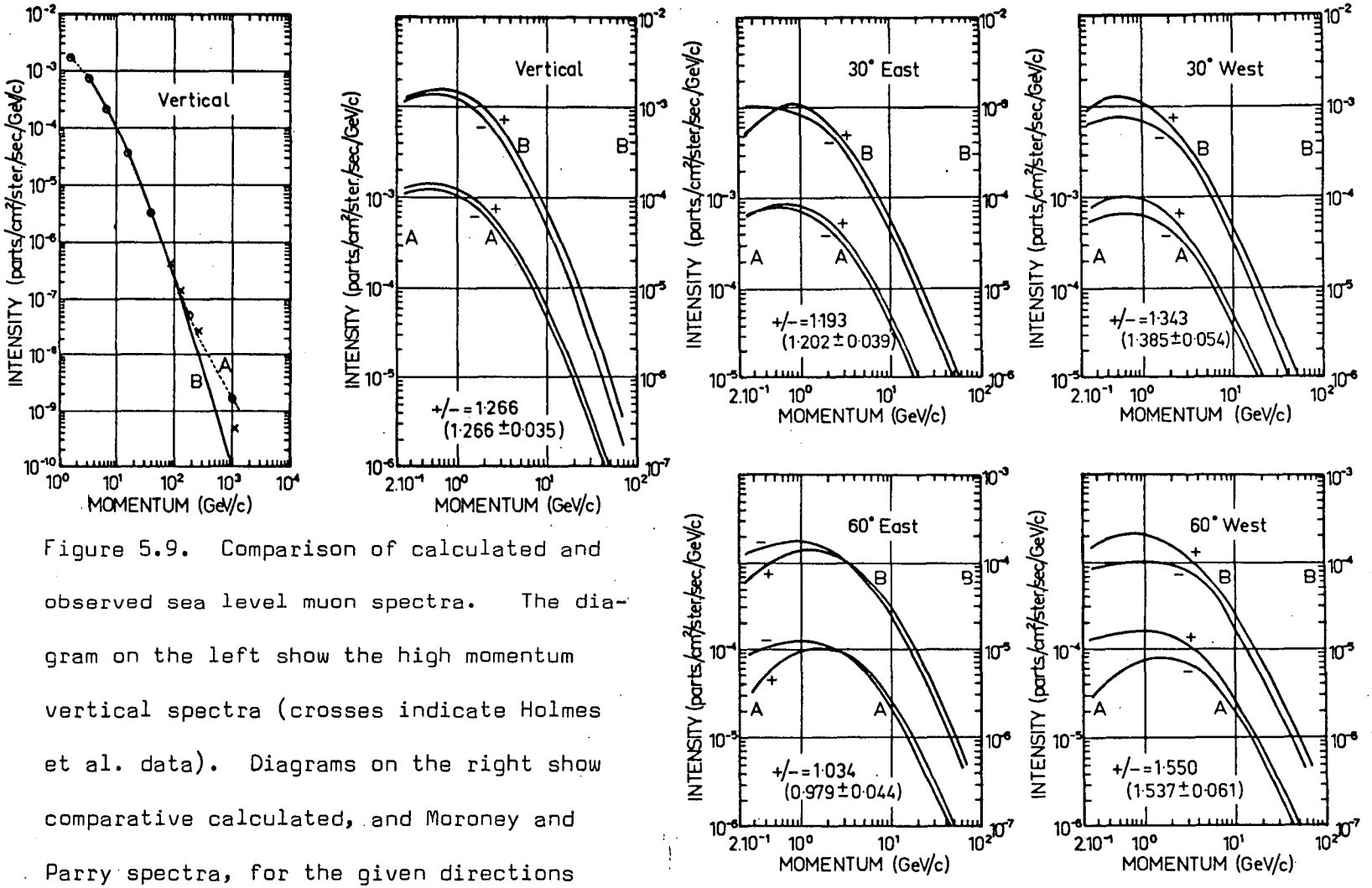

Figure 5.9. Comparison of calculated and observed sea level muon spectra. The diagram on the left show the high momentum vertical spectra (crosses indicate Holmes et al. data). Diagrams on the right show comparative calculated, and Moroney and Parry spectra, for the given directions (scales A, B apply to these spectra respectively, comparative charge ratio values also given).

[from page 199] In this range numerous experimental spectra have been determined. The observations of most workers, for example Pine et al. [1959], Hayman and Wolfendale [1962], Krasilnikov [1964], and Baber et al. [1968] agree closely in this momentum range, and are represented by a single line in Figure 5.9. The calculated spectrum, plotted in the same diagram, is seen to agree well for momentum values < 200 GeV/c, but to lie significantly above the experimental estimate at greater momenta, evidently more closely in agreement with the results of Holmes et al. [1961], which are represented by crosses in this diagram.

It is generally observed that at higher zenith angles the differential intensity of muons of high momenta increases (see for example the results of Mackeown et al. [1965], and Maeda [1964]), and the disparity between the predicted and experimental differential muon intensity would thus be expected to decrease. It is estimated that the maximum error in calculated total intensity values due to the high momentum disparity evident in Figure 5.9 is 0.5 %.

To test the predictions of our calculations in respect of sea level spectra in the presence of an appreciable primary cut-off, we have available the published results of experimental spectral determinations. In particular, a comparison has been made of the predictions of the modified Olbert production spectrum as used in the "muons in the atmosphere" program with the experimental vertical spectrum of Allkofer et al. [1968] (measured at a site with a vert-

ical cut-off of 14.1 GeV/c). Allkofer et al. themselves carried out a comparison against the predictions of Olbert's production spectrum. They overlooked, however, the limitation of the Olbert model (in that the muon cut-off is not taken into account), and by arbitrarily assuming merging of the zero cut-off spectrum and the finite value cut-off spectrum at the appropriate momentum, obtained a spectrum agreeing with the experimental result. In our calculations, the same good agreement is found, but obtained entirely through the operation of the internal provisions of the calculations.

5.10 Muon Deflections, Momentum Loss, and Survival Probabilities

It is of interest, for many purposes, to have access to information relating to the propagation of muons in the atmosphere, information such as deflections, momentum loss, and survival probabilities. A certain amount of information is available in the literature. For example, Bonnevier [1958] presented the calculated dependence of the deflection of muons arriving vertically at sea level, on horizontal field strength, and on magnetic dip angle.

We have taken the opportunity of using the facilities provided by the "muons in the atmosphere" program to carry out calculations relating to certain aspects of the passage of muons through the atmosphere, in order to supplement the available information.

Calculations have been made of the deflection of muons arriving from inclined directions, for passage normal to a horizontal magnetic field. In these computations the assumption [to page 204]

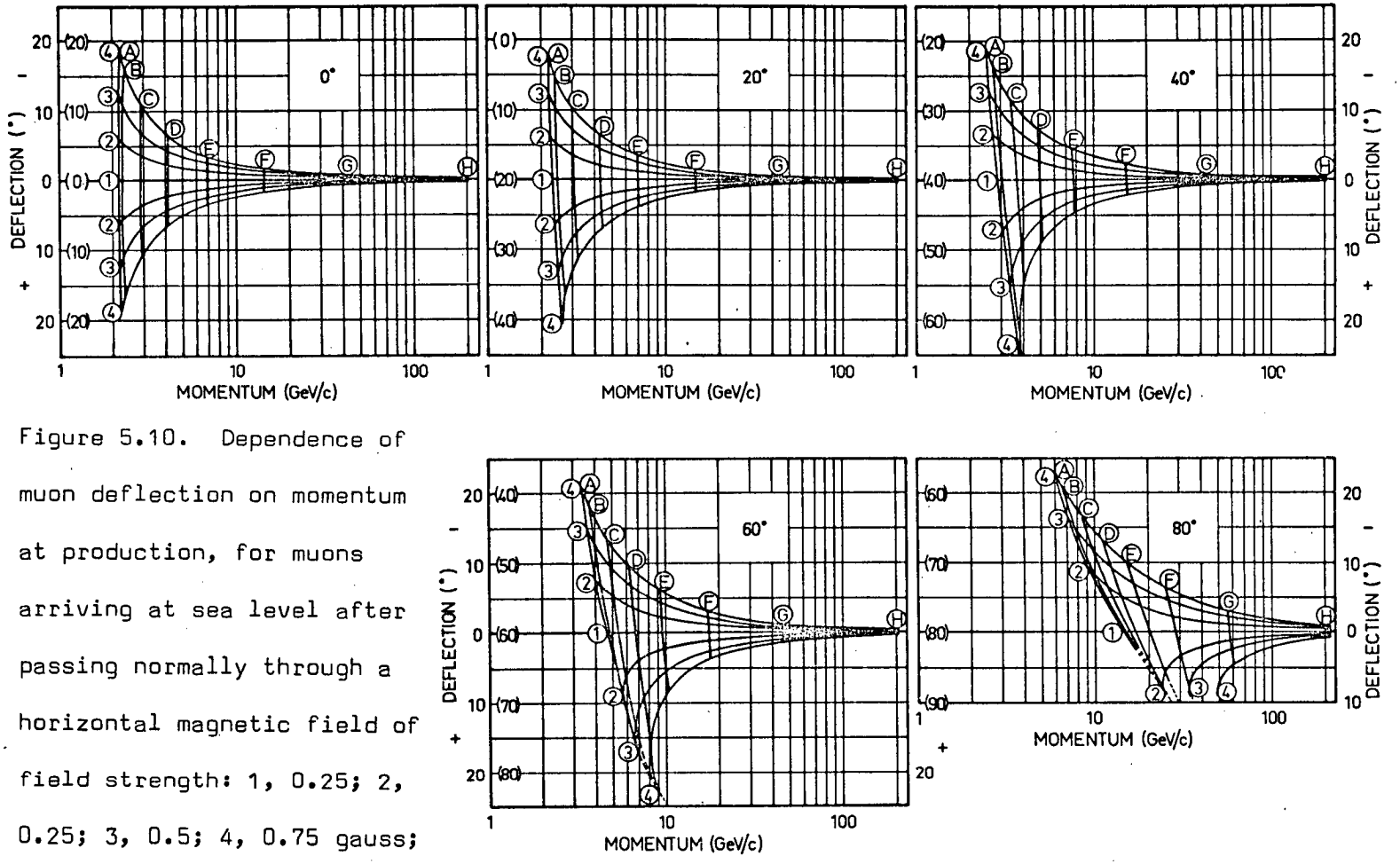

Figure 5.10. Dependence of muon deflection on momentum at production, for muons arriving at sea level after passing normally through a horizontal magnetic field of field strength: 1, 0.25; 2, 0.25; 3, 0.5; 4, 0.75 gauss; and arriving at sea level, at a number of zenith angles, with momenta: A, 0.25; B, 0.4; C, 0.9; D, 2.0; E, 4.5; F, 12; G, 40; H, 200 GeV/c. Momentum loss may be deduced from these diagrams.

[from page 202] was made that the muons are produced at the point in the standard mid-latitude atmosphere at which 125 gm cm^{-2} of air lies along the line of the trajectory extrapolated to the top of the atmosphere. Figure 5.10 presents muon deflection as a function of momentum at production for various momenta and zenith angles on arrival at sea level, and various horizontal field strengths. Because of the mode of presentation of these data, the graphs contain detailed information about muon momentum loss in the atmosphere under the various conditions. Estimation of the loss may be carried out by noting the difference between the momentum at production and the sea level value.

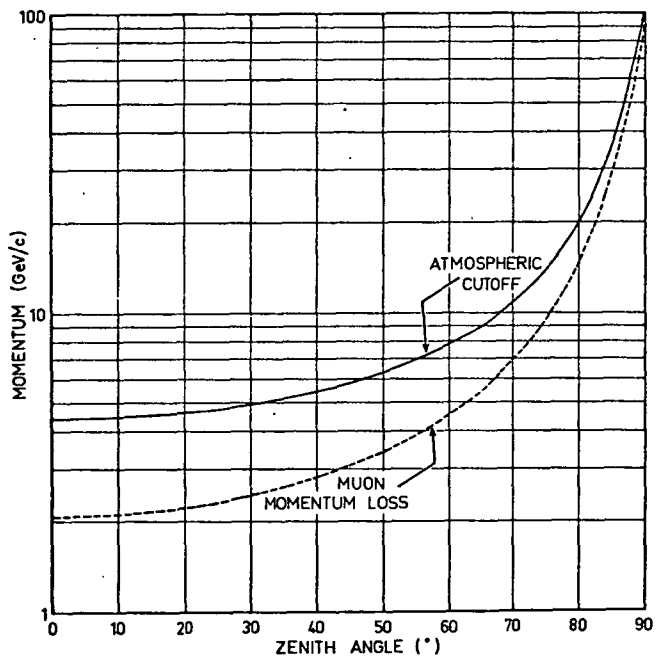

Figure 5.11. Dependence of atmospheric cut-off, and muon momentum loss, on zenith angle in the field-free standard mid-latitude atmosphere.

Figure 5.11 represents the calculated zenith angle dependence of muon momentum loss and atmospheric cut-off in the field-free, standard mid-latitude atmosphere. The atmospheric cut-off is the lowest value of momentum that a primary proton may possess in order to give rise to muons observable at sea level. The considerations involved in the determination of these quantities were discussed in Section 5.7.3.2.

Survival probabilities for muon arrival at sea level after production at the 125 gm cm^{-2} point in the field-free mid-latitude atmosphere were also calculated, and are presented in Figure 5.12.

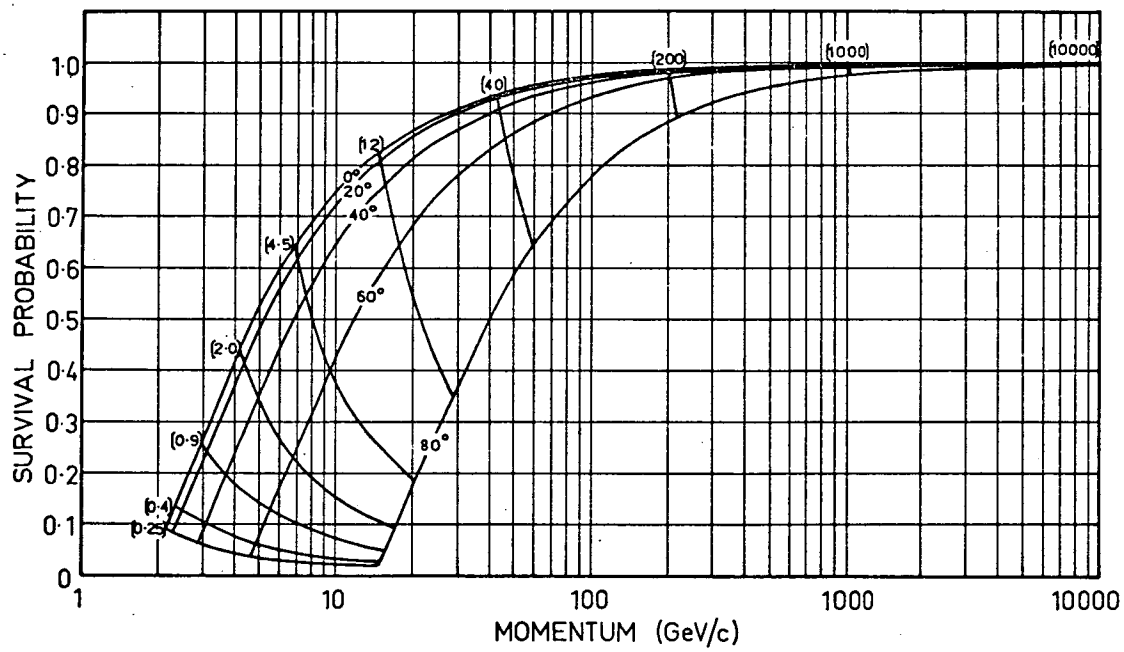

Figure 5.12. Dependence of muon survival probability on production momentum in field-free, standard mid-latitude atmosphere, for trajectories inclined at various indicated zenith angles, and for various values of sea level momentum (momentum values bracketed).

5.11 Theoretical Unidirectional Asymmetry Factors

In Section 5.7.1 we introduced the asymmetry function, A, a function relating the muon intensity I existing in any direction in the presence of a magnetic field in the atmosphere, to the intensity N that would exist in the absence of the field, such that N = I A.

An investigation has been carried out to ascertain the dependence of the asymmetry function on various geophysical factors - magnetic field strength and direction, atmospheric structure, altitude, and cut-off. The calculated asymmetry factors (pertaining to four zenith angles: 0^{o}, 22.5^{o}, 45^{o}, and 67.5^{o}; and six azimuths: 30^{o}, 90^{o}, 150^{o}, 210^{o}, 270^{o}, and 330^{o} E. of magnetic N.), deduced under the conditions listed in Table 5.2, are presented in Tables 5.3 to 5.9 inclusive, together with the associated charge ratio values. Table 5.2 lists the particular contents of these tables.

Table 5.2 Configuration of parameters in the various series of calculations, the results of which are presented in Tables 5.3 to 5.9 inclusive. (*) denotes the variable quantity in each table.

Table number	5.3	5.4	5.5	5.6	5.7	5.8	5.9
Field strength	*	0.55	0.55	0.55	0.55	0.55	0.55
Dip angle	-30^{o}	*	-30^{o}	-30^{o}	-60^{o}	-30^{o}	-60^{o}
Atmosphere	mid	mid	*	mid	mid	mid	mid
Altitude	0	0	0	*	*	0	0
Cut-off	0	0	0	0	0	*	*

The tabulated data refer to Southern hemisphere sites. In the Northern hemisphere the data relating to northern and southern azimuths would be transposed. The charge ratio values are given in the tables, although not further considered in this thesis, because they form in principle a useful basis for the comparison of experimentally observed charge ratios under various conditions. [to p.214]

Table 5.3 Asymmetry factor and charge ratio (bracketed) dependence on magnetic field strength; dip angle = -30^{o}, at sea level in standard mid-latitude atmosphere, zero value cut-off.

Field Strength (gauss)	Zenith Angle	Asymmetry factor and charge ratio at given azimuths					
		30^{o}	90^{o}	150^{o}	210^{o}	270^{o}	330^{o}
0.275	0^{o}	1.0010 (1.266)					
	22.5^{o}	1.0022 (1.236)	1.0038 (1.207)	1.0026 (1.236)	0.9998 (1.297)	0.9982 (1.328)	0.9994 (1.297)
	45^{o}	1.0042 (1.190)	1.0079 (1.118)	1.0055 (1.189)	0.9982 (1.347)	0.9932 (1.434)	0.9968 (1.347)
	67.5^{o}	1.0064 (1.097)	1.0020 (0.949)	1.0103 (1.096)	0.9933 (1.462)	0.9782 (1.689)	0.9896 (1.460)
0.55	0^{o}	1.0042 (1.266)					
	22.5^{o}	1.0064 (1.206)	1.0099 (1.149)	1.0082 (1.206)	1.0025 (1.329)	0.9985 (1.394)	1.0007 (1.329)
	45^{o}	1.0091 (1.117)	1.0164 (0.985)	1.0145 (1.117)	0.9997 (1.436)	0.9871 (1.627)	0.9944 (1.435)
	67.5^{o}	1.0084 (0.951)	1.0250 (0.690)	1.0234 (0.948)	0.9895 (1.690)	0.9562 (2.323)	0.9754 (1.685)

Table 5.4 Asymmetry factor and charge ratio (bracketed) dependence on dip angle; field strength = 0.55 gauss, sea level in standard mid-latitude atmosphere, zero value cut-off.

Dip Angle	Zenith Angle	Asymmetry factor and charge ratio at given azimuths					
		30°	90°	150°	210°	270°	330°
0°	0°	1.0055 (1.266)					
	22.5°	1.0092 (1.197)	1.0122 (1.132)	1.0093 (1.197)	1.0027 (1.339)	0.9991 (1.416)	1.0027 (1.339)
	45°	1.0144 (1.095)	1.0193 (0.947)	1.0144 (1.095)	0.9974 (1.463)	0.9854 (1.692)	0.9974 (1.463)
	67.5°	1.0184 (0.907)	1.0179 (0.637)	1.0184 (0.907)	0.9797 (1.767)	0.9418 (2.516)	0.9797 (1.767)
-30°	0°	1.0042 (1.266)					
	22.5°	1.0064 (1.206)	1.0099 (1.149)	1.0082 (1.206)	1.0025 (1.329)	0.9985 (1.394)	1.0007 (1.329)
	45°	1.0091 (1.117)	1.0164 (0.985)	1.0145 (1.117)	0.9997 (1.436)	0.9871 (1.627)	0.9944 (1.435)
	67.5°	1.0084 (0.951)	1.0250 (0.690)	1.0234 (0.948)	0.9895 (1.690)	0.9562 (2.323)	0.9754 (1.685)
-60°	0°	1.0014 (1.266)	Note: At -90° dip angle, asymmetry factor at 22.5°, 45° = 1.0000; at 67.5° = 1.0001.				
	22.5°	1.0023 (1.231)	1.0047 (1.197)	1.0041 (1.231)	1.0008 (1.302)	0.9982 (1.339)	0.9990 (1.301)
	45°	1.0030 (1.178)	1.0090 (1.096)	1.0083 (1.177)	0.9997 (1.361)	0.9921 (1.462)	0.9946 (1.360)
	67.5°	1.0028 (1.073)	1.0127 (0.908)	1.0169 (1.072)	0.9971 (1.496)	0.9742 (1.765)	0.9835 (1.494)

Table 5.5 Asymmetry factor and charge ratio (bracketed) dependence on atmospheric configuration; field strength 0.55 gauss, dip angle -30°, sea level, zero value cut-off.

Atmosphere	Zenith Angle	Asymmetry factor and charge ratio at given azimuths					
		30°	90°	150°	210°	270°	330°
Equatorial	0°	1.0044 (1.266)					
	22.5°	1.0065 (1.205)	1.0102 (1.146)	1.0084 (1.205)	1.0026 (1.330)	0.9985 (1.398)	1.0007 (1.330)
	45°	1.0094 (1.115)	1.0167 (0.981)	1.0151 (1.114)	1.0000 (1.439)	0.9868 (1.634)	0.9944 (1.438)
	67.5°	1.0090 (0.945)	1.0223 (0.686)	1.0235 (0.944)	0.9891 (1.698)	0.9534 (2.335)	0.9754 (1.695)
Mid-Latitude	0°	1.0042 (1.266)					
	22.5°	1.0064 (1.206)	1.0099 (1.149)	1.0082 (1.206)	1.0025 (1.329)	0.9985 (1.394)	1.0007 (1.329)
	45°	1.0091 (1.117)	1.0164 (0.985)	1.0145 (1.117)	0.9997 (1.436)	0.9871 (1.627)	0.9944 (1.435)
	67.5°	1.0084 (0.951)	1.0250 (0.690)	1.0234 (0.948)	0.9895 (1.690)	0.9562 (2.323)	0.9754 (1.685)
Polar	0°	1.0034 (1.266)					
	22.5°	1.0056 (1.211)	1.0087 (1.158)	1.0070 (1.211)	1.0017 (1.324)	0.9982 (1.384)	1.0003 (1.324)
	45°	1.0086 (1.127)	1.0157 (1.002)	1.0132 (1.126)	0.9994 (1.423)	0.9883 (1.599)	0.9949 (1.422)
	67.5°	1.0095 (0.961)	1.0325 (0.697)	1.0222 (0.959)	0.9896 (1.670)	0.9645 (2.299)	0.9776 (1.667)

Table 5.6 Asymmetry factor and charge ratio (bracketed) dependence on altitude; field strength 0.55 gauss, dip angle -30^{o}, standard mid-latitude atmosphere, zero value cut-off.

Altitude (km)	Zenith Angle	Asymmetry factor and charge ratio at given azimuths					
		30^{o}	90^{o}	150^{o}	210^{o}	270^{o}	330^{o}
0	0^{o}	1.0042 (1.266)					
	22.5^{o}	1.0064 (1.206)	1.0099 (1.149)	1.0082 (1.206)	1.0025 (1.329)	0.9985 (1.394)	1.0007 (1.329)
	45^{o}	1.0091 (1.117)	1.0164 (0.985)	1.0145 (1.117)	0.9997 (1.436)	0.9871 (1.627)	0.9944 (1.435)
	67.5^{o}	1.0084 (0.951)	1.0250 (0.690)	1.0234 (0.948)	0.9895 (1.690)	0.9562 (2.323)	0.9754 (1.685)
1.35	0^{o}	1.0043 (1.266)					
	22.5^{o}	1.0066 (1.205)	1.0104 (1.147)	1.0085 (1.205)	1.0026 (1.330)	0.9987 (1.398)	1.0007 (1.330)
	45^{o}	1.0103 (1.107)	1.0185 (0.967)	1.0163 (1.106)	1.0004 (1.449)	0.9875 (1.656)	0.9945 (1.448)
	67.5^{o}	1.0090 (0.917)	1.0202 (0.646)	1.0297 (0.908)	0.9905 (1.764)	0.9453 (2.481)	0.9719 (1.748)
3.0	0^{o}	1.0040 (1.266)					
	22.5^{o}	1.0065 (1.206)	1.0105 (1.149)	1.0084 (1.206)	1.0027 (1.329)	0.9991 (1.395)	1.0008 (1.329)
	45^{o}	1.0111 (1.098)	1.0210 (0.951)	1.0179 (1.097)	1.0010 (1.461)	0.9875 (1.685)	0.9944 (1.460)
	67.5^{o}	1.0088 (0.875)	1.0525 (0.534)	1.0559 (0.826)	0.9896 (1.854)	0.9569 (3.003)	0.9666 (1.831)

Table 5.7 Asymmetry factor and charge ratio (bracketed) dependence on altitude; field strength 0.55 gauss, dip angle -60°, standard mid-latitude atmosphere, zero value cut-off.

Altitude (km)	Zenith Angle	Asymmetry factor and charge ratio at given azimuths 30°	90°	150°	210°	270°	330°
0	0°	1.0014 (1.266)					
	22.5°	1.0023 (1.231)	1.0047 (1.197)	1.0041 (1.231)	1.0008 (1.302)	0.9982 (1.339)	0,9990 (1.301)
	45°	1.0030 (1.178)	1.0090 (1.096)	1.0083 (1.177)	0.9997 (1.361)	0.9921 (1.462)	0.9946 (1.360)
	67.5°	1.0028 (1.073)	1.0127 (0.908)	1.0169 (1.072)	0.9971 (1.496)	0.9742 (1.765)	0.9835 (1.494)
0.7	0°	1.0014 (1.266)					
	22.5°	1.0020 (1.231)	1.0046 (1.197)	1.0039 (1.231)	1.0006 (1.302)	0.9980 (1.339)	0.9987 (1.302)
	45°	1.0032 (1.174)	1.0096 (1.089)	1.0090 (1.174)	1.0001 (1.365)	0.9920 (1.472)	0,9945 (1.365)
	67.5°	1.0027 (1.062)	1.0132 (0.889)	1.0182 (1.061)	0.9974 (1.511)	0.9724 (1.803)	0.9822 (1.509)
1.35	0°	1.0014 (1.266)					
	22.5°	1.0022 (1.231)	1.0048 (1.195)	1.0041 (1.230)	1.0007 (1.303)	0.9980 (1.341)	0.9988 (1.303)
	45°	1.0034 (1.171)	1.0102 (1.083)	1.0095 (1.171)	1.0004 (1.368)	0.9919 (1.479)	0.9943 (1.368)
	67.5°	1.0021 (1.051)	1.0129 (0.871)	1.0191 (1.050)	0.9971 (1.527)	0.9699 (1.839)	0.9807 (1.524)

Table 5.8 Asymmetry factor and charge ratio (bracketed) dependence on geomagnetic cut-off; field strength 0.55 gauss, dip angle -30°, sea level in standard mid-latitude atmosphere.

Cut-off (GeV/c)	Zenith Angle	Asymmetry factor and charge ratio at given azimuths 30°	90°	150°	210°	270°	330°
0	0°	1.0042 (1.266)					
10		1.0037 (1.266)					
15		1.0032 (1.266)					
20		1.0028 (1.266)					
30		1.0022 (1.266)					
0	22.5°	1.0064 (1.206)	1.0099 (1.149)	1.0082 (1.206)	1.0025 (1.329)	0.9985 (1.394)	1.0007 (1.329)
15		1.0052 (1.215)	1.0083 (1.165)	1.0066 (1.215)	1.0016 (1.320)	0.9985 (1.376)	1.0003 (1.319)
20		1.0047 (1.219)	1.0075 (1.173)	1.0059 (1.219)	1.0014 (1.315)	0.9986 (1.366)	1.0002 (1.315)
30		1.0037 (1.226)	1.0061 (1.188)	1.0046 (1.226)	1.0009 (1.307)	0.9987 (1.349)	1.0000 (1.307)
0	45°	1.0091 (1.117)	1.0164 (0.985)	1.0145 (1.117)	0.9997 (1.436)	0.9871 (1.627)	0.9944 (1.435)
15		1.0085 (1.131)	1.0159 (1.010)	1.0131 (1.131)	0.9998 (1.417)	0.9895 (1.587)	0.9952 (1.417)
30		1.0071 (1.156)	1.0141 (1.054)	1.0105 (1.155)	0.9997 (1.387)	0.9926 (1.520)	0.9963 (1.387)

Table 5.8 (continued)

Cut-off (GeV/c)	Zenith Angle	Asymmetry factor and charge ratio at given azimuths 30°	90°	150°	210°	270°	330°
45	45°	1.0059 (1.175)	1.0121 (1.090)	1.0085 (1.175)	0.9996 (1.364)	0.9946 (1.470)	0.9971 (1.364)
0	67.5°	1.0084 (0.951)	1.0250 (0.690)	1.0234 (0.948)	0.9895 (1.690)	0.9562 (2.323)	0.9754 (1.685)
20		1.0094 (0.967)	1.0298 (0.712)	1.0232 (0.963)	0.9911 (1.665)	0.9640 (2.251)	0.9781 (1.658)
40		1.0104 (1.005)	1.0347 (0.772)	1.0215 (1.000)	0.9938 (1.602)	0.9772 (2.076)	0.9835 (1.596)
60		1.0105 (1.041)	1.0356 (0.832)	1.0193 (1.037)	0.9958 (1.545)	0.9863 (1.925)	0.9877 (1.540)

Table 5.9 Asymmetry factor and charge ratio (bracketed) dependence on geomagnetic cut-off; field strength 0.55 gauss, dip angle -60°, sea level in standard mid-latitude atmosphere.

Cut-off (GeV/c)	Zenith Angle	Asymmetry factor and charge ratio at given azimuths 30°	90°	150°	210°	270°	330°
0	0°	1.0014 (1.266)					
10		1.0012 (1.266)					
16		1.0011 (1.266)					
0	22.5°	1.0023 (1.231)	1.0047 (1.197)	1.0041 (1.231)	1.0008 (1.302)	0.9982 (1.339)	0.9990 (1.301)

Table 5.9 (continued)

Cut-off (GeV/c)	Zenith Angle	Asymmetry factor and charge ratio at given azimuths 30°	90°	150°	210°	270°	330°
10	22.5°	1.0021 (1.234)	1.0044 (1.202)	1.0038 (1.234)	1.0008 (1.299)	0.9983 (1.333)	0.9991 (1.299)
16		1.0019 (1.236)	1.0041 (1.207)	1.0035 (1.236)	1.0006 (1.297)	0.9984 (1.328)	0.9991 (1.297)
0	45°	1.0030 (1.178)	1.0090 (1.096)	1.0083 (1.177)	0.9997 (1.361)	0.9921 (1.462)	0.9946 (1.360)
16		1.0028 (1.187)	1.0084 (1.112)	1.0073 (1.186)	0.9997 (1.351)	0.9933 (1.441)	0.9953 (1.350)
24		1.0027 (1.192)	1.0079 (1.123)	1.0067 (1.192)	0.9996 (1.345)	0.9938 (1.427)	0.9957 (1.344)
0	67.5°	1.0028 (1.073)	1.0127 (0.908)	1.0169 (1.072)	0.9971 (1.496)	0.9742 (1.765)	0.9835 (1.494)
20		1.0034 (1.083)	1.0143 (0.925)	1.0162 (1.082)	0.9975 (1.482)	0.9778 (1.732)	0.9852 (1.480)
30		1.0038 (1.095)	1.0149 (0.947)	1.0151 (1.094)	0.9978 (1.465)	0.9810 (1.693)	0.9869 (1.463)

[from page 207] The particular conditions applying to the various sets of calculations do not correspond to those at any particular site, although certain of the parameter values (for example, altitude) were, in fact, selected to allow particular information to be obtained. These calculations, rather, were carried out in order to admit an understanding of the nature of the asymmetry function, and, in addition, to allow estimates to be made of the asymmetry factor

applicable to any particular situation, where the configuration of the variables lies within the ranges considered.

From the tabulated asymmetry factor values it may be seen that the magnetic field in the atmosphere can introduce very considerable perturbations into the sea level muon intensity distribution, particularly so at high zenith angles. Under the equatorial conditions simulated in Table 5.5, the calculations predict an east-west asymmetry of approximately 7 % at a zenith angle of 67.5^{o}, as a consequence of the muon deflections. This asymmetry is of the same order of magnitude as that produced by the geomagnetic cut-offs at low latitudes, so the importance of taking the atmospheric asymmetry effect into account when interpreting low latitude observations will be readily appreciated. It is interesting to note too, that the vertical asymmetry factor in this situation indicates a reduction of $\approx\frac{1}{2}$ % in vertical muon intensity, due to the local magnetic field, compared with the reduction of ≈ 0.1 % in magnetic field configurations corresponding to high latitude sites. Evidently a significant latitude dependence of vertical detector rate can arise out of the presence of the magnetic field in the atmosphere.

To illustrate more specifically the character of the asymmetry function, we present in Figure 5.13 a graphical representation of the variation of asymmetry factor with zenith and azimuth angle at sea level in the standard mid-latitude atmosphere, for magnetic field strength 0.55 gauss, and for dip angles of 0^{o}, -30^{o}, and -60^{o}.

The curves show, as expected, a maximum in the east and a minimum in the west. The azimuth position of the maximum is seen to be displaced towards higher values with increasing magnitude of the dip angle. The effect on the directional distribution of muons would be to cause a progressive increase in magnitude of the north-south asymmetry.

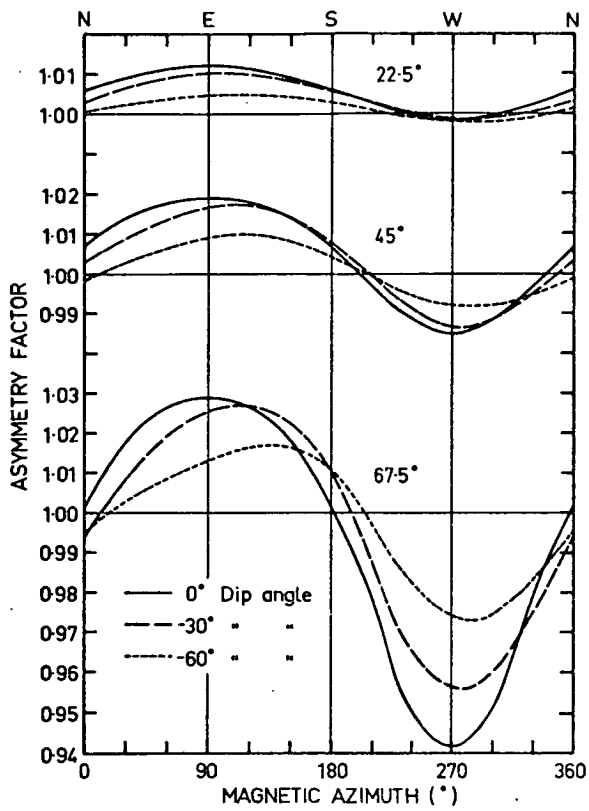

Figure 5.13. Dependence of the asymmetry factor on zenith and azimuth angle, for various values of dip angle.

It is to be noted that the curves are not symmetrically disposed about the ordinate 1.0000, confirming the conjecture in Section 5.2, that at high latitudes the western muon intensities are not necessarily enhanced by an amount equal to the diminuition of the eastern intensities. For a zenith angle of 22.5^{o} the curves are displaced well above the line corresponding to the unperturbed intensity, whilst for the 67.5^{o} zenith angle curves the mean is displaced below this line. At high zenith angles, as a result, there is an essential difference between the manifestation of the atmospheric asymmetry

effect and the asymmetries produced by the geomagnetic cut-offs. The cut-off produced effect appears as the result of reduction of the intensities in the east, whilst the atmospheric asymmetry, at the high zenith angle, arises mainly from the enhancement of western intensities, with a smaller decrease of intensity in the east.

This difference is readily illustrated graphically. In Figure 5.14a we present diagrams representing the dependence of intensity

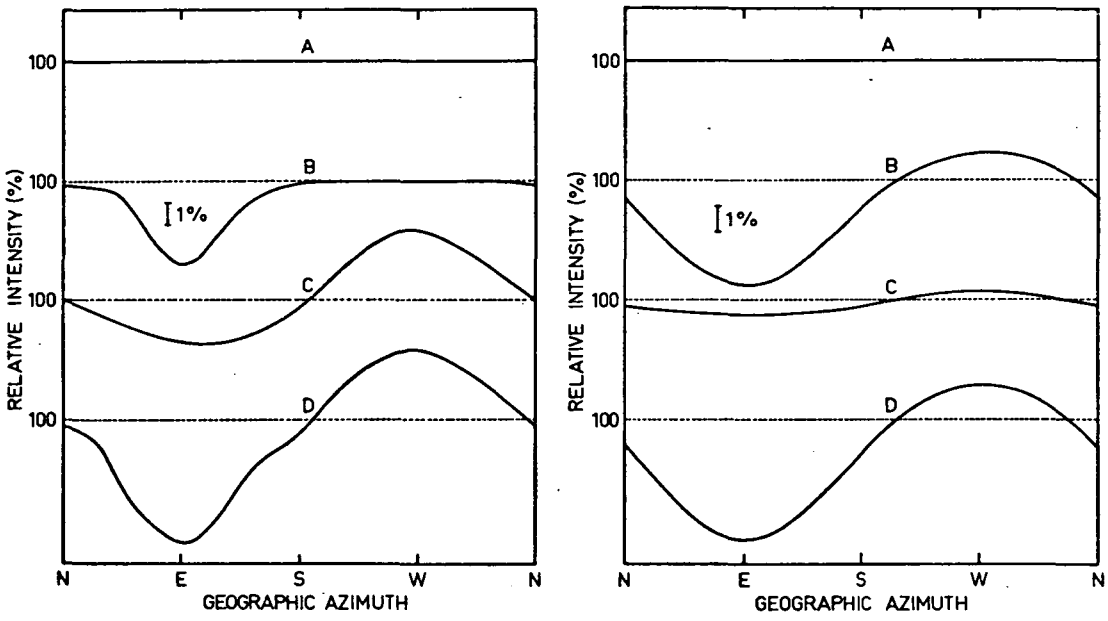

Figures 5.14a (left) and 5.14b (right). Graphical illustration of the typical magnitude and form of intensity contributions to azimuthal asymmetry at high and low zenith angles respectively due to geomagnetic cut-off and atmospheric asymmetry effects. The sequence of drawings A to D is explained in detail in the text. The origin of these curves is discussed in Section 5.12.4.

on azimuth as it might exist at a high zenith angle, at mid to low latitudes. The individual curves correspond to:

A. The intensity distribution in the absence of atmospheric and geomagnetic cut-off asymmetry components.

B. The geomagnetic cut-off produced intensity distribution, as it would exist in the absence of atmospheric asymmetry.

C. The intensity distribution produced by the atmospheric asymmetry effect in the absence of geomagnetic cut-offs.

D. The expected intensity variation with azimuth, in the presence of both effects.

This latter curve displays a kink, for the case illustrated, in the south. This occurs as the result of displacement of the intensity minimum associated with the atmospheric asymmetry to higher value azimuths in the presence of a non-zero dip angle, together with the presence of the cut-off produced intensity diminuition over a limited range of azimuths (the limiting is caused by the presence of a relatively high value of atmospheric cut-off).

The same sequence of curves A to D is displayed in Figure 5.14b, but in this case referring to the intensity distribution existing at a low zenith angle. Here the atmospheric asymmetry is manifested in a similar manner to the geomagnetic cut-off effect, and, notwithstanding the difference in magnitude, would not be expected to have any effect other than to displace the minimum in the resulting intensity pattern to higher values of azimuth angle.

In the vertical direction the presence of any magnetic field

(save that with the field lines vertical) must introduce trajectory curvature, lengthening the muon paths relative to what they would have been in the absence of the field. For this reason, the asymmetry factors relating to the vertical direction must, without exception, have magnitude in excess of unity (see for example, the values in Table 5.3 to 5.9). The displacement, to values > 1.0000, of the mean asymmetry factor values pertaining to 22.5^{o} zenith angle, as discussed earlier in this section in conjunction with Figure 5.13, is associated with the tendency for trajectories to lengthen in the presence of a field. At high zenith angles, on the other hand, the fact that the mean asymmetry factor values are less than unity indicates that the introduction of trajectory curvature tends to decrease the mean path lengths in the atmosphere. [to page 221]

Table 5.10 Configuration of the parameters applying to the results depicted in Figure 5.15. (*) denotes the independent variable in each of the six graphs displayed.

Graph number:	1	2	3	4	5	6
Zenith angle	*	-	-	-	-	-
Field strength	0.55	*	0.55	0.55	0.55	0.55
Atmos. config.	mid	mid	*	mid	mid	mid
Dip angle (^{o})	-30	-30	-30	*	-30 -60	-30 -60
Altitude	0	0	0	0	*	0
Cut-off	0	0	0	0	0	*

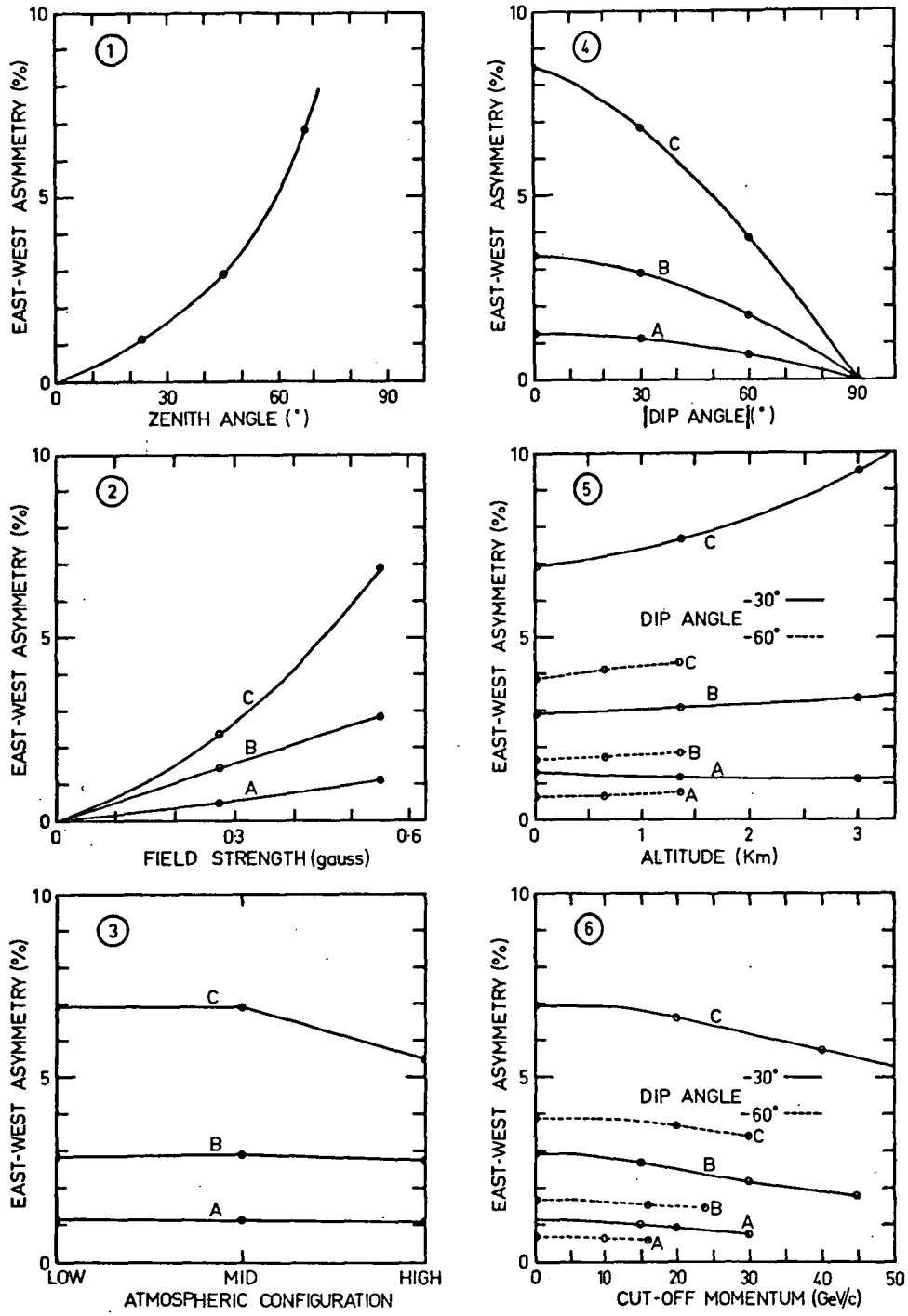

Figure 5.15 (containing graphs 1 - 6). Calculated dependence of east-west asymmetry on various parameters as listed in Table 5.10.

[from page 219] It is of interest to consider the east-west asymmetry as derived from the calculated asymmetry factors, and its dependence on the parameters introduced into those calculations. In Figure 5.15 we present a set of six graphs illustrating the behaviour of the east-west asymmetry under the conditions listed in Table 5.10.

These diagrams show that, although the magnitude of the asymmetry varies rapidly with change in magnetic field conditions, and zenith angle, it evidently does not have a very steep dependence on atmospheric conditions or on geomagnetic cut-off. It is fortunate, for the calculation of atmospheric asymmetry at any particular site, that those factors on which the asymmetry is most sensitively dependent, are those which most easily admit precise measurement.

It is interesting to note, in graph 2 of Figure 5.15, that as predicted by less detailed east-west asymmetry calculations, and discussed by Burbury and Fenton [1952] (see Section 5.2), the east-west asymmetry is proportional to the magnitude of the horizontal magnetic field component (even though, in our calculations, the total magnetic field was inclined at a dip angle of -30^{o}), although at high zenith angles there is some departure from precise proportionality.

5.12 Asymmetry Factors for Detectors of Finite Acceptance Angle

5.12.1 Derivation Technique

In the preceding section we examined the general dependence of

the atmospheric asymmetry effect on various geophysical factors that influence the production and motion of muons in the atmosphere. Calculation of the asymmetry factor has been carried out by simulating the arrival of an infinitesimally narrow angle beam of muons in specified directions, under given conditions. In practice it is necessary to be able to derive asymmetry factors applicable to detectors of finite acceptance angle in any particular situation, in order to remove the atmospheric asymmetry contamination from observational data.

In order to solve this problem we have investigated the relationship between the asymmetry factor values pertaining to such detectors and the unidirectional values. It was found, by representing the dependence of the asymmetry factor on zenith and azimuth by polynomial functions, and comparing the magnitude of the calculated directional muon intensities relative to the intensities calculated to exist in the absence of the atmospheric asymmetry effect, that the mean effective asymmetry factor values were nearly equal, for any given detector, to the unidirectional values applicable to a particular, "equivalent" zenith angle. This zenith angle was found to be dependent on the axial inclination of the telescope considered, and on the width of the acceptance cone. Not surprisingly, the "equivalent" zenith angle was found to correspond approximately to the zenith angle of maximum response of the telescope. Thus, for the purposes of calculating the asymmetry factors applicable to different viewing conditions, it is necessary only to determine the unidirectional values appropriate

to the "equivalent" zenith angle. In Table 5.11 we present the equivalent zenith angles of the latitude survey telescopes and the wide angle telescope at Mawson (these telescopes are described in Sections 2.2.1 and 5.4 respectively).

Table 5.11 Comparative values of axial and equivalent zenith angles of the narrow angle latitude survey telescopes, and the wide angle telescope at Mawson.

Telescope	Axial zenith angle	Equivalent zenith angle
Latitude survey narrow angle telescope	22.6^{o}	23.5^{o}
" "	45.2^{o}	45.2^{o}
" "	67.8^{o}	66.0^{o}
Mawson wide angle telescope	45.0^{o}	40.5^{o}

5.12.2 Re-examination of Mawson Data

We are now in a position to accurately predict the azimuthal asymmetry pattern at Mawson, for comparison with that observed. The expected azimuthal dependence of inclined wide angle telescope counting rate was deduced, by carrying out calculations for a range of azimuths, at the equivalent zenith angle discussed above, taking into account the atmospheric and magnetic field configurations at the site. The calculated asymmetry pattern is displayed in Figure 5.16, together with the experimental result, as reported in Section 5.4. The theoretical result is seen to be in considerably better

agreement with experiment (particularly in the case of the north-south asymmetry) than the theoretical calculations reported in Section 5.4. Evidently, the simple north-south asymmetry theory of Burbury [1952] does not completely represent the physical situation.

The residual asymmetry pattern, after the Mawson observations had been corrected by application of the calculated asymmetry factors, is also displayed in Figure 5.16. A small though significant north-south asymmetry (0.3 %) remains, in addition to an east-west asymmetry of the same magnitude, evidently as a result of the presence of a primary anisotropy, as discussed in Section 5.5.

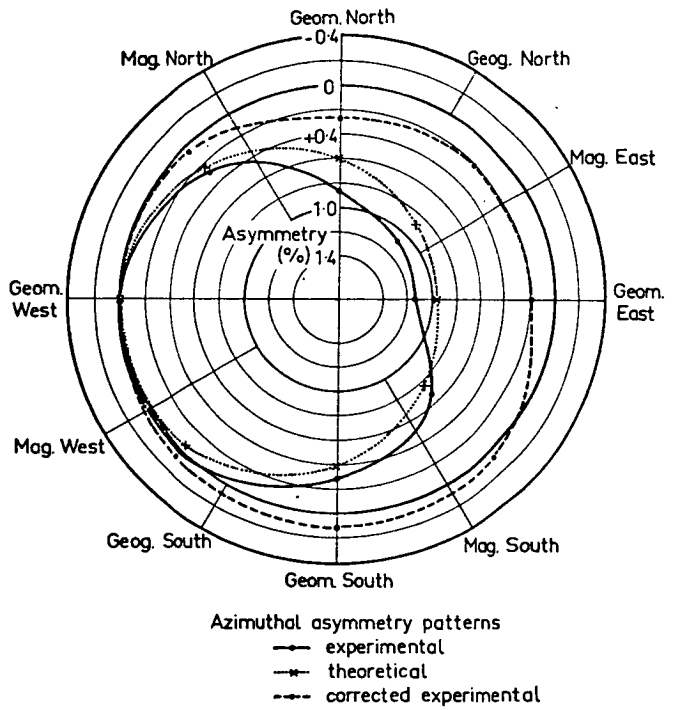

Figure 5.16. Comparison of the calculated asymmetry pattern at Mawson with that observed by inclined wide angle telescope. Also shown is the residual pattern obtained by correction of these data.

5.12.3 Correction of the Data of Mathews and Sivjee

A clear demonstration of the effectiveness of the use of calculated asymmetry factors in removing the atmospheric asymmetry contamination in directional muon intensity observations at low latitudes lies in the correction of the data of Mathews and Sivjee [1967]. In order to obtain atmospheric depths equivalent to those in the vertical direction at sea level, but with maximum cut-off momenta (to 25 GeV/c) very considerably in excess of those vertically, these authors carried out a series of measurements with an inclined detector at elevated sites near the equator. They hoped to obtain the extended form of the vertical sea level muon integral response curve in order to deduce the form of the coupling coefficients in the region of the function maximum (discussed further in Section 6.7).

It was found, however, (see Figure 5.17) that the curve expressing the intensity-cutoff relationship obtained from the high altitude measurements possessed considerably greater slope than that obtained by sea level latitude surveys with vertical detectors, in the range of momentum values common to both; and in addition, the curvature of the functions in the overlap region were of opposite sign.

Mathews and Sivjee, in interpreting their data, did not take into account the presence of the atmospheric asymmetry effect, which manifestly adds to the total east-west asymmetry and would, as a result, be expected to increase the slope of the momentum-

ordered data.

To test whether the atmospheric asymmetry effect could, in fact, have been responsible for the observed discrepencies, calculations

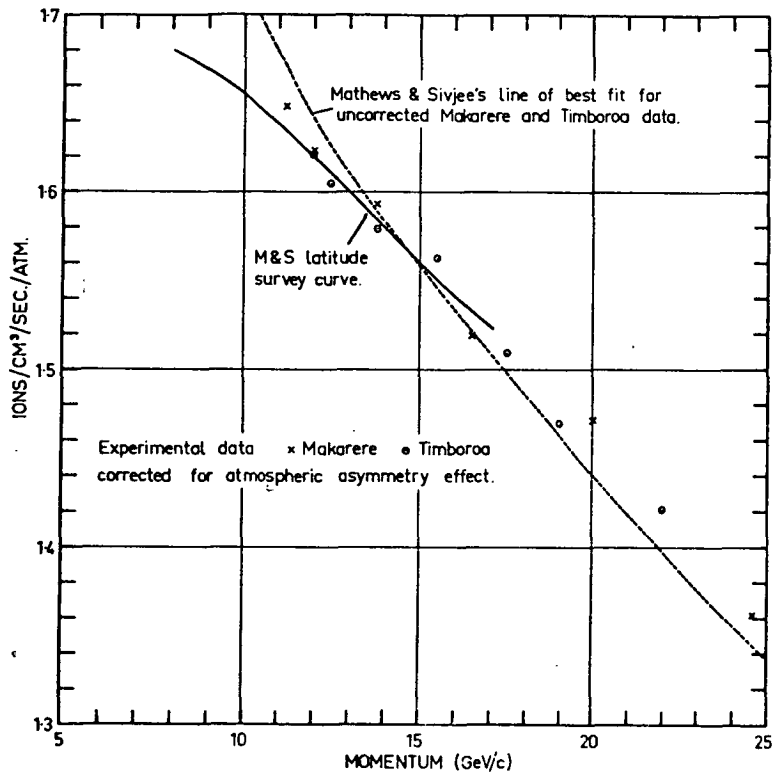

Figure 5.17. A reproduction of Figure 5 of Mathews and Sivjee [1967], showing the observed intensity of ions as functions of cut-off momentum, as deduced from latitude survey measurements (solid line), and mountain altitude azimuth survey (broken line). Also shown are the experimental data after correction for removal of the atmospheric asymmetry (calculated asymmetry factors applied). In the range of overlap, these data points are seen to be in very much better agreement with the latitude survey result (solid line) than the uncorrected data, as represented by the broken line.

have been carried out to deduce the asymmetry factors pertaining to the conditions of the observations. The equivalent angle of viewing of the telescope (see Section 5.12.1) at each site was estimated by determining the zenith angle of maximum telescope response in each situation, and used in the computations, in conjunction with the appropriate magnetic field configuration as predicted by the Finch and Leaton [1957] coefficients, the standard equatorial atmosphere (see Section 5.7.7), and the directions of viewing and associated cut-off momenta as published by Mathews and Sivjee. The intensity data were then corrected by application of these asymmetry factors, and replotted in Figure 5.17. The ordered data now appear to be in good accord with the vertical integral response curve.

We use the corrected data of Mathews and Sivjee in Section 6.7 as an important piece of evidence in the process of fixing the form of the directional muon coupling coefficients.

5.12.4 Correction of Latitude Survey Data

A series of calculations has been carried out to deduce the asymmetry factors pertaining to the latitude survey data. The known magnetic field configuration at each site, the equivalent zenith angles of viewing as listed in Section 5.12.1, and the atmospheric structure appropriate to each site were used as input data to the "muons in the atmosphere" computer program. The atmospheric profiles were adapted from information about the mean height and temperature of the significant pressure levels, as indicated by

the routine radiosonde flights conducted at the airport sites during the observing periods. At the sites where such information was not directly available (Mossman and Rockhampton), estimates of the atmospheric structures were obtained by interpolating details of the pressure levels for the corresponding periods at sites located at points either side of the survey stations (Port Moresby, Townsville and Brisbane). The technique involved in introducing the pressure data into the calculations is discussed in Section 5.7.7.

The cut-off values introduced into the asymmetry factor calculations were the mean effective cut-offs (or, when the mean effective cut-offs were indeterminate, the axial effective cut-offs) pertaining to the directions of viewing at each site. An approximation was implicit in the use of these cut-offs, inasmuch as a constant cut-off value is assumed, in the calculations, to apply to all the trajectory traces pertaining to any given direction at a site, rather than the cut-offs in the directions of entry of the primary particle destined to give rise to the muons, which, moving along curved trajectories, arrive at the site in the directions of interest. The "true" cut-off values could have been introduced into the calculations by arranging that the program deduce from the matrix of values representing the cut-off distribution at each of the sites (see Section 3.3.4) the appropriate cut-off value at the end point of each calculated trajectory. To have done this would have involved approximately double the computer time, as it would have been necessary to trace each trajectory twice - first to

deduce the "asymptotic direction" at the top of the atmosphere, and then again to allow the computation of the differential muon intensities, since this latter calculation involves knowledge of the cut-off in the evaluation of an integral along the trajectory.

It is estimated that the maximum error likely to arise from the use of the given cut-off values is small because of the comparative insensitivity of the asymmetry factor to change in cut-off and the relatively slow change in cut-off with direction. Because no observations were made in the direction of main cone folds (see Section 4.7), the rapid change in cut-off in these directions does not have to be considered. In addition, since the oppositely directed deflection of the positive and negative muons tend to give rise to "true" cut-offs both above and below the mean effective cut-off value, it might be expected that any error due to this source would be a second order effect.

The atmospheric asymmetry effect has been removed from the latitude survey data by application of correction factors calculated to take into account the asymmetry factor in both inclined and vertical directions. These corrected data are presented in Tables 5.12 to 5.14 inclusive, and plotted as a function of mean effective cut-off in the inclined direction, in Figure 5.18. In situations where the mean effective cut-off value is indeterminate (geomagnetic cut-off exceeded by atmospheric cut-off), inclined axial effective cut-off values have been used.

The improvement in the ordering of the experimental [to p.231]

Tables 5.12 and 5.13. Value of corrected inclined/vertical intensity ratio for various values of azimuth at latitude survey sites; zenith angle of inclined detectors: 22.6^{o} and 45.2^{o} respectively.

Table 5.12

Site	Inclined/vertical ratio at specified azimuths (*)							
	1	2	3	4	5	6	7	8
Mossman	0.8564	0.8220	0.8567	0.8761				
Townsville	0.8495	0.8307	0.8195	0.8351	0.8472	0.8594	0.8663	0.8621
Rockhampton	0.8434	0.8272	0.8345	0.8436	0.8535	0.8586	0.8522	
Brisbane	0.8417	0.8388	0.8405	0.8438	0.8463	0.8446	0.8434	
Williamtown	0.8453	0.8445	0.8434	0.8411				
Laverton	0.8417	0.8391	0.8370	0.8383				
Hobart	0.8399	0.8397	0.8400	0.8395				

* See Table 2.5.

Table 5.13

Site	Inclined/vertical ratio at specified azimuths (*)							
	1	2	3	4	5	6	7	8
Mossman	0.5001	0.4664	0.5015	0.5101				
Townsville	0.4880	0.4750	0.4613	0.4814	0.4947	0.4971	0.4976	0.4987
Rockhampton	0.4867	0.4732	0.4729	0.4884	0.4936	0.4886	0.4908	
Brisbane	0.4752	0.4772	0.4781	0.4777	0.4814	0.4792	0.4803	
Williamtown	0.4752	0.4726	0.4753	0.4753	0.4749			
Laverton	0.4704	0.4720	0.4655	0.4679				
Hobart	0.4711	0.4697	0.4735	0.4720				

* See Table 2.5.

Table 5.14 Value of corrected inclined/vertical intensity ratio for various values of azimuth at latitude survey sites; zenith angle of inclined detector: 67.8^{o}. NOTE: errors on ratios in Tables 2.2-2.4 apply to corresponding ratios in Tables 5.12-5.14.

Site	Inclined/vertical ratio at specified azimuths (*)							
	1	2	3	4	5	6	7	8
Mossman	0.1468	0.1392	0.1475	0.1487				
Townsville	0.1429	0.1406	0.1380	0.1434	0.1438	0.1434	0.1425	0.1438
Rockhampton	0.1412	0.1406	0.1410	0.1424	0.1443	0.1420	0.1415	
Brisbane	0.1376	0.1378	0.1389	0.1390	0.1396	0.1385	0.1379	
Williamtown	0.1376	0.1352	0.1357	0.1361				
Laverton	0.1344	0.1329	0.1350	0.1342				
Hobart	0.1344	0.1354	0.1352	0.1349				

* See Table 2.5.

[from page 229] data on introduction of the corrections is evident when these plots are compared with those in Figure 4.29. It may be seen that, if the vertical displacement between the various subsets of data was removed, the points at each zenith angle would lie close to a common curve, having, as expected, minimum slope at the lowest momentum values. The interpretation of these data is carried out in the following chapter.

The effectiveness of the applied asymmetry factors in removing the atmospheric asymmetry component is illustrated in Figure 5.19, which shows the latitude dependence of the east-west [to page 233]

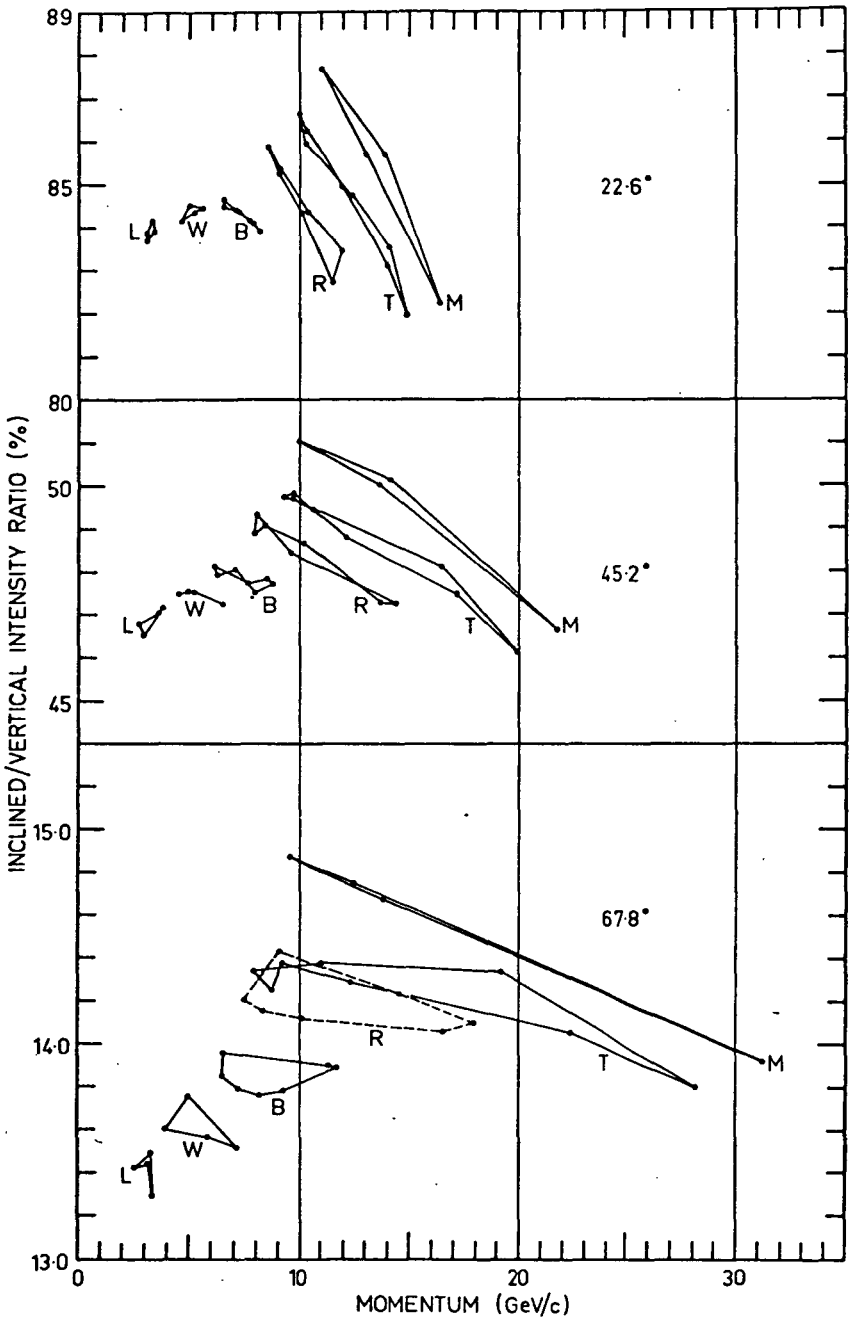

Figure 5.18. Corrected latitude survey data, plotted in the form of rates relative to that of a vertical detector at each site, of detectors inclined to 22.6^{o}, 45.2^{o} and 67.8^{o}, as function of mean effective cut-off momentum in the inclined viewing direction.

[from page 231] asymmetry in the corrected latitude survey data (compare this diagram with Figure 5.2, which shows the corresponding dependence in the uncorrected data). It may be seen that the magnitude of the residual asymmetry at the higher latitudes is essentially zero in the corrected data, becoming finite at latitudes where the geomagnetic cut-offs start to exert a significant influence.

By comparing the mean effective cut-off momentum values

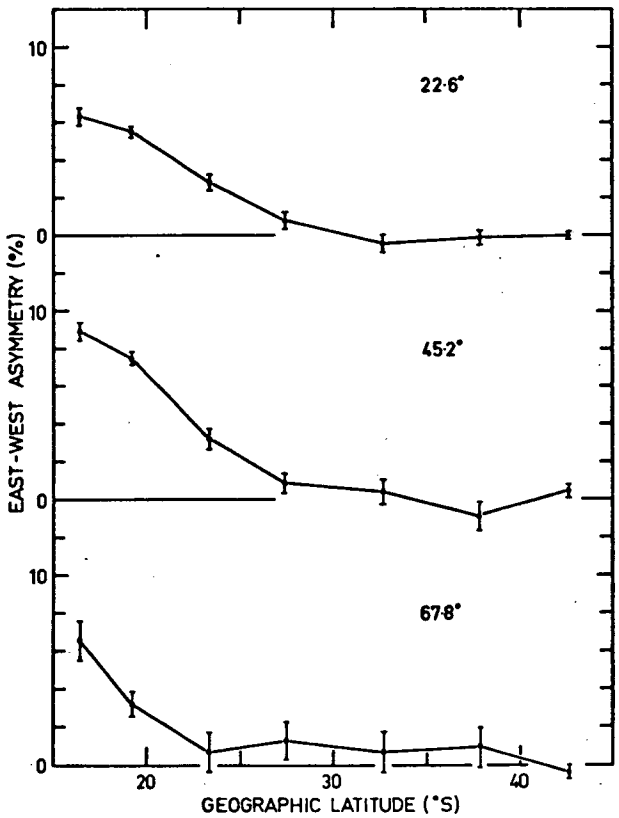

Figure 5.19. Latitude dependence of east-west asymmetry as indicated by the atmospheric asymmetry-corrected latitude survey data (compare this diagram with Figure 5.2).

Section 4.6) in the east and west with the mean effective atmospheric cut-off value pertaining to telescopes at each inclination, predictions have been made of the latitude position of the "knee" in these directions. These positions are listed in Table 5.15.

Table 5.15 Predicted position of latitude "knee" in the east and west, corresponding to observation by the inclined latitude survey telescopes.

Zenith angle (^{o}) of telescope axis	Position of "knee" (^{o}S. Geographic)	
	In east	In west
22.6	35	32
45.2	34	27
67.8	27	17

The latitude dependence of the east-west asymmetry could be expected to reflect the presence of the "knees" in the east and west. In Figure 5.19 it can be seen that the experimental result, whilst not showing distinct evidence of the "knee" in the west, does show very clearly the effect in the east (the experimental positions agree closely with those predicted). The effect is pronounced, for it is at these latitudes that the cut-offs first influence the east-west asymmetry.

Having demonstrated, in the preceding discussion, the apparent validity of certain predictions made on the basis of the calculations, it is pertinent to explain the origin of the intensity

distributions illustrated in Figures 5.14a and 5.14b. These curves correspond to the azimuth distribution of intensity at 67.8^{o} and 22.6^{o} zenith angle respectively at Townsville, as predicted using the calculated asymmetry factors, and the integral response functions derived in the following chapter. The "kink", visible in the higher zenith angle curve, and discussed in Section 5.11, is predicted on this basis. It is interesting to note that the experimental data show evidence of this effect (see Figure 2.13). This fact supports the assumption that the atmospheric asymmetry and the geomagnetic cut-off produced asymmetry co-exist at low latitudes in the manner predicted by calculation.

5.13 Conclusions

Although the atmospheric asymmetry effect is responsible for very significant contributions to the azimuthal asymmetry of the directional distribution of muon intensity deep in the atmosphere (at low latitudes and at high zenith angles the effect is of the same order of magnitude as that produced by the geomagnetic cut-offs), almost without exception the investigators examining muon intensity distributions have overlooked the effect, and have carried out interpretation in terms of cut-offs alone.

The investigation reported in this chapter was carried out in order to determine the nature of the atmospheric asymmetry effect, and to calculate its dependence on direction, and on various geophysical factors - atmospheric structure, magnetic field

configuration, altitude, and geomagnetic cut-offs.

It was found convenient to express the results of the calculations (which were carried out using the Olbert production spectrum model, modified in certain respects) in terms of "asymmetry factors" - values of the ratio (intensity of muons that would exist in a given situation in the absence of a local magnetic field) / (intensity that would exist in the same physical situation in the presence of the field). The calculated sets of asymmetry factor values have been presented in full, as, in principle, through their use, the atmospheric asymmetry in any related situation may be determined.

Examination of these data reveals that the azimuthal asymmetries produced by the atmospheric asymmetry effect are relatively insensitive to change in atmospheric structure, and geomagnetic cut-offs, but are very directly dependent on magnetic field configuration. As one result of this latter sensitivity, a latitude dependence of vertical muon intensity ($\approx \frac{1}{2}\%$) is predicted, due to change in local field conditions with latitude.

The relationship between the unidirectional asymmetry factors and those pertaining to detectors of finite acceptance angle has been investigated, and it is apparent that, to an acceptable accuracy, the asymmetry factor values applicable to given inclined detectors correspond to those unidirectional values pertaining to the zenith angle of maximum telescope response in the same situation.

On application of asymmetry factors to experimental data from Mawson, for removal of the atmospheric asymmetry component, a residual

asymmetry pattern remains, suggesting the presence of a steady primary anisotropy, such as could be produced by a density gradient of cosmic ray intensity normal to the ecliptic plane.

Finally, the techniques developed in this chapter have been applied in the atmospheric asymmetry-correction of the latitude survey data. It was found possible to obtain more satisfactory momentum ordering of the corrected, than of the uncorrected, data, the peculiarities associated with the integral response curves deduced from the uncorrected data having been removed.

In the following chapter we use these atmospheric asymmetry-corrected latitude survey data in the determination of directional muon coupling coefficients.

CHAPTER 6

DETERMINATION OF COUPLING COEFFICIENTS

6.1 Introduction

As the result of investigations described in the preceding chapters, the latitude survey data have been corrected to remove the effects of the atmospheric asymmetry, and ordered by the use of calculated mean effective cut-offs pertaining to the various directions of viewing at the sites (see Figure 5.18). These data, after normalization to remove the displacement between the various subsets of data applying to each zenith angle, will represent the integral response functions (see Section 1.2) for telescopes inclined to three zenith angles. In addition, because of the use of the inclined/vertical mode of data presentation, the integral response function pertaining to the vertical telescope may be deduced from the normalization factors, as discussed in Section 2.3.4.

The coupling coefficients, which express the fractional contribution to the detector rate attributable to primary particles within any particular momentum interval, are related to the first differential of the integral response function (equation 1.4). In order to form an estimate of the coupling coefficients from the experimental integral response functions, it is necessary to determine the slope of these functions as a function of momentum. Since these estimates will apply to values of momentum corresponding

to the range of cut-offs encountered on the latitude survey, extrapolation to high momentum values is necessary in order to obtain complete specification of the detector coefficients.

Because the coupling coefficients applying to particular detectors are of limited general application, it is obviously desirable to obtain the coefficients in the form of a basic unidirectional set, which may then be used to derive the coupling coefficients applying to any detector.

This chapter describes the derivation of a unidirectional coupling coefficient function from the experimental data. A technique is developed by which the zenith angle dependence of parameters controlling the form of an empirical function fitted to the experimental integral response functions is examined, so that the zenith angle dependence of the coupling coefficient function may be deduced. Other techniques are then used to extrapolate the function to high momentum values and to high zenith angles.

Because of the importance of the ratio method of analysis in extracting information from the experimental data, it is desirable, before proceeding further in the data analysis, to justify the technique and to estimate the possible errors associated with its implementation.

6.2 Justification of the Ratio Method of Analysis

The ratio technique (qualitatively discussed in Section 2.3.4) relies on the constancy, over a wide zenith angle range, of the

coefficients expressing the dependence of muon intensity on atmospheric structure. In the absence of primary spectral changes, variation in atmospheric conditions would thus be expected to produce sensibly the same fractional change in muon intensity at each zenith angle, causing the ratio of inclined to vertical intensity to be independent of atmospheric structure. The ratio would, of course, be dependent on the zenith angle of the inclined direction and the cut-off values associated with the directions considered.

The near constancy of the atmospheric coefficients with zenith angle is supported both theoretically and experimentally. Fenton [1952] investigated the zenith angle dependence of the barometer coefficient and found theoretically that, whilst the coefficients pertaining to muons of any particular momentum increase appreciably with zenith angle, the integral coefficients, due to the progressive hardening of the spectrum with increasing zenith angle, display only a small change, a decrease, with zenith angle. The effect was undetectable in the experimental evidence available at the time. The theoretical calculations of Wada [1960] support Fenton's finding.

Dorman, Kovalenko and Milovidova [1965] experimentally determined the dependence of the barometer coefficient on zenith angle. Their results, like those of Fenton, fail to show any significant change in coefficient value with zenith angle. The experimental results of Fenton, and Dorman et al. are summarized in Figure 6.1. It is apparent from this diagram that the magnitude of any systematic change in the barometer coefficient must be of the order of 0.02 % per mb or

less over the range 0^{o}-70^{o}. It is of interest to calculate what effect a zenith angle variation in the coefficients of this magnitude would have on the experimental ratio values.

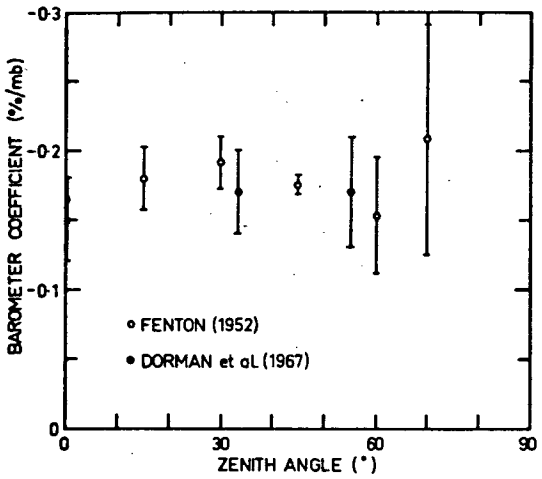

Figure 6.1. Zenith angle dependence of sea level muon barometer coefficient, as experimentally determined by Fenton [1952], and Dorman et al. [1967].

As indicated in Table 2.1, the mean pressures experienced during the observing periods at the sites lay within a 13 mb range. If, as a first approximation, the assumption is made that all the observations were made at different levels within a common atmosphere (overlooking for the moment the effect of the temperature distribution within the atmosphere on the ratios), then the maximum error in the ratio values due to the observed pressure differences would be of the order of 0.3%, at a telescope inclination of 67.8^{o}. This error is of the order of the observational errors inherent in the ratio values (see Table 2.4) and consequently would not be expected to affect the validity of the ratio technique.

That the zenith dependence of the barometer coefficient may be ignored is supported by the results of the experiment described in Section 2.3.2, in which the inclined/vertical ratio was

measured over a large pressure range at Hobart. In this case the indicated differential pressure coefficient relating observations at 67.8^{o} and 0^{o} was +0.018 % per mb; the corresponding value for the 45.2^{o} and 0^{o}, +0.002 % per mb; and for 22.6^{o} and 0^{o}, -0.001 % per mb. As discussed in Section 2.3.3, the errors in the ratio values due to pressure changes are evidently small compared with the other errors of observation.

To test the dependence of the ratios on other than simple pressure changes (for example, on changes in the height of the pressure levels in the upper atmosphere), calculations have been made by means of the "muons in the atmosphere" computer program, to determine the expected values of inclined/vertical ratio in atmospheres of widely varying structure.

Firstly, calculations were carried out for a given pressure level (1013.2 mb) in the "standard" equatorial, mid-latitude, and polar atmospheres (see Section 5.7.7 for details of the calculation techniques, and the method of representing these atmospheres). Directional muon intensities were evaluated at zenith angles of 8.2^{o}, 23.5^{o}, 45.2^{o}, and 66^{o} (the "effective" zenith angles* of viewing of the 0^{o}, 22.6^{o}, 45.2^{o}, and 67.8^{o} latitude survey telescopes respectively), in the absence of geomagnetic cut-offs. The ratios are

* The zenith angle at which the unidirectional integral response function best matches the mean effective response function for each particular detector.

presented in Table 6.1, together with the percentage departure of each ratio value from the corresponding mid-latitude value.

Table 6.1 Values of inclined/vertical ratio calculated for the "standard" equatorial, mid-latitude, and polar atmospheres. The bracketed figures refer to the percentage departure of the ratios from the mid-latitude values.

Zenith angle	8.2^{o}	23.5^{o}	45.2^{o}	66.0^{o}
Atmosphere				
Equatorial	1.0000	0.8304 (+0.024)	0.4165 (+0.313)	0.1269 (+1.28)
Mid-latitude	1.0000	0.8302 -	0.4152 -	0.1253 -
Polar	1.0000	0.8316 (+0.169)	0.4171 (+0.458)	0.1254 (+0.080)

It is evident that, whilst some differences are predicted to arise in the ratio values because of the variation of atmospheric configuration, particularly at the higher zenith angles, these are small compared with the magnitude of the total intensity variation with latitude, and must not be regarded as serious, in view of the uncertainties associated with removing the dependence on atmospheric structure directly.

A further series of calculations has been carried out to estimate the likely dependence of the ratio values on both local atmospheric configuration and on the pressure level at the observing site.

The details of the atmospheres at each site have been introduced into the computer program and the directional muon intensities have been deduced, in the absence of cut-offs. The results are presented in Table 6.2, in the form (like Table 6.1) of inclined/vertical ratio values, as calculated for the effective zenith angles of viewing of the latitude survey detectors, together with the percentage departures of the values from the corresponding value at Hobart.

The indicated maximum departure of the ratios from constant values over the range of conditions is seen to be extremely small (0.05%) in the case of a telescope inclined to 22.6^{o}, and 1% for one at 67.8^{o} inclination, a value comparable with the other errors of observation. Test calculations have shown that, if anything, the computer program tends to indicate larger differences than actually are observed. In any case it is evident that ratios may be analysed on the assumption of independence from atmospheric effects without the introduction of serious systematic errors. This conclusion is supported by the internal consistency observed in the data during the detailed analysis.

6.3 Analysis of Experimental Data

The intensity-corrected and momentum-ordered ratio data, as shown in Figure 5.18, have, at each zenith angle, the form of displaced sections of a common integral response curve. This displacement, as mentioned in Section 2.3.4, is produced as a result of the change from site to site of the mean effective cut-off in the

Table 6.2 Values of inclined/vertical ratio calculated for atmospheric structures representative of those at the latitude survey sites. The bracketed figures refer to the percentage departure of the ratios from the Hobart values.

Zenith angle / Site	8.2°	23.5°	45.2°	66.0°
Mossman	1.0000	0.8305 (+0.00)	0.4166 (+0.10)	0.1270 (+0.79)
Townsville	1.0000	0.8304 (-0.01)	0.4165 (-0.05)	0.1267 (+0.56)
Rockhampton	1.0000	0.8309 (+0.05)	0.4175 (+0.31)	0.1272 (+0.95)
Brisbane	1.0000	0.8305 (+0.00)	0.4165 (+0.07)	0.1262 (+0.16)
Williamtown	1.0000	0.8304 (-0.01)	0.4159 (-0.07)	0.1258 (-0.16)
Laverton	1.0000	0.8308 (+0.04)	0.4163 (+0.02)	0.1258 (-0.16)
Hobart	1.0000	0.8305 -	0.4162 -	0.1260 -

direction of viewing of the vertical telescope. By correlating the indicated relative intensities with the mean effective cut-off values it is possible, in principle, to obtain the integral response curve from those pertaining to the inclined directions.

Estimates of the coupling coefficients for telescopes at each inclination may be made by calculating the slope of the experimental integral response curves as a function of momentum. These

estimates would, however, be the coefficients pertaining to the particular telescopes rather than estimates of the unidirectional coefficients at a number of zenith angles. It is obviously more desirable to use the available information as the basis for deriving a set of unidirectional coupling coefficients. For this reason, and to take the detector characteristics more fully into account, a general empirical function has been sought to represent the dependence of directional muon intensity on mean effective cut-off at each zenith angle. In addition, functional representation would allow an appreciably more efficient analysis of the observational data, and a more useful expression of the results, to be made.

A function of the form

$$I(\theta,P) = 100 - k(\theta)\,[P - P_{at}(\theta)]^{n} \;\% \quad \text{for } P > P_{at}$$
$$= 100 \quad \text{for } P \leq P_{at} \qquad (6.1)$$

was found, by trial and error, to be eminently suitable for this purpose. In this function, which applies to momentum values within the range of cut-offs at which the latitude survey observations were made, $I(\theta,P)$ is the directional muon intensity (normalized to percent of intensity in the absence of cut-offs), $P_{at}(\theta)$ is the **mean effective atmospheric cut-off*** for the detector

* Mean effective atmospheric cut-off - the weighted mean atmospheric cut-off applying to any particular detector configuration, calculated by the technique described in Section 6.6.

inclined to zenith angle θ, k is a zenith angle-dependent constant describing the general slope of the function, and n is a constant used to fix the curvature of the function. The conditional values take into account the fact that the integral response function must have zero slope for momenta below the atmospheric cut-off.

P_{at}, in contrast to the constants k and n, is not determined from the experimental data, rather being the weighted mean of the known zenith dependent unidirectional atmospheric cut-offs over the acceptance cone of the telescopes. Since the weighting depends on the other parameters to a certain extent, it is necessary to deduce the mean effective atmospheric cut-off for the telescopes by means of successive approximations over the cycle of operations involved in the optimization of the values of the other parameters. It was found possible to choose values of the parameters that brought about a close fit of the empirical function to the observational data at each zenith angle, so enabling the response functions pertaining to the telescopes to be determined.

It is appropriate at this point to outline the principles involved in deducing the unidirectional muon response functions from the experimental functions (obtained by the use of detectors of finite acceptance angle). If it can be shown that the unidirectional integral response curve is well represented by a function of the same basic form as the empirical function, then the problem becomes one of determining what zenith dependence of n and k, together with the known dependence of P_{at} on zenith angle (see Section

5.10), is required in order that calculations of telescope response reproduce precisely the experimental result. (The means of carrying out the response calculations have already been developed, in Chapter 3).

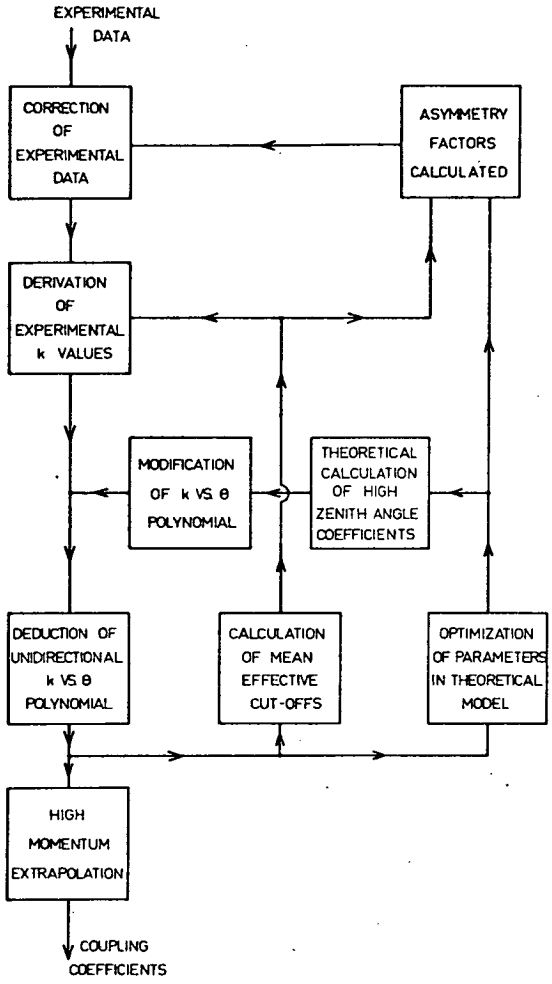

Figure 6.2. Flow chart representing the relationship between the various operations involved in the optimization of the parameters in the coupling coefficient model.

Because of the involved interdependence of the mean effective values of k and P_{at}, and the dependence of the asymmetry factors (necessary for the correction of the experimental data) upon the final response functions, the entire process of determining the unidirectional response functions has the form of a cyclic series of operations in which the parameters are adjusted progressively until a stable series of values is found. The relationship between the various operations in the determination, and the position of the optimization "loops" are represented in Figure 6.2 by a flow chart. The processes

represented in the chart are elucidated in the following sections.

The different relative "powers" of the parameters in the various parts of the overall operation (for example, the lesser dependence of the asymmetry function than the integral response function on momentum) leads to the presence of a single maximum in the multidimensional parametric surface, and so the final set of parameters represents a unique solution to the problem. It is found, as a result, that the difficulty discussed in Section 5.6, that of separating the genuine azimuthal asymmetry produced by the geomagnetic cut-offs from the effects of the overlaid atmospheric asymmetry, can be resolved.

Correction of the experimental data for removal of the effects of atmospheric asymmetry were initially made on the assumption that the asymmetry factors were independent of cut-off momentum, and later successively improved models were used in the "muons in the atmosphere" computer program to derive the correction factors. Similarly, progressively improved estimates of mean effective geomagnetic cut-off were used, both in the numerical calculations, and in the data analysis.

6.4 Determination of the Empirical Response Function Parameters

A computer program was written to aid in the data analysis, which, given values of P_{at} and n, calculated the values of the constant k in equation (6.1) appropriate to the various subsets of data. It did this by means of a weighted regression analysis of

intensity I on $(P - P_{at})^n$, producing k as the normalized regression coefficient, and estimating the associated correlation coefficient of the fit of the empirical function (the normalization was necessary to obtain k in the correct percentage form). The weighting was applied according to the accuracy of the individual data points.

Estimation of the value of n was made by examination of the dependence of the correlation coefficient on n for the Townsville data. These particular data were used for this purpose as they formed the most complete and accurate set, and the range of mean effective cut-offs at each zenith angle extended over a wide range. A maximum was observed in the correlation coefficient for a particular value of n (n = 1.6 in the final estimate) for the 22.6° and 45.2° data sets, whilst for the 67.8° data, although no distinct maximum was evident because of the considerably poorer accuracy of the data, the same value nevertheless allowed a satisfactory representation of the observational data to be obtained. The parameter n was therefore chosen to have constant value, independent of zenith angle.

At each zenith angle, for the given value of n, the data subsets were found to predict essentially the same k values (after normalization to adjust for the intensity displacement between the various sections of the curves). The effectiveness of the empirical function, exemplified by this correspondence, is illustrated in Figure 6.3. In this diagram, sections of a common integral response curve are fitted to the 22.6° data; in this case the curves are displaced by an amount predicted by the empirical function

appropriate to the vertical telescope.

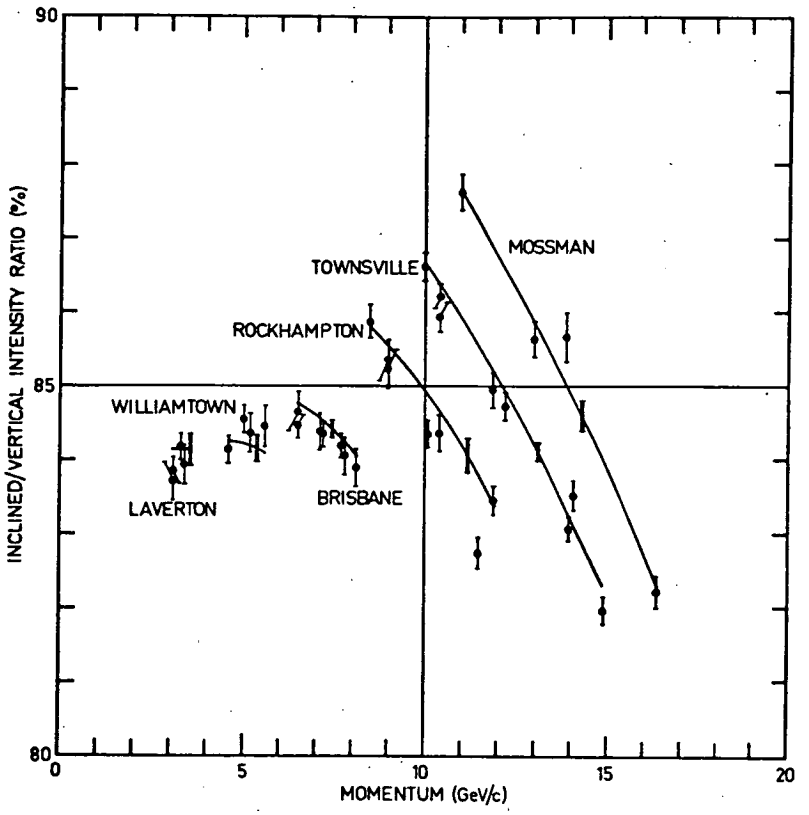

Figure 6.3. Comparison between the individual subsets of 22.6° observational data and the empirical integral response function, which, having been derived by the use of the collected 22.6° data, has been displaced in sections by amounts predicted by the empirical function appropriate to the vertical telescope. The errors indicated are standard deviation statistical errors. An additional uncertainty of magnitude ± 0.095 % pertains to each of the individual observations. The double error bars on the integral response curve sections represent the uncertainty in relative position of each subset (see Section 2.3.3).

In order to make the best estimates of the k values appropriate to the full sets of inclined telescope data, multiplication factors were applied to the points in each subset (data relating to single sites), to bring the weighted mean intensity of each set onto the regression line fitted to the Townsville data at the given zenith angle (see Figure 6.4), and a new estimate of the value of k made from the collected data. In this way, three k values were obtained, one for each of the telescope inclinations.

6.5 Determination of Response of the Vertical Telescope

6.5.1 Integral Response

The sets of multiplication factors are not merely numbers calculated for the convenient handling of the inclined direction intensity data. They contain information, as discussed previously, about the change in the true "corrected" vertical telescope rate over the latitude range of the survey. By carrying out regression

Figure 6.4 (opposite). Experimental data after application of normalizing factors to bring the weighted mean of each data subset onto the regression line fitted to the Townsville data at the given zenith angle. The error bars represent the calculated statistical standard deviation errors pertaining to each point. An additional uncertainty is associated with the observations (see Section 2.3.3) which has magnitude ± 0.12% at 22.6^{o}, ± 0.16% at 45.2^{o}, and ± 0.49% at 67.8^{o}.

analyses on the appropriately normalized sets of multiplication factors, one derived from each zenith angle data set, three indep-

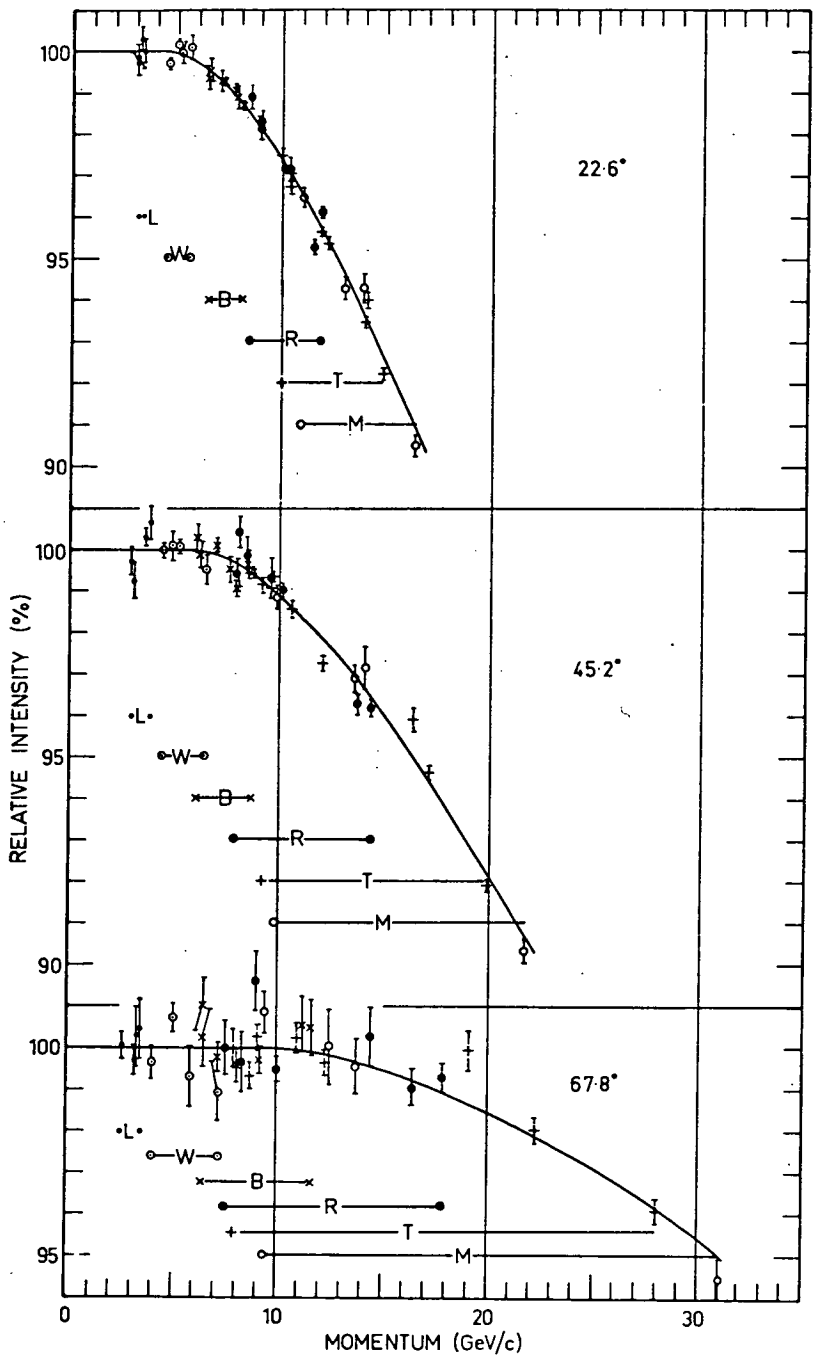

endent estimates of the value of k pertaining to the vertical telescope were obtained (see Table 6.3).

Table 6.3 Values of k for vertical latitude survey telescope as deduced from various data sets.

Data set	Estimated k value for vertical telescope
22.6^{o}	0.231 ± 0.010 (S.D. error)
45.2^{o}	0.260 ± 0.015
67.8^{o}	0.249 ± 0.032

The fact that these values agree very closely tends to confirm the validity of the ratio method of analysis. If there had been appreciable systematic atmospheric dependence in the data, the k values would have been expected to reflect this. Because of the possibility of a small residual atmospheric dependence in the higher zenith angle data, the k estimate derived from the 22.6^{o} data was in fact used for the purposes of further analysis.

By the use of the ratio technique in this way, the integral response of the vertical latitude survey telescope has been obtained, effectively corrected for changes in atmospheric configuration at the different sites. Because the integral response function is produced as the product of independent measurements at each site, it, unlike other direct methods, does not depend on the absolute counting efficiency of the detectors.

6.5.2 Dependence of Vertical Muon Intensity on Atmospheric Configuration

(This section may be omitted at a first reading)

It is of interest to compare the ratio derived integral response function for the vertical telescope with that obtained by direct observation of vertical muon intensity, and to note the significant dependence of the latter on atmospheric structure. The dependence of the vertical telescope rate on latitude is illustrated in Figure 6.5. These relative intensity values were obtained from the wide angle telescope data, corrected to take into account the difference in opening angle compared with the vertical narrow angle telescope (the corrections are small, amounting to about 0.25 %), and corrected to remove the effect of differences in mean pressure at each site. The ratio derived relative intensity values are plotted in the same diagram. The slight differences in mean effective cut-off value relating to the intensity values derived by the two methods arise out of the difference in opening angle of

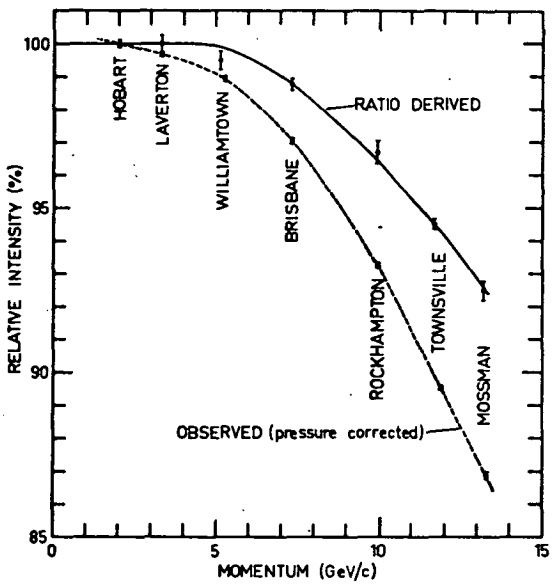

Figure 6.5. Integral response function of vertical narrow angle telescope, as deduced by the ratio method, and as observed experimentally.

the vertical telescopes used in the measurements.

It is interesting to note that the experimentally determined function showing the dependence of pressure corrected muon intensity on latitude has maximum slope at about 12 GeV/c. Thus, unless the corrections for differences in atmospheric structure were to remove this feature, the coupling coefficients that would be determined from these data would have a maximum at this momentum.

The difference between the observed and ratio derived intensities in Figure 6.5, a measure of the dependence of the muon intensity on atmospheric configuration, is shown as a function of geographic latitude in Figure 6.6.

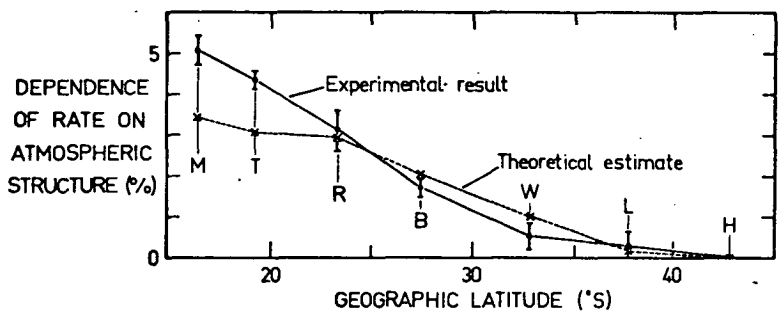

Figure 6.6. Dependence of vertical telescope rate on atmospheric structure over the latitude range of the survey - comparative experimental and calculated results.

Figure 6.7 shows the atmospheric profiles representative of the alternate latitude survey sites. The differences between these structures is responsible for the latitude dependence of muon intensity of muon intensity displayed in Figure 6.6.

These atmospheric profiles have been used in the "muons in the atmosphere" computer program to calculate the expected form of the muon intensity dependence on latitude. These predictions were made by computing the muon intensity at a zenith angle of 8.2^{o} (the effective zenith angle of the vertical narrow angle telescopes), for a pressure level of 1013 mb, and in the presence of the calculated mean effective geomagnetic cut-offs for vertical telescopes at each site. The calculated dependence of telescope rate on latitude is plotted in Figure 6.6. Good general agreement is evident between the predicted and experimental results, particularly at the higher latitudes. The results tend to confirm the validity of the techniques, both in experiment and calculation.

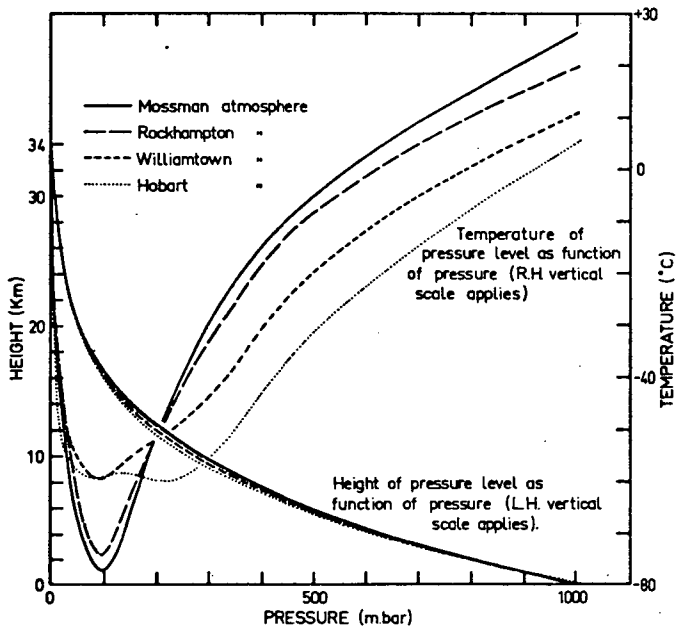

Figure 6.7. Mean atmospheric structures at Mossman, Rockhampton, Williamtown and Hobart, as used in the "muons in the atmosphere" computer program.

6.6 Unidirectional Dependence of k on Zenith Angle

In the preceding sections we have described the process of evaluation of the integral response function parameter k from the latitude survey data. The values pertaining to telescopes at each inclination are given in Table 6.4.

Table 6.4 Values of k for latitude survey telescopes.

Telescope inclination to zenith	k Value
0^{o}	0.231 ± 0.010 (S.D. error)
22.6^{o}	0.185 ± 0.006
45.2^{o}	0.116 ± 0.005
67.8^{o}	0.0353 ± 0.007

The coupling coefficients for these telescopes are readily obtained by differentiation of the empirical integral response function and insertion of the appropriate values of the parameters into the resulting differential response function,

$$\text{i.e., since } W = -\frac{dI}{dP} \quad (I \text{ normalized to } \%)$$

$$\text{then } W = n\,k\,[P - P_{at}(\theta)]^{n-1} \tag{6.2}$$

These coefficients are of very limited use, since they strictly pertain only to the latitude survey detectors, and to the momentum range corresponding to the cut-off momentum values encountered on the survey.

In order to obtain an estimate of the zenith angle dependence of the unidirectional coupling coefficients from the response functions applying to these detectors, it is necessary to deduce a model of the unidirectional response function that can be used to reconstitute the observed detector responses. To a first approximation the k values were assumed to apply to the zenith angles to which the telescopes were inclined. A polynomial function passing through the four established k values was constructed for use in representing the dependence of k on zenith angle. This function, together with a further function representing the dependence of P_{at} on zenith angle, was used in the "telescope response" computer program to allow the response of the latitude survey telescopes to be predicted.

The constant cut-off technique, mentioned in Chapter 3, was employed to derive the mean effective values of k and P_{at} for the latitude survey telescopes. In detail, the technique operates as follows: If muon intensities I_1, I_2, and I_3 are calculated for a particular direction in the presence of cut-off values P_1, P_2, and P_3, and if the form of the dependence of intensity on cut-off is known, i.e.

$$I = 100 - k\,[P - P_{at}]^{1.6}$$

in the present case, then the mean effective k and P_{at} values corresponding to the particular telescope configuration simulated may be deduced, since it may be shown that (if P_1 is chosen to be = 0, making I_1 = 100)

$$P_{at} = \frac{P_3 - P_2 \left\{\frac{100 - I_3}{100 - I_2}\right\}^{1/1.6}}{1 - \left\{\frac{100 - I_3}{100 - I_2}\right\}^{1/1.6}}$$

and $$k = \frac{100 - I_3}{(P_3 - P_{at})^{1.6}}$$

The assumption that the functional dependence of the telescope rate on mean effective cut-off is the same as the unidirectional intensity dependence on directional cut-off is acceptable, since it is found that the mean effective values of k and P_{at} are sensibly independent of the choice of P_2 and P_3, if these cut-off values exceed the mean atmospheric cut-off value for the particular detector.

It is pertinent to note here that at small telescope inclinations the effective zenith angle of viewing as deduced independently from the mean effective k and P_{at} values (deduced by determining at what zenith angle the values of the mean effective parameters are equal to the unidirectional values) are found to be essentially the same. On the other hand, at large zenith angles of viewing, the estimates of the effective angle of viewing of the telescope, as deduced from the two parameters, may differ very considerably. Thus, for large detector inclinations, the integral response functions do not correspond to the unidirectional function at any particular zenith angle.

When using the first estimate of the polynomial function rep-

resenting the unidirectional dependence of k on zenith angle, the calculated mean effective k values were found to be well removed from the actual observed values (i.e. those listed in Table 6.4), and considerable modification was necessary in order to obtain satisfactory agreement. Adjustment of this function also affected the calculated mean effective P_{at} values, and through these, the analysis of the experimental data. As a result, it was necessary to cycle around the sequence of operations shown in Figure 6.2, in order to optimize the values of the various parameters. In addition, as the optimization proceeded, the parameters in the production spectrum model used in the "muons in the atmosphere" computer program had to be adjusted, and as these also affected the experimental data (through the asymmetry factors), a series of operations was

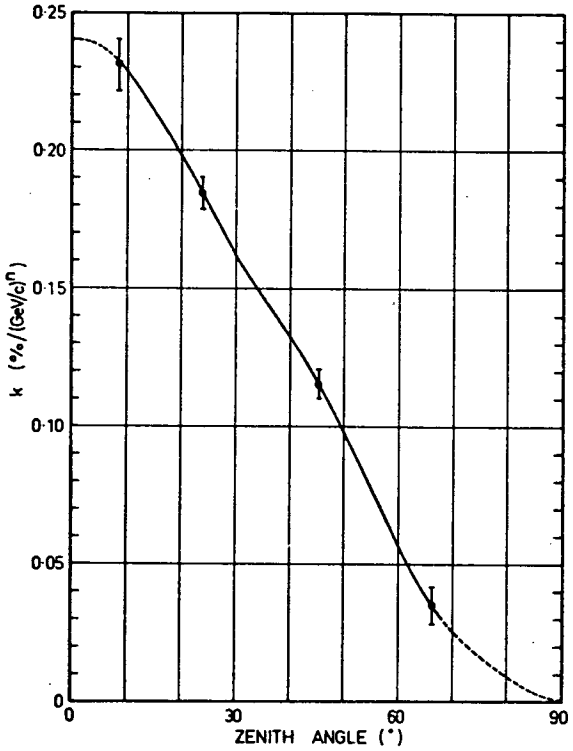

Figure 6.8. Dependence of k on zenith angle. The solid line section was deduced from the experimental k values (shown with the calculated S.D. errors), and the dotted section was predicted with the aid of the "muons in the atmosphere" computer program.

necessary to optimize these parameters at the same time as adjusting the form of the k - θ polynomial function. It was found, in practice, that because the asymmetry factor values were not greatly dependent on the parameters affected in the production spectrum model, it was necessary to traverse this particular loop only three times before arriving at satisfactory stability.

The result of this sequence of operations was the derivation of a polynomial representing the unidirectional dependence of k on zenith angle (see Figure 6.8). When used in telescope response calculations, this function allowed the mean effective k values pertaining to the latitude survey telescopes to be predicted correctly. Because information is now available about the zenith angle dependence of all the parameters in equation (6.2), the zenith angle dependence of the coupling coefficients is known.

6.7 High Momentum Extrapolation of Coupling Coefficients

The empirical coupling coefficient function, because it is derived basically from the experimental data, applies only to the "envelope" of angle - momentum values defined by the mean effective cut-off values encountered during the course of the latitude survey, as shown in Table 6.4. To be of any practical use in cosmic ray astronomy, the coupling coefficient values have to be known at all momentum values. It is therefore necessary to extrapolate the empirical low momentum function.

As discussed in Section 1.2, Dorman [1957] showed that this

extrapolation could be carried out by the use of an empirical function, whose parameters are determined by application of the known restraints on the expression. These restraints are that the low momentum function and the extrapolation function be continuous at the point of connection, and that the area enclosed by the entire coupling coefficient function (corresponding to the total directional muon intensity) be of given value.

Table 6.4 Highest values of cut-off momentum (GeV/c) encountered at each telescope inclination on the latitude survey.

Telescope inclination	Maximum cut-off value
0^o	13.2
22.6^o	16.3
45.2^o	21.7
67.8^o	31.1

Dorman used a function of the form

$$W_{P>P_o} = K \left[\frac{P}{P_o}\right]^{(-\alpha + bP_o/P)}$$

for the extrapolation, where P is momentum, P_o is the point of connection of the two functions, and K, α and b are determinable constants.

For the purposes of the present determination a different extrapolation function has been employed, one which has essentially the exponential character required by theory, but which has an

assigned asymptotic slope at high momenta, rather than a slope determined by the value of the constants as in the Dorman equation. The equation is

$$W' = \frac{A}{f(\theta)} P^{-2.5} e^{-(P_o/P)^m}$$

where A, P_o and m are constants determined, as in the case of the Dorman equation, by application of the restraints; and $f(\theta)$ is a function representing the zenith angle dependence of total muon intensity (see Section 3.3).

This function has asymptotic slope equal to the slope of the differential spectrum at high momenta, corresponding to the assumption that the multiplicity of production of muons detectable at sea level asymptotically approaches a constant value. This tendency to constant multiplicity is indicated by the theoretical calculations of Krimsky et al. [1965], and is not inconsistent with the experimental evidence relating to the multiplicity of pion production as summarized by Sitte [1961]. It is useful to introduce the constancy because of the added flexibility in the later analysis. It should be noted that in the extrapolation function, the rate at which the curves asymptote to a line of constant slope can be controlled over extremely wide limits by the choice of the constants P_o and m. If, in the process of optimization of the parameters, the data are not consistent with the assumption of constant multiplicity at high momenta, the parameters are capable of taking this fact into account with acceptable efficiency. They accordingly take values that delay the rate of approach to the line of constant

slope, thereby decreasing the slope of the function at moderate momenta (whilst the true coupling coefficient slope may be equal to, or less negative than, the slope of the primary differential spectrum, it cannot have greater negative slope).

Since the low momentum empirical coupling coefficient function is known, i.e.

$$W = 1.6\ k\ [P - P_{at}]^{0.6}$$

the Dorman conditions relating W and W' (the extrapolation function) at the point of connection of the two functions (at momentum P_a) may be established:

a) Equality of absolute values of W and W', i.e.

$$W_{P=P_a} = W'_{P=P_a}$$

In terms of the functions, this conditions is

$$1.6\ k\ [P_a - P_{at}]^{0.6} = \frac{A}{f(\theta)}\ P_a^{-2.5}\ e^{-(P_o/P_a)^m}$$

b) Continuity of slope, i.e.

$$\frac{dW'}{dP}(P = P_a) = \frac{dW}{dP}(P = P_a)$$

which may be shown to be given by

$$\frac{A\ e^{-(P_o/P_a)^m}}{f(\theta)\ P_a^{3.5}}\ [m(P_o/P_a)^m - 2.5] = 0.96\ k\ (P_a - P_{at})^{-0.4}$$

c) The area condition. If the coefficients are expressed in the units % per GeV/c then this condition, in terms of the functions, is

$$\int_{P_a}^{\infty} \frac{A\, P^{-2.5}}{f(\theta)}\, e^{-(P_o/P)^m}\, dP + k\,(P_a - P_{at})^{1.6} = 100$$

These equations are sufficient to determine the values of the constants A, P_o and m for any given value of P_a. On the other hand, if one of A, P_o or m is assigned a value, then the remaining three unknowns may be evaluated.

A computer program was written to carry out the evaluation of these parameters, using the equations representing the Dorman conditions. In a first series of calculations P_a values were chosen corresponding to the highest cut-off values for which the experimental observations had been made (i.e. those in Table 6.4). The program selected the value of A which provided the most suitable extrapolation of the low momentum function at each of a number of nominated zenith angles (in a loop involving the successive adjustment of the P_a values at each zenith angle), and then deduced values of P_o and m appropriate to each zenith angle.

It became apparent, after these calculations, that this method of selecting P_a was very arbitrary. Since the choice of P_a effectively fixed the position of the maximum in the coupling coefficient functions, the overall shape of the curves were thus dependent on values of momentum quite fortuitously associated with the observational data. It was found that a more useful starting point in the evaluation of the extrapolation parameters was the choice of a value of A, from which the remaining constants were deduced appropriate to each zenith angle.

Depending on the choice of A, one of a family of coupling coefficient curves could be produced at any particular zenith angle, as represented, for example, by the curves in Figure 6.9a. It can be seen that the shape of the function is very directly dependent on A, these differences causing very great variation in the shape of the corresponding integral response curves (see Figure 6.9b). No particular one of these curves can be selected a priori as being the most suitable, or as best representing the actual situation, since each extrapolation is equally valid, on the basis of the experimental evidence. It is apparent that very small A values are not appropriate, because of the patent artificiality of the form of the extrapolation (see Figure 6.9a). It is obvious that some other means must be found to select the value of A best representing the true primary-secondary relationship.

In principle, if experimental evidence of the shape of the muon integral response curves in the region of the maximum could be acquired, then this could form the basis for the selection. In practice the limited range of cut-offs available in the geomagnetic field preclude the execution of decisive observations at sea level. On the other hand, suitable experimental observations do exist, those of Mathews and Sivjee [1967], of muon intensity in inclined directions at mountain altitudes. As discussed in Section 5.12.3, these investigators hoped to extend the experimental determination of vertical muon coupling coefficients to higher momentum values by making observations through atmospheric depths equivalent to that in

the vertical direction at sea level, but in the presence of high cut-off values. Because of contamination by the atmospheric

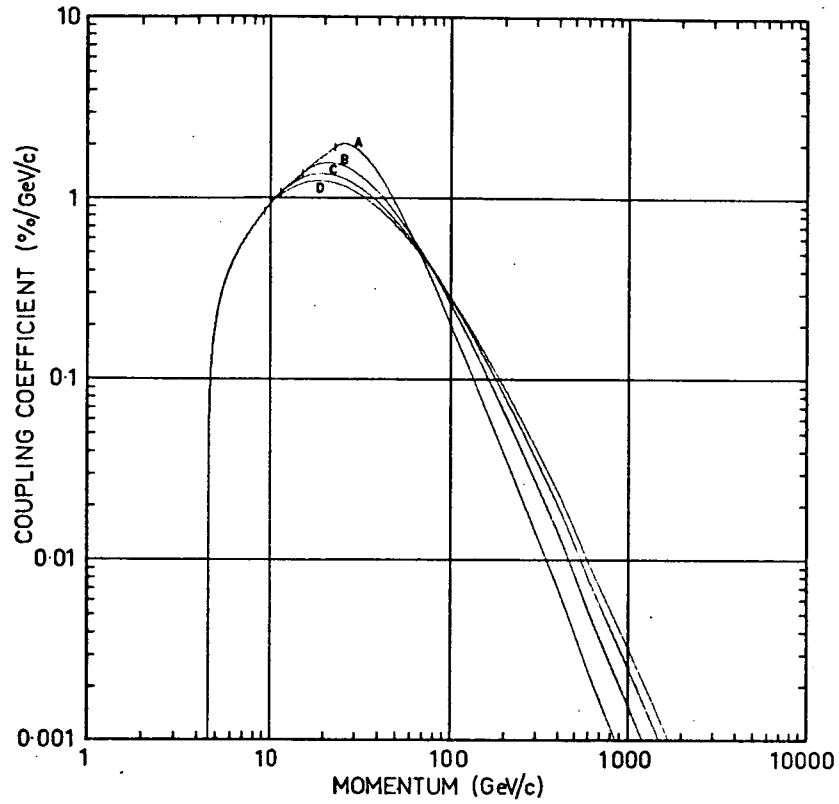

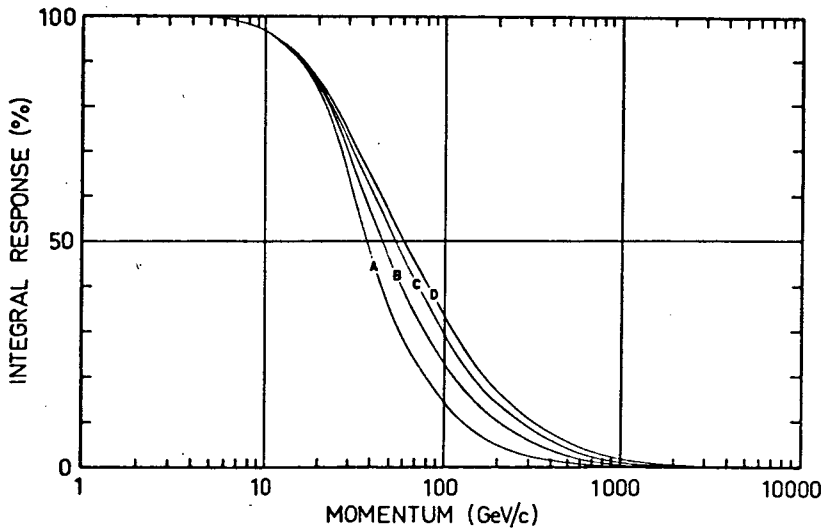

asymmetry effect, Mathews and Sivjee were unable to obtain the result they sought (they themselves attributed their anomalous result to failure to take into account the differences in geometry of the detectors used in the sea level and mountain altitude observations). We have been able to correct these data (see Section 5.12.3) and use them to resolve the problem of selecting a suitable value of the constant A.

Calculations were made of the effective values of the constants k and P_{at} pertaining to the configuration of the Mathews and Sivjee telescope when directed vertically at sea level, and as a result the low momentum portion of the integral response function for this telescope could be drawn (see Figure 6.10). This response curve is equivalent to the unidirectional response function at 16.6^{o} zenith angle (this fact is utilized in later work).

The experimental data were normalized so that the corrected

Figure 6.9 (opposite).

Figure 6.9a (upper diagram). 16.6^{o} zenith angle coupling coefficient function, for various values of the parameter A: curve A, $A = 2\times10^{4}$; B, $A = 5\times10^{4}$; C, $A = 10^{5}$; D, $A = 1.575\times10^{5}$. The short vertical bars intersecting the lines indicates the join between the two empirical functions.

Figure 6.9b (lower diagram). Integral response curves corresponding to the coupling coefficient curves represented in Figure 6.9a.

data points could be plotted on the same diagram. This normalization was carried out by fitting a straight line of best fit to the data (the points collectively do not exhibit any appreciable curvature), and then a multiplication factor applied to bring the regression line into coincidence with the empirical function at 12.5 GeV/c (see Figure 6.10). It may be seen that the general slope of

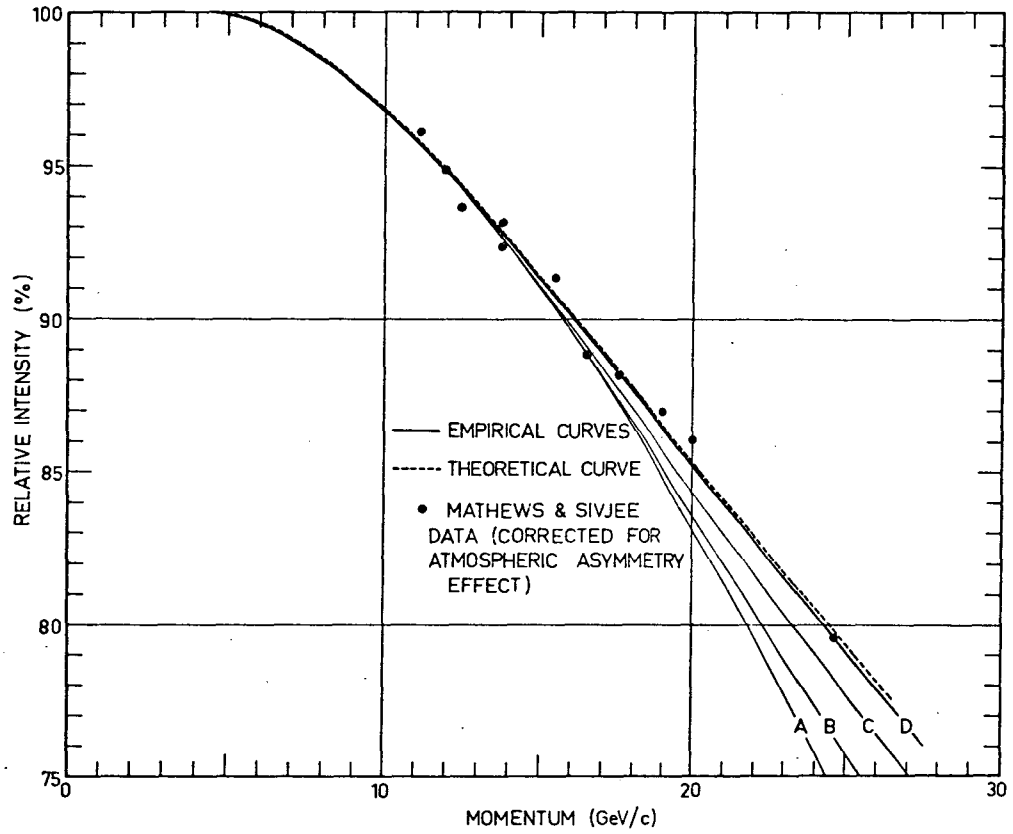

Figure 6.10. Low momentum portion of the 16.6° zenith angle integral response curves displayed in Figure 6.9. The data points represent the corrected observations of Mathews and Sivjee, and the dashed line the integral response curve as predicted by the modified Olbert production spectrum.

the empirical function is preserved in the distribution of the data points.

We now have an estimate of the position (although not the detailed shape) of the integral response curve, for momenta as high as 25 GeV/c. By comparison of this integral response curve with the various curves representing the possible range of values of A, as illustrated in Figure 6.10, it was found that a value of A = 1.575×10^5 produced the best representation of the experimental data. In this way it was possible to select a value of A out of the large range of possible values, and confidently use it to represent the actual physical situation. In determining A, a definite high momentum form has been assigned to the coupling coefficient function, so that for the zenith angle range covered by the experimental observations a complete specification of the coupling coefficients is available.

It should be noted here that the choice of A = 1.575×10^5 causes the point of connection of the low and high momentum empirical functions to lie at momenta lower than the highest cut-off values encountered in the latitude survey (see Table 6.4). As a result, the experimental data should, in principle, have been represented by two functions in the data analysis, rather than by a single function. Fortunately, the modification to the shape of the integral response curve is minute in the momentum range affected (see for example, the relative positions of the integral response curves in Figure 6.10, for momenta $\leq$ 14 GeV/c), and the resulting

errors are negligible.

It would be of very great value to obtain the high zenith angle form of the muon coupling coefficients, both for use in the analysis of data from high zenith angle detectors such as those in use at Mawson and Hobart in the study of primary cosmic ray anisotropies, and as a means of obtaining evidence about the form of the coupling coefficients pertaining to moderate depths of absorber. At large zenith angles the atmospheric depth is approximately equivalent to the absorber depth in the viewing cone of underground detectors at tens of metres water equivalent.

6.8 Coupling Coefficient Extrapolation to High Zenith Angles

It would be quite invalid simply to extrapolate the k function to high zenith angles, as there is no means of knowing a priori the true extrapolated form of the dependence. It is therefore necessary to look elsewhere for evidence on which to base the extrapolation.

The key to the solution of this problem lies in the use of the "muons in the atmosphere" computer program. The adjustment of the parameters in the calculations executed by the program was made by matching the predictions of the calculations to the form of the semi-empirical integral response curve at a zenith angle of 16.6^{o}. At this zenith angle the best evidence exists concerning the true shape of the muon integral response functions (i.e. the Mathews and Sivjee data). It is particularly interesting to note that, whilst

change of the parameters K and D in the computer program (defined in Sections 7.7.3.1 and 5.7.3.3) could cause variation in slope, and to a certain extent the overall curvature of the calculated integral response function, the predicted position of the point of maximum slope remained virtually unchanged, this point agreeing very closely with that obtained by the use of the chosen value of the parameter A in the extrapolation formula. It was found possible to choose a pair of values of K and D that allowed the predicted integral response function to be in very close correspondence to the experimental curve. The comparitive calculated and experimental integral response curves are depicted in Figure 6.10. and the corresponding differential response curves (coupling coefficients) are shown in Figure 6.11. The agreement is

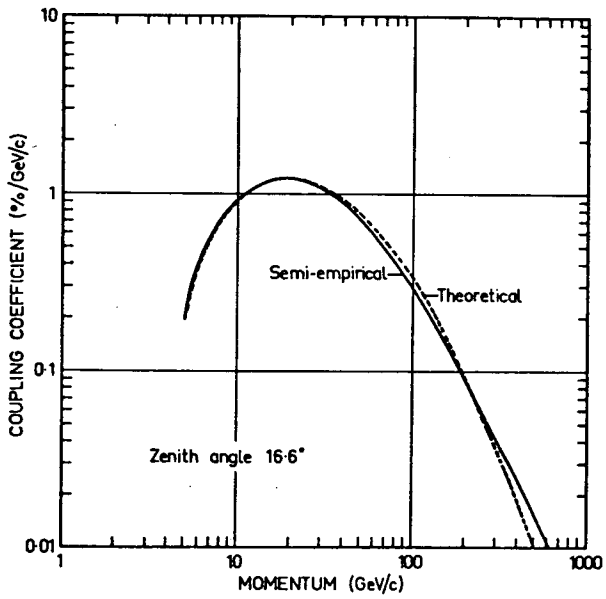

Figure 6.11. 16.6^{o} zenith angle coupling coefficients as predicted by calculation, and by the empirical model ($A = 1.575 \times 10^{5}$).

remarkably good for momenta $\leq$ 300 GeV/c, although at higher momenta the estimates diverge. In view of the demonstrated departure of the calculations based on the modified production spectrum from reality at high momenta (see Section 5.9.2), the observed disparity between the semiempirical and calculated coefficients at high momenta is in no way an indication of lack of plausibility of the semiempirical result.

It is of interest to find how closely the computer calculations predict the experimental result at other zenith angles. A series of calculations was carried out to derive the coupling coefficients at 8.2^{o}, 23.7^{o}, 46.5^{o}, and 66^{o} zenith angle ("effective" zenith angles of viewing of the latitude survey telescopes). These results were then compared with the coefficients as predicted by the empirical functions. The comparative results are presented graphically in Figure 6.12.

Although a shift is evident in the relative position of the curves obtained by the two methods (as a result of the difference in high momentum behaviour), a close correspondence is displayed between the positions of the maxima. The sensitivity of the position of the maxima to change in the values of the parameters in the empirical extrapolation formula has already been indicated (Section 6.7; see, in particular, Figure 6.9). In principle then, by ensuring that at high zenith angles the maxima in the semiempirical coefficients occur at the same momentum values as predicted by calculation, a means is available for choosing the form of the zenith angle dependence of k

at high zenith angles. The sensitivity of the position of the maximum to change in k is large, a change of 10% in k causing a shift of approximately 6% in the momentum value at the peak, at medium and high zenith angles.

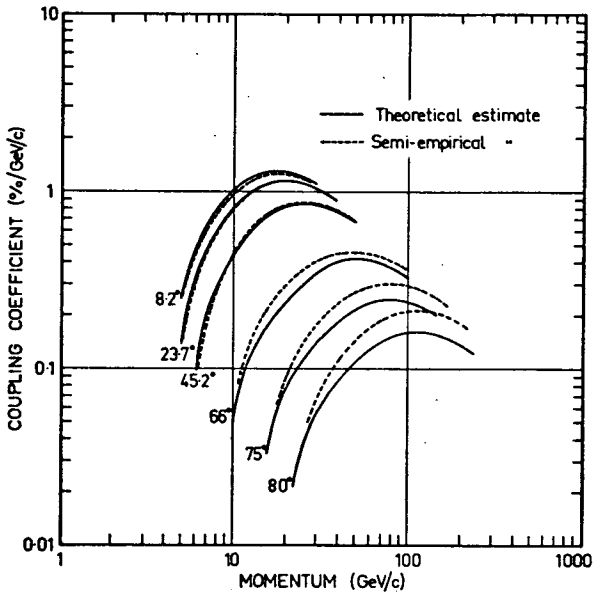

Figure 6.12. Coupling coefficients for a range of zenith angles, as predicted by calculation, and by the semiempirical model.

In the high zenith angle extrapolation, the general empirical function, equation (3.4), has been used to represent the zenith angle dependence of total muon intensity, rather than equation (3.5), which was developed for use in conjunction with the experimental data. At zenith angles $< 70^{o}$ these functions, as used in establishing the empirical coupling coefficient model, are essentially equivalent.

At very small zenith angles ($\lesssim 5^{o}$) the experimental data do not

allow the precise form of the k - θ polynomial to be fixed; however, the "muon in the atmosphere" computer program provides a means for doing this. The selection of the k value appropriate to 0^{o} zenith angle was made by noting the indicated displacement between members of the family of calculated coupling coefficient curves relating to small zenith angles.

Modification at both the high and low zenith angle regions of the polynomial representing the zenith angle dependence of k necessitated further repetition of the cycle of operations involved in deducing the unidirectional coupling coefficients, in all its detail, as indicated by the flow chart in Figure 6.2.

As the end result of this involved process, a polynomial function was determined, expressing the zenith angle dependence of k, whose use in the various functions satisfied all the derivation conditions. This function (illustrated in Figure 6.8), together with the chosen value of the constant A, specifies completely the muon coupling coefficients, at all momenta, and at zenith angles up to approximately 85^{o}. The coupling coefficients, which relate the

Figure 6.13 (opposite).

Figure 6.13a (upper diagram). Coupling coefficients for a range of zenith angles at sea level in the "field-free" standard mid-latitude atmosphere, in the absence of geomagnetic cut-offs.

Figure 6.13b (lower diagram). The family of integral response curves corresponding to the coupling coefficients in Figure 6.13a.

primary cosmic ray intensity to the directional muon intensity at "field free", mid- to low-latitude sites during periods of low

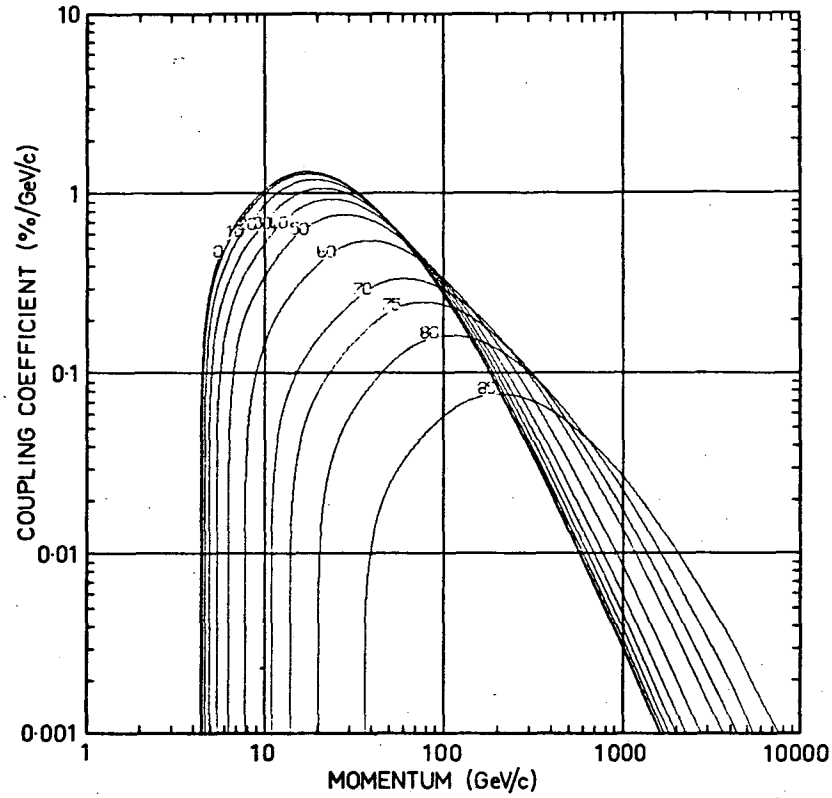

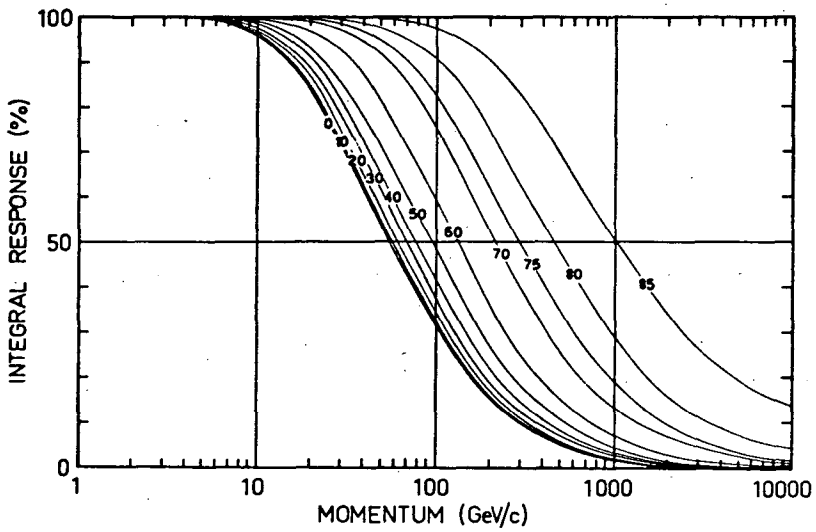

solar activity, are presented graphically in Figure 6.13a, and the corresponding integral response curves in Figure 6.13b. Table 6.5 contains the values of the parameters k, P_a, P_{at}, P_o and m, and also the values of the function $f(\theta)$, at the various zenith angles.

Table 6.5 Values of empirical coupling coefficient parameters for range of zenith angles. At momenta $P_{at} < P \leq P_o$, and $P > P_a$, the following functions, respectively, apply:

$$W = 1.6\ k\ [P - P_{at}]^{0.6} \qquad W = \frac{1.575 \times 10^5}{f(\theta)}\ P^{-2.5}\ e^{-(P_o/P)^m}$$

where bold face denotes zenith dependency. The coupling coefficient values have the units (% per GeV/c).

Zenith angle	k	P_{at}	P_a	P_o	m	$f(\theta)$
0	0.2401	4.41	7.63	273	0.549	1.0000
10	0.2289	4.47	8.26	279	0.550	0.9675
20	0.1983	4.64	9.55	298	0.551	0.8729
30	0.1629	4.94	11.00	340	0.548	0.7296
40	0.1322	5.46	12.17	429	0.534	0.5578
50	0.0985	6.31	13.99	602	0.516	0.3800
60	0.0565	7.82	20.01	913	0.505	0.2197
70	0.0256	10.91	32.18	1729	0.488	0.0967
75	0.0165	14.01	39.44	2948	0.464	0.0536
80	0.0091	20.09	51.67	6182	0.435	0.0239
85	0.0030	36.25	88.76	17310	0.408	0.0075

It is obviously desirable to present the coupling coefficients in a form capable of allowing the determination of the coupling coefficient value corresponding to any particular momentum and zenith angle, for use in computer programs, for example. Polynomials have therefore been derived to represent the zenith angle dependence of the various parameters. Details of these polynomials are given in Appendix 4, in the body of a computer program which may be used to calculate the coupling coefficient value at any particular momentum and zenith angle.

6.9 Adaption of the Coupling Coefficients to Change in Primary and Secondary Conditions

Having available an accurate, basic set of muon coupling coefficients, the question arises of how to adapt these to take into account the conditions affecting the primary and secondary cosmic rays, should they differ from those for which the standard coefficients apply. In addition to change in the primary spectrum, the factors which must be considered include the presence of a magnetic field in the atmosphere, the existence of geomagnetic cut-off values in excess of the atmospheric cut-offs, and change in the observing level in the atmosphere.

6.9.1 Coupling Coefficient Dependence on Primary Spectrum

Kane [1963] has shown that long term changes in the primary spectrum produce relatively small changes in the sea level muon

coupling coefficients, of considerably smaller magnitude than the disparity between the vertical coefficient estimates by various investigators. On the other hand, large short term changes do occur, during periods of solar disturbance (as a manifestation of Forbush decreases or solar flares), which would appreciably affect the form of the coupling coefficients, particularly at low momenta and at low zenith angles. It is desirable to be able to adapt the coefficients for use during such periods.

In Section 1.2 it was shown that the relationship between the coupling coefficients $W(P,\theta,x)$ and the primary differential spectrum $J(P)$ may be expressed as

$$W(P,\theta,x) = J(P)\ S(P,\theta,x) / N$$

where N is the integrated directional muon intensity at zenith angle θ at the level x, and $J(P,\theta,x)$ is the specific yield function.

Webber and Quenby [1959] pointed out that contributions to the sea level muon flux from α particles are significant, and so should be taken into account when yield functions are being derived. Because of the similarity in shape of the proton and α particle rigidity spectra, and since contributions within a given rigidity interval from particles with charge number ≥ 2 are approximately equal to the contributions from protons, Webber and Quenby showed that it was possible to express the "gross" yield function $S_G(R,x)$ as

$$S_G(R,x) = S_p(R,x) + S_p(\tfrac{1}{2}R,x)$$

(where the proton specific yield function S_p is here expressed in terms of rigidity R), and from this expression, by means of an iteration process, to deduce the proton specific yield function.

Using the technique described by Webber and Quenby, in conjunction with the quiet solar period primary differential spectrum of Ormes and Webber [1965] ($J = 1.05\ P^{-2.5}$ particles per cm^2 per ster. per sec. per GeV/c), we have obtained firstly the gross yield functions as predicted by our coupling coefficient model for

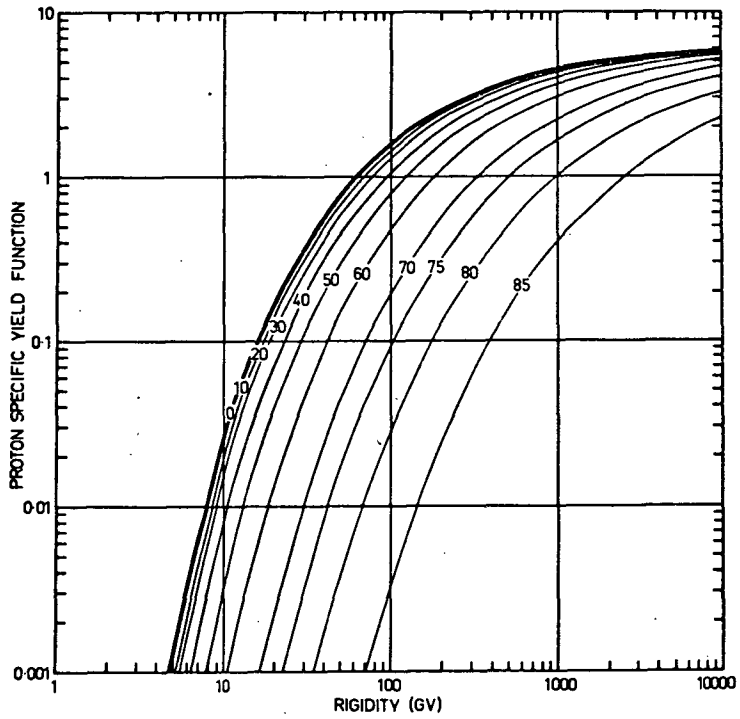

Figure 6.14. Proton specific yield functions deduced from semi-empirical coupling coefficients, for a range of zenith angles.

various zenith angles, and then deduced the corresponding proton specific yield functions. These latter functions are shown in Figure 6.14. Using these specific yield functions it is possible to estimate the coupling coefficients pertaining to any particular primary spectrum, by evaluating the expression

$$W(R,\theta) = J(R)\,[S_p(R,\theta) + S_p(\tfrac{1}{2}R,\theta)]$$

6.9.2 The Effect of the Local Magnetic Field

As discussed in Section 1.2 and in Chapter 5, the presence of the magnetic field in the atmosphere is responsible for introducing appreciable deflections in the paths of muons travelling through the atmosphere, causing systematic intensity changes in the sea level directional muon flux. It is obviously desirable to know what effect this phenomenon will have on the primary-secondary intensity relationship. It is not valid, as pointed out in Section 1.4, to obtain the appropriate relationship by using data from a latitude survey in which telescopes are directed at fixed azimuths, since implicit in this means of determination is the erroneous assumption that the atmospheric asymmetry effect is constant, independent of cut-off and local magnetic field configuration.

In order to deduce the modified form of the coupling coefficients appropriate to any particular direction at a given site, it is necessary to have sufficient information to allow the form of the perturbed integral response function in that direction to be deduced.

As a result of the investigation described in Chapter 5, it was

shown (Section 5.7.1) that a function A could be introduced to relate the directional intensity I of muons in any situation in the presence of a magnetic field to the intensity N that would exist in the absence of the field, such that $N = I A$. Of particular interest in this discussion is the dependence of these quantities on cut-off momentum. In any particular situation the function N(P) is simply the integral response function. Therefore I(P) corresponds to the required perturbed integral response function. It is evident that if the dependence of the asymmetry function A on cut-off can be deduced, then the perturbed integral response function may be obtained, and the corresponding coupling coefficients derived.

It was in anticipation of this usage of the asymmetry factor that the calculations of the asymmetry factors were carried out, in some situations, for momenta well in excess of the maximum cut-off existing in the geomagnetic field (see Table 5.8). Under these conditions, which are representative of a mid- to low-latitude sea level site (0.55 gauss field at a dip angle of -30^{o}, standard mid-latitude atmosphere), we have calculated the coupling coefficients applicable to magnetic east and west azimuths, at 45^{o} to the zenith. These coefficients are displayed in Figure 6.15, together with the unperturbed coupling coefficient function. It can be seen that, whilst the curves are displaced relative to each other, the position of the maxima agree closely in momentum.

The differences between the coupling coefficients for east and

west, as determined in this way, are very much smaller than when obtained directly by latitude survey (as, for example, by Mazaryuk [1966], and Dorman et al. [1967]). Evidently the variation in local field conditions from site to site, in addition to producing distortion of the coupling coefficient functions, tends to produce exaggerated estimates of the differences between the coupling coefficients for different azimuths.

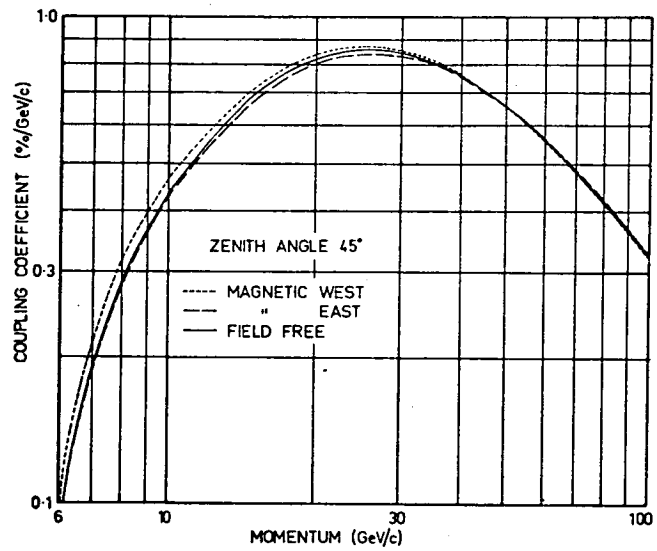

Figure 6.15. Coupling coefficients applying to magnetic east and west azimuths, at 45° zenith angle, at sea level in the standard mid-latitude atmosphere, in a magnetic field of strength 0.55 gauss and dip angle -30°.

It is evident, from our calculations, that the magnitude of the differences between the coupling coefficients for particular azimuths and the basic functions are sufficiently small ($\lesssim 2\%$ in Figure 6.15) that for most purposes they could be ignored, and the basic function

used.

6.9.3 Coupling Coefficients in the Presence of Geomagnetic Cut-offs

It is necessary to modify the coupling coefficients in order that they apply at low latitude sites, where the geomagnetic cut-offs have appreciable effect. The modification, which is readily made, involves truncating the lower momentum end of the coupling coefficient function at the momentum equal in value to the cut-off momentum in the direction of interest, and renormalizing the position of the curve to obtain the correct area under the function. In Figure 6.16 the coupling coefficients appropriate to 45^{o} zenith angle in the "field free" mid-latitude atmosphere are presented, modified to take into account cut-off values of 10, 15 and 20 GeV/c.

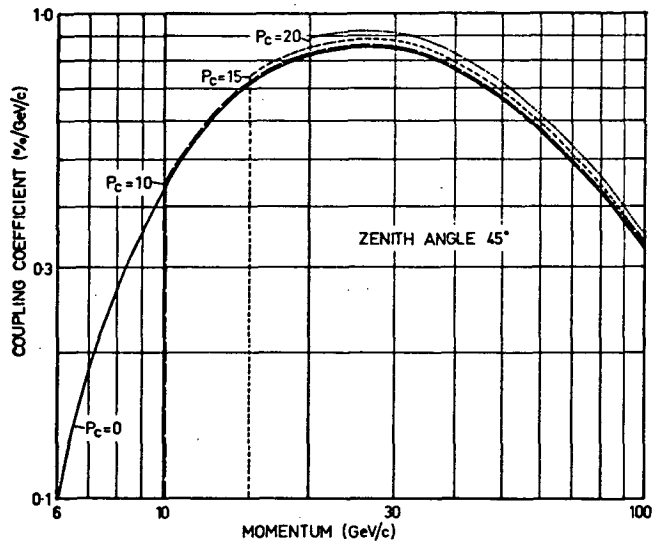

Figure 6.16. Coupling coefficients pertaining to 45^{o} zenith angle in the "field free" mid-latitude atmosphere, in the presence of geomagnetic cut-offs of value 0, 10, 15, and 20 GeV/c.

6.9.4 Coupling Coefficients for Different Depths of Absorber

If observations at other than sea level are to be carried out, then it is desirable to adapt the coupling coefficients accordingly.

Dorman [1959] presented an approximate relationship between the coupling coefficients for the vertically incident muon component at two different atmospheric depths. This is given by

$$\frac{dN}{dP}(P,x_1) = \frac{P_2}{P_1}\frac{dN}{dP}(P\frac{P_2}{P_1},x_2)$$

where P is momentum, x_1 and x_2 are the two levels of registration of the muon component, $\frac{dN}{dP}(P,x_1)$ is the differential response at the momentum P and depth x_1, and $\frac{P_2}{P_1}\frac{dN}{dP}(P\frac{P_2}{P_1},x_2)$ is the differential response at the momentum $P\frac{P_2}{P_1}$ and depth x_2. P_1 and P_2 are the lowest momenta that primaries can possess in order to give rise to muons detectable at the two levels x_1 and x_2 respectively.

This expression implies that the coupling coefficient curves appropriate to different depths of absorber have essentially the same form, on a log-log plot, and that approximate coupling coefficients for any particular level may be obtained by bodily displacing the curves, in momentum, by an amount indicated by the ratio of the thresholds for detector response from primaries at each level, and in intensity by the reciprocal of the same ratio (in order to obtain correctly normalized curves, with 100% area under each curve).

The validity of Dorman's assumption of the similarity in form

of the similarity in form of the coupling coefficients at different absorber depths is borne out by the similarity in general shape of the different members of the family of curves representing the coupling coefficients at different zenith angles, deduced in this chapter (see Figure 6.13).

As discussed in Section 1.3, Mathews [1963] used Dorman's technique to deduce the coupling coefficients corresponding to the vertical direction at sea level, and those applying to 40 and 60 m.w.e. absorber, from the coefficients pertaining to 312 gm cm^{-2} absorber. The close correspondence between the vertical sea level curve of Mathews and our own is evident in Figure 6.17. It is of interest, too, to note the similarity in the position of maxima, and general high momentum behaviour, of Mathews' 40 and 60 m.w.e. results and our own at zenith angles 75^{o} and 80^{o}. The differences at lower momenta may arise out of the difference in path length under the conditions represented, nevertheless the discrepancy between these two sets of coefficients is smaller than those to be found between the other independent estimates of the underground coupling coefficients.

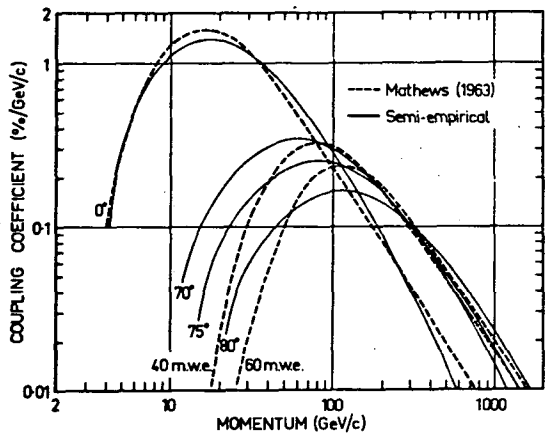

Figure 6.17. Comparison of the coupling coefficients of Mathews [1963] with those derived in this chapter.

The possibility is raised of using the high zenith angle coefficients to represent, in a very convenient form, the underground coupling coefficients corresponding to any moderate depth of absorber, since the coefficients deduced in this chapter are available in the form of known, continuous functions of zenith angle and momentum (see Section 6.7). If the primary threshold for detector response were to be determined in any situation (on the basis of known depth of rock plus known atmospheric depth), then the coefficients corresponding to that situation could be obtained, by calculating what particular zenith angle in air possesses that threshold, and constructing the appropriate values of the parameters from the polynomial functions. In order to facilitate the implementation of this technique a polynomial function has been derived, representing zenith angle as a function of atmospheric cut-off. The coefficients of this polynomial function are given in Appendix 4.

By means of this technique it would be possible to determine detector response in any situation where the absorber configuration is known. An additional piece of information is required in these calculations, that is, the variation of total muon intensity with absorber depth. Published data may be used to yield this information, for example, those of Barton and Stockel [1968].

It is reiterated that this technique will be subject to errors at low momenta, due to the differences in muon behaviour in air and rock, but that these errors are likely to be of magnitude smaller than the differences between the various independent estimates of

the underground coupling coefficients.

6.9.5 The Use of Atmospheric "Multiplicities"

A rigorous means of deriving muon coupling coefficients in any situation lies in the use of muon "multiplicities". These express the average spectrum of muons produced by primaries of any particular rigidity. Using this information it is possible to deduce the relationship between the muon flux at any level and the primary cosmic ray flux, by considering in detail the interactions occurring in the atmosphere. The muon multiplicities, in short, represent a complete specification of the primary-secondary relationship, although the calculations necessary to make use of this information may be very complex.

A set of three-dimensional muon multiplicities pertaining to muon of momenta $\leq$ 50 GeV/c was deduced by Astrom [1968]. This information was obtained from analysis of published data from accelerator studies. Although Astrom has shown that sea level muon spectra are predicted satisfactorily by the use of these functions, it appears that no information on primary-secondary intensity relationship has been published in a form allowing direct comparison with muon coupling coefficients as derived directly by measurements of the sea level muon flux.

In principle, the multiplicities may be calculated from the sea level muon coupling coefficients. A simplified approach to this problem has been adopted here to illustrate generally the

principles involved.

If the directional muon coupling coefficients are expressed in the form of relative intensities rather than in the units (% per GeV/c), then the coefficients may be replotted in a form showing the intensity of muons descendant from primaries of any particular momentum, as a function of zenith angle (see Figure 6.18). This diagram shows the reduction in the intensity of the beam of muons initiated by primary particles of particular momentum as the angle of the beam to the vertical increases.

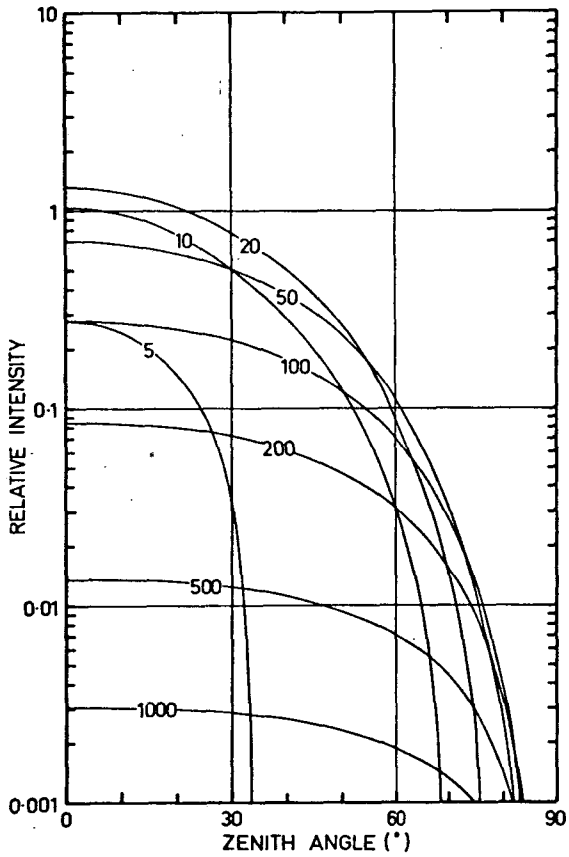

Figure 6.18. Relative intensity of muons descended from primaries of given momentum, as function of zenith angle.

As illustrated in Figure 5.12, the probability of survival of muons arriving at any zenith angle, for particular momentum at production, may be calculated, on the assumption of single layer muon production. Knowledge of these survival probabilities $F(P,\theta)$, together with the observed zenith angle variation of intensity $I(\theta,P')$ of muons descendant from primaries of particular

momentum P', may be used to deduce the average "multiplicity" N(P) of muons, by means of the following expression, which is readily seen to relate these quantities

$$I(\theta,P') = \int_{P_{min}}^{P_{max}} N_{P'}(P)\ F(P,\theta)\ dP \qquad (6.3)$$

where P_{max} is the highest momentum a muon can possess when descended from the primary of momentum P', and P_{min} is the lowest momentum that a muon may possess at production and be observed at sea level. These momentum values may be determined explicitly (see Appendix 3 and Section 5.10).

A technique was developed for representing the "multiplicity" by a polynomial function, and for applying systematic distortion to this function to a degree described by two independent parameters. A standard minimization procedure was used to optimize the values of these parameters so that a suitable function could be derived, subject to the restraints of equation (6.3).

Attempts to deduce multiplicities using this simplified approach were successful for primary particle momenta > 15 GeV/c, yielding multiplicities superficially like those of Astrom, but failing at lower momenta, probably as a result of the assumptions of single layer production and muon production by protons only. Whilst, in principle, these factors could be taken into account, the technique necessary for producing the multiplicities would of necessity be very much more sophisticated, and beyond the scope of the present investigation.

6.10 Coupling Coefficients Pertaining to Detectors of Finite Acceptance Angle

In Section 6.6 it was shown that mean effective values of the constants k and P_{at}, used in the empirical functions expressing the detector integral response, could be calculated by means of the constant cut-off technique in the "telescope response" computer program. Having assigned values to these constants, a complete specification of the coupling coefficients may be obtained, by extrapolating the empirical function to high-momentum values, as outlined in Section 6.7.

Coupling coefficients appropriate to a number of detector configurations in use by the Hobart and Antarctic Division cosmic ray research groups have been determined in this way. The coupling coefficient functions presented in Figure 6.19a are identified in Table 6.6, which also lists the values of the parameters describing these curves. The corresponding integral response curves are presented in Figure 6.19b.

Whilst these coupling coefficients and integral response curves may conveniently be used to gain an understanding of the overall

Figure 6.19 (opposite).

Figure 6.19a (upper diagram). Coupling coefficients pertaining to the detector configurations listed in Table 6.6.

Figure 6.19b (lower diagram). Integral response curves corresponding to the coupling coefficient curves in Figure 6.19a.

response of these detectors to the primary cosmic radiation, and indeed could be used to facilitate detailed analyses, greater

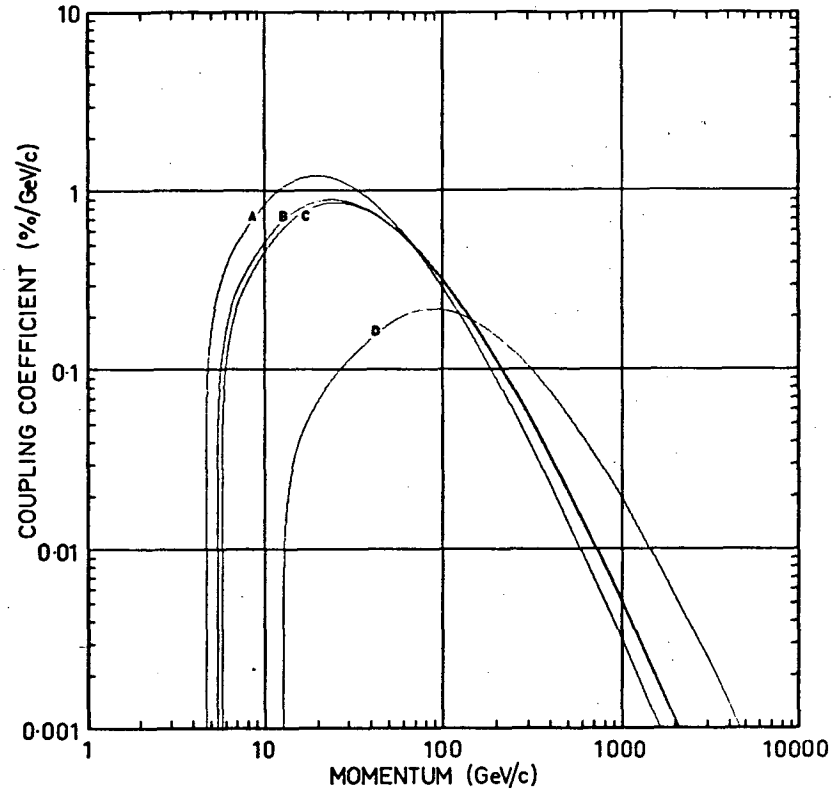

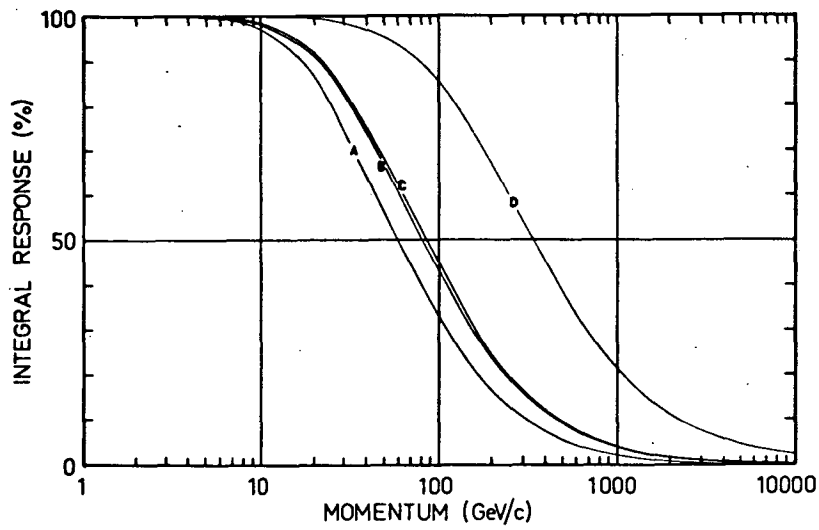

accuracy would be attainable through the use of the unidirectional coupling coefficient model as represented by the information in Table 6.5 or by the use of the polynomial representation of the parameters (see Appendix 4), in conjunction with information about the directional properties of the detectors.

Table 6.6 Specification of the configuration of the detectors referred to in the text, and values of the parameters determining the form of the corresponding coupling coefficients (as displayed in Figure 6.19).

	Detector specification		Parameter values				
	Inclination	Dimensions	k	P_{at}	P_a	P_o	m
A	0^o	1x(1x1) units	0.1916	4.69	10.66	245	0.580
B	45^o	1.5x(1x1)	0.1285	5.39	11.60	536	0.511
C	45^o	1.5x(0.4x0.4)	0.1184	5.71	12.65	509	0.522
D	76.5^o	0.5x(0.08x1)	0.0129	12.82	46.91	3521	0.459

6.11 Conclusions

Unidirectional sea level muon coupling coefficients have been deduced from the latitude survey data, using a number of new techniques. Extrapolation of the coefficients to high momentum values and high zenith angles has been effected with the aid of published observational data, and through the use of calculations based on the Olbert production spectrum.

The resulting vertical coefficients are very similar in form to the coupling coefficients of Mathews [1963], and as a result would be expected to predict essentially the same response to a primary anisotropy.

For convenience in the application of the directional coupling coefficients, in particular for use in computer-aided calculations, the zenith angle dependence of the parameters in the basic momentum-dependent empirical coupling coefficient functions have been expressed in terms of polynomial functions. Thus a completely continuous mathematical description of the coefficients is available.

Methods have been examined for deducing the form of the coupling coefficients under different conditions, to take into account change in primary spectrum, the presence of a local magnetic field, the effects of geomagnetic cut-offs, and change in level of observation. A method was discussed, of using the sea level coupling coefficients to represent the coefficients pertaining to underground situations.

Finally, the effective coupling coefficients applying to a number of detector configurations currently in use, have been deduced.

In the following chapter, an application of the unidirectional coupling coefficient model is described. A computer technique is developed to facilitate the completely automatic determination of the response of any sea level muon telescope to primary cosmic ray anisotropies.

CHAPTER 7

ASYMPTOTIC CONE OF ACCEPTANCE OF MUON DETECTORS

7.1 Introduction

In the preceding chapters of this thesis consideration has been given to the means by which the intensity relationship between the primary cosmic ray flux and the directional muon component of the secondary cosmic ray flux may be established. The complete specification of the primary-secondary relationship involves, in addition, the correlation of the directions of viewing at the detector with primary particle directions of arrival at the outer boundary of the geomagnetic field.

In this chapter we consider some of the factors influencing the motion of charged primary particles within the domain of the geomagnetic field. We then go on to develop a technique of combining the primary-secondary intensity and direction information in a completely automatic operation within a computer program, so that predictions may be accurately and rapidly made of the response of muon detectors in any situation to anisotropies that exist in the primary cosmic ray flux on entry into the geomagnetic field. We do not here consider the effects of any factors, such as the interplanetary magnetic field, whose manifestations are external to the terrestrial field.

Except for primaries of very high energy the directions of

arrival of primaries at the top of the atmosphere do not correspond to the directions of entry into the field (asymptotic directions of approach), as a result of deflections in the field. It is obvious that interpretation of the time variations of muon intensity observed by any particular detector must take these deflections into account if information is to be obtained about anisotropies in the distribution of primary particles outside the geomagnetic field.

Two methods have been used in the past to obtain details of asymptotic directions of approach to sites on the earth's surface. The first, originally developed by Birkeland [1901], involves the use of an experimental "scale model" technique to trace trajectories in a simulation of the terrestrial magnetic field. Brunberg [1953], and Brunberg and Dattner [1953] carried out a series of measurements, using this technique, to enable them to deduce the dependence of asymptotic direction on zenith and azimuth angles of approach at sites of varying latitude, for a range of values of primary particle rigidity. Whilst information such as this was invaluable for early studies of the primary cosmic ray distribution external to the geomagnetic field, it was necessary, in later generations of experiments, to have access to information of greater accuracy, to represent better the effects of the magnetic field.

The electronic computer provides the means of obtaining information to the accuracy required, by allowing trajectory paths to be calculated in a simulation of the geomagnetic field as produced by

both internal and external sources. This technique, because of its great power, has come into almost universal use for theoretical studies of cosmic ray motion in the geomagnetic field, and a great many calculations have been carried out, by many investigators, to obtain information relating to particular sites and sets of conditions. Details of the operation of trajectory tracing, as applied to the problem of directional cut-off determination, were discussed in Section 4.4.

In deducing asymptotic directions of approach pertaining to particular sites, the trajectories of negatively charged particles are traced outwards from the site in the given directions, and the calculations proceed until a displacement from the centre of the earth is reached at which the geomagnetic field is deemed to terminate. The direction of the velocity vector in velocity space at the termination of the field becomes the asymptotic direction of approach of positively charged particles. McCracken et al. [1962] presented a detailed discussion of this technique.

7.2 Asymptotic Directions for Primaries of Rigidity $\gtrsim$ 10 GV

The determination of asymptotic directions pertaining to primaries with rigidity $\gtrsim$ 10 GV is relatively simple, since it is found (as noted for example, by Gall et al. [1969]) that external field sources do not greatly affect the form of the cosmic ray trajectories. It is generally found sufficient to utilize the internal magnetic field as represented by 6th or 8th order field

terms. For these particle rigidities the field may be regarded as time independent, and a set of asymptotic directions appropriate to different values of particle rigidity and directions of arrival at any given site is readily calculated, these directions co-rotating with the earth. Results of calculations of this type have been published by McCracken et al. [1962], Hatton and Carswell [1963], Shea et al. [1965, 1968], among others.

7.3 Asymptotic Directions for Primaries of Rigidity $\lesssim$ 10 GV

The trajectories of particles of rigidity $\lesssim$ 10 GV are found to be significantly influenced by external magnetic field sources. In particular, for very low rigidities ($R < 4$ GV), the situation is very complex, because the external field contributions to the total magnetic field (magnetopause current field, magnetospheric tail field, and ring current field) have a great influence on cosmic ray trajectories. Under most conditions the direction of particle entry into the field is found to stay roughly fixed with respect to the earth-sun line, for a given direction of arrival on the surface of the earth. Gall, Jimenez and Orozco [1969] pointed out that the concept of an "asymptotic" direction of approach is not strictly applicable in such cases, and they suggested that these arrival directions be referred to simply as "directions of approach". The formidable complexity of the problem prevents detailed analyses appropriate to any particular situation being made. Instead, investigations (by Gall et al. [1968], Gall [1968], Gall et al.

[1969], for example) have been aimed at elucidating the general characteristics of particle motion under these conditions.

Because sea level muon detectors do not respond to primaries of rigidity $R < 4$ GV (experimentally determined by McCracken [1962], and demonstrated by calculation in Section 5.10), these very severe distortions of the primary cosmic ray trajectories will not seriously affect the form of the telescope asymptotic cone of acceptance.

Primaries of rigidity $5 < R < 10$ GV are found (Gall [1968]), in general, to possess asymptotic directions that, while rotating with the earth, exhibit appreciable daily variation (and, because of the inclination of the axis of rotation of the earth to the ecliptic plane, a certain yearly variation). Due to the lengthy nature of the calculations in even relatively simple situations, the difficulties of effectively studying the dependence of asymptotic direction on time are considerable.

Gall investigated the local time dependence of asymptotic directions for particles arriving at high latitude sites. In this investigation, because coefficients representing the magnetopause and magnetospheric tail field were used in conjunction with a dipole representation of the internal field, the annual time dependence was of course removed. Nevertheless, because of the large expected difference in the magnitudes of the daily and yearly variations, such an approach is acceptable. From Gall's diagrams it appears that at sites with latitude in the range 60-70^{o}, the asymptotic longitude daily variation is of the order of 10^{o} at 5 GV,

and $< 5^{o}$ for rigidities > 10 GV. Because the contribution to a vertical telescope counting rate (for example, a vertical cube, see Figure 6.19), due to primaries with rigidity $R < 10$ GV is of the order of 3 %, and for a telescope inclined at 45^{o}, 1.5 %, it is evident that the resultant daily variation of muon intensity in the presence of anisotropy will be extremely small. Gall's results indicate that at sites near the poles the daily variation of asymptotic longitude will be somewhat larger; however, due to the small telescope response to primaries in the differential rigidity interval affected, a very small change in telescope response to external anisotropies would be expected.

It is interesting to examine the dependence of asymptotic latitude and longitude on rigidity and on direction of arrival at a site. At any given high latitude site, the asymptotic directions pertaining to a particular direction of arrival of particles of low rigidity would be expected to exhibit a degree of periodicity with change in momentum, as a consequence of the multiple looping of trajectories about the local field line bundle. The change in latitude and longitude would occur as the angle of entry into the first loop (in the region of the geomagnetic equator) changed with particle rigidity (trajectory looping is discussed in Chapter 4). The phenomenon is to be seen manifested in the results of Gall [1968], where, for rigidity in the range 3-20 GV approximately, distinct changes in asymptotic latitude and longitude occur, indicative of the periodicity.

Primaries with rigidity lying close to the main cone cut-off, or within the penumbra, in any direction at a site, move along trajectories that have a form similar to the closed periodic orbits, in that the trajectories oscillate from hemisphere to hemisphere before being restrained to loop along the bundle of field lines associated with the site (see Section 4.7). As a result the asymptotic directions associated with these particular directions of arrival and values of rigidity exhibit a further systematic variation with change in rigidity, this variation being responsible for a "smearing" of the lower rigidity portions of the telescope asymptotic cone of acceptance. Allowance for the "smearing" of the cone at these rigidities may in principle be made using the results of calculations of asymptotic directions of approach at the appropriate rigidity values in the internal field. Because of the small range of rigidities affected, the "smearing" would be expected to lead to only a very small dilution of the response of a detector to a primary anisotropy. Since, in any case, as discussed in Chapter 4, the cut-off values at mid- to low-latitude regions are not appreciably dependent on the external contributions to the geomagnetic field, it would be expected that, for a detector in such a situation, any daily variation in the form of the asymptotic cone of acceptance would be a second order effect.

It would thus appear that, for muon detectors at sea level, the effects of the external field contributions on asymptotic directions may for most purposes be overlooked, as the perturbation in the time

dependence of telescope response to external anisotropies is evidently very small.

7.4 Determination of Detector Response to Primary Anisotropies

In order to obtain an estimate of the reponse of any particular telescope to a primary anisotropy, it is necessary to make use of the intensity and direction relationships calculated to exist between the primary and secondary cosmic ray fluxes (i.e. coupling coefficients, such as determined in the preceding chapter, and calculated asymptotic directions of approach).

Bostrom [1965] discussed the general problems involved in the transformation of elements of a telescope acceptance cone through the geomagnetic field in order to deduce the detector response to external anisotropies. He presented a detailed discussion of the general properties of transformed elements under various conditions, and reviewed the methods of Brunberg [1958], and Rao et al. [1963], by which detector response may be calculated. Sandstrom [1965] also presented a detailed review of these techniques. Very briefly, the pertinent details are as follows:

Brunberg's technique involves the division of the asymptotic cone into small elements (spatial and rigidity elements), and calculation of the response of the detector to radiation arriving within each element. The relative contributions are expressed by means of these "sensitivity coefficients", and the response to anisotropy is then calculated by summation over all elements, each

weighted according to the form of the anisotropy.

The method of Rao et al. is essentially similar, in that the detector response to radiation arriving within given elements of the asymptotic cone is calculated, except that in this case the coefficients used to express the response, the "variational coefficients, represent the response of the detector to fractional change in the intensity incident within each element (the variation occurring according to an anisotropy of a given form).

A third method (used by Jacklyn and Humble [1965], for example) is that in which, instead of the initial division of the asymptotic cone of acceptance into elements, the determination of response commences with the division of the acceptance cone of the detector into elements. These elements are then transformed through the geomagnetic field onto the asymptotic cone of directions.

In this latter technique it is in practice found unnecessary to consider the transformed shape of the element, but sufficient to determine the asymptotic direction corresponding to the zenith and azimuth angles defining the position of the centre of the particular element in the detector, for the particular rigidity. The elements are chosen to be of sufficiently small size that the intensity variation over the corresponding element in the asymptotic cone may be neglected (this is readily achieved, except where the solid angle "magnification", as referred to by Brunberg, is extremely small, such as, for example, in portions of the cone where the rigidity is close to the cut-off value).

The fractional contribution to the telescope rate from each element, due to particles having rigidity within small rigidity intervals, is initially calculated on the assumption of primary isotropy, by applying the coupling coefficient value appropriate to the zenith angle of the element and the rigidity under consideration. Having a complete set of these "differential sensitivities", the response of the detector to any form of primary anisotropy may be readily calculated, by summation over the appropriately weighted element sensitivities.

This technique is a particularly convenient way of calculating telescope response by means of computer, since the division of the acceptance cone of the detector into elements is carried out as a part of the process of determining the sensitivity pattern of the detector in any case. The element radiation sensitivities can then be carried over into the next phase of the process, to be modified by application of the pertinent coupling coefficient value to become the differential sensitivities.

From the discussion in this section it will be apparent that the principles by which the reponse of a detector to primary anisotropy may be determined are well established. In the absence of accurate information on the functional dependence of muon coupling coefficients on zenith angle and rigidity, the use of very detailed techniques for accurately determining the asymptotic cone of the detector has not been warranted. Accordingly, in most investigations certain simplifications have been made, such as the use of a

fixed coupling coefficient function to apply to all points within the acceptance cone of the detector, and the division of the acceptance cone into only a small number of elements.

7.5 Automated Process of Asymptotic Cone Determination

The investigations in this thesis have been oriented towards the development of techniques by which more general and accurate determinations of muon detector response may be effected, with the aid of computers. A program has been written, capable of automatically deducing the details of the asymptotic cone for telescopes of any configuration, estimating the differential response of the telescope to any given form of primary anisotropy, and pictorially representing the asymptotic cone.

The program utilizes the approach in which the determination of telescope response commences with the division of the telescope acceptance cone into elements. The division is carried out by means of the technique described in Chapter 3, and each element is assigned a radiation sensitivity $r_{\theta,\phi}$, where θ and ϕ refer to the zenith and azimuth angles defining the position of the element.

The differential element sensitivities $s_{\theta,\phi,R}$ are then evaluated by multiplication of the radiation sensitivity of each element by the appropriate value $W_{\theta}(R)$ of the coupling coefficient function (determined by means of the computer procedure described in Appendix 4), i.e.

$$s_{\theta,\phi,R} = r_{\theta,\phi}\, W_{\theta}(R)$$

The remaining task in establishing the asymptotic cone is the determination of the asymptotic direction of approach corresponding to the zenith and azimuth angle associated with each element, for primaries of given rigidity.

If the acceptance cone has been divided into a large number of elements then it is completely impractical to calculate the asymptotic directions from first principles for each element, because of the very great time involved. It is far more desirable that the asymptotic direction pertaining to any particular direction and rigidity be interpolated from a set of asymptotic directions previously determined, for a range of values of zenith and azimuth direction, and rigidity.

The problems of interpolating from such a set are considerable because of the complexity, in many cases, of the locus of asymptotic direction with, for example, changing azimuth for a given zenith angle at low rigidity. It is obvious that curvilinear interpolation must be used because of the extremely poor fit, in most cases, of a great circle section to successive points on the locus. Further, it is preferable that the interpolation process use as independent variables, parameters other than latitude and longitude, because of the complications introduced into the interpolation process by the clustering of meridian lines at the poles.

For this reason, an interpolation technique was developed, that makes use of two angles (σ,γ) to express the relative position of two points on a spherical surface, where σ is the angle between the

great circle connecting the points and the meridian line intersecting one of them, and γ is the angle subtended at the centre of the sphere by the two points (see Figure 7.1). It may be shown that, in terms of the latitude and longitude of the two points (λ_1,ψ_1) and (λ_2,ψ_2), the angles are given by

$$\sigma = \arctan\left[\frac{\sin(\psi_2 - \psi_1)\cos\lambda_2}{\sin\lambda_1\cos\lambda_2 - \sin\lambda_1\cos\lambda_2\cos(\psi_2 - \psi_1)}\right]$$

$$\gamma = \arccos\left[\cos(\psi_2 - \psi_1)\cos\lambda_1\cos\lambda_2 + \sin\lambda_1\sin\lambda_2\right]$$

The use of these angles (whose magnitude is independent of the latitude and longitude position of the points) allows the representation, by parabolic sections, of the locus of asymptotic direction for variation of zenith angle for constant azimuth angle, and vice versa, on the surface of a unit sphere. In principle, it would be a relatively matter to interpolate in rigidity, too, although this facility has not yet been incorporated into the program. The interpolation process is described in detail in Appendix 6. It is sufficient for the present purpose to say that it is possible to use standard sets of asymptotic

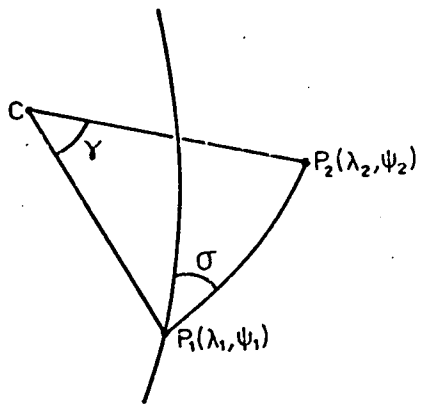

Figure 7.1. Diagram defining the angles σ and γ used to express the relative position of the two points P_1 and P_2 on a spherical surface. C is the centre of the sphere.

directions pertaining to widely spaced zenith and azimuth directions at given sites to deduce, by means of this interpolation process, the asymptotic direction corresponding to any intermediate zenith and azimuth angle.

Obviously, in order to minimize the number of calculations required to derive a basic set of asymptotic directions, it is preferable to use a relatively low number of zenith and azimuth directions. In practice it has been found that a satisfactory specification of the asymptotic cone of directions corresponding to the observing hemisphere at any site may be obtained in terms of 49 asymptotic asymptotic directions for any rigidity in excess of 25 GV. At these rigidities, directions spaced 15^{o} in zenith and 45^{o} in azimuth have been found satisfactory for use in the standard asymptotic direction set, and for rigidities $\leq$ 25 GV, 22.5^{o} spacing in azimuth for zenith angles $\geq 45^{o}$; additional directions are inserted in the set to aid the interpolation where curvature reversals are present in the loci. This information is readily assembled in the correct form by the computer program used to derive the trajectories.

That the interpolation procedure is satisfactory is evidenced by the very smooth form of the asymptotic cones deduced in this way, the elements lying in ordered progression without sign of the irregularities that would accompany poor interpolation. A certain amount of testing has been carried out to determine the effect of altering the zenith and azimuth intervals used in the asymptotic

direction sets, in particular by comparing the interpolated latitude and longitude when interpolated from a set in which the zenith spacing was 10^{o} and the azimuth spacing 22.5^{o}, with the predictions of the standard set, for a rigidity of 50 GV. The differences in latitude and longitude were small, at most 2^{o}, and no significant differences arose in the associated response calculations (magnitude and phase of response equal to the fourth decimal place).

The differential sensitivities and asymptotic directions pertaining to the telescope elements together constitute a perfectly general specification of the asymptotic cone of acceptance of the detector at any particular rigidity (since the sensitivities are calculated on the assumption of primary isotropy). Having determined them once for a particular detector at a particular site, it is unnecessary at any stage to repeat the calculations. For this reason the computer program, if required, outputs these data in the form of punched tape, for use in later analyses.

In the next stage of its operation, the program calculates the differential response of the telescope to any given form of primary anisotropy (for example, an anisotropy having a given form of ecliptic latitude dependence). It does this by applying appropriate weighting to the differential element sensitivities, and then estimating the amplitude and phase of the first and second harmonic components of the indicated daily variation of detector rate.

Although, as the result of the calculations at a single rigidity, there is insufficient information to allow the estimation of the

fractional contribution to the telescope counting rate from primaries within a given rigidity interval about the rigidity value concerned, the program outputs a "relative" response figure. By comparison of this figure with those from calculations at other rigidities, the rigidity dependence of the response may be precisely determined. The "relative" response figures are equivalent to the coupling coefficients, except that the values have not been normalized to allow the figures to represent the response in percentage form.

The program then calculates the total counting rate of the telescope in the particular situation, by taking the product of the integrated radiation sensitivity and the sea level vertical muon intensity (0.009 particles per cm^2 per ster. per sec.). This facility is particularly useful when the program is being used for purposes of experiment design.

On completion of these calculations, the program causes the detector asymptotic cone to be drawn, in the form of a grid of lines on a spherical surface, as seen in perspective from any desired asymptotic direction. If required, the diagrams are drawn with the lines representing the element positions raised in proportion to the differential sensitivities at the particular rigidity.

In summary then, the main phases of the operation of the "asymptotic cone" computer program are as follows:

1) Data input.

   a) Standard asymptotic direction set,

b) Telescope details - dimensions, orientation.

2) Calculations.

a) Viewing cone split into elements,

b) Radiation sensitivities calculated,

c) Coupling coefficient values determined,

d) Differential sensitivities produced,

e) Asymptotic directions interpolated from standard set,

f) "Relative" response figure determined,

g) Differential response to given anisotropy calculated,

h) Counting rate of detector in given situation calculated.

3) Output.

a) Tape containing differential sensitivities,

b) Asymptotic cone drawn, from specified viewpoint,

c) Response figures printed.

7.6 The Computer Program in Operation

As an example of the operation of the program, we present in Figure 7.2 a series of computer drawn asymptotic cones of acceptance, for the 76.5° zenith angle telescope described in Section 6.10, viewing towards geographic north at Mawson (geomagnetic coordinates 73° S, 103°E), for rigidities 1000, 300, 100, 50, 35, 25, and 18 GV. In these diagrams the change in the asymptotic cones with decreasing rigidity is very clearly displayed. At high rigidities the asymptotic cone corresponds closely to the "line of sight" cone of the detector, but with diminishing rigidity the magnetic [to page 314]

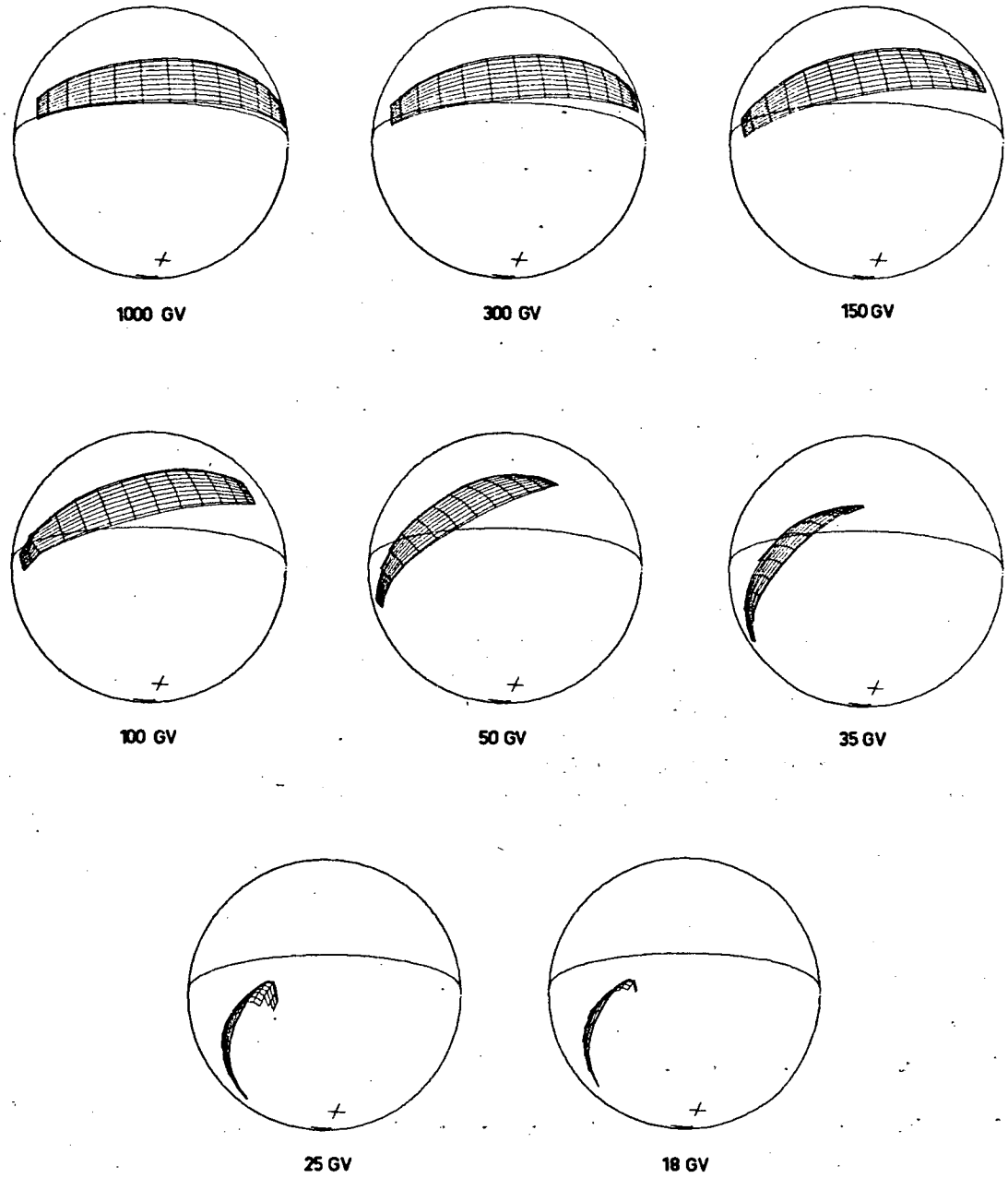

Figure 7.2. Computer drawn asymptotic cone of acceptance for the north pointing 76.5^{o} zenith angle telescope (described in Section 6.10) at Mawson, for a range of rigidity values. The location of Mawson is shown by the upper cross, the south pole by the lower.

[from page 312] field is seen to exert a progressively greater focussing effect. Each of these drawings and the associated calculations took approximately 3 minutes on an Elliott 503 computer.

It would be true to say that, in general, the differences in predicted response when the detailed form of a detector acceptance cone is taken into account to that predicted on the assumption of a single, or limited number, of asymptotic directions of approach, are of magnitude sufficient to affect significantly the interpretation of experimentally observed daily variation of telescope rate.

The diagrams in Figure 7.2 illustrate clearly the necessity of taking into account the effects of contributions to the telescope rate from all portions of the telescope acceptance cone. It is seen that the asymptotic cone at high rigidities lies parallel to the equator, extending over a large range of longitudes. The response of the telescope at high rigidities would, as a result, be smeared, particularly in the response to a second harmonic anisotropic component. If the "fan" beam of the telescope were to be rotated through 90^{o}, then the response to an anisotropy would obviously be considerably greater, as then the asymptotic cone, for high rigidities, would lie over only a very narrow band of longitudes. Rotation of the telescope would similarly produce a change in response at the lower rigidities.

The potential power of the "asymptotic cone" program lies in its capacity to facilitate the optimization of detector configuration for use in studies of primary anisotropies, since it in essence

provides a means of "conducting the experiment" at the console keyboard of a computer. The calculations are sufficiently rapid to allow a thorough investigation to be made of the effects of change in detector orientation and opening angle.

Calculations, carried out as an aid to the design of proposed experiments at Mawson, have shown that very real gains may result from the optimization of the detector configuration. In a number of situations it has proved possible, for a given sensitive area of detecting elements, to obtain increases in counting rate of the order of five over the rates expected with telescopes of standard design (for example, cubic geometry), without appreciably affecting the predicted amplitude of response to any particular anisotropy. The increase in counting rate has been obtained by an increase in opening angle of the telescopes in one or more dimensions, in conjunction with a selected change in orientation.

Because of the very large opening angles of telescopes in such situations, the orientation required to obtain the desired result is found to be critical. The wide angle detectors "view" over a very large range of zenith angles, and the availability of an accurate zenith angle-dependent coupling coefficient function (such as that produced in the preceding chapter and used in the "asymptotic cone" program) is most important.

In experiment design with the aid of the computer program, it has proved possible to take more subtle considerations into account. In given situations, detector configurations have been predicted

that are capable of producing, at high counting rates, particular forms of detector response to given anisotropies, broadly analogous to the "band pass" and "notch" characteristics of electronic filters. These response characteristics are potentially valuable in the study of the rigidity dependence of primary anisotropies. As an aid to achieving these and other particular forms of telescope response, it is useful to introduce into the calculations, in addition to other details of telescope design, the angle of rotation of the telescope about the axis of the acceptance cone, particularly if a "fan" beam telescope or multiple beam telescope array is to be used.

So much for the use of the program as a tool in experiment design. In the basic function of predicting the response of any given telescope, the program differs from previous methods of computation most significantly in the introduction of the directional coupling coefficient model, and the division of the viewing cone into small elements.

Comparisons made between the predictions if the program and those of a less detailed approach (in particular, those of Jacklyn [private communication]) have shown that, for a telescope of moderate width of acceptance cone, whilst the predictions are essentially similar, significant differences do occur in the detailed estimates of the response. In Table 7.1 we present the comparative estimates of the differential response of telescopes of dimensions (1.5 units in length x 1 x 1), inclined at 45^{o} zenith

angle in the geomagnetic east and west at Mawson, to a solar anisotropy having a cosine form of ecliptic latitude dependence. Jacklyn used the 45^{o} zenith angle coupling coefficients of Webber [1962], and divided the acceptance cone of the telescope into 16

Table 7.1 Comparison of calculated amplitude A and phase Ø of the first harmonic response of east and west pointing telescopes at Mawson to a solar anisotropy having a cosine form of ecliptic latitude dependence, as estimated by Jacklyn and by the computer technique. The amplitude A is the response of the telescope to the anisotropy relative to the response that would occur if the asymptotic cone were unidirectional and located on the equator. The phase Ø is the amount by which the mean longitude of viewing of the detector is "ahead" of the station

Rigidity	East				West			
(GV)	Jacklyn		Computer		Jacklyn		Computer	
	A	Ø	A	Ø	A	Ø	A	Ø
25	0.96	-5^{o}	0.94	-3^{o}	0.34	5^{o}	0.40	5^{o}
35	0.95	8^{o}	0.92	9^{o}	0.17	-20^{o}	0.26	-13^{o}
50	0.94	20^{o}	0.90	18^{o}	0.18	-63^{o}	0.22	-47^{o}
100	0.89	32^{o}	0.84	30^{o}	0.34	-95^{o}	0.33	-78^{o}
150	0.85	35^{o}	0.81	34^{o}	0.42	-97^{o}	0.37	-83^{o}
300	0.82	39^{o}	0.78	38^{o}	0.48	-95^{o}	0.43	-86^{o}
1000	-	45^{o}	0.76	41^{o}	-	-95^{o}	0.47	-87^{o}

segments (compared with approximately 150 in the computer calculations).

The order of the disparity between the differential responses calculated by the computer technique and the less detailed approach, although relatively small for the case considered, would be expected to increase with increasing width of telescope acceptance cone. The precise manner in which the integral response of a telescope in any situation would be affected by such differences, in conjunction with the different coupling coefficients, would of necessity have to be determined by calculation. It is apparent, however, that significant differences will arise, particularly in the case of detectors whose differential response phase angle is a sensitive function of rigidity.

7.7 Concluding Remarks

The research reported in this thesis consists of a number of investigations, by their nature separate, but aimed overall at improving the accuracy in the specification of the relationship between the sea level directional muon component and the primary cosmic ray flux. Where the inherent interest in the problem has justified it, these investigations have been carried further than strictly necessary for the resolution of the main problem (for example, the investigations of the loop cone phenomenon, and the atmospheric asymmetry effect).

With the aid of a number of new techniques, experimental data

from a latitude survey, corrected for removal of the atmospheric asymmetry effect and ordered by the use of calculated mean effective cut-offs, have been used to derive a comprehensive unidirectional muon coupling coefficient model. Techniques for modifying the coefficients to take account of change in the conditions affecting the primary and secondary components have been discussed, and developed where necessary. In order to facilitate the accurate implementation of the coefficients, the basic coupling coefficient set has been described in terms of continuous functions of zenith angle and momenta, by means of polynomial representation of the parameters.

The possession of a complete functional coupling coefficient model has facilitated the development of a computer program capable of accurately and automatically determining the asymptotic cone of acceptance of any sea level muon telescope. This program offers the means of introducing an increased degree of sophistication in certain aspects of cosmic ray astronomy - at the planning level, because of the possibility of effective optimization of detector configuration (thus allowing greatly improved efficiency of detection of anisotropic effects); and in the analysis of data, as a result of the greater accuracy attainable in the determination of detector response.

APPENDIX 1

DEFINITION OF THE TERM "RE-ENTRANT"

The term "re-entrant" has been used in two different senses in the literature for referring to properties of the trajectories of charged particles in the geomagnetic field.

The original usage was introduced by Lemaitre and Vallarta [1936a], who defined the allowed (or main) cone of radiation as the solid angle of directions along non-reentrant trajectories. Schremp [1938] formally defined re-entrancy in terms of the shape of orbital "sections", where a "section" is any segment of an orbit lying between two consecutive points at which a certain function associated with the trajectories attains relative minima. To be "re-entrant", the two ends of an orbital section have to be directed towards the dipole.

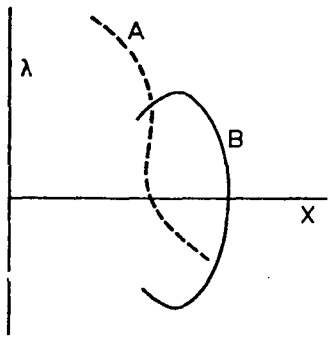

Figure A1.1. Typical trajectory sections. "A" represents a looped trajectory, and "B" a trajectory oscillating in the region of the bound periodic orbits. By definition, only B is re-entrant.

The minima appear on X-λ plots (see Section 4.3) as maxima in the curvature of the trajectories. A section such as that labelled A in Figure A1.1 would, in view of the orientation of the section ends, be regarded as "re-entrant". This trajectory segment is typical of

an orbit oscillating in the region of the bound periodic orbits.

On the other hand, the looping of trajectories around field lines would not produce re-entrancy, in spite of possible reversals in the sense of motion relative to the dipole, because these sections would not satisfy the requirements of the re-entrant definition (see, for example, trajectory A in Figure A1.1).

It should, perhaps, be noted here that the definition of re-entrancy given by Vallarta [1961] does allow trajectory loops having such reversals in the sense of motion relative to the dipole to be regarded as re-entrant sections. Since these loops may occur in trajectories associated with primary particles having momenta in excess of the main cone cut-off (as determined by invoking the requirement for the main cone edge trajectory to be associated with asymptotic entrance to bound periodic orbits), it would thus appear that the Vallarta definition is in conflict with Lemaitre and Vallarta's definition of the allowed cone in terms of non-reentrant trajectories. The disparity arises out of an apparent error in the definition of "re-entrant" as given by Vallarta, in which the re-entrant sections are referred to as lying between consecutive relative maxima (rather than minima) of the function associated with the trajectories.

The second usage of the term "re-entrant" occurs in the later literature, where it is used (by Shea et al. [1965], for example) to refer to calculated trajectories commenced at a point on the earth that subsequently intersect the surface of the earth.

APPENDIX 2

STEREOSCOPIC DRAWINGS

Stereoscopic drawings of cosmic ray trajectories and cut-off information have proved a useful aid to the visualization and interpretation of the cosmic ray trajectory effects described in Chapter 4, and a number of the stereo pictures have been presented to illustrate the discussions in that chapter (the frontispiece, and Figures 4.12, 4.15 and 4.19).

A2.1 Viewing the Stereoscopic Drawings

These drawings, constructed by means of a computer program written by the author, have been prepared for viewing in two different ways:

a) Over-printed Colour Image Technique (Frontispiece)

In order to obtain visual separation of the two over-printed images in the frontispiece, it is necessary to make use of the coloured filter "spectacles" enclosed inside the back cover of this thesis. This diagram is designed to be viewed from a distance of 12 - 15 inches, with the red filter over the left eye and the green over the right. This presentation has the advantage over the separate image stereo pair pictures in that a wider field of view may be encompassed. On the other hand, it is difficult to prepare pictures of this type because of the problem of obtaining colours pure enough and of the right intensity to ensure

satisfactory image separation. Because the coloured inks available for use on the computer X-Y plotter were unsuitable for use directly, it was necessary to prepare separate pairs of drawings in black, and to over-print these in colour by means of the offset printing process.

b) Stereo pair pictures (Figures 4.12, 4.15, and 4.19)

These pictures may be viewed with the aid of the prism enclosed inside the back cover of this thesis, from a distance of 10 - 12 inches. In using the prism, hold the thin edge towards the nose, immediately in front of one eye. With little difficulty the images should rearrange themselves so that there appear to be only three images, of which the centre one is the fused stereoscopic image.

This type of drawing is easily prepared, and can be drawn directly by the computer plotter for direct viewing. These particular drawings were, in fact, prepared twice the size required, and photographically reduced, in order to minimize the visual effects of the finite step size of the digital X-Y plotter.

A2.2 Preparation of the Stereoscopic pictures

Although the computer program is relatively simple in function, the basic angle conversions necessary for the production of the drawings are involved, and so these are presented here in detail.

In the preparation of the stereoscopic drawings in this thesis, the information to be represented was available in the form of

sets of points whose positions were available in spherical coordinates (latitude, longitude and radius, in the case of the trajories; zenith, azimuth and radius (cut-off) for the cut-off information). Angle conversions had to be applied to allow the calculation of the position of each data point on a plain two dimensional surface to represent the "scene" when viewed from given, related pairs of positions outside the scene (corresponding to the "point of view" of each eye).

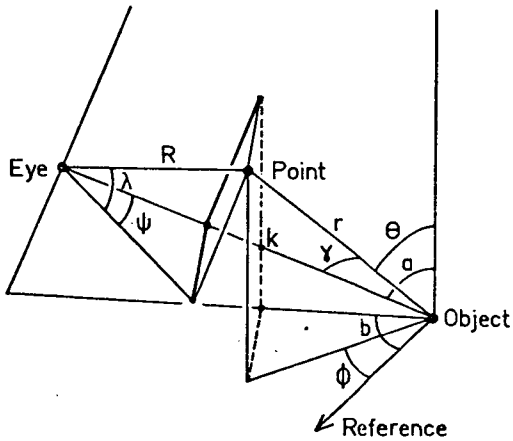

Figure A2.1. Diagram showing the quantities used to define the relative positions of eye, the origin of the coordinate system fixed in the object, and a generalized point.

Consider the scene as viewed by an eye situated at a point (k,a,b) relative to a spherical coordinate system centred on the object of interest (see Figure A2.1). We wish to determine the values of the angles λ,ψ describing the apparent position of the point relative to the eye. It may be shown that:

$$\psi = \arctan\left[\frac{r \sin\theta \sin(b - \phi)}{k - r \cos\gamma}\right]$$

$$\lambda = \arccos\left[\frac{\cos\left(\arctan\left(\frac{r \sin\gamma}{k - r \cos\gamma}\right)\right)}{\cos\psi}\right]$$

where

$$\gamma = \arccos[\cos(\arcsin(\sin\theta \sin(b - \phi)))$$
$$\sin(a + \arctan(\tan\theta \cos(b - \phi)))]$$

Having determined these angles, the position (x,y) of the point of intersection of the line of sight with the plane on which the scene is being recorded (at distance V from the eye, normal to the eye-object origin line) may be found using the equations

$$y = V \tan\psi$$
$$x = V \frac{\tan\lambda}{\cos\psi} \qquad \text{(A2.1)}$$

It is necessary to determine the apparent position, in the same plane, of the given point as viewed by a second eye, displaced a distance X laterally from the first. In this case the position of the point is given by

$$\psi' = \arctan\left(\frac{R \cos\lambda \sin\psi - X}{R \cos\lambda \cos\psi}\right)$$
$$\lambda' = \arctan\left(\frac{\tan\lambda \cos\psi'}{\cos\psi}\right)$$

where R is the displacement of the point from the first eye, given by

$$R = \frac{k - r \cos\gamma}{\cos\lambda \cos\psi}$$

The corresponding position in the X-Y plane is found using ψ' and λ' in equations (A2.1) instead of ψ, λ.

The computer, in operation, required specification of the view-point (k,a,b) to be used for the particular plot, and of

a magnification figure to fix the simulated size of the "object". For plotting the cut-off directional distributions, data were provided in the form of prepared data tapes, whilst for drawing trajectories the program carried out the trajectory trace using standard numerical integration methods, plotting simultaneously the first of the traces. On completion of the first trace, the second was automatically drawn, from the correct view-point, using the trajectory details stored in the computer memory.

The basic perspective drawing technique was also utilized in the "asymptotic cone" computer program described in Chapter 6, for representing the detector asymptotic cones on a unit sphere (see Figure 7.2).

APPENDIX 3

MAXIMUM MOMENTUM TRANSFERABLE TO MUON BY PROTON OF GIVEN MOMENTUM

Most muons in the atmosphere are produced as a result of the decay pf pions produced in the initial interaction of primary protons in the atmosphere. Rossi [1952] described the physical processes involved, and outlined the nature of the calculations by which the energies of the particles may be deduced.

The production of pions is described by the equations

$$p + p \longrightarrow p + n + \pi^{+}$$

$$p + n \longrightarrow p + p + \pi^{-}$$

and the production of muons from pions, by the equation

$$\pi^{\pm} \longrightarrow \mu^{\pm} + \text{one or more neutrinos.}$$

The muon energy is a maximum when the mesons are ejected in the forward direction in the c.m. systems of each of the groups of particles associated with each reaction, the maximum available energy goes into the pion production, and a single neutrino is produced in the pion decay.

We have derived equations relating the momentum of the maximum energy muon to the momentum of the parent primary proton. In these equations the following notation is used: m, rest mass; P, T, E, the momentum, kinetic energy, and total energy respectively in the laboratory system, and the same letters with an asterisk refer to these quantities measured in the appropriate c.m. system.

For determining the maximum muon momentum possible for a given

proton momentum these equations have the form

$$P_\mu c = \frac{E_\pi \sqrt{(E^{*2}_\mu - m^2_\mu c^4)} + E^*_\mu \sqrt{(E^2_\pi - m^2_\pi c^4)}}{m_\pi c^2}$$

where $E^*_\mu = \frac{1}{2} m_\mu c^2 \, (m_\pi/m_\mu + m_\mu/m_\pi)$

$$E_\pi = T_p + 2m_p c^2 - 2\sqrt{(m^2_p c^4 + T_p m_p c^2/2)}$$

$$T_p = \sqrt{(m^2_p c^4 + p^2_p c^2)} - m_p c^2$$

Conversely, to determine the minimum proton momentum required to produce a muon of given momentum, the equations may be used in the following form

$$P_p c = T_p \sqrt{(1 + 2m_p c^2/T_p)}$$

where $T_p = E_\pi - m_p c^2 + \sqrt{(m_p c^2 (2E_\pi + m_p c^2))}$

$$E_\pi = m_\pi c^2 \left(\frac{E^*_\mu \sqrt{((P_\mu c)^2 + E^{*2}_\mu)} - P_\mu c \sqrt{(E^{*2}_\mu - m^2_\mu c^4)}}{m^2_\mu c^4}\right)$$

$E^*_\mu = \frac{1}{2} m_\mu c^2 \, (m_\pi/m_\mu + m_\mu/m_\pi)$

The momentum relationship predicted by these equations is illustrated in Figure A3.1 (where the calculations were carried out assuming a pion mass of 273 x electron mass, and a muon mass of 207 x electron mass). In this diagram the ratio of proton momentum to muon maximum momentum is shown as a function of muon and proton momentum. In Table A3.1 we present, for a range of values of muon

momentum, the calculated minimum momentum required by a proton in order to give rise to a muon of given momentum.

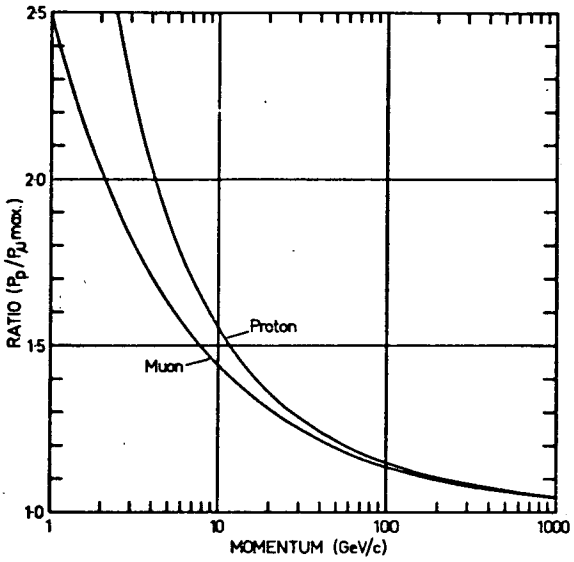

Figure A3.1 (left). Proton momentum - muon maximum momentum ratio as a function of muon and proton momentum.

Table A3.1 Value of minimum proton momentum required to allow production of muons of given momentum (GeV/c).

Muon momentum	Proton momentum	Ratio $\frac{\text{proton}}{\text{muon}}$ momentum
1.00	2.503	2.503
1.50	3.300	2.200
2.50	4.774	1.910
4.00	6.835	1.709
6.50	10.074	1.550
10.00	14.403	1.440
15.00	20.367	1.358
25.00	31.900	1.276
40.00	48.706	1.218
65.00	76.079	1.170
100.00	113.727	1.137
150.00	166.801	1.112
250.00	271.679	1.087
400.00	427.413	1.069
650.00	684.938	1.054
1000.00	1043.330	1.043

APPENDIX 4

COUPLING COEFFICIENT EVALUATION

Chapter 6 describes the derivation of a unidirectional coupling coefficient model from experimental data. Two empirical functions were used to describe the momentum dependence of the coefficients (at low and high momenta), where the parameters in these functions took values dependent upon the zenith angle under consideration. In order to obtain functional representation of the dependence of the coupling coefficients on zenith angle, polynomial functions were derived to represent the zenith angle dependence of the individual parameters.

So that a form of parameter zenith angle dependence suitable for accurate representation by polynomial functions could be obtained, it was necessary, in deriving the polynomial expressions, to modify first the values of some of the parameters by insertion into suitable arbitrary functions. Thus, for example, a polynomial was derived to represent, instead of the dependence of atmospheric cut-off P_c on zenith angle, the dependence of $\ln(\ln(P_c))$ on zenith angle. Necessarily these secondary functions must be taken into account when using the polynomial functions.

The computer program presented in this Appendix calculates the coupling coefficient value appropriate to any given zenith angle and momentum. It takes into account the secondary functions in the polynomial evaluations, and selects the correct empirical function.

```
Coupling Coefficient Evaluation;
      begin real k,m,pi,ze,atmos,I,P,Pa,Pc,Po;
            integer a,b,c,d,e,i;
            real array Aa,Ab,Ac,Ad,Ae[0:11];
comment The following procedure evaluates the polynomial expressions;
            procedure assemble(j,x,B);
            value j; real x; integer j; array B;
                  begin for i:=j step -1 until 0 do
                        if i=0 then x:=x+B[i] else x:=x+B[i]*ze↑i
                  end assemble;
comment The following procedure calculates coupling coefficient value
  I appropriate to given zenith angle ze (radians) and momentum P;
            procedure coco;
                  begin Pa:=Pc:=Po:=k:=m:=0;
comment Pc polynomial evaluated;
                  assemble(a,Pc,Aa);
                  if P≤Pc then I:=0 else
                        begin assemble(b,Pa,Ab);
comment Pa polynomial evaluated;
                              Pa:=exp(exp(Pa));
                              if P≤Pa then
                                    begin assemble(c,k,Ac);
comment k polynomial evaluated;          k:=exp(11-exp(k))/10^5;
comment Low momentum empirical function invoked;
                                    I:=1.6*k*(P-Pc)↑0.6
```

```
                                    end else
                                    begin assemble(d,Po,Ad);
comment Po polynomial evaluated;            Po:=exp(exp(Po));
comment m polynomial evaluated;             assemble(e,m,Ae);
comment High momentum empirical function invoked;
                                            I:=1.575_10 5/atmos*
                                            exp(-(Po/P) m)/(P)↑2.5
                                    end
                            end
                        end coco;
comment List of polynomial coefficients follows, first the Pc
  coefficients;
            a:=8;
            Aa[0]:=3.94343496_10-1;   Aa[1]:=2.83884720_10-2;
            Aa[2]:=3.18442428_10-1;   Aa[3]:=-0.16828682_101;
            Aa[4]:=6.99170487_100;    Aa[5]:=-0.12935522_102;
            Aa[6]:=1.24020400_101;    Aa[7]:=-0.59915204_101;
            Aa[8]:=1.16222237_100;
comment Pa coefficients;
            b:=11;
            Ab[0]:=7.08785201_10-1;   Ab[1]:=5.64229237_10-2;
            Ab[2]:=1.06625323_100;    Ab[3]:=1.40906421_100;
            Ab[4]:=-0.21538617_102;   Ab[5]:=7.63781066_101;
            Ab[6]:=-0.1398355_103;    Ab[7]:=1.30777139_102;
            Ab[8]:=-0.41757523_102;   Ab[9]:=-0.23013499_102;
```

```
            Ab[10]:=2.1424339_10 1;    Ab[11]:=-0.46189787_10 1;
comment k ccefficients;
            c:=11;
            Ac[0]:=-0.94776962_10 -1;  Ac[1]:=-0.13363799_10 0;
            Ac[2]:=1.62128649_10 0;    Ac[3]:=9.69825069_10 0;
            Ac[4]:=-0.25649371_10 2;   Ac[5]:=-0.68015002_10 2;
            Ac[6]:=4.02677287_10 2;    Ac[7]:=-0.80381229_10 3;
            Ac[8]:=8.66742904_10 2;    Ac[9]:=-0.53638738_10 3;
            Ac[10]:=1.79171694_10 2;   Ac[11]:=-0.25040684_10 2;
comment Po coefficients;
            d:=9;
            Ad[0]:=1.72573354_10 0;    Ad[1]:=-0.49085898_10 -1;
            Ad[2]:=1.63812338_10 -1;   Ad[3]:=3.27545817_10 0;
            Ad[4]:=-0.20060650_10 2;   Ad[5]:=5.17553067_10 1;
            Ad[6]:=-0.69388286_10 2;   Ad[7]:=5.07210045_10 1;
            Ad[8]:=-0.19193853_10 2;   Ad[9]:=2.95101927_10 0;
comment m coefficients;
            e:=10;
            Ae[0]:=5.48965579_10 -1;   Ae[1]:=-0.10698337_10 -1;
            Ae[2]:=1.49861853_10 -1;   Ae[3]:=3.19583393_10 -1;
            Ae[4]:=-0.79977262_10 1;   Ae[5]:=3.71731038_10 1;
            Ae[6]:=-0.84547734_10 2;   Ae[7]:=1.05937600_10 2;
            Ae[8]:=-0.74223833_10 2;   Ae[9]:=2.72343586_10 1;
            Ae[10]:=-0.40758739_10 1;
comment Program reads zenith angle (degrees) and momentum (in GeV/c),
```

and then prints out the appropriate coupling coupling coefficient value (units: % per GeV/c);

```
        sameline;  top of form;  pi:=3.141593;
        read ze,P;  ze:=ze*pi/180;
        atmos:=(cos(ze))↑2.2+0.001909*ze;
        coco;
        print aligned(4,1),ze*180/pi,££t??,P,££t??,aligned(1,5),I
    end of program;
```

As mentioned in Section 6.9.4, a polynomial function has been deduced to express the dependence of zenith angle on atmospheric cut-off. The following computer program evaluates the zenith angle appropriate to any given value of atmospheric cut-off. This angle may then be inserted in the preceding program to evaluate the coupling coefficient value for any given value of momentum.

Zenith Angle Equivalent of Atmospheric Cut-off;

```
    begin real x,pi,ze,Pc;
        integer m,n;
        real array A[0:7];
        m:=7;
        A[0]:=1.22879907₁₀1;     A[1]:=-0.10852344₁₀3;
        A[2]:=3.86597802₁₀2;     A[3]:=-0.73939884₁₀3;
        A[4]:=8.45104302₁₀2;     A[5]:=-0.57151438₁₀3;
        A[6]:=2.10075228₁₀2;     A[7]:=-0.32267157₁₀2;
```

```
comment Program reads atmospheric cut-off value (in GeV/c), and
prints out corresponding zenith angle (degrees);
        sameline;  top of form;  pi:=3.141593;  x:=0;
        read Pc;
        for n:=m step -1 until 0 do
        if n=0 then x:=x+A[n] else x:=x+A[n]*(ln(ln(Pc)))↑n;
        if x<0 then print ££l?Pc too low? else
              begin ze:=pi/180*(abs(x))↑0.3333;
                    print ££l?Pc=?,aligned(3,3),Pc,££t?Angle=?,ze
              end
    end of program;
```

APPENDIX 5

TABULATED DETECTOR MEAN EFFECTIVE RESPONSE VALUES

We present here values of mean effective coupling coefficient W and integral response N at various momenta P, for the detectors listed in Table 6.6 (and identified A, B, C and D). The coupling coefficient values have the units % per GeV/c, whilst the integral response figures represent the percentage of the detector rate due to primaries of momentum greater than the given momentum values.

P	A		B		C		D	
	W	N	W	N	W	N	W	N
4	0.000	100.00	0.000	100.00	0.000	100.00	0.000	100.00
5	0.150	99.97	0.000	100.00	0.000	100.00	0.000	100.00
6	0.360	99.71	0.153	99.94	0.090	99.98	0.000	100.00
7	0.506	99.27	0.273	99.72	0.221	99.82	0.000	100.00
8	0.628	98.70	0.365	99.40	0.312	99.55	0.000	100.00
9	0.736	98.02	0.443	99.00	0.387	99.20	0.000	100.00
10	0.834	97.23	0.513	98.52	0.454	98.78	0.000	100.00
11	0.925	96.35	0.577	97.97	0.515	98.30	0.000	100.00
12	1.002	95.39	0.637	97.37	0.571	97.75	0.000	100.00
13	1.065	94.35	0.689	96.70	0.624	97.16	0.007	100.00
14	1.115	93.26	0.734	95.99	0.670	96.51	0.023	99.98
15	1.153	92.13	0.772	95.24	0.711	95.82	0.033	99.96
16	1.181	90.96	0.804	94.45	0.745	95.09	0.041	99.92

P	A		B		C		D	
	W	N	W	N	W	N	W	N
17	1.201	89.77	0.830	93.63	0.774	94.33	0.049	99.87
18	1.214	88.56	0.851	92.79	0.798	93.54	0.055	99.82
19	1.220	87.34	0.867	91.93	0.818	92.73	0.062	99.76
20	1.221	86.12	0.879	91.06	0.833	91.91	0.067	99.70
25	1.175	80.11	0.897	86.59	0.866	87.63	0.092	99.30
30	1.086	74.45	0.871	82.16	0.850	83.33	0.114	98.78
35	0.986	69.27	0.824	77.92	0.812	79.17	0.133	98.16
40	0.889	64.58	0.770	73.93	0.764	75.23	0.150	97.46
50	0.720	56.56	0.661	66.78	0.662	68.10	0.180	95.80
60	0.588	50.05	0.565	60.66	0.569	61.96	0.201	93.89
80	0.405	40.27	0.418	50.91	0.425	52.11	0.218	89.65
100	0.293	33.38	0.318	43.61	0.324	44.68	0.217	85.29
120	0.220	28.30	0.249	37.98	0.254	38.93	0.207	81.04
150	0.151	22.83	0.180	31.63	0.184	32.44	0.188	75.10
200	0.090	16.98	0.114	24.48	0.117	25.11	0.155	66.56
300	0.041	10.84	0.056	16.46	0.058	16.88	0.106	53.74
500	0.015	5.89	0.021	9.50	0.022	9.72	0.056	38.28
1000	0.003	2.43	0.005	4.20	0.005	4.29	0.019	21.71
5000	0.000	0.27	0.000	0.53	0.000	0.54	0.001	4.53
10000	0.000	0.11	0.000	0.22	0.000	0.22	0.000	2.43

APPENDIX 6

TECHNIQUE OF INTERPOLATING FROM STANDARD ASYMPTOTIC DIRECTION SET

A technique has been developed to allow the asymptotic direction pertaining to any given direction at a site (for any particular rigidity) to be deduced from a standard set of asymptotic directions relating to widely spaced directions at the site. As mentioned in Section 7.5, this interpolation process involves the use of two variables (σ,γ) to describe the relationship between two asymptotic directions. If the asymptotic directions are considered as being represented by points on a spherical surface, then σ is the angle between the great circle section connecting the points and the meridian line (line of constant asymptotic longitude) passing through one of the points, and γ is the angle subtended at the centre of the sphere by the two points (see Figure 7.1). The relationship between σ,γ and the latitudes and longitudes of the points is given by equations (7.1).

A single phase of the process of interpolation of the required intermediate asymptotic direction is described here. In the operation considered, the asymptotic direction pertaining to a site direction with given zenith and azimuth angles is determined from the set of asymptotic directions pertaining to a range of zenith angles at the given azimuth angle. In the "asymptotic cone" computer program the interpolation is carried out in both zenith and azimuth, and in principle the technique could also be used to

interpolate in rigidity.

Assume that, for primaries of a given rigidity approaching the site of interest, the asymptotic directions $(\lambda,\psi)_1$, $(\lambda,\psi)_2$, and $(\lambda,\psi)_3$ apply to three site directions $(\theta_1,\emptyset)$, $(\theta_2,\emptyset)$, and $(\theta_3,\emptyset)$, where λ,ψ refer to asymptotic latitude and longitude respectively, and $\theta,\emptyset$ to zenith and azimuth angles respectively. We wish to determine the asymptotic direction $(\lambda,\psi)'$ corresponding to a site direction $(\theta',\emptyset)$, where $\theta_1 < \theta < \theta_3$.

The relationship between the asymptotic directions is first established, in particular, the pair of angles $(\sigma,\gamma)_2$ relating the asymptotic directions $(\lambda,\psi)_1$ and $(\lambda,\psi)_2$, and the angles $(\sigma,\gamma)_3$ relating $(\lambda,\psi)_1$ and $(\lambda,\psi)_3$ are calculated. We then examine the dependence of σ,γ on the independent variable in the interpolation (in this case θ). Since it is possible to say that the value of γ_1 (the angle subtended at the centre of the sphere by the direction $(\lambda,\psi)_1$ relative to itself) is zero, three values of γ are known, pertaining to the three zenith angles θ_1, θ_2 and θ_3. The value of γ' corresponding to the zenith angle θ' may be found by fitting a quadratic to the three points $(\theta,\gamma)_1$, $(\theta,\gamma)_2$ and $(\theta,\gamma)_3$, as shown in Figure A6.1, and interpolating accordingly.

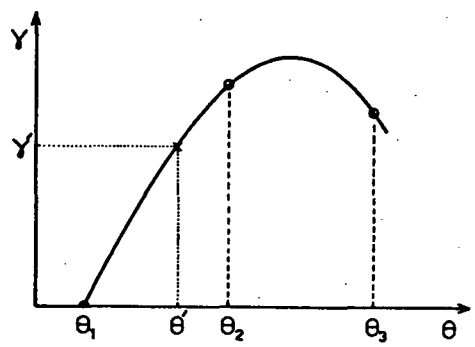

Figure A6.1. Diagram illustrating interpolation from the assumed θ-γ relationship.

In the case of the variable

σ (the angle between the great circle section connecting two points, and the meridian through one of them), the value σ_1 is indeterminate from a consideration of the point $(\lambda,\psi)_1$ alone. Therefore, since only two σ values are known, a linear relationship between σ and θ is assumed to exist. The value σ' corresponding to the zenith angle θ' is deduced by making use of the equation of the straight line passing through points $(\theta,\sigma)_2$ and $(\theta,\sigma)_3$, as illustrated in Figure A6.2.

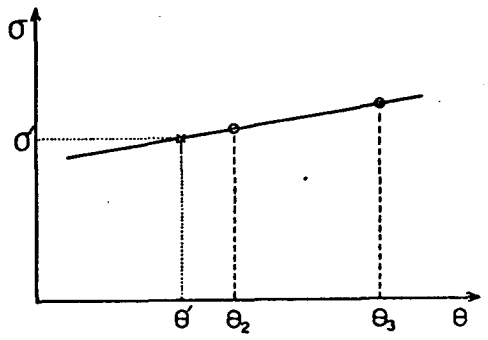

Figure A6.2. Diagram illustrating interpolation from the assumed θ-σ relationship.

Thus the angles $(\sigma,\gamma)'$ describing the position of the required intermediate asymptotic direction relative to other asymptotic directions in the standard set are known. The asymptotic latitude and longitude appropriate to the indicated direction are found using the equations

$$\lambda' = \pi/2 - \arccos(\cos\sigma \sin\gamma \cos\lambda_1 + \cos\gamma \sin\lambda_1)$$

$$\psi' = \psi_1 + \arcsin\left(\frac{\sin\sigma \sin\gamma}{\cos\lambda'}\right)$$

The operation described in the preceding discussion involved interpolation in zenith angle θ alone. In order to establish the asymptotic direction $(\lambda,\psi)'$ for the intermediate direction at the site $(\theta,\phi)'$, four interpolation cycles are required, three to determine the asymptotic directions appropriate to, for example, (θ',ϕ_1),

(θ',ϕ_2) and (θ',ϕ_3), and then one interpolation in azimuth to find $(\theta,\phi)'$. The interpolation may of course be carried out in the reverse order, i.e. interpolation in azimuth first, and then in zenith. Figure A6.3 illustrates the relationship of the asymptotic directions (plotted on a spherical surface) for $\theta = \theta_1, \theta_2, \theta_3$ and $\phi = \phi_1,\phi_2,\phi_3$, and the lines fitted to aid the interpolation of the asymptotic direction pertaining to the site direction $(\theta,\phi)'$ when the interpolation is carried out in either order (the lines represent the asymptotic direction loci for change in zenith and azimuth). The thick lines represent the "loci" constructed for use in the interpolation in the order zenith-azimuth, and the thin lines those used for interpolation in the reverse order.

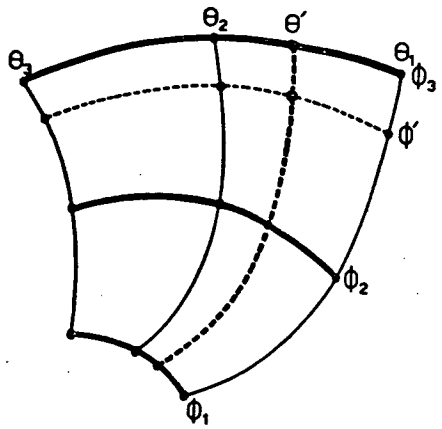

Figure 6.3. Diagram showing the "loci" constructed in the interpolation process.

For greater accuracy, in situations where asymptotic direction loci are complex (for example at low momenta), it would be advantageous to use higher order interpolation, using sets of four, rather than three, points. In this case γ would be determined from a third order, and σ from a second order, function. Necessarily the time involved in the interpolation would increase accordingly.

Although the facility for interpolation in rigidity has not

been incorporated into the "asymptotic cone" computer program, the principles involved would be the same as those discussed, although because of the network of interrelationships to be established in order to interpolate in zenith, azimuth and rigidity, the volume of calculations would increase by a factor of three minimum.

Although the use of the variables σ and γ removes, in principle, the difficulty in the interpolation process in the region of the poles, in practice a difficulty is encountered in unambiguously defining the correct quadrant in which the angle values lie, so that the angle values are introduced into the interpolation in the correct order. To overcome this difficulty, an angle transformation has been employed that, when asymptotic latitudes greater than 50^{o} are encountered, allows the asymptotic direction to be calculated relative to a frame of reference in which the poles lie on the "equator" of the sphere (and thus causing the former poles to lie on the "equator" of the new coordinate system). The transformation into this coordinate system is given by

$$\lambda' = \arcsin(\cos\psi \cos\lambda)$$

$$\psi' = \pi/2 - \arccos(\sin\lambda / \cos\lambda')$$

and the transformation from the new system back into terrestrial latitude and longitude by

$$\lambda = \arcsin(\sin\psi' \cos\lambda')$$

$$\psi = \pi/2 - \arcsin(\sin\lambda' / \cos\lambda)$$

This transformation is potentially useful in the calculation of cosmic ray trajectories that pass close to the geographic poles. Because of the rapid change in longitude in such cases, the Runge-Kutta integration process is sometimes found to fail, or more often to introduce a step size which, while small enough to facilitate the completion of the trajectory, increases the calculation time considerably. In these cases there may be advantages in applying the coordinate transformation and recalculating the trajectory in the new coordinate system.

PUBLICATIONS

1. D.J. Cooke, Cosmic Ray Azimuthal Asymmetry Measurements at Mawson, Antarctica. Il Nuovo Cimento 39, 43, 1965

2. D.J. Cooke & A.G. Fenton, A New Determination of Muon Directional Coupling Coefficients. Proc. Astron. Soc. Aust. 1, 154, 1968.

3. R.J. Francey, A.G. Fenton, K.B. Fenton, D.J. Cooke, L.R. Barnden, L.E. Doherty, A.G. Gregory, K.G. McCracken & I.R. Tuohy, The Development of UAT Rocket Instrumentation for X-Ray Astronomy. Proc. Astron. Soc. Aust. 1, 240, 1969.

4. D.J. Cooke & J.E. Humble, Directional Cosmic Ray Cut-offs and the Loop Cone Phenomenon at Mid Latitude Sites. J.G.R. 75, 5961, 1970.

REFERENCES

Allkofer, O.C., R.D. Andresen & W.D. Dau [1968], Proceedings of International Conference on Cosmic Rays; Can. J. Phys., 46, S301, 1968.

Alpher, R.A. [1950], J.G.R. 55, 437, 1950.

Astrom, K. [1968], Proceedings of International Conference on Cosmic Rays, Calgary; Can. J. Phys., 46, S1064, 1968.

Baber, S.R., W.F. Nash & B.C. Rastin [1968], Nucl. Phys. B4, 549, 1968.

Barton, J.C. & C.T. Stockel [1968], Proceedings of International Conference on Cosmic Rays, Calgary; Can. J. Phys., 46, S319, 1968.

Beiser, A. [1954], J.G.R. 59, 253, 1954.

Bel'skiy, S.A., B.A. Dmitriyev & A.M. Romanov [1969], Geomag. and Aeronomy 9, 119, 1969.

Birkeland, K. [1901], Vid. Selsk. Skv. Math. Nat. Kl., 1, 1901.

Bonnevier, B. [1958], Ark. Fys., 14, 255, 1958.

Bostrom, R. [1965], J.G.R. 69, 1217, 1965.

Bowen, I.S. [1934], Phys. Rev., 45, 349, 1934.

Brooke, G., P.J. Hayman, Y. Kamiya & A.W. Wolfendale, Proc. Phys. Soc. Lond., 83, 853, 1964.

Brunberg, E.A. [1953], Tellus, 5, 135, 1953.

Brunberg, E.A. [1958], Arkiv. Fysik., 14, 195, 1958.

Brunberg, E.A. & A. Dattner, A. [1953], Tellus, 5, 269, 1953.

Burbury, D.W.P. [1952], Phys. Rev., 86, 577, 1952.

Burbury, D.W.P. & K.B. Fenton [1952], Aust. J. Sci. Res., A5, 47, 1952.

Burbury, A.W.P. & A.C. McClaren [1952], Aust. J. Sci. Res., A5, 782, 1952.

Bush, V. [1931], J. Frank. Inst., 212, 447, 1931.

Carmichael, H., M. Bercovitch, M.A. Shea, M. Magidin & R.W. Peterson [1968], Proceedings of International Conference on Cosmic Rays, Calgary; Can. J. Phys., 46, S1006, 1968.

Carmichael, H., M.A. Shea, D.F. Smart & J.R. McCall [1969], Can. J. Phys., 47, 2067, 1969.

Cooke, D.J. [1965], Il Nuovo Cimento, 39, 43, 1965.

Cooke, D.J. & J.E. Humble [1970], J.G.R., 75, 5961, 1970.

Daniel, R.R. & S.A. Stephens [1966], Proc. Ind. Acad. Sci. A63, 275, 1966.

Dorman, L.I. [1957], Cosmic Ray Variations, State Publishing House for Technical and Theoretical Literature (Moscow, 1957). Translation by Tech. Doc. Liaison Office, Wright-Patterson Air Force Base (Washington, 1958).

Dorman, L.I. [1959], Section VII, IGY Programme (C.R.), No. 1, 1959.

Dorman, L.I., V.A. Kovalenko & N.P. Milovidova [1967], Il Nuovo Cimento, 850, 27, 1967.

Dorman, L.I., V.A. Kovalenko & S.B. Cherkov [1969], preprint, similar in content to paper by Dorman, L.I., V.A. Kovalenko, N.P. Milovidova & S.B. Cherkov, in the Proceedings of the International Conference on Cosmic Rays, Budapest, 1970.

Fasoli, U., I. Modena, E. Pohl & J. Pohl-Ruling [1957], Il Nuovo Cimento, 6, 869, 1957.

Fenton, A.G. & D.W.P. Burbury [1948], Phys. Rev., 74, 589, 1948.

Fenton, K.B. [1952], Ph.D. Thesis, University of Tasmania, 1952.

Finch, H.F. & B.R. Leaton [1957], Mon. Not. Roy. Astron. Soc. Geophys. Supp., 7, 314, 1957.

Fonger, W. [1953], Phys. Rev., 91, 351, 1953.

Fowler, G.N. & A.W. Wolfendale [1961], Handb. d. Phys., 46, 272, 1961.

Freon, A. & K.G. McCracken [1962], J.G.R., 67, 888, 1962.

Froman, D.K. & J.C. Stearns [1934], Phys. Rev., 46, 535, 1934.

Gill, S. [1951], Cam. Phil. Soc. Proc., 47, 96, 1951.

Gill, P.S. & A.N. Mitra [1958], Il Nuovo Cimento, 9, 400, 1958.

Gall, R. [1968], J.G.R., 4400, 1968.

Gall, R., J. Jimenez & L. Camacho [1968], J.G.R., 1593, 1968.

Gall, R., J. Jiminez & A. Orozco [1969], J.G.R., 74, 3529, 1969.

Handbook of Geophysics [1961], U.S. Air Force Tables, MacMillan Co., New York, 1961.

Harris, F.B. & I. Escobar [1955], Phys. Rev., 100, 255, 1955.

Harris, F.B. & I. Escobar [1956], Phys. Rev., 104, 542, 1956.

Hatton, C.J. & D.A. Carswell [1963], Atomic Energy of Canada Ltd., Report No. AECL-1824, 1963.

Hayman, P.J. & A.W. Wolfendale [1962], Proc. Phys. Soc., 80, 710, 1962.

Holmes, J.E.R., B.G. Owen & A.L. Rodgers [1961], Proc. Phys. Soc., 78, 505, 1961.

Hovi, V. & A. Aurela [1961], An. Acad. Sci. Fen., A6, No. 97, 1961.

Hutner, R.A. [1939a], Phys. Rev., 55, 15, 1939.

Hutner, R.A. [1939b], Phys. Rev., 55, 614, 1939.

Jacklyn, R.M. [1959a], "The 27-Day Type of Intensity Variation ...", Proc. Antarctic Symposium, Buenos Aires, Nov., 1959.

Jacklyn, R.M. [1959b], "Short Term Decreases of the Cosmic Ray East-West Asymmetry ...", Proc. Ant. Symp., Buenos Aires, Nov., 1959.

Jacklyn, R.M. & A.G. Fenton [1957], Phys. Rev., 106, 809, 1957.

Jacklyn, R.M. & J.E. Humble [1965], Aust. J. Phys., 18, 451, 1965.

Jakeman, D. [1956], Can. J. Phys., 34, 432, 1956.

Janossy, L. [1948], Cosmic Rays, Oxford University Press, London, 1948.

Jensen, D.C. & J.C. Cain [1962], J.G.R., 67, No. 9, (Abstract), August, 1962.

Johnson, T.H. [1941], Phys. Rev., 59, 11, 1941.

Johnson, T.H. & J.C. Street [1933], Phys. Rev., 43, 381, 1933.

Johnson, T.H. & E.C. Stevenson [1933], Phys. Rev., 44, 125, 1933.

Judge, R.J.R. & W.F. Nash [1965], Il Nuovo Cimento, 35, 1025, 1965.

Kane, R.P. [1962], J.G.R., 67, 1295, 1962.

Kane, R.P. [1963], Il Nuovo Cimento, 30, 681, 1963.

Kasper, J.E. [1959], Suppl. Il Nuovo Cimento, 11, 1, 1959.

Kellogg [1960], J.G.R., 65, 2701, 1960.

Kellogg, P.J. & M. Schwartz [1959], Il Nuovo Cimento, 13, 761, 1959.

Kilfoyle, B.P. & F. Jacka [1968], Nature, 220, 773, 1968.

Kondo, I. & M. Kodama [1965], Proceedings of the International

Conference on Cosmic Rays, London, 1, 558, 1965.

Krasilnikov, D.D. [1964], Bull. Acad. Sci. USSR (Phys. Ser.), 28, 1742, 1964.

Kraushaar, W.L. [1949], Phys. Rev., 76, 1045, 1949.

Krimsky, G.F., P.A. Krivoshapkin & G.V. Skripin [1965], Proccedings International Conference on Cosmic Rays, London, 1, 503, 1965.

Leaton, B.R., S.R.C. Malin & M.J. Evans [1965], J. Geomagn. and Geoelect., 17, No. 3-4, 187, 1965.

Lemaitre, G. & M.S. Vallarta [1936a], Phys. Rev., 49, 719, 1936.

Lemaitre, G. & M.S. Vallarta [1936b], Phys. Rev., 50, 493, 1936.

Lindgren, S. [1965], Ark. Fys., 5, 23, 1965.

Mackeown, P.K., S.S. Said, J. Wdowezyk & A.W. Wolfendale [1965], Proceedings International Conference on Cosmic Rays, London, 2, 965, 1965.

Maeda, K. [1964], J.G.R., 69, 1725, 1964.

Mathews, T. [1963], Phil. Mag., 8, 387, 1963.

Mathews, T. & G.G. Sivjee [1967], Can. J. Phys., 45, 1643, 1967.

Mazaruyk, E.A. [1966], Bull. Acad. Sci. USSR (Phys. Ser.), 30, 1947, 1966.

McCracken, K.G., U.R. Rao & M.A. Shea [1962], M.I.T. Technical

Report 77, 1962.

McCracken, K.G. [1962], J.G.R., 67, 423, 1962.

Mead, G.D. [1964], Phys. Rev., 69, 1181, 1964.

Montgomery, D.J.X. [1949], Cosmic Ray Physics, (Princeton), 1949.

Moroney, J.R. & J.K. Parry [1954], Aust. J. Phys., 7, 423, 1954.

Olbert, S. [1953], Phys. Rev., 92, 454, 1953.

Olbert, S. [1954], Phys. Rev., 96, 1400, 1954.

Ormes, J.F. & W.R. Webber [1965], Proceedings International Conference on Cosmic Rays, London, 1, 349, 1965.

Pine, J., R.J. Davisson & K. Greisen [1959], Il Nuovo Cimento, 14, 1181, 1959.

Pak, W., S. Ozaki, B.P. Roe & K. Greisen [1961], Phys. Rev., 121. 905, 1961.

Pal, Y. & B. Peters [1964], Mat. Fys. Med. Dan. Vid. Selk., 33, 1, 1964.

Parsons, N.R. [1957], Rev. Sci. Instr., 28, 265, 1957.

Parsons, N.R. [1959], Ph.D. Thesis, University of Tasmania, 1959.

Parsons, N.R. [1960], Australian National Antarctic Research Expedition Interim Report No. 17, 1960, (Antarctic Division, Department of Supply, Melbourne).

Quenby, J.J. & W.R. Webber [1959], Phil. Mag., 4, 90, 1959.

Quenby, J.J. & G.J. Wenk [1962], Phil. Mag., 7, 1457, 1962.

Rao, U.R., K.G. McCracken & D. Venkateson [1963], J.G.R., 68, 345, 1963.

Rossi, B. [1952], High Energy Particles, (Prentice Hall), 1952.

Rothwell, P. [1958], Phil. Mag., 3, 961, 1958.

Rothwell, P. & J.J. Quenby [1958], Suppl. Il Nuovo Cimento, 8, 249, 1958.

Sands, M. [1950], Phys. Rev., 77, 180, 1950.

Sandstrom, A.E. [1965], Cosmic Ray Physics, (North Holland Publ. Comp.), 1965.

Sauer, H.H. [1963], J.G.R., 68, 957, 1963.

Schremp, E.J. [1938], Phys. Rev., 54, 153, 1938.

Seidl, F.G.P. [1941], Phys. Rev., 59, 7, 1941.

Shea, M.A. & D.F. Smart [1967], J.G.R., 72, 2021, 1967.

Shea, M.A. & D.F. Smart [1970a], J.G.R., 75, 3921, 1970.

Shea, M.A. & D.F. Smart [1970b], Proceedings of International Conference on Cosmic Rays, Budapest, 1970.

Shea, M.A., D.F. Smart & K.G. McCracken [1965], J.G.R., 70, 4117, 1965.

Shea, M.A., D.F. Smart, K.G. McCracken & U.R. Rao [1968], Supplement to IQSY Instruction Manual 10, Cosmic Ray Tables, Special Report No. 71, AFCRL, 68-0030, 1968.

Shea, M.A., D.F. Smart & J.R. McCall [1968], Proceedings of International Conference on Cosmic Rays, Calgary; Can. J. Phys., 46, S1098, 1968.

Sitte, K. [1961], Handbuch der Physik, 46/1, 157, 1961.

Smart, D.F., M.A. Shea & R. Gall [1969], J.G.R., 74, 4731, 1969.

Stensland, B. [1965], Ark. Geophys., 5, 31, 1965.

Stern, D. [1960], Suppl. Il Nuovo Cimento, 16, 153, 1960.

Tidman, D.A. & K.W. Ogilvie [1957], Il Nuovo Cimento, 6, 735, 1957.

Vallarta, M.S. [1961], Handbuch der Physik, 46/1, 88, 1961.

Wada, M. [1960], Sci. Papers of the Inst. of Phys. Chem. Res., Tokyo, 54, 335, 1960.

Webber, W.R. [1962], Progress in Elementary Particle and Cosmic Ray Physics, 6, 75, 1962.

Webber, W.R. & J.J. Quenby [1959], Phil. Mag., 4, 654, 1959.

Wilson, B.G. [1959], Can. J. Phys., 37, 28, 1959.